The role of CaSR signalling in adipocytes and its regulation by ADMA

Erin Dawn Higgins BSc (Hons) MRes

PhD Thesis

School of Cardiovascular & Metabolic Health
College of Medical, Veterinary and Life Sciences
University of Glasgow

March 2023

Abstract

The amino acid sensitive calcium-sensing receptor (CaSR) plays a critical role in regulating extracellular calcium ($[Ca^{2+}]_o$) levels. In addition to maintaining $[Ca^{2+}]$ homeostasis, the CaSR is involved in a variety of non-calciotropic functions, among which it has emerged as a mediator of adipocyte (patho)physiology.

Recent work in our lab has revealed that adipocyte hypertrophy is stimulated by the amino acid asymmetric dimethylarginine (ADMA) via a nitric oxide-independent, CaSR pathway. However, the underpinning mechanisms and relevance in adipocytes was not clearly identified. This thesis aimed to delineate CaSR signalling pathways *in vitro*, and subsequently test the effect of ADMA on CaSR downstream signalling and functions. CaSR was investigated first in HEK293 cells overexpressing CaSR, which showed CaSR-dependent $ERK_{1/2}$ signalling in response to pharmacological CaSR stimulation and exogenous ADMA. Next, CaSR/ADMA signalling pathways were examined using 3T3-L1 cells modelling mature adipocytes. Agonist-induced CaSR signalling caused adipocyte hypertrophy, leptin secretion and lipogenic gene expression. ADMA enlarged adipocytes, and ADMA-induced lipogenic gene expression was perturbed by CaSR blockade indicating ADMA/CaSR crosstalk in adipocytes. However, ADMA was unable to fully replicate the effects of CaSR acting in adipocytes highlighting the complexity of CaSR signalling pathways requiring further investigation.

Adipose tissue (AT) dysfunction is a key mechanism linking metabolic disorders and cardiovascular disease (CVD). The CaSR is associated with CVD, but the relevance of adipocyte CaSR in cardiovascular health has not been directly examined. Therefore, this thesis also aimed to investigate the function of adipocyte CaSR, and determine its significance in AT and cardiovascular biology. To investigate the role of adipocyte CaSR *in vivo*, this thesis generated a murine model of adipocyte-specific CaSR deficiency. In female mice specifically, body weight, adipocyte size and AT-induced vascular contractility was reduced. This thesis establishes ADMA as a potentially novel ligand of CaSR, and demonstrates that adipocyte CaSR can impact on AT biology as well as cardiometabolic health in the intact animal.

Contents

List of tables

List of figures

Publications

Dowsett L, Duluc L, **Higgins E**, Alghamdi F, Fast W, Salt I.P., Leiper J. *Asymmetric dimethylarginine positively modulates Calcium-Sensing Receptor signalling to promote lipid accumulation and adiposity.* Preprint – bioRxiv. (2021) [https://www.biorxiv.org/content/10.1101/2022.07.26.501411v1]

Dowsett L, **Higgins E**, Alanazi S, Alshuwayer NA, Leiper FC and Leiper J. *Asymmetric dimethylarginine: A key player in the relationship between vascular dysfunction and inflammation in atherosclerosis*. J. Clin. Med. (2020) 9 (9):3026

Abstracts: Oral Presentations

Dowsett L, **Higgins E**, Duluc L, and Leiper J. *ADMA can act as a positive regulator of endothelial nitric oxide production by modulation of signalling via the calcium sensing receptor.* European Society of Hypertension 2019, Milan.

Dowsett L, Duluc L, **Higgins E**, Boruc O, and Leiper J. *ADMA can positively regulate NO production through the Calcium Sensing Receptor.* Nitric Oxide Society Biennial Conference 2018, Oxford.

Abstracts: Poster Presentations

Higgins E, Leiper J, Dowsett L. *Adipocyte-specific CaSR deletion in vivo.* The Biochemical Society/Society for Endocrinology: The adipocyte across biological scales 2021, Edinburgh.

Dowsett L, **Higgins E**, and Leiper J. *The Calcium Sensing Receptor (CaSR) Is a Bi-Phasic Regulator of Vascular Reactivity and Can Be Modulated by the Cardiovascular Risk Factor Asymmetric Dimethylarginine (ADMA).* The 21st International Vascular Biology Meeting 2020, South Korea (e-poster due to Covid-19 travel restrictions).

Dowsett L, Duluc L, **Higgins E**, Leiper J. *ADMA increases Calcium- Receptor signalling to promote endothelial NO production.* British Society of Cardiovascular Research Spring Conference 2019, Manchester.

Acknowledgements

Firstly, I would like to thank the British Heart Foundation for their generous funding and stipend which underpinned my PhD work.

I would like express gratitude to my primary supervisor James Leiper, who I was initially drawn to because of his enthusiasm and humour. During my project, it was often hard for me to match James' unbridled optimism, but in truth I found great comfort in his positivity. Most certainly, James encouraged me to be a self-sufficient (and patient!) student and scientist. I must also thank my secondary supervisor Graeme Milligan who showed much welcomed kindness when personal events impacted my studies.

It is not an exaggeration to say that working within ICAMS has been a wonderful experience. I feel incredibly fortunate to have met a great number of interesting, intelligent and kind people during my studies, many of whom are now fond friends. Of these people, there are several I would like to thank in particular. Firstly, Leiper lab group members Fiona, Zaniah, Noha and Sara for their feedback and encouragement. John McAbney, for his technical assistance and banter during long myography days. Nic Britton, for her invaluable histology skills. Antoniya, Simon & Eleni, my officemates who I was never actually in the office with, for their friendship. Not forgetting others who provided support, fun, or caring words – Jim, Wendy, Dan, Gabby, Arun, Elaine, Linda, Anne, the other Anne, and Steven.

Of those within my institute who deserve acknowledgement, my most heartfelt appreciation must be extended to Laura Dowsett. A wonderful, caring human being who played a fundamental role in shaping my PhD experience and guiding the work within this thesis. Laura, I don't think you will ever really know how fantastic you are. For your mentorship, pastoral support and friendship – thank you.

In addition to my colleagues, I would like to recognise the essential role played by my parents Tracy & Scott. Their love and support has been a key driving force for me throughout my life generally, but particularly so during my PhD. Whenever I was uncertain of myself, my ability or worth, I could always find comfort in their reassurance. Mum & Dad – it is without doubt that I am here because of you. I would also like to acknowledge my Gran who, despite still not really knowing what it is I actually do, is an unwavering source of support and one of my biggest fans.

Thank you to my cats Micah and Fergie, who were always there to keep my lap warm and my heart full during quiet moments where I struggled most.

Lastly but perhaps most importantly, I want to thank Fraser. My partner and very best friend who has been by my side throughout my – by this point, quite extensive - academic career. It is difficult to articulate how much I appreciate your support, patience, and the countless sacrifices you have made to make this possible for me. This thesis, built on a foundation of coffee offered without ask, is dedicated to you.

Author's declaration

I confirm that the work presented within this thesis is my own. Information which is obtained from other sources has been referenced appropriately, and experiments which have been performed by others or as part of a collaboration have been clearly indicated.

Erin Dawn Higgins

"I don't know where I am going from here, but I promise it won't bore you"

Definitions & abbreviations

$[Ca^{2+}]_i$	Intracellular/cytosolic calcium
$[Ca^{2+}]_o$	Extracellular calcium
18S	18S ribosomal RNA
ACC1	Acetyl-CoA carboxylase
ACE	Angiotensin-converting enzyme
ACh	Acetylcholine
ADIS	Agonist-driven insertional signalling
ADMA	Asymmetric NG,NG-dimethylarginine
AGXT2	Alanine-glyoxylate aminotransferase 2
AKT	Protein kinase B
ApoE	Apolipoprotein E
AT	Adipose tissue
ATGL	Adipose triglyceride lipase
BAT	Brown adipose tissue
BMSC	Bone marrow stem cell
BODIPY	Boron-dipyrromethene
BSA	Bovine serum albumin
C/EBP	CCAAT/enhancer- binding-protein
CAD	Coronary artery disease
cAMP	Cyclic AMP
CaSR	Calcium-sensing receptor
$CaSR^{Ad-/-}$	Adipocyte-specific CaSR deficient mouse
$CaSR^{fl/fl}$	CaSR homozygous floxed mouse
CAT	Cationic amino acid transporter
CREB	cAMP response element-binding protein
CVD	Cardiovascular disease
DAPI	4′,6-diamidino-2-phenylindole
DBP	Diastolic blood pressure
DDAH	Dimethylarginine dimethylaminohydrolase
Dex	Dexamethasone
DMEM	Dulbecco’s Modified Eagle’s Medium

DX	Doxycycline
EC	Endothelial cell
EDN-1	Endothelin-1
ELISA	Enzyme-linked immunosorbent assays
eNOS	endothelial nitric oxide synthase
$ERK_{1/2}$	Extracellular signal-regulated kinase
FABP4/aP2	Fatty acid binding protein
FASN	Fatty acid synthase
FBS	Foetal bovine serum
FFA	Free fatty acid
GAPDH	Glyceraldehyde 3-phosphate dehydrogenase
gAT	Gonadal adipose tissue
GLUT-4	Glucose transporter-4
GPCR	G-protein coupled receptor
HEK293-CaSR	human calcium-sensing receptor transfected HEK293 cells
HEK293-vec	vector transfected HEK293 cells
HR	Heart rate
HSL	Hormone sensitive lipase
IBMX	3-isobutyl-1-methylxanthine
IK_{Ca}	Calcium-sensitive K^+ channels
IL	Interleukin
IP_3	Inositol trisphosphate
L-Arg	L-arginine
LD	Lipid droplet
L-NAME	NG-Nitroarginine methyl ester
L-Phe	L-phenylalanine
LPL	Lipoprotein lipase
MAP	Mean arterial blood pressure
MCP-1	Monocyte chemoattractant protein-1
mGluR	Metabotropic glutamate receptor
MMA	NG-monomethylarginine
MMP2	Matrix metalloproteinase-2
NBS	Newborn calf serum
NO	Nitric oxide
NOX	NADPH oxidase

NRF2	Nuclear factor erythroid 2-related factor 2
ORO	Oil red O
p90RSK	p90 ribosomal S6 kinase
PBS	Phosphate buffered saline
PCR	Polymerase chain reaction
PE	Phenylephrine
PGI_2	Prostacyclin
PKA	Protein kinase A
PKG	Protein kinase G
PLC	Phospholipase C
PLN-1	Perilipin-1
PPARγ	Peroxisome proliferator-activated receptor gamma
PRMT	Protein methyltransferase
PSS	Physiological salt solution
PTH	Parathyroid hormone
PVAT	Perivascular adipose tissue
PVCF	Perivascular contractile factor
PVRF	Perivascular relaxing factor
qPCR	Quantitative PCR
ROS	Reactive oxygen species
RPL13	60S ribosomal protein L13
RSK	S6 kinase
SBP	Systolic blood pressure
scAT	Subcutaneous adipose tissue
SDMA	Symmetric NG,NG'-dimethylarginine
SDS	Sodium dodecyl sulfate
SDS-PAGE	Sodium dodecyl sulfate polyacrylamide gel electrophoresis
SNP	Sodium nitroprusside
SOD	Superoxide dismutase
sGC	Soluble guanylate cyclase
SREBP1	Sterol regulatory element-binding protein 1
TBS	Tris-buffered saline
TBS-T	Tris buffered saline with Tween20
TG	Triglyceride
TGFβ	Transforming growth factor beta

TNFα	Tumour necrosis factor α
UCP-1	Uncoupling protein-1
VFT	Venus fly trap
VGCC	Voltage-gated calcium channels
VSMC	Vascular smooth muscle cell
WAT	White adipose tissue

Chapter One

General Introduction

Chapter 1: General Introduction

1.1 Adipose Tissue

1.1.1 General anatomy

For a very long time, adipose was considered an inert tissue, acting simply to store energy and provide insulation as a by-product. However, this dogma was rapidly altered following the discovery that a protein, termed adipsin (complement D), could be secreted by cultured 3T3-L1 cells and murine adipose (Cook *et al.*, 1987). This realisation triggered a scientific renaissance, compelling many investigators to reconsider the importance of adipose tissue (AT), the mechanism(s) involved in its function and its significance in disease. Though adipose is now recognised as a highly complex tissue capable of regulating a wide variety of endocrine and metabolic functions, the identification of novel and yet undiscovered aspects of AT biology indicate that our present understanding of AT is far from complete.

Adipose is a heterologous tissue. Though adipocytes comprise the greatest volume, adipose also contains fibroblasts, macrophages, vascular cells, preadipocytes and stem cells (Oikonomou and Antoniades, 2019). Adipose tissue (AT) is classified by several methods. When grouped according to *morphology*, adipose can be defined as white adipose tissue (WAT) or brown adipose tissue (BAT). Morphological differences in WAT and BAT arise due to the distinct appearance and function of adipocytes within these tissues (Fig. 1-1). Beige or brite AT demonstrates features of both BAT and WAT, though it is recognised as a specific AT subtype (Hildebrand, Stümer and Pfeifer, 2018).

Figure 1-1

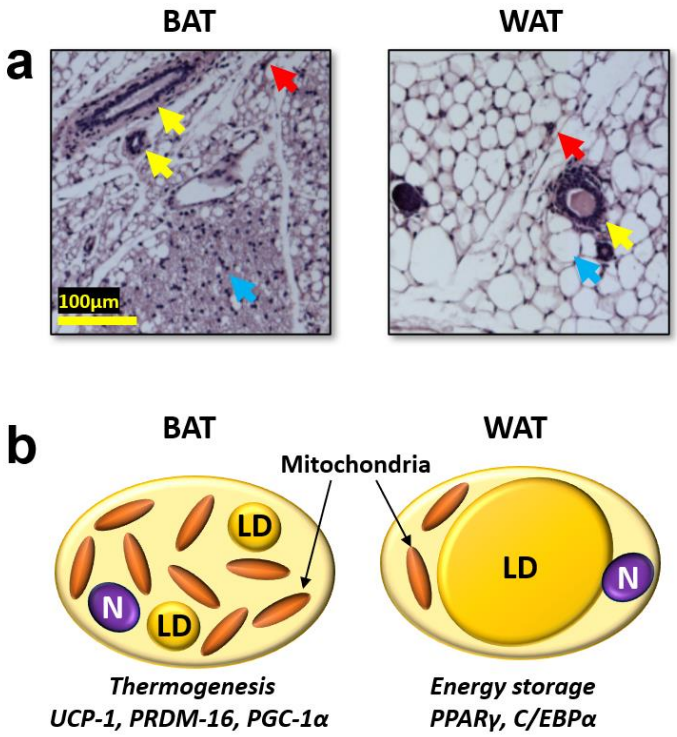

Figure 1-1: Adipose tissue morphology and phenotype.
(a) Brown adipose tissue (BAT) and white adipose tissue (WAT) stained with hematoxylin and eosin and imaged with light microscopy. BAT and WAT display common features such as adipocytes (blue arrows), blood vessels (yellow arrows) and tissue immune cells (red arrows). The microscopic appearance of BAT and WAT however differs significantly due to adipocyte morphology. **(b)** Schematic depicting structural and functional differences in BAT and WAT adipocytes. C/EBPα= CCAAT/enhancer- binding-protein α; LD=Lipid droplet. N=Nucleus. PGC-1α=PPARγ coactivator 1-alpha; PPARγ=Peroxisome proliferator-activated receptor gamma; PRDM-16=PR domain containing 16; UCP-1=Uncoupling protein-1 Scale bar=100µM. Schematic produced using information from Hildebrand, Stümer and Pfeifer (2018).

WAT is the predominant adipose type in mammals (Trayhurn and Wood, 2004) and main focus of this thesis. Besides its morphological appearance, WAT can be further stratified based on *anatomy*. Generally, WAT classed according to locality is defined as either subcutaneous or visceral AT, corresponding to its presence beneath the skin or in association with organ systems, respectively. In humans, subcutaneous WAT resides predominantly in the upper body (abdominal

AT) and lower body (gluteal-femoral AT). In contrast, visceral WAT is closely associated with the stomach (omental AT), gastrointestinal tract (mesenteric AT) and heart (epicardial AT) (Kwok, Lam and Xu, 2016). Mice are frequently used as preclinical models of human AT pathophysiology. As with humans, rodents accumulate both subcutaneous and visceral WAT. However, subcutaneous WAT is largely present in anterior and posterior depots, while visceral WAT is situated within gonadal, mesenteric and peritoneal depots (Fig. 1-2) (Chusyd *et al.*, 2016).

Figure 1-2

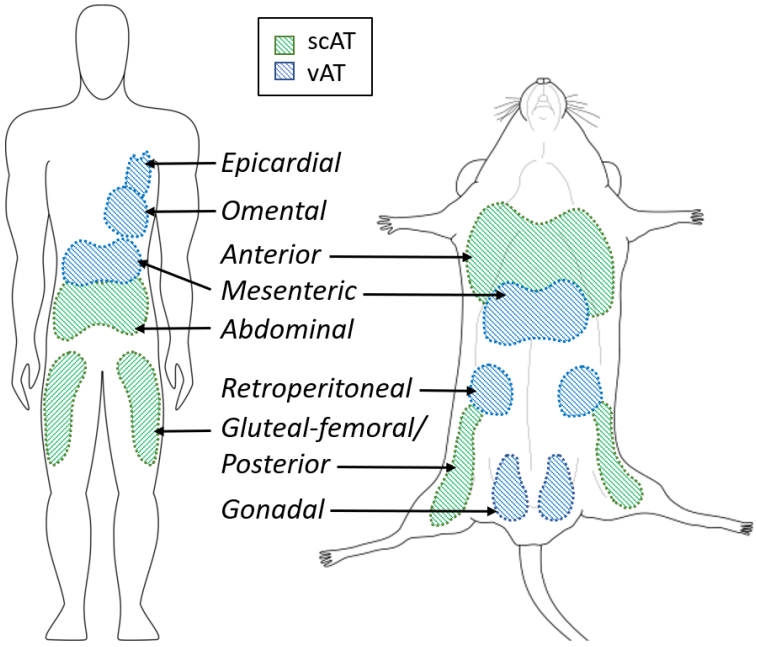

Figure 1-2: Distribution of white adipose tissue in humans and rodents.

Humans accumulate subcutaneous adipose tissue (scAT) around the abdomen and gluteal-femoral region. Mice demonstrate scAT distributed anteriorly and dorsally. Humans possess epicardial, omental and mesenteric visceral adipose tissue (vAT) concentrations, whereas vAT accumulates within mesenteric, retroperitoneal and gonadal depots in mice. Figure adapted from Chusyd *et al.* (2016).

1.1.2 Adipocyte differentiation

High nutritional states stimulate AT expansion. Key features of this process are increased adipocyte number (hyperplasia) and increased adipocyte size (hypertrophy) (Oikonomou and Antoniades, 2019). Physiological, hyperplastic AT

remodelling is regulated by a mechanism known as adipogenesis, which involves two defined phases: stem cell commitment, followed by the differentiation of adipocyte lineage precursors (i.e. preadipocytes) into adipocytes. Commitment of stem cells to the preadipocyte lineage is achieved when pluripotent mesenchymal stem cells in the vascular tissue of AT are stimulated by elevated nutrients, particularly glucose (Tang and Lane, 2012).

Once committed, preadipocytes proliferate until they reach growth arrest. At this stage, primed preadipocytes can be stimulated to undergo differentiation by a specific cocktail of hormonal inducers which enhance insulin, glucocorticoid and cyclic AMP (cAMP) signalling pathways (Tang and Lane, 2012). CCAAT/enhancer- binding-protein (C/EBP)-ß and C/EBPδ accumulate early in differentiation, activating C/EBPα and the key adipocyte transcription factor peroxisome proliferator-activated receptor gamma (PPARγ) (Yeh *et al.*, 1995; Rosen, Eguchi and Xu, 2009). In turn, these transcriptional activities induce expression of key adipocyte gene markers acetyl-CoA carboxylase (ACC1), fatty acid synthase (FASN) and fatty acid binding protein (FABP4/aP2). The chronological expression of such genes and corresponding accumulation of triglyceride lipid signals the acquisition of an adipocyte phenotype (Spiegelman *et al.*, 1993; Rosen and Spiegelman, 2003). Though differentiating adipocytes undergo lipogenesis, this process and others also regulate intracellular lipid content in the mature adipocyte, as explained in the next section.

1.1.3 Function

The earliest reports of AT function indicated its role in energy storage, owing to its accumulation of triglycerides. However, adipocyte-specific production of adipsin and later leptin showed a potentially important role for AT secretory function in metabolism (Cook *et al.*, 1987; Zhang *et al.*, 1994). Since then, AT has been revealed as a *bona fide* endocrine organ and a key regulator of metabolism, cardiovascular function, immune responses and reproduction (Coelho, Oliveira and Fernandes, 2013). AT function is regulated by the activities of stromal cells and adipocytes. However, adipocyte lipid storage, insulin sensitivity and secretory function are particularly important in maintaining AT biology and health, since derangement of these mechanisms manifests a range of cardiometabolic disease states (Coelho, Oliveira and Fernandes, 2013;

Oikonomou and Antoniades, 2019). This section will highlight key features of adipocyte function.

1.1.1.1. Lipogenesis

Cellular lipid accumulation is determined by the relative balance between lipid synthesis and lipid catabolism, termed as lipogenesis and lipolysis, respectively. Though other cells such as hepatocytes accumulate and release lipid, adipocytes are highly specialised for this function (Coelho, Oliveira and Fernandes, 2013).

Lipogenesis is highly regulated by the prevailing nutritional environment, since the process is triggered in response to circulating glucose and insulin (Rosen, Eguchi and Xu, 2009). Broadly, lipogenesis describes the process of cellular lipid accumulation via the esterification of glucose and free fatty acid (FFA) to the neutral lipid triglyceride. FFAs are key constituents of triglyceride biosynthesis, the availability of which is determined by two main processes described here in brief. Firstly, FFAs are liberated from circulating lipoproteins and chylomicrons by the action of AT lipoprotein lipase (LPL), after which fatty acid transporters facilitate adipocyte entry. The second process involves the uptake of glucose by adipocyte glucose transporter-4 (GLUT-4). Glucose then undergoes glycolysis and citric acid cycle processing to form citrate, which is converted to FFAs by the stepwise enzymatic action of citrate lysate, ACC1 and FASN (Fig. 1-3) (Saponaro *et al.*, 2015; Song, Xiaoli and Yang, 2018). The process governing the synthesis of lipids from carbohydrates is known as *de novo* lipogenesis (Song, Xiaoli and Yang, 2018).

Once formed, triglycerides are packaged and stored in highly specialised organelles known as lipid droplets (LDs). LDs display a unique structure comprising a hydrophobic neutral lipid core, which is shielded by phospholipid monolayer bound by scattered perilipin proteins (Krahmer *et al.*, 2013). In times of nutritional excess, increased triglyceride synthesis necessitates a corresponding increase in LD storage capacity. This is fulfilled by LD biogenesis and expansion, which in WAT adipocytes causes enlargement of its characteristic unilocular LD and cellular hypertrophy (Richard *et al.*, 2000).

Figure 1-3

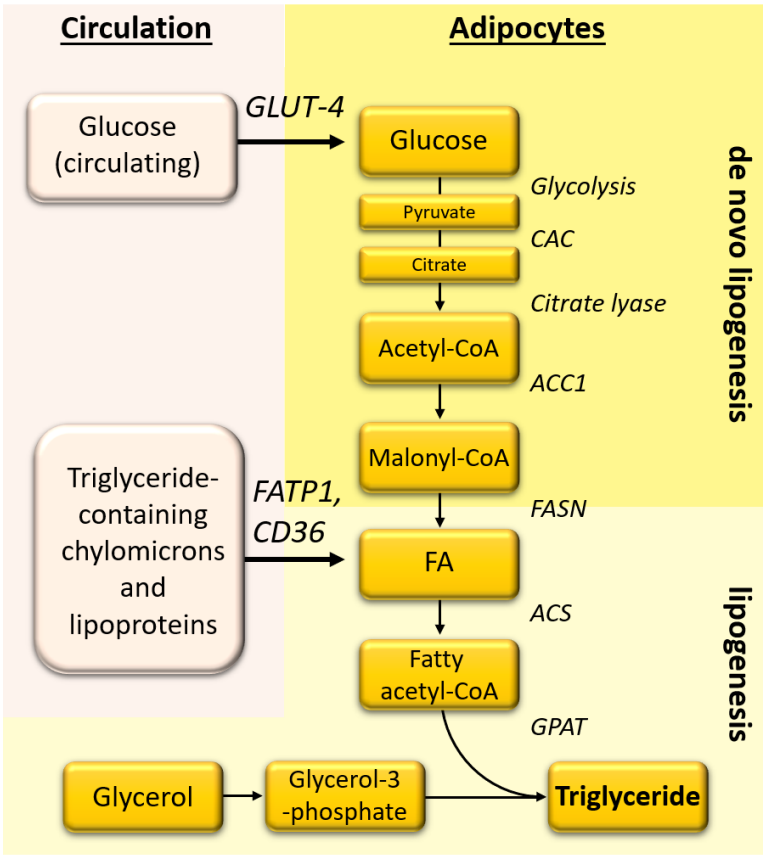

Figure 1-3: The lipogenesis pathway in adipocytes.

Adipocyte lipid accumulation occurs due to the conversion of glucose and FA to triglyceride. This occurs through two key pathways: sequestering and uptake of FFAs from the circulation by catabolism of triglyceride-rich chylomicrons and lipoproteins, and secondly via the intracellular entry of glucose and its stepwise conversion to FAs. The biosynthesis of triglyceride from fatty acetyl-CoA and Glycerol-3-phosphate is initialised by GPAT, but involves a number of enzymatic steps not shown. ACC1= Acetyl-CoA carboxylase; ACS=Acyl-CoA synthetase; CAC=Citric acid/Kreb's cycle; FA=Fatty acid; FASN=Fatty acid synthase; FATP1= Fatty acid transport protein-1; GLUT-4=Glucose transporter-4; GPAT=Glycerol-3-phosphate acyltransferase. Figure produced using information from Saponaro *et al.* (2015) and Song, Xiaoli and Yang (2018).

1.1.1.2. Lipolysis

As discussed above, adipocytes undergo lipogenesis to sequester and store circulating lipids as triglycerides. While conditions of nutritional excess stimulate adipocyte uptake of glucose and FFAs, periods of low nutrition stimulates sympathetic and catecholamine signalling pathways, triggering degradation of adipocyte LDs, promoting lipolysis (Kwok, Lam and Xu, 2016). Opposing lipogenesis, lipolysis describes the process by which stored cellular triglycerides are hydrolysed and released as glycerol and FFA (Saponaro *et al.*, 2015).

Lipolysis is predominantly regulated by the actions of cAMP-mediated protein kinase A (PKA). Activated PKA stimulates hormone sensitive lipase (HSL) and perilipin-1, the latter of which results in adipose triglyceride lipase (ATGL) recruitment. The sequential action of ATGL, HSL and monoacylglycerol lipase catalyse the conversion of triglyceride into diglyceride, monoacylglycerol, then finally glycerol. Glycerol and fatty acids liberated throughout stepwise triglyceride catabolism then serve as substrates for cellular gluconeogenesis and oxidation, respectively (Richard *et al.*, 2000).

1.1.1.3. Secretion

Adipocyte secretory function was first revealed by Cook et al., who demonstrated that the serine protease adipsin was elaborated by 3T3-L1 adipocytes and murine AT (Cook *et al.*, 1987). It is now known that adipocytes and stromal cells secrete a wide variety of bioactive factors, including mRNA, lipids, cytokines, and adipocyte-specific peptide hormones (i.e. adipokines) which mediate potent metabolic effects influencing insulin responses, appetite, lipid metabolism and the cardiovascular system (Richard *et al.*, 2000). Though some mediators, particularly cytokines such as tumour necrosis factor α (TNFα) and interleukin-6 (IL-6) are predominantly elaborated by AT stromal cells, others such as leptin and adiponectin are secreted principally by adipocytes (Hocking *et al.*, 2010).

Leptin is a circulating protein produced predominantly by subcutaneous WAT and positively correlated with adiposity (Wajchenberg, 2000). First known as the

obese (*ob*) mutation, leptin was identified as a hormonal regulator of appetite and adiposity since its deficiency in mice (*ob*/*ob*) perpetrated an obese and diabetic phenotype. This genetic identity of this factor was reconciled by Zhang and colleagues, who demonstrated that the *ob* gene was expressed exclusively in AT and highly conserved across species, including humans (Zhang *et al.*, 1994). The importance of leptin in metabolic regulation is demonstrated by studies which administer leptin in *ob*/*ob* mice and humans with leptin deficiency. In both instances, hypertriglyceridemia, insulin responses and body weight are corrected by leptin infusion (Harris *et al.*, 1998; Farooqi *et al.*, 2002). Other models of dysfunctional leptin signalling such as the *db*/*db* mouse display similar metabolic derangement but are insensitive to leptin infusion. In this case however, leptin signalling deficiency arises due to leptin receptor mutation (Chen *et al.*, 1996), corroborating the importance of this pathway in metabolic homeostasis. Regarding metabolism, key biological targets of leptin are the central nervous system and hypothalamic-pituitary-adrenal axis, which when stimulated produces responses favouring appetite suppression and energy disposal (La Cava and Matarese, 2004). Leptin also exhibits many additional targets such as macrophages, T- and B-cells, endothelial cells (ECs) and vascular smooth muscle cells (VSMCs) where it fulfils important roles in immune function, vascular reactivity and vascular remodelling (La Cava and Matarese, 2004; Li *et al.*, 2014; Nava and Llorens, 2019).

In contrast to leptin which is typically proinflammatory and linked with AT accumulation, adiponectin is negatively correlated with adiposity and exerts anti-inflammatory effects (Wajchenberg, 2000). Adiponectin, at the time termed as Arcp30, was originally cloned from 3T3-L1 cells. In a series of experiments, Scherer and colleagues demonstrated that adiponectin mRNA was abundant in mature 3T3-L1 adipocytes, murine AT and plasma, but was absent in undifferentiated preadipocytes and other sampled tissues (Scherer *et al.*, 1995). Today, several tissues are known to generate adiponectin (Mukohira *et al.*, 2019), though its high systemic levels are maintained principally by WAT (Ghantous *et al.*, 2015). Circulating adiponectin binds its receptors AdipoR1 and R2 in a variety of tissues including skeletal muscle, vascular tissue, the liver, and adipocytes themselves. Though adiponectin mediates a range of effects at these sites, it plays an important role in metabolism by improving adipocyte, myocyte and

hepatic glucose utilisation (Achari and Jain, 2017). Adiponectin exerts particularly potent anti-inflammatory effects in the vasculature. For instance, adiponectin stimulates AMP kinase in ECs, causing increased endothelial nitric oxide synthase (eNOS) elaboration of nitric oxide (NO) and suppression of inflammatory pathways perpetrated by factors such as TNFα and hyperglycaemia. This mechanism promotes endothelial-dependent relaxation and counteracts EC activation (Goldstein, Scalia and Ma, 2009). Adiponectin also induces vasodilation through direct effects on VSMC calcium-sensitive K^+ channels (IK_{Ca}) (Lynch *et al.*, 2013) and further regulates VSMC biology by inhibiting extracellular signal-regulated kinase ($ERK_{1/2}$) signalling, which attenuates the VSMC proliferation and migration response to platelet derived growth factor (Arita *et al.*, 2002). The importance of adiponectin in metabolism and vascular biology is corroborated by studies performed in adiponectin deficient mice, since this model develops hyperglycaemia and hypertension (Ouchi *et al.*, 2003).

In addition to leptin and adiponectin, the adipocyte secretome comprises over 50 adipokines (Trayhurn and Wood, 2004). Other major adipokines such as resistin, omentin and vaspin have been identified. Though resistin is implicated in vascular remodelling and inflammation (Pereira and Alvarez-Leite, 2014; Chang, Garcia-Barrio and Chen, 2020), the mechanistic actions and functional role(s) of these factors are not well understood.

1.1.4 WAT Heterogeneity

1.1.4.1 General WAT depots

In general, excessive AT accumulation is considered harmful. However, clinical data demonstrate that the anatomical localisation of WAT is also important, since WAT distribution is an independent determinant of insulin sensitivity, circulating triglycerides, glucose and blood pressure (Mårin *et al.*, 1992; Abate *et al.*, 1995; Grundy, Adams-Huet and Vega, 2008). Correlations between AT locality and function arise due to AT biology, which demonstrates distinct and depot-specific differences. For instance, visceral WAT is more resistant to insulin when compared to subcutaneous depots (Abate *et al.*, 1995). Metabolic activity is also greater in visceral compared to subcutaneous depots; basal and catecholamine- and insulin-stimulated lipolysis is increased in visceral compared to subcutaneous adipocytes (Östman *et al.*, 1979; Mårin *et al.*, 1992). In

adipocytes, lipolytic activity is stimulated by ß-adrenoreceptors, but is inhibited by insulin and α-adrenoreceptors. In part, comparatively higher lipolytic activity in visceral WAT arises due to increased ß-adrenoreceptor sensitivity, alongside decreased responsiveness to α-adrenoreceptor- and insulin-mediated lipolysis inhibition (Frayn, 2000).

As above, lipid metabolism is greater in visceral compared to subcutaneous WAT. However, lipid storage capacity is substantially greater in the latter. This is partly because subcutaneous WAT adipocytes demonstrate a greater capacity for triglyceride synthesis (Maslowska *et al.*, 1993). In addition, adipocyte differentiation potential is markedly greater in subcutaneous WAT (Hauner, Wabitsch and Pfeiffer, 1988). Insulin sensitivity is enhanced and FFA and triglyceride uptake occurs more readily in smaller adipocytes. As such, avid proliferation of new, small adipocytes within subcutaneous WAT facilitates effective sequestering and storage of systemic lipids. Subcutaneous WAT therefore acts as an important buffer regulating circulating lipid levels (Freedland, 2004; Ibrahim, 2010).

Aside from metabolic parameters, WAT depots differ in their secretory function. Though the synthesis and release of bioactive substances is a general feature of AT, depot-specific differences are evident. For example, the secretory repertoire of visceral WAT is greater than subcutaneous WAT. Interestingly, this effect is apparent in adipocytes, but is similarly conserved in visceral AT preadipocytes and vascular ECs (Hocking *et al.*, 2010). Of note, visceral WAT exhibits an increased propensity for inflammation, since secreted cytokines such as monocyte chemoattractant protein-1 (MCP-1/CCL2), IL-6 and IL-8 are increased versus subcutaneous AT (Fried, Bunkin and Greenberg, 1998; Bruun *et al.*, 2004, 2005). Visceral WAT also displays increased macrophage infiltration (Bruun *et al.*, 2005). Collectively, these studies demonstrate depot-specific regulation of inflammatory pathways in AT.

The above observations underscore the functional significance of AT phenotype, but the heterogenous phenotype of WAT becomes especially relevant when considering the (patho)physiological role of AT. In humans, AT expansion is bias towards visceral accumulation in males, but amasses within subcutaneous WAT

depots in females. Differing patterns of AT accumulation are thought to explain sex-dependent differences in metabolic function, and greater cardiovascular risk in males versus females (Fuente-Martín *et al.*, 2013). These and similar findings ascribe added significance to AT research, since total adiposity (quantity) and adipose location (quality) must be considered in the context of physiological function.

1.1.4.2 Perivascular adipose tissue

Perivascular adipose tissue (PVAT) is an anatomically distinct type of AT which is closely associated with the microvasculature, medium diameter vessels, and large conduit vessels like the aorta (Cheng *et al.*, 2018). The association between PVAT and the vasculature is extremely intimate. Indeed, the boundary between PVAT and the vascular unit adventitia is not easily distinguishable (Szasz, Bomfim and Webb, 2013), but is recognised as an important interface mediating adipocyte-vascular signalling, and interactions between adventitial adipocytes and neuronal cells (Cheng *et al.*, 2018).

Though adipokines typically have defined central functions, they are frequently vasoactive. An array of adipokines with vasomotor properties are produced by both peripheral AT and PVAT (Nava and Llorens, 2019). Regarding AT, many of its physiological effects, including its influence the vasculature, are achieved through the release of adipokines into the circulation, i.e. endocrine signalling. However, the unique localisation of PVAT facilitates direct, paracrine AT-vascular cell interactions. As a result of its proximity to the vasculature, PVAT is a highly distinct and significant mediator of vascular biology, especially vasoreactivity (Cheng *et al.*, 2018).

The role of PVAT in vascular function was initially established by Soltis and Cassis, who demonstrated that contractile responses in rat aorta were attenuated in vessels with intact PVAT compared to those with PVAT removed (Soltis and Cassis, 1991). This effect was replicated with PVAT-conditioned media suggesting that PVAT induced vasorelaxations were attributed to a secreted factor, though at the time this substance could not be identified (Löhn *et al.*, 2002). The secretory function of PVAT was later confirmed by Gao and colleagues, who showed that PVAT could potentiate vascular contraction. Subsequent experiments indicated

that this effect was sensitive to reactive oxygen species (ROS) scavengers and that PVAT could elaborate superoxide, suggesting that PVAT-mediated superoxide release could regulate vascular function (Gao *et al.*, 2006). Since these early investigations, our knowledge of PVAT and its secretory function has evolved significantly to recognise a variety of vasoactive molecules and their effects; PVAT produces substances defined as perivascular relaxing factors (PVRFs) which promote vasorelaxation, and perivascular contractile factors (PVCFs) conferring contractile responses. Adiponectin, angiotensin 1-7 and NO are putative PVRFs, while ROS, angiotensin II and endothelin-1 are procontractile (Szasz, Bomfim and Webb, 2013; Nava and Llorens, 2019). PVAT also generates cytokines such as IL-6, TNFα and MCP-1 which regulate vascular tone (Qi *et al.*, 2018). More recently, our understanding of PVAT function has expanded to reveal PVAT actions which are not directly related to its role in vasoreactivity. For instance, PVAT-derived leptin has been implicated in VSMC de-differentiation and proliferation, potentially accelerating pathological vascular remodelling (Li *et al.*, 2014). In contrast, PVAT-derived adiponectin stimulates macrophage death, attenuating vascular plaque formation (Li *et al.*, 2015). These functions implicate PVAT as a specific regulator of vascular health, as well as vasoreactivity.

As above, PVAT fulfils several roles in the vasculature, in part facilitated by its vascular distribution. However, PVAT is also morphologically unique; it displays features consistent with both WAT and BAT, though the degree to which PVAT emulates WAT or BAT is dependent on the vasculature studied. For instance, thoracic periaortic PVAT morphology and uncoupling protein-1 (UCP-1) gene expression resembles that of BAT. However, abdominal periaortic PVAT demonstrates large LDs and modest UCP-1 expression, corresponding most closely to WAT (Hildebrand, Stümer and Pfeifer, 2018).

Because of its discrete composition, PVAT differs from AT in other depots due to its biology; though PVAT and systemic AT generate a range of adipokines, their respective secretory profiles are disparate. Compared to WAT, PVAT shows reduced production of key adipokines leptin and adiponectin (Chatterjee *et al.*, 2009). On the other hand, PVAT demonstrates a greater propensity for inflammation, since it releases more IL-6, IL-8 and MCP-1 (Chatterjee *et al.*,

2009). PVAT and systemic AT also demonstrate highly distinct patterns of gene expression. For instance, adipocyte marker genes PPARγ and C/EBPα are reduced in PVAT versus subcutaneous WAT. In addition, PVAT demonstrates decreased expression of genes involved in lipid turnover, such as FABP4, FASN and LPL (Chatterjee *et al.*, 2009; Fitzgibbons *et al.*, 2011). These data support the idea that adipocyte maturation and lipid handling functions are differentially regulated in PVAT and general WAT depots.

As above, the biology of PVAT is distinct to that of peripheral AT. However, PVAT and systemic AT dysfunction are implicated during the development and presence of AT-related pathologies, such as obesity (Ha and Bauer, 2018). Accordingly, though PVAT and peripheral AT demonstrate differing biology, both are important in disease.

1.1.5 Dysregulation and disease

The metabolic syndrome describes a cluster of cardiometabolic conditions which associate with an increased risk of cardiovascular disease (CVD). Though the exact definition varies, the main feature is insulin resistance concurrent with two or more further metabolic abnormalities which can include obesity, hypertension, hyperlipidaemia and microalbuminuria, the latter being indicative of kidney dysfunction (Rochlani *et al.*, 2017). A central feature of the metabolic syndrome and the risk factors which it comprises is the biological and functional derangement of AT (Kolovou, Anagnostopoulou and Cokkinos, 2005; Grundy, 2015).

While general adiposity increases the risk for metabolic syndrome, visceral WAT expansion has been specifically implicated (Klöting *et al.*, 2010). AT enlarges during periods of high nutrition, resulting in adipocyte hyperplasia and hypertrophy; while the former characterises healthy AT responses, the latter is detrimental and linked with AT derangement (Oikonomou and Antoniades, 2019). As discussed earlier, circulating lipids are preferentially sequestered and stored by subcutaneous WAT. However, overnutrition or chronic physiological stress results in saturation or impairment of this system, reducing its protective effects (Ibrahim, 2010). As a result, circulating lipids are deposited in peripheral ectopic

sites poorly adapted for lipid storage, such as visceral WAT, skeletal muscle, the liver and pancreas. At these sites, lipid accumulation exerts damaging effects (i.e. lipotoxicity) (Ibrahim, 2010; Longo *et al.*, 2019).

Systemic pathology is also perpetrated by adipocytes themselves. Enlarged adipocytes become dysfunctional; lipid loading capacity is progressively reduced, lipolysis is enhanced and adipocytes become insulin resistant (Ibrahim, 2010; Klöting and Blüher, 2014). As metabolic stress continues, adipocytes express inflammatory factors such as IL-6 and MCP-1. Inflamed adipocytes undergo autophagy and apoptosis, leading to impaired adipogenesis, hypoxia and altered secretion within AT (Klöting and Blüher, 2014). In concert, adipocyte dysfunction stimulates immune cell recruitment, reinforcing adipocyte and AT derangement (Weisberg *et al.*, 2003).

Obesity, coinciding adipocyte enlargement and insulin resistance have been correlated for some time (Salans, Knittle and Hirsch, 1968). Though many mechanisms are known to contribute to and exacerbate AT pathology, adipocyte enlargement may constitute an early and fundamental trigger for AT derangement leading to metabolic dysfunction and inflammation (Klöting and Blüher, 2014). In obese individuals, adipocyte size is significantly larger in subjects with insulin resistance compared to those which retain effective insulin responses. Importantly, adipocyte size predicts insulin sensitivity independent of total adiposity (Klöting *et al.*, 2010). Therefore, metabolic outcomes in obesity could vary as a function of adipocyte biology specifically. In support of this view, weight loss in obese subjects resulting in reduced insulin levels coincide with a decrease in adipocyte size but not number (Stern *et al.*, 1972). Interestingly, the relationship between adipocyte size and circulating insulin is conserved in lean subjects (Stern *et al.*, 1972), again suggesting that adipocyte biology can influence metabolism independent of the obese state. This is corroborated by investigations examining adipose morphology in healthy individuals, since adipocyte enlargement is positively correlated with other measures of adipocyte function such as lipolysis (Laurencikiene *et al.*, 2011) and secretion of proinflammatory cytokines IL-6, IL-8 and MCP-1, as well as adipokines leptin and adiponectin (Skurk *et al.*, 2007). Considering the clear relationship between adipocyte phenotype and metabolic function, mechanisms

which regulate adipocyte biology, size and pathological dysfunction are of considerable interest.

1.2 The CaSR

1.2.1 Discovery

The importance of extracellular calcium ($[Ca^{2+}]_o$) as an endogenous signalling molecule was first demonstrated by Sydney Ringer, who discovered by way of accident that inorganic salts contained in common tap water, particularly calcium, could regulate cardiac contractility (Ringer, 1883). Since this early description, subsequent studies showed that $[Ca^{2+}]_o$ ions were virtually ubiquitous among cells types and were a critical mediator of physiological function (Carafoli, 2003). Considering the broad range of biological functions which are regulated by $[Ca^{2+}]_o$ signalling, it is perhaps unsurprising that $[Ca^{2+}]_o$ homeostasis in intact animals is controlled within very narrow limits. Systemically, $[Ca^{2+}]_o$ levels are determined by the relative activity of three key hormones: parathyroid hormone (PTH), vitamin D3 and calcitonin (Mundy and Guise, 1999).

PTH plays a role in regulating circulating $[Ca^{2+}]_o$, but it has long been known that PTH secretion operates under a negative feedback loop, whereby PTH secretion is determined by plasma $[Ca^{2+}]_o$ levels. In very early bovine models, PTH was shown to vary inversely with $[Ca^{2+}]_o$ in plasma. Upon recognition of this relationship, Care and colleagues showed that $[Ca^{2+}]_o$ infusion in cows increased circulating $[Ca^{2+}]_o$ levels and triggered a sharp decline in circulating PTH. Conversely, infusion of the chelating agent EDTA reduced plasma $[Ca^{2+}]_o$ and elevated PTH (Care *et al.*, 1966). Studies examining parathyroid cells later showed that $[Ca^{2+}]_o$-induced intracellular calcium ($[Ca^{2+}]_i$) signalling was involved in PTH regulation, since increasing $[Ca^{2+}]_o$ caused a fall in PTH secretion, but enhanced $[Ca^{2+}]_i$ mobilisation (Shoback *et al.*, 1983). The observation that divalent cations could trigger $[Ca^{2+}]_i$ mobilisation in the absence of $[Ca^{2+}]_o$ led Nemeth and Scarpa to suggest that $[Ca^{2+}]_o$-induced $[Ca^{2+}]_i$ effects could not be attributed membrane permeation by $[Ca^{2+}]_o$. They instead proposed that this pathway was regulated by an extracellular mediator (Nemeth and Scarpa, 1987). Nemeth and Carafoli later suggested that the $[Ca^{2+}]_o$ sensing, cell surface mechanism could be a receptor. In addition to previous data, the idea was based on the observation that $[Ca^{2+}]_o$ stimulated inositol trisphosphate (IP_3) and diacylglycerol accumulation, consistent with the actions of other receptors known to potentiate $[Ca^{2+}]_i$ signalling (Nemeth and Carafoli, 1990). The identity

of this receptor was finally reconciled by Brown and colleagues who cloned an unidentified G-protein coupled receptor (GPCR) from bovine parathyroid cells. This novel receptor displayed functional responses which were consistent with those observed in parathyroid cells upon stimulation with divalent cations. Hence, this receptor was coined as 'the calcium-sensing receptor' (CaSR) (Brown *et al.*, 1993).

1.2.2 Structure

The first structural description of the CaSR was provided by Brown et al., based on the novel CaSR clone derived from bovine parathyroid tissue. Bovine parathyroid CaSR cDNA demonstrates a length of 5275bp and encodes a 1085 amino acid protein composed of three main regions: 7 central transmembrane helices (250 amino acids); an extracellular carboxyl region (222 amino acids) and a large hydrophilic amino terminus (613 amino acids). These structural features were typical of receptors belonging to the GPCR superfamily, thus the CaSR was designated as a novel GPCR (Brown *et al.*, 1993).

Shortly after the identification of bovine CaSR, Garrett and colleagues cloned human CaSR from a parathyroid adenoma. This protein was composed of 1078 amino acids and was sensitive to divalent cations and neomycin, thus showing structural and functional similarity to bovine CaSR (Garrett *et al.*, 1995). Early genetic studies investigating the clinical effects of CaSR mutation showed that the human CaSR gene was comprised of 6 coding exons (Pollak *et al.*, 1993) and mapped to human chromosome 3q13.3-21 (Janicic *et al.*, 1995). The genomic organisation of CaSR was later expanded to recognise an initial non-translated region, termed exon 1A and 1B, which precedes coding exons 2-7 (Fig. 1-4) (Chikatsu *et al.*, 2000). Immunoblotting analyses of HEK293 cells overexpressing CaSR under reducing conditions demonstrate that CaSR migrates in two distinct bands; a high molecular weight band of 240-310kDa corresponding to CaSR in its dimeric form, and a lower molecular weight band of 121-167kDa indicative of variably glycosylated, monomeric CaSR (Ward, Brown and Harris, 1998).

Figure 1-4

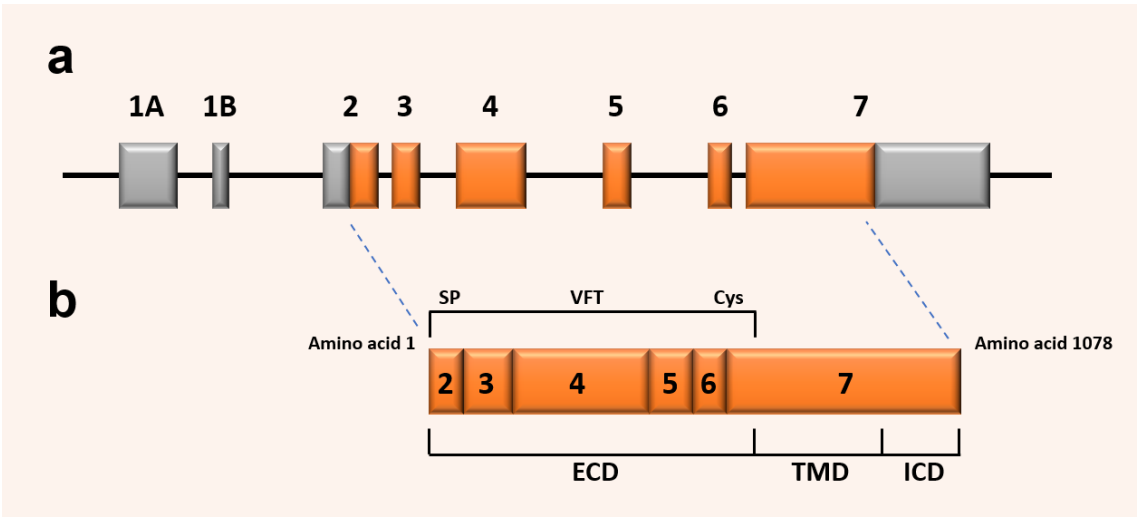

Figure 1-4: Organisation of the human CaSR gene and CaSR protein.
(a) The genomic organisation of CaSR comprises 8 exons in total. Protein coding regions are coloured orange, including exons 3-6 and part of exons 2 and 7. Sequences which are not translated are grey. They are contained within exonal regions 1A and 1B, with additional non-translated regions within exons 2 and 7. **(b)** The human CaSR protein is 1078 amino acids in length and is encoded by exons 2-7. Cys=Cysteine rich domain; ECD=Extracellular domain; ICD=Intracellular domain; SP=Signal peptide; TMD=Transmembrane domain; VFT=Venus flytrap domain. Figure adapted from Hendy and Canaff (2016).

In terms of sequence structure, the CaSR shares small but significant similarities with other GPCRs. For instance, sequence conservation between bovine CaSR and metabotropic glutamate receptors (mGluRs) 1-6 is 25-30%, whereby mGluRs 1 and 5 demonstrate the greatest alignment. These similarities were realised in the identification of a large C-terminus, in addition to conserved cysteine residues in the N-terminus, extracellular loops and a transmembrane domain. Regions within intracellular loops 1 and 3 were also significantly similar (Brown *et al.*, 1993). The bovine CaSR and human CaSR sequences are highly conserved, whereby significant dissimilarities are limited to the intracellular C-terminus. When compared to rat mGluR1, the alignment of cysteine residues observed in bovine CaSR is similarly conserved in human CaSR (Garrett *et al.*, 1995).

The CaSR is member of a specific subfamily of GPCRs known as the class C or family C GPCRs. Class C GPCRs are unique in that they possess a unusually enlarged extracellular region, termed the venus fly trap (VFT) domain, which serves to bind endogenous ligands (Kniazeff *et al.*, 2011). The VFT is also crucial to CaSR structure, since this is recognised as the site where cysteine residues form disulphide bonds, enabling CaSR homodimerization (Hu and Spiegel, 2007).

1.2.3 Regulation

At the gene level, several mechanisms regulate CaSR expression. The CaSR gene demonstrates two promotor regions, P1 and P2, which precede non-coding exons 1A and 1B, respectively. Both promotors are implicated in baseline and stimulated CaSR expression (Hendy and Canaff, 2016). Contained within these promotors are response elements for vitamin D, which stimulates CaSR expression (Canaff and Hendy, 2002). Interestingly, CaSR gene expression appears to be linked to inflammation, since CaSR is upregulated in animal models of acute inflammatory states such as burn injury (Murphey *et al.*, 2000), and in response to cytokines IL-1β, TNFα (Canaff and Hendy, 2005) and IL-6 (Canaff, Zhou and Hendy, 2008). Of these cytokines, at least IL-1β and TNFα upregulate CaSR expression by stimulating a nuclear factor kappa B response element contained within each CaSR promotor (Canaff and Hendy, 2005). CaSR gene expression can also be regulated reciprocally by CaSR ligands. Evidence for this effect is evident *in vitro*, where CaSR expression is increased by calcimimetics, and also by $[Ca^{2+}]_o$ itself (Huang and Breitwieser, 2007; Hénaut *et al.*, 2014; Hendy and Canaff, 2016).

The CaSR is also subject to significant post-translational regulation. CaSR expression at the cell surface is, in part, regulated by the stimulation intensity of available receptors, i.e. agonist-driven insertional signalling (ADIS). Through this mechanism, enhanced CaSR signalling results in increased anterograde trafficking of CaSR from the endoplasmic reticulum to its functional site at the plasma membrane (Breitwieser, 2013). In addition to ADIS, the abundance of CaSR is also determined by agonist-dependent desensitisation, a mechanism whereby agonist binding triggers GPCR deactivation, internalisation, and degradation. However, CaSR regulation is likely biased toward ADIS, as CaSR

protein is evident predominantly in the endoplasmic secretory system, rather than the plasma membrane (Breitwieser, 2012).

1.2.4 General signalling

Among the many characteristics which define the CaSR as a unique GPCR, perhaps the most remarkable feature is its signalling properties. CaSR mediated signal transduction is exquisitely complex; its activation is regulated by a range of ligands, including cations (Ca^{2+}, Gd^{3+}, Mg^{3+}, Zn^{2+} and Fe^{2+}), L-amino acids (L-tryptophan, L-phenylalanine and L-tyrosine), polypeptides (poly-L-arginine), polyamines, select antibiotics and $[Ca^{2+}]_o$ emulating calcimimetics and calcilytics (Fig. 1-5) (Colella *et al.*, 2016).

In response to ligand binding, the CaSR couples to $G\alpha_{q/11}$, $G\alpha_s$, $G\alpha_{i/0}$ or $G\alpha_{12/13}$ proteins, in turn activating distinct intracellular messengers and downstream targets. Moreover, while many ligands such as $[Ca^{2+}]_o$ function as primary (orthosteric) agonists directly activating the CaSR, orthosteric signalling can be altered by allosteric modulators. In this way, allosteric activity at the CaSR can modulate or redirect G-protein recruitment in response to orthosteric activation (Conigrave and Ward, 2013; Colella *et al.*, 2016).

Figure 1-5

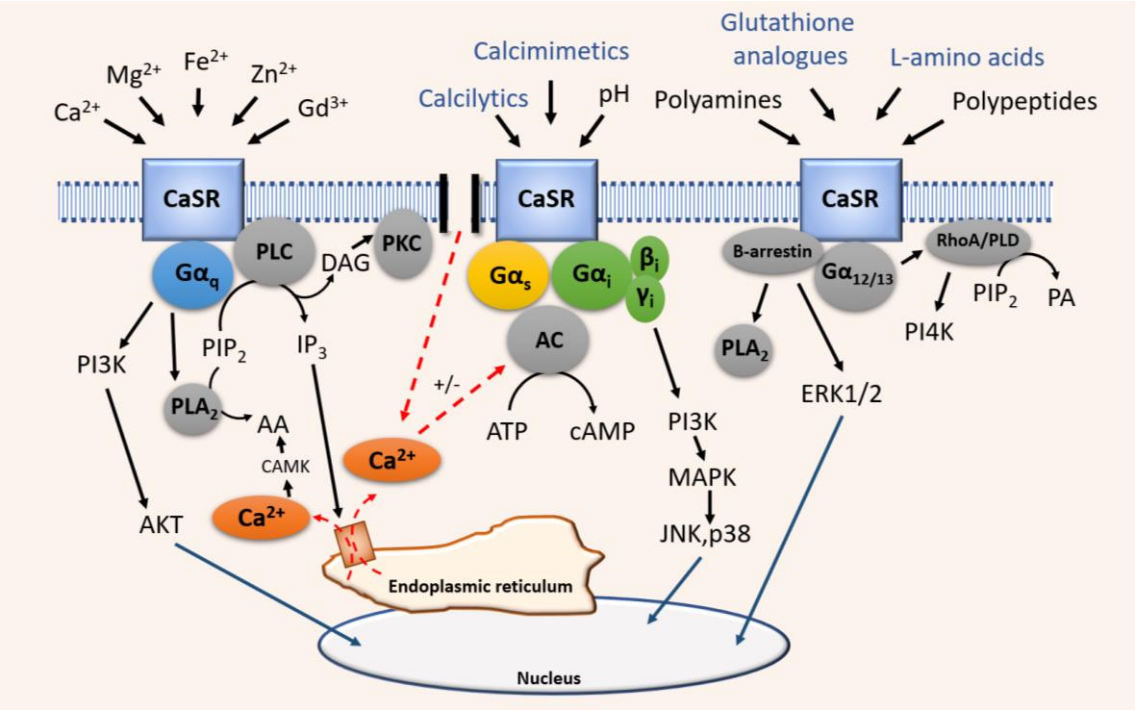

Figure 1-5: CaSR pharmacology, heterotrimeric G-protein coupling and associated downstream mechanisms.

Primary ('orthosteric') ligands (indicated in black) interact with the CaSR to stimulate a variety of possible G-protein signalling pathways ($G\alpha_q$, $G\alpha_s$, $G\alpha_i$, $G\alpha_{12/13}$), which in turn can recruit many distinct intracellular messengers and signalling complexes. Orthosteric agonist signalling can be altered by allosteric modulators (indicated in blue) which facilitates recruitment of specific G-proteins pathways at the expense of others, which may be reduced or deactivated, i.e. biased signalling. Blue arrows represent translocation of nuclear transcription factors or activation of intranuclear transcription factors. AA=Arachidonic acid; AC=Adenylyl cyclase; AKT=Protein kinase B; ATP=Adenosine triphosphate; CaMK=Calmodulin-dependent protein kinase; cAMP=Cyclic AMP; CaSR=Calcium-sensing receptor; DAG=Diacylglycerol; $ERK_{1/2}$=Extracellular-signal regulated kinase; IP_3=Inositol triphosphate; JNK=C-jun N-terminal kinase; MAPK=Mitogen-activated protein kinase; PA=Phosphatidic acid; PI3K/PI4K=Phosphatidylinositol 3- and 4-kinase; PIP_2=Phosphatidylinositol biphosphate; PKC=Protein kinase C; PLA_2=Phospholipase A_2; PLC=Phospholipase C; PLD=Phospholipase D; RhoA=Ras homolog gene family. Image adapted from Colella et al. (2016).

As above, a broad range of ligands are capable of stimulating CaSR. However, attempts to characterise these signalling pathways have been complicated by the finding that CaSR signalling is agonist-dependent, whereby specific agonists recruit distinct CaSR signalling pathways. Among the many descriptions of CaSR ligand directed signalling, a notable example is realised in work by Makita et al., who demonstrated that autoantibodies derived from a subject with hypocalciuric hypercalcemia potentiated G_q-signalling (stimulating inositol phosphate accumulation), but inhibited G_i-signalling (reducing $ERK_{1/2}$ activation). This was not recapitulated by the allosteric CaSR modulator NPS R-568, which increased both inositol phosphate and $ERK_{1/2}$ activation (Makita *et al.*, 2007). The concept that CaSR signalling pathways could be selectively activated by specific agonists is underscored by other studies which demonstrate the effect of CaSR agonists on $[Ca^{2+}]_i$ mobilisation. Previously considered to be a hallmark of CaSR activation, $[Ca^{2+}]_i$ is stimulated by $[Ca^{2+}]_o$ but not neomycin (Bruce *et al.*, 1999). On the other hand, CaSR ligands can invoke $[Ca^{2+}]_i$ signalling but exhibit divergent CaSR responses downstream of $[Ca^{2+}]_i$. For instance, both $[Ca^{2+}]_o$ and the allosteric CaSR ligand L-phenylalanine (L-Phe) significantly elevate cytosolic $[Ca^{2+}]_i$ in CaSR overexpressing HEK293 cells, but the effect of L-Phe on CaSR-dependent $ERK_{1/2}$ activation is highly limited compared to $[Ca^{2+}]_o$ (Lee *et al.*, 2007). The idea that CaSR agonists can impose differing effects on CaSR mediators downstream of $[Ca^{2+}]_i$ is supported by earlier investigations in HEK293 cells. Rey and colleagues demonstrated that CaSR-dependent phospholipase C (PLC) pathways are activated by $[Ca^{2+}]_o$ but are unaffected by L-Phe, despite both ligands triggering significant $[Ca^{2+}]_i$ mobilisation (Rey *et al.*, 2005). This same effect is observed when examining the influence of $[Ca^{2+}]_o$ and L-Phe on CaSR-dependent cAMP response element-binding protein (CREB) activation (Avlani *et al.*, 2013). Though CaSR ligands are thought to invoke alternative signalling pathways by redirecting G-protein recruitment, these data implicate additional control points for CaSR signalling downstream of G-protein coupling (Avlani *et al.*, 2013). Considering that CaSR function is likely to be regulated endogenously by nutrient (amino acid) and acidity (pH) levels in addition to $[Ca^{2+}]_o$, there is a clear need to delineate the diverse signalling mechanism(s) through which CaSR ligands regulate CaSR function.

In addition to demonstrating agonist-specific signalling, CaSR signalling pathways are also cell-specific. Indeed, evidence of cell-specific CaSR intracellular signalling can be traced back to the earliest CaSR studies. For instance, pertussis toxin sensitivity in *X. laevis* oocytes expressing bovine CaSR differed from that in native cells (Brown *et al.*, 1993). The authors suggested that PLC could be differentially regulated by CaSR in these models. Since this first description, investigators have demonstrated significant cell type-dependent signalling with regard to CREB activation (Avlani *et al.*, 2013) and cAMP inhibition (Mamillapalli *et al.*, 2008). Considering the number of signalling pathways invoked by CaSR, and the detection of CaSR in a variety of distinct cell types (Schreckenberg and Schlüter, 2018), it is highly likely that other CaSR targets are regulated in a cell-dependent manner. Taken together, agonist- and cell-specific signalling imposes unique challenges on investigations seeking to characterise CaSR signalling, since findings derived from a specific ligand or model may not be easily applied to other systems.

1.2.5 Amino acid signalling

Class C GPCRs are characterised by their ability to bind amino acids. Generally, amino acids act as orthosteric ligands at class C GPCRs such as mGluR, γ-aminobutyric acid receptor $(GABA)_B$ and GPRC6A. In contrast, amino acids are unable to independently activate the CaSR, but instead function as allosteric modulators (Wellendorph and Bräuner-Osborne, 2009).

Driven by reports that protein intake regulates both PTH and $[Ca^{2+}]_o$, in addition to the recognition of structural homology between CaSR and glutamate-sensitive mGluRs, CaSR amino acid sensing was studied in HEK293 models of CaSR overexpression (Conigrave, Quinn and Brown, 2000). In their investigations, Conigrave and colleagues analysed in some detail how amino acids influenced $[Ca^{2+}]$-induced $[Ca^{2+}]_i$ mobilisation. Except for L-lysine, -leucine and -isoleucine, amino acids (at supraphysiological concentrations) reduced the EC_{50} for $[Ca^{2+}]_o$-induced $[Ca^{2+}]_i$ signalling. Crucially, $[Ca^{2+}]_o$ was requisite in this response, since amino acid responses were absent below a threshold $[Ca^{2+}]_o$ concentration of 1mM (Conigrave, Quinn and Brown, 2000).

Very recently, interactions between amino acids and CaSR were investigated in isolated cell membranes using high sensitivity FRET-biosensor assays to detect CaSR activation (Liu *et al.*, 2020). This approach is considered superior to those testing amino acid sensitivity in intact cells, since it should mitigate the confounding influence of CaSR-active compounds in physiological solutions and within the cellular structure itself (Liu *et al.*, 2020). However, the results generated by Liu and colleagues agreed with those of Conigrave, Quinn and Brown (2000), with few exceptions (Tb. 1-1). Among the amino acids studied, aromatic amino acids L-tryptophan, -tyrosine, -histidine and L-Phe were most effective at raising CaSR sensitivity for $[Ca^{2+}]_o$ (Conigrave, Quinn and Brown, 2000; Liu *et al.*, 2020). As aromatic amino acids stimulate CaSR-dependent $[Ca^{2+}]_i$ signalling, others have sought to characterise how amino acids affect molecular targets of CaSR transduction. As previously discussed, $[Ca^{2+}]_o$ activates CaSR-dependent PLC, $ERK_{1/2}$ and CREB signalling in CaSR overexpressing HEK293 cells. L-Phe in contrast has a minor effect on $ERK_{1/2}$, and is unable to stimulate PLC or CREB (Rey *et al.*, 2005; Lee *et al.*, 2007; Avlani *et al.*, 2013). Though these studies highlight profound and potentially significant differences in CaSR activation kinetics between amino acids and $[Ca^{2+}]_o$, CaSR-dependent amino acid signal transduction remains poorly described. It is unclear how CaSR activation might be affected by amino acid potency, or whether amino acid transduction pathways in heterologous cell systems can be applied to native cells.

Table 1-1

Group	Amino acid	Assays which observe increased $[Ca^{2+}]_o$ sensitivity
Aromatic	L-Trp	Intact cells, cell-free
	L-Tyr	Intact cells, cell-free
	L-Phe	Intact cells, cell-free
	L-His	Intact cells, cell-free
Aliphatic	L-Ala	Intact cells, cell-free
	L-Val	Intact cells, cell-free
	L-Ile	Cell-free only
	L-Met	Intact cells, cell-free
	L-Leu*	None
Polar	L-Ser	Intact cells, cell-free
	L-Thr	Intact cells, cell-free
	L-Asn	Intact cells, cell-free
	L-Gln	Intact cells, cell-free
Charged	L-Glu	Intact cells, cell-free
	L-Asp	Intact cells only
	L-Arg	Intact cells, cell-free
	L-Lys*	None
Other	L-Cys	Intact cells, cell-free
	Gly	Intact cells, cell-free
	L-Pro	Intact cells only

Table 1-1: Amino acids which allosterically modulate CaSR signalling.

The ability of amino acids to allosterically modulate CaSR behaviour was examined. The investigations differed in the assay approach to measuring CaSR activation; the first study measured $[Ca^{2+}]_o$-induced $[Ca^{2+}]_i$ signalling in HEK293-CaSR overexpressing cells (intact cells), while more recent work measured $[Ca^{2+}]_o$-induced conformational changes in CaSR within (cell-free) assays utilising isolated membranes. As determined by these methods, CaSR could be sensitive to all amino acids except L-Leu and L-Lys (denoted *). Studies in intact cells indicate that L-Pro and L-Asp stimulates CaSR, though this is not validated by high sensitivity FRET-biosensor studies which detect CaSR activation in cell-free assays. Conversely, cell-free assays determined that L-Ile is CaSR-active, whereas previous studies in intact cells are unable to demonstrate CaSR sensitivity to L-Ile. Table is produced using data from Conigrave, Quinn and Brown (2000) and Liu et al. (2020).

The biological significance of CaSR amino acid sensing was first interrogated by Conigrave and colleagues, who performed a series of studies examining the effect of amino acids on parathyroid cell PTH secretion. In addition to confirming that amino acids allosterically enhance CaSR-induced $[Ca^{2+}]_i$ signalling in native cells, amino acids (at concentrations typical in plasma) also acutely potentiate $[Ca^{2+}]_o$-mediated inhibition of parathyroid cell PTH secretion (Conigrave *et al.*, 2004), therein highlighting a definitive role for CaSR in nutrient sensing. Considering the obvious implications of these findings in the context of dietary protein intake, it is perhaps unsurprising that investigations seeking to delineate the functional significance of CaSR amino acid sensing have centred on its role in gastrointestinal physiology (Mace, Schindler and Patel, 2012; Alamshah *et al.*, 2017; Acar *et al.*, 2020). However, there is a paucity of information regarding the potential relevance of this mechanism in other tissues.

1.2.6 Cardiovascular CaSR

Since its initial description, the CaSR has become widely recognised as an endogenous $[Ca^{2+}]_o$ sensor, regulating systemic levels of both PTH and $[Ca^{2+}]_o$ (Brown *et al.*, 1993; Garrett *et al.*, 1995). Since then, the CaSR has been identified in variety of tissues such as the gut, kidneys, bone, nervous system, reproductive tissue and inflammatory cells. Within these systems, the CaSR mediates important functional roles not directly related to systemic $[Ca^{2+}]_o$ regulation; these include intestinal motility, water balance and numerous cellular activities such as hormone secretion, differentiation and proliferation (Schreckenberg and Schlüter, 2018).

In addition to the tissues mentioned above, the CaSR has been detected in ECs, VSMCs and cardiac tissue (Wonneberger, Scofield and Wangemann, 2000; Wang *et al.*, 2003; Weston *et al.*, 2005), indicating that CaSR would likely play a role in cardiovascular biology. The first description of CaSR expression and function in the vascular system was provided by Wonneberger and colleagues, who detected CaSR in porcine artery homogenate. In these vessels, $[Ca^{2+}]_i$ mobilisation and vascular contraction was triggered by CaSR agonists $[Ca^{2+}]_o$, divalent cations and neomycin, which the authors attributed to stimulation of vascular CaSR (Wonneberger, Scofield and Wangemann, 2000). As predicted by

Wonneberger and colleagues, subsequent studies confirmed CaSR expression in VSMCs specifically (Smajilovic *et al.*, 2006). The expression and significance of CaSR was later demonstrated in aortic primary VSMCs. In these cells, Chow and colleagues illustrated that $[Ca^{2+}]_o$ stimulation triggered CaSR-dependent $[Ca^{2+}]_i$ mobilisation. This effect was associated with PLC activation and was sensitive to inhibition of both PLC and transient receptor potential channels, suggesting that CaSR stimulation in VSMCs activates PLC signalling pathways, triggering transient receptor potential channel activation and permeation of $[Ca^{2+}]_o$ (Chow *et al.*, 2011). Independent investigations in pulmonary VSMCs confirmed that $[Ca^{2+}]_o$ stimulates PLC, leading to IP_3 activation and $[Ca^{2+}]_i$ mobilisation (Li *et al.*, 2011). Considering that $[Ca^{2+}]_i$ elevation is a key event in VSMC contraction (Brozovich *et al.*, 2016), these findings combined with previous functional studies suggest that CaSR mediates VSMC contraction.

In addition to VSMCs, CaSR is additionally present in ECs (Weston *et al.*, 2005). Curiously, where Wonneberger, Scofield and Wangmenn (2000) had demonstrated that CaSR activation induced vascular contraction in vessel segments, Weston et al. (2005) in contrast showed that CaSR regulates IK_{Ca} channels in ECs leading to VSMC hyperpolarisation, a mechanism known to favour vasodilation. Indeed, later work confirmed CaSR-mediated activation of IK_{Ca} in ECs (Greenberg, Shi, *et al.*, 2016). EC CaSR-mediated NO release has been indicated as an additional mechanism. In the vasculature, both pathways would favour endothelium-dependent vasorelaxation (Ziegelstein *et al.*, 2006; Greenberg, Shi, *et al.*, 2016). Collectively, these studies implicate CaSR in vascular biology, though its role in vasoreactivity is cell-dependent (Fig. 1-6). As such, the functional and potentially antagonistic roles of CaSR in VSMC and ECs require further exploration.

Figure 1-6

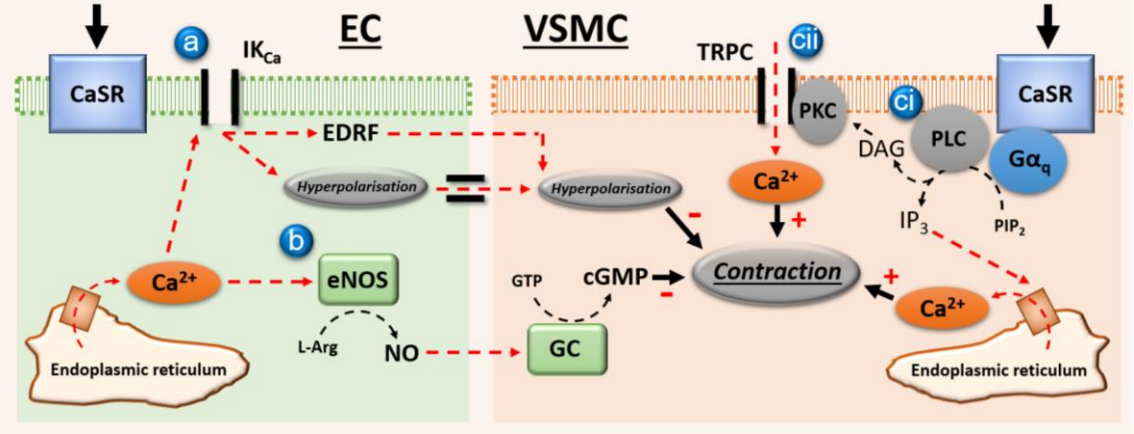

Figure 1-6: The proposed antagonistic actions of vascular CaSR.

In endothelial cells (ECs), CaSR stimulation activates IK_{Ca} channels and NO production. EC CaSR could trigger these events by recruiting G_q-signalling pathways and increasing intracellular $[Ca^{2+}]_i$, since both IK_{Ca} channels and NO generation by eNOS are sensitive to Ca^{2+}. **(a)** CaSR-mediated activation of EC IK_{Ca} channels permits cellular efflux of K^+, increasing EC membrane potential and hyperpolarisation. Stimulation of EC CaSR results in VSMC hyperpolarisation; the mechanisms were not identified but may involve charge transference via EC-VSMC intracellular junctions, or secretion of EDRF. **(b)** CaSR also stimulates EC NO production, which would diffuse into VSMCs, stimulating GC and causing synthesis of cGMP, PKG activation and VSMC relaxation. In VSMCs, CaSR stimulation causes $[Ca^{2+}]_i$ mobilisation. This effect is dependent on **(ci)** PLC, which may increase $[Ca^{2+}]_i$ through DAG or IP_3 pathways, and **(cii)** TRPC activation, which would promote intracellular entry of cations, including Ca^{2+}. CaSR-mediated $[Ca^{2+}]_i$ elevation likely facilitates VSMC contraction. CaSR=Calcium-sensing receptor; cGMP=Cyclic guanosine monophosphate; EDHF=Endothelial derived hyperpolarising factor; eNOS=Endothelial nitric oxide synthase; DAG=Diacylglycerol; GC=Guanylate cyclase; IK_{Ca}=Calcium-sensitive K^+ channel; IP_3=Inositol triphosphate; PIP_2=Phosphatidylinositol biphosphate; PKG=Protein kinase G; PLC=Phospholipase C; TRPC=Transient receptor potential channel. Figure produced using information from Chow et al. (2011), Greenberg et al. (2016) and Li et al. (2011).

As above, *in vitro* studies suggest that CaSR mediates opposing roles in the vasculature. To clarify the antagonistic CaSR actions in VSMCs and ECs, CaSR function has been explored using vascular myography in isolated vessels. Corroborating EC *in vitro* data, $[Ca^{2+}]_o$ caused endothelial-dependent relaxation in rabbit mesenteric arteries. This effect was sensitive the CaSR inhibitor Calhex-231, antagonism of IK_{Ca} and NO signalling pathway components, illustrating that EC CaSR regulates vascular tone via IK_{Ca} and NO (Greenberg, Shi, *et al.*, 2016). However, findings in this area are far from uniform. For instance, CaSR activation by calindol in aorta and mesenteric arteries which are denuded of endothelium causes vasodilation, suggesting CaSR can promote VSMC relaxation (Thakore and Vanessa Ho, 2011; Loot *et al.*, 2013). Though this could be due to calindol-mediated inhibition of $[Ca^{2+}]_o$ influx via L-type channels rather than CaSR (Thakore and Vanessa Ho, 2011), there is dissonance regarding the exact role of CaSR in VSMCs.

To delineate the specific roles of vascular CaSR, cell-specific CaSR function would need to be determined in the vasculature of intact animals. Very recently, the importance of VSMC CaSR was confirmed *in vivo*. Schepelmann et al. produced mice with VSMC-specific CaSR deletion by disrupting exon 7 under the activity of SMC22α. These mice demonstrated a broad cardiovascular dysregulation including decreased vascular contractility and blood pressure, indicating that VSMC CaSR is crucial in the vasculature where it likely fulfils a procontractile role (Schepelmann *et al.*, 2016). Though the participating mechanism(s) are disputed, especially regarding CaSR in VSMCs, these studies underscore the importance of CaSR in maintaining vascular tone.

In humans, CaSR expression has been confirmed in VSMCs (Molostvov *et al.*, 2007) and ECs (Ziegelstein *et al.*, 2006). However, data regarding the relevance of CaSR in vascular function is quite limited. Interestingly, clinical studies examining the effect of CaSR modulation have demonstrated that cinacalcet decreases blood pressure in renal disease (Kuczera, Adamczak and Wiecek, 2015; Chang *et al.*, 2016). As discussed in the previous section, CaSR mediates antagonistic roles in VSMCs and ECs. This concept is further complicated upon consideration of other tissues known to influence vascular function, especially those proximate and integral to the vascular unit, such as PVAT (Nava and Llorens, 2019). As explained

in the following section, CaSR is expressed in adipocytes, where it regulates adipocyte biology. However, the role of adipocyte CaSR regarding vascular function has not been assessed to date. To fully delineate the role played by CaSR in the vasculature, a comprehensive understanding of CaSR actions in VSMCs, ECs, in addition to adipocytes, is required.

1.2.7 Adipocyte CaSR

The adipocyte CaSR was first identified in primary adipocytes isolated from human visceral adipose tissue (Cifuentes, Albala and Rojas, 2005). This description is corroborated by others which have detected CaSR in multiple cell line models, including LS14, SW872 and 3T3-L1 adipocytes (Jensen *et al.*, 2004; Cifuentes *et al.*, 2010; He, Zhang, *et al.*, 2011). As such, the role of adipocyte CaSR is of considerable interest.

In preadipocytes and adipocytes, CaSR activation by cinacalcet or the divalent cation $GdCl_3$ induces PPARγ expression (He *et al.*, 2012; Villarroel *et al.*, 2013). In adipocytes, PPARγ regulates several key functions, such as lipogenesis, differentiation, lipid accumulation and adipokine secretion (Rosen, Eguchi and Xu, 2009), suggesting that CaSR could potentially regulate a broad scope of biological functions in adipocytes.

Consistent with reports that CaSR regulates the key adipocyte transcription factor PPARγ, several investigations have identified a role for CaSR in adipocyte lipid handling. In primary adipocytes, CaSR agonists $GdCl_3$, $CaCl_2$ and cinacalcet attenuate glycerol release (Cifuentes and Rojas, 2008), suggesting that CaSR activity favours triglyceride preservation and lipid loading. This same effect was demonstrated by He et al. in SW872 adipocytes. Interestingly, CaSR stimulation was associated with reduced expression of lipolytic enzymes, since HSL and ATGL gene and protein levels were decreased by $GdCl_3$ (He, Zhang, *et al.*, 2011). In both studies, antilipolytic effects were abolished by the CaSR inhibitor NPS-2390, suggesting a role for CaSR in lipid accumulation.

Adipocyte CaSR also mediates inflammation. Gene expression of MCP-1 (CCL2), IL-6 and IL-1β cytokine expression is increased by the CaSR activator cinacalcet

in differentiated LS14 cells. Interestingly, cinacalcet was also found to elevate IL-6, IL-1ß secretion in human visceral AT (Cifuentes et al., 2012). Although Cifuentes et al. did not establish which cells within AT were responsible for this effect, it is possible that adipocytes play a contributing role.

Based on the findings above, adipocyte CaSR is emerging as a mediator of AT dysfunction (Bravo-Sagua *et al.*, 2016). However, the (patho)physiological relevance of these mechanisms had not been investigated until very recently. To explore the importance of adipocyte CaSR *in vivo*, the mechanism(s) involved in its activity and its significance in disease, Sundararaman and colleagues developed apolipoprotein E (ApoE) deficient mice with conditional, adipocyte-specific CaSR deletion. Surprisingly, these mice demonstrated no evidence of enhanced atherogenesis or altered lipid metabolism. Moreover, AT inflammation was unremarkable compared to control counterparts (Sundararaman *et al.*, 2021). From these data, Sundararaman et al. concluded that CaSR does not participate in AT inflammation, or the progression of CVD. However, this study did not examine the effect of adipocyte CaSR specifically; rather, they investigated how adipocyte CaSR affects AT inflammation and metabolism in the context of CVD. Notably, ApoE deletion has profound and beneficial effects in murine AT, evidenced by decreased adipocyte size, fat mass and obesity resistance in this model (Kypreos *et al.*, 2018). Consequentially, the investigation of adipocyte CaSR by Sundararaman and colleagues may have been confounded, since small beneficial CaSR effects in adipocytes may have been saturated by the significant documented effects of ApoE deletion on AT health. Thus, it remains conceivable that adipocyte CaSR regulates adipocyte function *in vivo*, and that deletion of CaSR may elicit positive effects in adipocytes.

1.2.8 CaSR and cardiometabolic disease

As discussed in sections 1.2.6 and 1.2.7, CaSR is a mediator of cardiovascular and adipocyte function. These observations raise questions regarding the pathophysiological role of CaSR in cardiovascular risk and the development of CVD. In humans, increased expression of CaSR in VSMC has been shown to play a role in the development of pulmonary arterial hypertension (Yamamura *et al.*, 2012). There is also evidence that CaSR derangement could have a wider influence on CVD, since CaSR polymorphisms have been identified as an

independent risk factor for coronary artery disease (CAD) and myocardial infarction (März *et al.*, 2007). At present, there is no clear mechanism linking CaSR and CVD. The relationship could be attributed to CaSR dysfunction in cardiovascular tissue specifically. On the other hand, CaSR may mediate cardiovascular risk indirectly if CaSR function was disturbed in tissues which influence the cardiovascular system, such as AT.

As outlined in section 1.1.5, metabolic derangement is a significant etiological factor in the development of CVD risk factors and CVD itself. Though heritable and *de novo* CaSR mutations manifest primarily as calcitropic disorders, CaSR signalling abnormalities also impact on glucose, insulin and lipid handling (Vahe *et al.*, 2017), suggesting that CaSR may be involved in metabolic function. Data regarding the status of CaSR status in conditions such as obesity and diabetes is limited. There is some evidence to suggest that CaSR could be upregulated in the obese state, based on the observation that $[Ca^{2+}]_o$ sensitivity is increased in obese versus lean individuals (Villarroel *et al.*, 2014). Possibly, this effect could be attributed to elevated CaSR activation (Villarroel *et al.*, 2014). However, $[Ca^{2+}]_o$ sensitivity could also be due to CaSR expression, which is positively correlated with body fat % (Mattar *et al.*, 2020). The idea that increased CaSR expression associates with AT expansion is corroborated by studies which examine how AT-conditioned media affects CaSR expression in LS14 adipocytes. Interestingly, cells which are stimulated using media conditioned by obese AT show increased CaSR expression, but the magnitude of this effect is reduced when cells are exposed to media derived from lower body mass index individuals (Cifuentes *et al.*, 2010). These data underscore a clear association between CaSR and metabolic dysregulation.

The importance of CaSR in metabolic function has also been demonstrated *in vivo*. Recently, Babinsky and colleagues developed mice with global CaSR activation, based on the gain of function CaSR mutation responsible for human autosomal dominant hypocalcaemia. Murine models of CaSR activation demonstrated impaired glucose homeostasis characterised by hyperglycaemia and hypoinsulinemia. These effects were reversed following infusion of the CaSR antagonist roncalaret, confirming that CaSR could mediate a causal role in metabolic dysfunction (Babinsky *et al.*, 2017). Though the CaSR is emerging as a

mediator of metabolic derangement, the tissues and mechanism(s) involved have not been intensively investigated. Derangement of AT and adipocytes specifically is a key etiological mechanism in metabolic dysfunction, leading to the development of CVD risk factors and CVD itself (Oikonomou and Antoniades, 2019). Consequentially, the significance of adipocyte CaSR in cardiovascular health must be established.

1.3 ADMA

1.3.1 Generation and regulation

Monomethyl- and dimethylarginines are endogenous, non-proteinogenic amino acids which are generated through post-translational modification of arginine guanidino groups. Arginine methylation is catalysed by protein methyltransferase (PRMT) enzymes, of which nine PRMT homologues are expressed in humans. PRMTs are classified as either type I (PRMT1-4, -6 and -8), type II (PRMT5 and -9) or type III (PRMT7) (Morales *et al.*, 2016; Tain and Hsu, 2017); while all PRMT isoforms modify terminal guanidino nitrogen atoms to form NG-monomethylarginine (MMA), type I and type II PRMTs can catalyse an additional methylation step, leading to the synthesis of asymmetric NG,NG-dimethylarginine (ADMA) and symmetric NG,NG'-dimethylarginine (SDMA), respectively (Fig. 1-7) (Morales *et al.*, 2016).

Figure 1-7

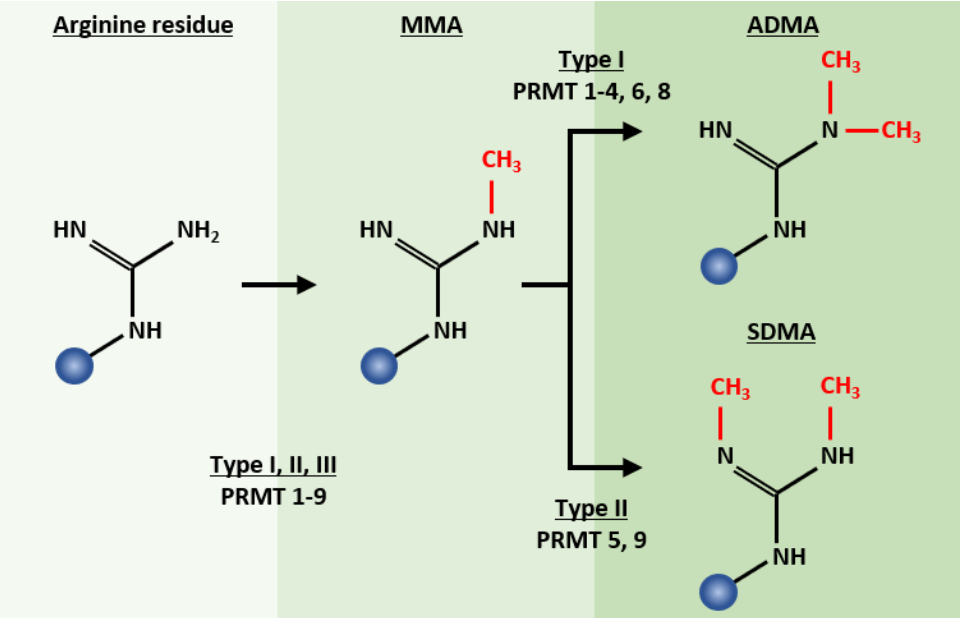

Figure 1-7: Generation of methylarginines.

MMA is produced by Type I, II or III PRMTs through single step methylation of arginine. Formation of ADMA and SDMA involve subsequent posttranslational modification, which is catalysed by Type I and II PRMTs, respectively. ADMA=asymmetric dimethylarginine; MMA=monomethylarginine; PRMT=protein methyltransferase; SDMA=symmetric dimethylarginine. Adapted from Morales et al. (2016) and Bedford & Clarke (2005).

ADMA and SDMA possess a shared functional group, but discrete geometry and hydrogen bonding patterns are produced by asymmetric and symmetric methylation, in turn allowing ADMA and SDMA to mediate isomer-specific biological effects (Morales *et al.*, 2016). Target protein methylation mediates numerous processes, including RNA splicing, processing and transcription, nuclear-cytoplasmic translocation and intracellular signalling (Bedford and Richard, 2005; Bedford and Clarke, 2009). Though arginine methylation can influence protein function, free ADMA and SDMA are also biologically active (Caplin and Leiper, 2012). Through proteolysis, ADMA is liberated from arginine-methylated residues and released into the cytoplasm, where it can then be transported across the membrane and into the extracellular environment via amino acid handling proteins, termed cationic amino acid transporters (CATs) (Teerlink *et al.*, 2009). ADMA formation in humans occurs at a rate of ~300μM per day (Achan *et al.*, 2003), resulting in plasma ADMA concentrations of ~0.5μM (Horowitz and Heresztyn, 2007).

Three main mechanisms are responsible for regulating systemic ADMA levels. These comprise the formation of ADMA by PRMT, the clearance of ADMA by renal excretion and metabolic ADMA degradation by the dimethylarginine dimethylaminohydrolase (DDAH) family of enzymes, DDAH-1 and DDAH-2. By virtue of their ability to influence ADMA formation and degradation, these pathways determine endogenous ADMA levels (J. M. Leiper and Vallance, 2006; Teerlink *et al.*, 2009). While SDMA is predominantly eliminated by renal clearance, urinary excretion of ADMA is considerably lower and is cleared primarily via DDAH mediated catabolism (Tain and Hsu, 2017). The proportion of ADMA that is metabolised by DDAH varies depending on species, although DDAH may be responsible for between 87-95% of ADMA clearance in rat and rabbit (McDermott, 1976; Ogawa *et al.*, 1987) and at least 83% in humans (Achan *et al.*, 2003). Though its expression is limited to the liver and kidneys, the enzyme alanine-glyoxylate aminotransferase 2 (AGXT2) also controls ADMA catabolism, which in turn impacts regulation of systemic ADMA levels (Fig. 1-8) (Amir *et al.*, 2018).

Figure 1-8

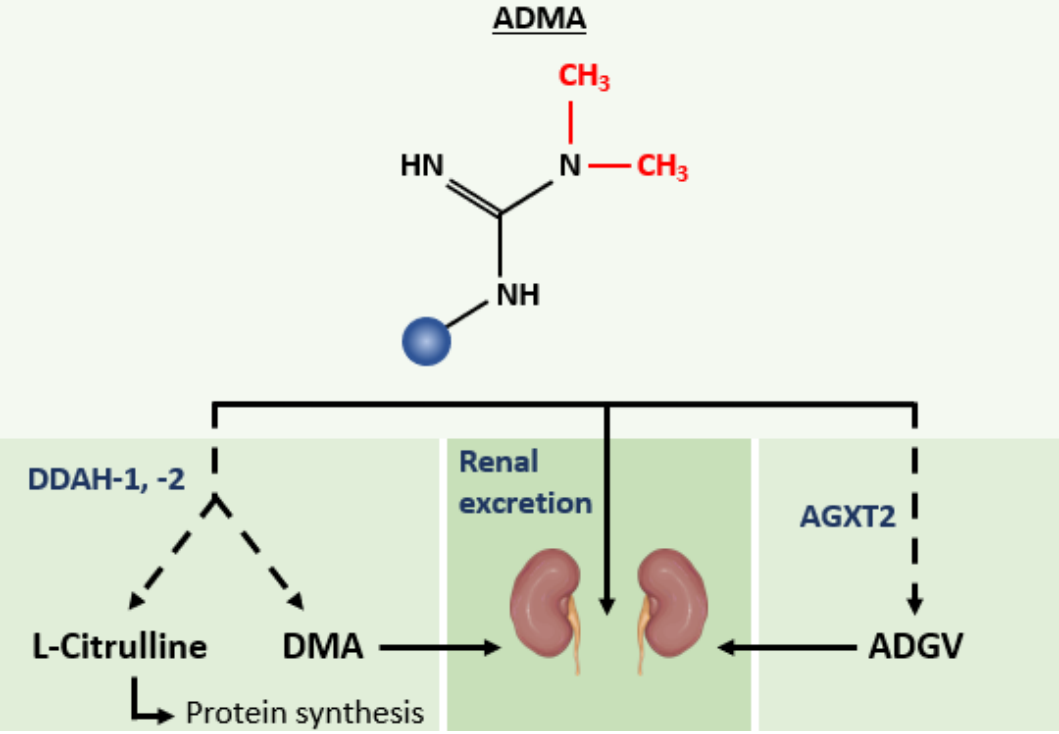

Figure 1-8: Metabolic and renal ADMA clearance.

Removal of circulating ADMA is regulated principally by DDAH metabolism and renal excretion. DDAH catabolism of ADMA produces L-citrulline and DMA; L-citrulline is reincorporated into tissues, while DMA is cleared by the kidneys. ADMA is additionally subject to AGXT2 metabolism, which produces ADGV and excreted by the kidneys. ADGV=Asymmetric dimethylguanidino valeric acid; ADMA=Asymmetric dimethyl arginine; AGXT2=Alanine-glyoxylate aminotransferase 2; DDAH=Dimethylarginine dimethylaminohydrolase; DMA=Dimethyl arginine. Figure produced using information from Amir et al. (2018) and Ogawa et al. (1987).

1.3.2 ADMA and cardiometabolic disease

A myriad of risk factors have been implicated in the development and advancement of CVD, many of which associate with raised ADMA (Dowsett *et al.*, 2020). In health, serum ADMA is ~0.5μM, infrequently exceeding 1μM (Horowitz and Heresztyn, 2007). In 1992, Vallance and colleagues were the first to observe that endogenous ADMA was elevated in chronic kidney disease patients (Leone *et al.*, 1992). 30 years on, raised ADMA is recognised as a hallmark of many CVD states and risk factors, including endothelial dysfunction (Böger *et al.*, 1998), hypertension (Surdacki *et al.*, 1999), stroke (Yoo and Lee, 2001),

hypercholestremia (Vladimirova-Kitova *et al.*, 2008), and atherosclerosis (Miyazaki *et al.*, 1999), among others (Bode-Böger, Scalera and Ignarro, 2007; Leiper and Nandi, 2011). Furthermore, ADMA accumulation is also linked with cardiometabolic diseases such as obesity (Eid *et al.*, 2004; Arlouskaya *et al.*, 2019), hypertriglyceridemia (Lundman *et al.*, 2001), type I diabetes (Altinova *et al.*, 2007) and type II diabetes (Abbasi *et al.*, 2001). Collectively, these studies underscore the association between ADMA and CVD. Interestingly, the shift in circulating ADMA levels during disease is frequently small. For instance, plasma ADMA can be 2-fold greater in renal failure when compared to healthy controls, whereas smaller increases of ~57% are reported in cardiovascular disease states such as hypercholesteremia and hypertension (Horowitz and Heresztyn, 2007). Such observations would suggest that minor fluctuations in plasma ADMA concentrations could be biologically significant.

In addition to the link between increased circulating ADMA and CVD risk factors, longitudinal studies reveal that ADMA predicts cardiovascular morbidity and mortality. For instance, in end-stage renal failure, the risk of cardiovascular events and death increased progressively in line with ADMA concentration percentile in 225 patients (Zoccali *et al.*, 2001). Mortality arising from coronary artery disease complications also correlates with increased ADMA (Meinitzer *et al.*, 2007). In addition to renal and coronary artery disease, ADMA predicts risk in cardiometabolic disease states. When 170 diabetic men were examined, subjects with ADMA concentrations in the upper tertile were at increased risk of adverse cardiovascular outcomes and death (Cavusoglu *et al.*, 2010). Crucially, several studies have demonstrated that ADMA imposed cardiovascular risk is conserved, even when traditional and non-traditional risk factors are controlled, suggesting that incident events may be predicted by ADMA independent of other factors (Zoccali *et al.*, 2001; Meinitzer *et al.*, 2007; Cavusoglu *et al.*, 2010). While observational studies highlight the prognostic value of ADMA as a marker of CVD and CVD associated risk, a causal role in CVD cannot be inferred. However, these studies raise important questions regarding the role of ADMA in the development of CVD.

As aforementioned, DDAH-mediated catabolism plays a key role in ADMA clearance. The importance of DDAH in human ADMA regulation is underscored

by an abundance of studies which link with genetic variation in DDAH1 with ADMA levels (Abhary *et al.*, 2010; Ding *et al.*, 2010; Amir *et al.*, 2018) as well as DDAH2 (Abhary *et al.*, 2010; Xuan *et al.*, 2016). Considering that ADMA is broadly associated with CVD, it is perhaps unsurprising that that genetic variation in DDAH leading to increased ADMA levels has been found to be clinically significant, highlighted by how ADMA levels impact on cardiovascular risk. In Chinese populations, DDAH1 polymorphisms which correlate with raised plasma ADMA, such as the promotor variant -396 4N, confers an increased risk of stroke, thrombosis and coronary heart disease (Ding et al., 2010). Subsequent work has linked -396 4N (Zhu et al., 2020), as well as the DDAH1 polymorphism rs1241321 (Lu et al., 2011) with type 2 diabetes. Smaller cohort studies demonstrating a positive association between ADMA accumulation and DDAH1 genotype have linked DDAH1 variation with hypertension (Valkonen, Tuomainen and Laaksonen, 2005) and CAD (Amir et al., 2018). Though DDAH1 would appear to be a significant determinant of circulating ADMA levels and CVD risk, the role of DDAH2 is less clear. For instance, the DDAH2 variant rs2272592 associates with type II diabetes (Seo et al., 2012), but several studies have failed to show an association between DDAH2 genotype and CAD (Xu et al., 2012; Xuan et al., 2016). Nonetheless, these studies offer compelling evidence that the association between ADMA and CVD could, at least some cases, arise due to DDAH followed by ADMA dysregulation.

Compared to DDAH, ADMA catabolism by AGXT2 is considered far less significant (Ogawa *et al.*, 1987). However, recent work in CAD patients examining the role of AGXT2 and ADMA metabolism in the context of cardiovascular risk have demonstrated that ADMA levels and CAD incidence are increased by AGXT2 variants rs37369 and rs16899974 (Amir et al., 2018). Taken together, studies which examine how genetic variation in DDAH and AGXT2 affects cardiovascular risk supports the view that ADMA levels could impact the development of cardiovascular risk factors and hence susceptibility to CVD.

1.3.3 Acute vascular actions

In addition to its status as a marker of cardiovascular risk, a causal role for ADMA in CVD may be realised in its status as a haemodynamic modulator. In rat aortic ring preparations, supraphysiological doses of ADMA enhances phenylephrine (α_1-

adrenoreceptor) mediated vascular contraction (Al-Zobaidy, Craig and Martin, 2010). Aside from enhancing contraction, ADMA also reduces relaxation by causing a concentration-dependent attenuation of acetylcholine induced responses in isolated human thoracic and radial arteries (Segarra *et al.*, 2000). Together, these data indicate that ADMA can regulate contractile and pro-relaxant vascular mechanisms. Aside from influencing the vascular response to vasoactive mediators, ADMA also acts, in a concentration dependent manner, as an independent pro-contractile mediator. This effect is demonstrated in mouse carotid artery (Torondel *et al.*, 2010) and in human thoracic and radial artery *ex vivo* preparations (Segarra *et al.*, 2000). Therefore, as well as modifying classical vasoconstriction/vasorelaxation mechanisms, ADMA also participates in direct modulation of vascular tone.

As above, ADMA regulates vascular responses in isolated vessels. Accordingly, several studies sought to address whether this effect was conserved in intact animal models. In rat, chronic, 14-day 10mgkg^{-1} ADMA infusion increases plasma ADMA levels from 0.65 to 1.25μM. ADMA treatment caused a 26% increase in baseline blood pressure and a 32% increase in coronary perfusion pressure in response to angiotensin-II pressor challenge, suggesting that small increases in circulating ADMA levels can cause vascular dysregulation (De Gennaro Colonna *et al.*, 2007). Interestingly, endothelial-dependent relaxation is reduced by ~40% in aortic ring preparations derived from the ADMA treated cohort, suggesting that ADMA exposure disturbs vascular reactivity chronically.

In addition to its effects in rodents, the role of ADMA in vascular function has been validated in humans. In healthy subjects, ADMA blunts renal blood flow by 11% (Kielstein *et al.*, 2004) and cerebral blood flow by 15% (Kielstein *et al.*, 2006). Aside from the haemodynamic effects of ADMA infusion, Kielstein et al. observed that arterial stiffness was significantly increased by ADMA (Kielstein *et al.*, 2006). Collectively, these observations led Kielstein and colleagues to suggest that the association between ADMA and cardiovascular risk could be explained, at least in part, by the effect of ADMA in the vasculature (Kielstein *et al.*, 2004, 2006). Though these data implicate ADMA as a vasoactive mediator, ADMA infused subjects demonstrated supraphysiological plasma ADMA concentrations (~15-42μM) in these investigations, indicating that ADMA-

mediated vascular effects might not be relevant in physiological settings. However, intravenous infusion of ADMA resulting in a plasma ADMA concentration of 2.6μM acutely perturbs vascular function, increasing blood pressure by 6% and systemic vascular resistance by ~24% (Achan *et al.*, 2003). Although performed on a small cohort, these observations demonstrate that pathologically relevant fluctuations in circulating ADMA can underpin dysfunction in the human vasculature. In intact systems, it is not possible to discern whether ADMA augments vascular reactivity by directly modulating vascular function, or indirectly by stimulating remote target(s) involved in the regulation of vascular tone. Irrespective of the mechanisms implicated, ADMA-mediated regulation of both vasoreactivity and haemodynamic function raise the possibility that ADMA could impose meaningful effects on vascular health and hence CVD risk.

1.3.4 Causal indications

As ADMA metabolism is influenced by PRMT and DDAH, strategies to modulate their activity and/or expression to manage endogenous ADMA levels may be of therapeutic use. Due to the difficulties associated with selectively inhibiting PRMT isoforms which are involved in ADMA formation, pharmacological targeting of PRMTs is not considered viable (Leiper and Nandi, 2011). As such, efforts to control ADMA levels *in vivo* have focused on DDAH modulation. In recent years, several studies have sought to manipulate DDAH genetically and pharmacologically to alter intracellular ADMA levels and thus interrogate the effect of altered ADMA levels *in vivo*. The systemic importance of DDAH1 was first demonstrated by Leiper and colleagues, who generated mice with global DDAH1 deletion via disruption of DDAH1 exon 1. Heterozygous DDAH1$^{+/-}$ mice displayed reduced protein and mRNA expression of DDAH1 and ~50% reduction in DDAH activity. Reduced DDAH1 function coincided with ADMA accumulation, since serum ADMA measures were elevated by ~30%, while ADMA elaboration from pulmonary ECs was increased by ~10%. Importantly, DDAH1$^{+/-}$ mice showed enhanced phenylephrine mediated vasoconstriction and impaired endothelial-dependent vasorelaxation, which corresponded with elevated blood pressure and systemic vascular resistance, suggesting that ADMA fulfils a causal role in CVD (Leiper *et al.*, 2007). In another set of experiments, Leiper et al. demonstrated that ADMA accumulation could also be triggered by the small molecule DDAH1 inhibitor L-291. In this model, endothelial nitrite release was

reduced by ~40%, while endothelial-dependent relaxation was also attenuated. Crucially, L-arginine (L-Arg) normalised endothelial-dependent vasorelaxation in both genetic and pharmacological ADMA accumulation models, therein indicating that the harmful effects linked with DDAH1 dysregulation *in vivo* likely arise via ADMA accumulation and reduced NO signalling (Leiper et al., 2007).

As global DDAH1 deletion causes ADMA accumulation and significant vascular dysregulation, several studies have attempted to delineate the role of ADMA specifically in the vasculature. As with $DDAH^{+/-}$ mice, targeted endothelial deletion of DDAH1 led to plasma ADMA accumulation, increased blood pressure and endothelial dysfunction, therein implying that the endothelium is a key site of ADMA regulation (Hu *et al.*, 2009). While other studies examining endothelial-specific DDAH1 deficient mice were unable to demonstrate an effect on ADMA or vasoreactivity, endothelial DDAH1 deletion resulted in impaired vascularisation endothelial outgrowth. ADMA was implicated in the regulation of endothelial function in these studies as endothelial outgrowth was improved by L-Arg (Dowsett et al., 2015).

Where DDAH1 deletion stimulates ADMA accumulation, viral transfection and genetic strategies to induce DDAH1 expression leads to reduced ADMA levels (Dayoub *et al.*, 2003; Matsuguma *et al.*, 2006). Endothelial dysfunction was not directly examined in these studies, but blood pressure was decreased. This would suggest that DDAH1 upregulation has a beneficial effect on vascular function, since this haemodynamic phenotype is consistent with the expected effects of ADMA withdrawal and improved NO signalling (Dayoub *et al.*, 2003; Matsuguma *et al.*, 2006). To test the concept that ADMA suppression could alleviate the development of CVD, Jacobi et al. developed a DDAH1 overexpressing, pro-atherogenic mouse model to study the significance of DDAH1 in atherosclerosis pathogenesis. In this model, reduced ADMA levels were associated with decreased lesion burden and improved endothelial relaxation (Jacobi *et al.*, 2010). While this study was unable to demonstrate a beneficial effect on blood pressure, these observations support the notion that ADMA mediates a causal, rather than simply indicative, role in the development of vascular derangement.

Studies which have modulated DDAH2 have been somewhat less informative with regards to the effect on ADMA on vascular function. In mice, global deletion of DDAH2 generated through targeted disruption of exon 2 of the DDAH2 gene leads to reduced ADMA accumulation in the myocardium and kidneys, but not in plasma. Blood pressure was similarly unaffected. Despite the lack of systemic effects, Lambden et al. showed that DDAH2 deficiency elevated aortic elaboration of ADMA *ex vivo*. These aortas exhibited decreased endothelial-dependent relaxation and increased vasoconstriction (Lambden *et al.*, 2015), supporting the notion that DDAH2 determines ADMA (tissue) concentrations *in vivo*, which in turn modulates vascular function. As DDAH2 deletion influences vascular function and localised ADMA levels, strategies to enhance DDAH2 expression might be predicted to mediate positive vascular effects. In mice overexpressing DDAH2, blood pressure is unaffected, despite decreased ADMA accumulation (Hasegawa *et al.*, 2007). This observation seems erroneous considering the wealth of literature which associates ADMA accumulation with adverse vascular effects. However, the reduction in plasma ADMA levels in DDAH2 overexpression models was only 43% of that observed in DDAH1 models (Hasegawa *et al.*, 2007). Consequentially, models which target DDAH2 may have a decreased effect on ADMA levels and hence disease phenotype compared to those which manipulate DDAH1. Taken together, studies examining the effect of pharmacological and genetic manipulation of DDAH implicate ADMA in cardiovascular dysfunction.

1.3.5 Molecular targets

Supraphysiological doses of ADMA inhibits cellular NOS activity, decreasing NO synthesis through competition with L-Arg, the requisite NOS substrate and structural analogue of ADMA (Fig. 1-9) (Leone *et al.*, 1992). Since this early work, these findings have been corroborated *in vitro* (Böger et al., 2000) and *in vivo* (Leiper et al., 2007).

Figure 1-9

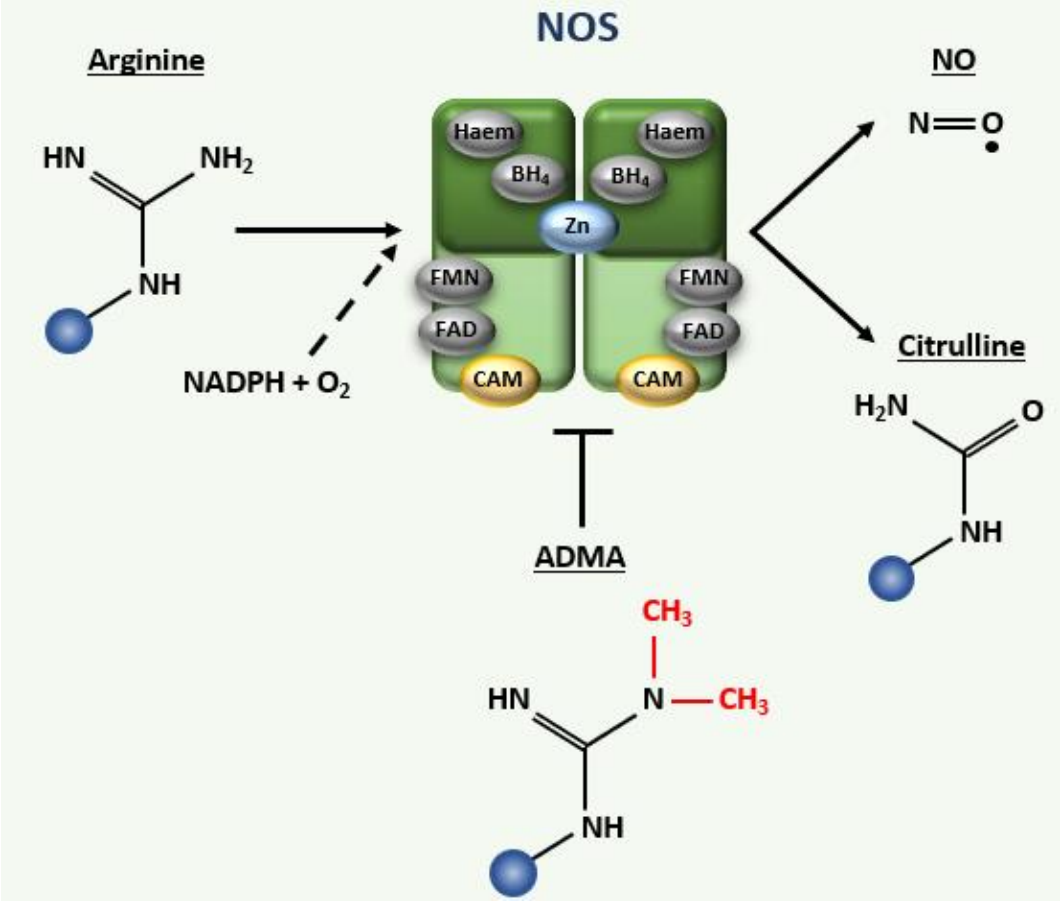

Figure 1-9: Inhibition of NOS by ADMA.

NOS exists as a homodimer, which comprises two domains; the oxygenase domain which binds cofactors haem and BH_4, and the reductase domain which requires cofactors FMN and FAD. Each dimer demonstrates a bound CAM molecule, and a shared Zn exists at the interface between NOS dimers. Arginine is a NOS substrate. In the presence of O_2, NOS converts arginine residues to citrulline, where NO is produced as a biproduct. ADMA is a structural analogue of arginine and thus competes with arginine at NOS to reduce NO production. ADMA=Asymmetric dimethylarginine; BH_4= Tetrahydrobiopterin; CAM=Calmodulin; FAD=Flavin adenine dinucleotide; FMN= Flavin mononucleotide; NOS=Nitric oxide synthase. Figure adapted from Leiper and Vallance (2004).

Aside from directly interacting with NOS, an additional ADMA target, the system Y^+ family of CAT proteins, may also contribute towards dysregulation of NO. CATs facilitate bidirectional transmembrane amino acid transport, of which CAT-1, CAT-2A and CAT-2B are sensitive to ADMA and L-Arg; through CAT saturation,

ADMA is thought to competitively inhibit intracellular influx of L-Arg, therein indirectly regulating NOS substrate availability and hence NO production (Teerlink *et al.*, 2009). Due to its targeting of NOS, the biological effects of ADMA and its occurrence alongside cardiovascular risk factors and CVD have been largely attributed to ADMA-mediated NOS inhibition and subsequent dysregulation of NO-dependent cardiovascular functions (Caplin and Leiper, 2012).

The suggestion that ADMA confers an effect on cardiovascular risk via inhibition of L-Arg/NO signalling is substantiated by interventional studies which show that L-Arg supplementation is associated with beneficial cardiovascular effects. CAD patients in receipt of oral L-Arg supplementation for 6 months show 143% improvement in acetylcholine induced coronary blood flow compared to placebo counterparts (Lerman et al., 1998). Acute exposure also improves endothelial function, as flow-induced vasodilation in the brachial artery is increased by ~7% in subjects with hypercholesteremia following intravenous infusion of L-Arg (Böger et al., 1998). Despite these findings, evidence supporting the potential benefits of L-Arg lack uniformity. Some clinical studies observe no improvement in vascular function despite increased circulating L-Arg /ADMA ratios (Walker *et al.*, 2001). Moreover, studies in isolated arteries show that ADMA-induced vascular dysfunction is not reversed with L-Arg (Veresh *et al.*, 2012). Indeed, examination of ADMA and L-Arg biochemistry acting at NOS raises doubt over the physiological relevance of this pathway. In health, the L-Arg/ADMA ratio is ~170 in plasma (Bode-Böger, Scalera and Ignarro, 2007) and >18 in the cytosol (Teerlink *et al.*, 2009). Given that intracellular L-Arg concentrations are reportedly 3000-fold greater than the K_m of L-Arg acting at NOS (Shin, Thapa and Fung, 2017), comparatively low prevailing concentrations of ADMA, or subtly increased levels in CVD, might not be expected to produce significant inhibition of NOS *in vivo*. These observations indicate that ADMA may act at other intracellular sites.

The idea that ADMA may mediate cellular dysfunction through NO-independent mechanisms is not novel. In fact, several studies suggest that ADMA may regulate biological effects through additional, NO-independent mechanism(s). In early animal studies, Suda et al. observed that eNOS deficient mice are not protected

from vascular lesions triggered by exogenous ADMA administration. Importantly, ADMA infusion did not modify vascular or plasma NO content, and the development of vascular injury was not alleviated by L-Arg supplementation. Collectively, these data suggest that NOS inhibition and reduced NO production may not be critical in vascular injury (Suda *et al.*, 2004). Arguably, eNOS depletion could have been counteracted by NO production from other NOS isoforms. However, Suda et al. proposed that the renin-angiotensin system was involved in ADMA induced vascular injury, since vascular angiotensin-converting enzyme expression, superoxide formation and lesioning were prevented when mice were treated with angiotensin-converting enzyme or angiotensin II receptor type 1 inhibitors (Suda *et al.*, 2004).

Other studies which have investigated how ADMA affects the renin-angiotensin system in the vasculature consistently show that ADMA stimulates this pathway in isolated vessels causing superoxide production (Veresh *et al.*, 2008, 2012). Veresh et al. suggested that superoxide elaboration could interfere with NO bioactivity. However, NO scavenging is only one mechanism among many through which superoxide and its derivative hydrogen peroxide mediates vascular injury (Touyz and Briones, 2010). Accordingly, ADMA-induced superoxide production could invoke a broad range of possible targets beyond NO. Studies examining the effects of NO inhibition *in vitro* provide additional data supporting the view that ADMA may mediate cardiovascular dysfunction independent of NO. For example, ADMA treatment in human coronary artery ECs causes gene changes which are not replicated when NO is inhibited pharmacologically with L-NIO (Smith *et al.*, 2005). More recently, our lab has shown that exogenous ADMA promotes cellular hypertrophy in adipocytes. Again, synthetic NO blockade could not reproduce these results (Dowsett *et al.*, 2022). Collectively, these studies suggest that the biological effects of ADMA may not be limited to its influence on NO signalling (Smith *et al.*, 2005; Dowsett *et al.*, 2022). Given that altered NO bioavailability is both a predominant marker and etiological factor in the development of endothelial dysfunction (Drenjancevic *et al.*, 2018), it is perhaps unsurprising that efforts to delineate the pathophysiological role of ADMA in CVD have been directed towards its effect on NO formation, while alternative ADMA signalling pathways remain largely unexplored. As emerging evidence suggests that ADMA may have biological functionality beyond NOS inhibition, NO-independent

mechanism(s) which contribute towards ADMA associated cardiovascular risk are of considerable interest.

As discussed in section 1.2.4 and 1.2.5, the CaSR can be activated by cations and synthetic calcimimetics, but also L-amino acids which may regulate the biological actions of CaSR *in vivo*. Studies in HEK293-CaSR cells consistently indicate that aromatic amino acids are most potent at CaSR, but a broad range of basic amino acids have been confirmed to stimulate CaSR (Conigrave, Quinn and Brown, 2000; Liu *et al.*, 2020). Notably, L-Arg invoked CaSR signalling in both instances. Due to the structural similarities between ADMA and L-Arg, ADMA competitively inhibits L-Arg binding at NOS as well as amino acid transporters (Teerlink *et al.*, 2009). Considering that CaSR is responsive to L-Arg and that ADMA and L-Arg demonstrate common molecular bindings sites, ADMA could comprise a potentially novel agonist of CaSR. Very recently, our lab examined the effect of ADMA in 3T3-L1 adipocytes and found that ADMA stimulated NO-independent cellular hypertrophy. Interestingly, the response was recapitulated by cinacalcet and was abolished by calcilytic treatment, suggesting that ADMA might regulate adipocyte biology via a CaSR mechanism. Subsequent experiments interrogating the effect of ADMA in HEK293 cells overexpressing CaSR showed that $GdCl_2$-mediated $[Ca^{2+}]_i$ and cAMP signalling were potentiated in the presence of ADMA. Interestingly, ADMA stimulated $[Ca^{2+}]_i$ mobilisation was sensitive to the CaSR inhibitor NPS-2143, again implicating CaSR as a mediator of ADMA signalling (Dowsett *et al.*, 2022). Though these observations highlight a potentially novel ADMA signalling pathway, the effect of ADMA on downstream CaSR signalling and the biological relevance of ADMA/CaSR signalling remains to be established.

1.4 Hypotheses

CaSR signalling maintains adipocyte health; altered CaSR signalling causes adipocyte dysregulation, which negatively impacts vascular function and perturbs haemodynamic homeostasis.

ADMA constitutes a novel allosteric agonist of CaSR and potentiates known CaSR signalling pathways.

1.5 Aims

To model and characterise CaSR signalling *in vitro*.

To determine whether ADMA influences CaSR signalling and explore the biological relevance of ADMA/CaSR signalling in cellular and vascular function.

To establish the role of adipocyte CaSR in adipose and cardiovascular function.

Chapter Two

Methods

Chapter 2: Methods

2.1 In vitro

2.1.1 Cell culture

The study used Flp-In T-REx- human embryonic kidney cells-293 (#R78007 Thermofisher, UK) transfected with Hu-myc-tagged CaSR pcDNA/FRT/TO vector to model CaSR mediated intracellular signal transduction. Transfection was conducted as previously described (Ward, Alvarez-Curto and Milligan, 2011) by Lucie Duluc (Imperial College London). CaSR transfected Flp-In T-REx-HEK293 (HEK293-CaSR) cells were thawed from nitrogen storage and grown in Dulbecco's Modified Eagle's Medium (DMEM) High Glucose with Glutamax (Gibco, #61965-026) containing 10% foetal bovine serum (FBS; Gibco, #10500064) and 1% penicillin/streptomycin (37°C, 5% CO2). DMEM was supplemented with 50µg/mL hygromycin (Sigma, #0654) to select for gene integration and 5µg/mL blasticidin (Life Technologies, #R21001) to repress non-DX CaSR expression. HEK293-CaSR cells were treated with 0.1µg/mL doxycycline hyclate (DX; Sigma, #9891) for 24h to induce CaSR expression. Vector-only transfected HEK293 cells (HEK293-vec) and uninduced HEK293-CaSR cells were used as negative controls.

3T3-L1 murine preadipocyte fibroblasts (ATCC, #CL-173) were grown in DMEM High Glucose with Glutamax, 10% newborn calf serum (NBS; Thermo, #16030074) and 1% penicillin/streptomycin (37°C, 10% CO_2). Differentiation efficiency was maintained by passaging 3T3-L1 cultures at 80% confluency.

2.1.2 3T3-L1 differentiation

To initiate differentiation, 3T3-L1 fibroblasts were grown to 100% confluency in DMEM/NBS. Three days post-confluency (i.e. differentiation day 0; D0), 3T3-L1 cells were treated with DMEM, 10% FBS, 10µg/mL insulin, 0.5mM 3-isobutyl-1-methylxanthine (IBMX), 1µM dexamethasone and 5µM troglitazone induction medium. On D3-6, 3T3-L1 cells were treated with insulin in DMEM/FBS medium, with a final change of DMEM/FBS on D6-10. 3T3-l1 cells were taken to be mature adipocytes from differentiation day 10 (Fig. 2-1).

Figure 2-1

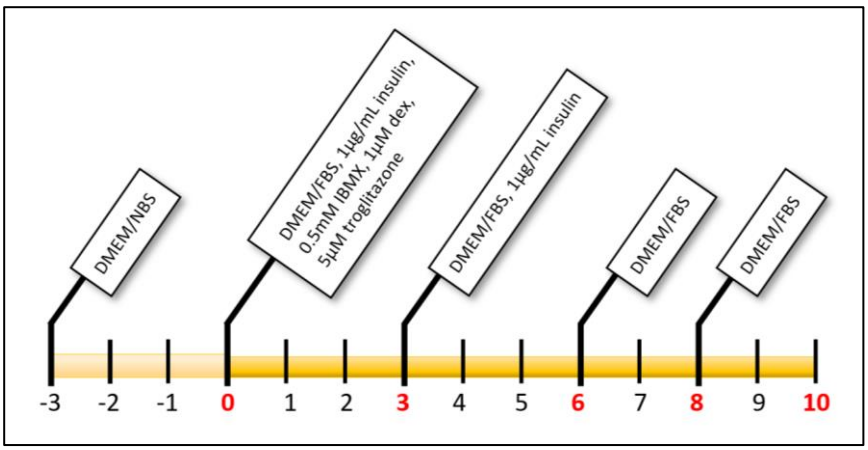

Figure 2-1: Differentiation of 3T3-L1 murine preadipocyte fibroblasts.
3T3 cultures were grown to 100% confluency and maintained in DMEM/NBS media for three days prior to differentiation. Underside of timeline denotes time in days (D), where D0 indicates differentiation induction. The upper bound of the timeline details media changes. 3T3-L1 murine preadipocyte fibroblasts were considered to be fully differentiated into adipocyte-like cells by D10. Dex=Dexamethasone; DMEM=Dulbecco's Modified Eagle's Medium; FBS=Foetal bovine serum; IBMX=3-isobutyl-1-methylxanthine; NBS=Newborn calf serum.

2.1.3 Oil-red-O absorption

3T3-L1 cells were washed once with PBS then fixed with 10% formalin in PBS at RT for 15min. Cells were incubated with oil Red O (ORO; 0.2% ORO, 40% 2-propanol in ddH_2O) at RT for 30min, and then rinsed five times with ddH_2O. ORO dye was eluted by immersing cells in 100% 2-propanol (12-well, 1mL; 6-well, 2.5mL) and incubating at RT for 10min on an orbital shaker. Elutate absorption was measured in duplicate at 510nm and recorded using the VictorX3 multilabel plate reader system (PerkinElmer, UK). Absorbance (A) is expressed as mean±SEM.

2.1.4 3T3-L1 morphology and lipogenesis

3T3-L1 cells were grown and differentiated on 1.5mm borosilicate coverslips. Mature 3T3-L1 cells were treated on D10 for 72h. Cells were washed twice in PBS, fixed with 4% paraformaldehyde for 3min and washed a further twice in PBS. 3T3-L1 cells were then incubated in 1µg/mL DAPI and 1µg/mL boron-dipyrromethene 493/503 (BODIPY; ThermoFisher, #D3921,) at RT for 30min. 3T3-

L1 cells were washed twice in PBS and mounted in ProLong Diamond Antifade Mountant (Thermofisher, #P36965) cured at RT overnight. Imaging was performed using the Zeiss LSM510 Meta Confocal Microscope System at x20 magnification. Typically each treatment consisted of two technical replicates, where three images were taken of each.

Cell dimensions were assessed by manual identification of the cell periphery; in each image, up to 30 cells were measured (maximum 180 total cells per treatment) to give cell area (μm^2) ±SEM for each condition. Technical and analytical assistance was provided by Dr. Laura Dowsett (University of Glasgow). Differentiation efficiency was quantified by assessing the proportion of lipid-positive (i.e., differentiated) cells relative to lipid-negative cells in each condition. Total nuclei were counted by thresholding and segmenting DAPI stained regions and counting the resulting particles. Cells in which nuclei were seen to associate with LDs were taken as lipid-positive by manual counting. Differentiation efficiency was derived by dividing lipid-positive cells by total nuclei and expressed as % of total cells ±SEM. LD dimensions were calculated by thresholding and segmenting BODIPY stained regions and quantifying the area of each particle, expressed as mean area (μm^2) ±SEM. LDs per cell (LD/cell) was quantified by dividing BODIPY segmented particles by the number of lipid-positive cells in an image, expressed as mean LDs/cell ±SEM. Cell area and counting were conducted manually (Image J: v1.52). All other morphological quantification was performed using a customised image analysis pipeline (Cellprofiler: v.3.1.8) (Fig. 2-2).

Figure 2-2

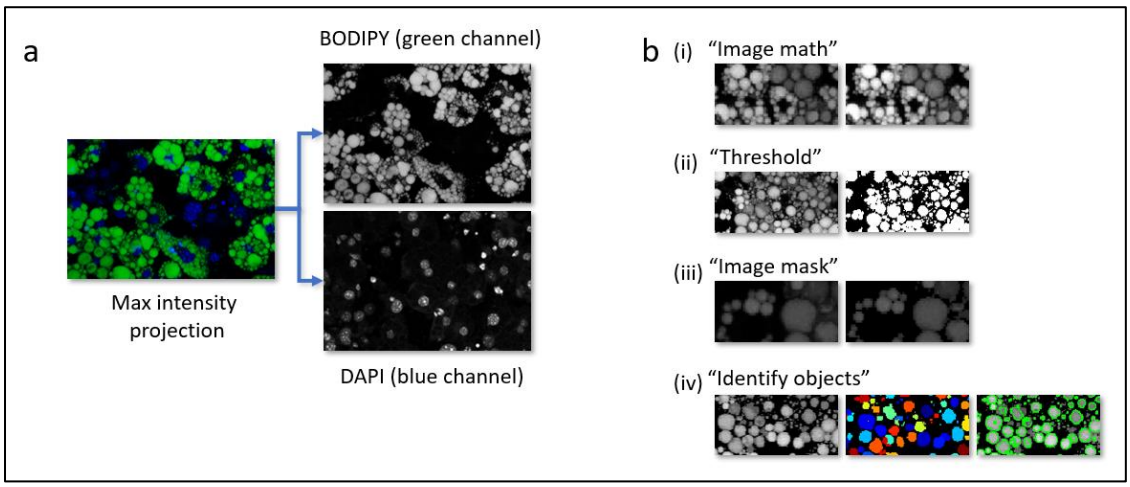

Figure 2-2: CellProfiler image processing and analysis pipeline.

(a) Confocal microscopy was used to record Z-stack images of 3T3-L1 cells stained for nuclear proteins (DAPI, blue) and neutral lipids (BODIPY, green). Channels were split to generate separate images for LD and nuclear analysis. **(b)** (i) Image intensity was enhanced using image math, which multiplied the original image by itself. (ii) LDs were subject to thresholding and segmentation. (iii) Using the segmented image generated in the previous step as a mask, image areas containing LDs were isolated. (iv) The identify objects function was designed to capture as many types of LDs as possible. This can be seen to be mostly successful, but some LD particles are omitted due to their small size, shape, or overt clustering. DAPI= boron-dipyrromethene 493/503; LD=Lipid droplet.

2.1.5 Immunocytochemistry

Media was removed and cells washed twice times with PBS. HEK293-CaSR cells were fixed in 100% methanol for 3min, and 3T3-L1 cells in 5% PFA for 5min. Cells were blocked using 5% bovine serum albumin (BSA) in PBS for 1h. Cells were incubated with 1/1000 mouse anti-human c-myc primary antibody (Santa Cruz Biotech, #40), 1/500 rabbit anti-mouse CaSR primary antibody (Abcam, #137408) or 1/500 mouse anti-mouse CaSR primary antibody (Abcam, #19347) at 4°C overnight, then 1/500 donkey anti-mouse Alexa Fluor 488 secondary antibody (Thermofisher, #21202) or 1/500 donkey anti-mouse Alexa Fluor 488 secondary antibody (Thermofisher, #21206) at 22°C for 1h. Cells were stained with 1µg/mL DAPI in PBS at 22°C for 30min. Antibody incubations were conducted in 5% BSA in PBS, with two PBS washes between each incubation step. Cells were held in

PBS during and imaged using the Zeiss Live Cell Microscope System at x10 or x20 magnification (HEK293-CaSR cells) or the Zeiss Axio Imager A1 at 40x magnification (3T3-L1 cells). Typically each condition was represented by a minimum of two technical replicates, with three images collected from each. HEK293-CaSR expression was characterised by analysing fluorescence intensity, where mean intensity was calculated for each condition. Intensity was expressed as absolute intensity (AU) ±SEM.

2.1.6 Phosphorylation studies

HEK293-CaSR cells were prepared for protein activation western blot analysis by incubating overnight in Ca^{2+}-free DMEM (Gibco, #21068-028) supplemented with 1% L-glutamine, 1.5mM $CaCl_2$ and 0.2% BSA. Prior to stimulation, HEK293-CaSR cells were incubated for 30min in physiological salt solution (PSS) pre-treatment buffer (125mM NaCl, 4mM KCl, 20mM HEPES, NaH_2PO_4, 1mM $MgCl_2$ hexahydrate and 0.1% glucose, 0.1% BSA and 0.5mM $CaCl_2$ in ddH_2O). HEK293-CaSR cells were then treated for 10min in (BSA-free) PSS treatment solution (125mM NaCl, 4mM KCl, 20mM HEPES, NaH_2PO_4, 1mM $MgCl_2$ hexahydrate and 0.1% glucose) supplemented with the required $CaCl_2$ concentration ±treatments. The reaction was terminated by removing the treatment solution and washing in ice-cold PBS. Chronic stimulation of HEK293-CaSR cells was performed by incubating cells for 24h in Ca^{2+}-free DMEM supplemented with the required $CaCl_2$ concentration and treatments.

Mature 3T3-L1 cells were used at D10-14 post differentiation. These were incubated overnight in Ca^{2+}-free DMEM, 1% L-glutamine, 1.5mM $CaCl_2$ and 0.5% FBS. 3T3-L1 cells were starved for 2h in serum-free Ca^{2+}-free DMEM, 1% L-glutamine and 0.2mM $CaCl_2$. Treatments were added directly to the starvation media.

2.1.7 $[Ca^{2+}]_i$ imaging

HEK293-CaSR cells were seeded in black, flat-bottom 96-well plates (Griener, #655090) and grown to >60% confluency. All experiments were conducted using HEPES or HBSS buffer (140mM NaCl, 5mM KCl, 1mM $CaCl_2$, 0.4mM $MgSO_4$-$7H_2O$, 0.5mM $MgCl_2$-$6H_2O$, 0.3mM Na_2HPO_4-$2H_2O$, 0.4mM KH_2PO_4, 4mM $NaHCO_3$ and 6mM

glucose in dH2O), ±treatment. As necessary, HEK293-CaSR treatments were present throughout Fura-8 incubation, in buffer during the experiment and in treatment plates. Cells were incubated with 3μM Fura-8 (Stratech, #21055-AAT) in buffer for 45min (37°C, 5% CO2), washed twice with buffer warmed to 37°C and allowed to acclimatise for 20min. HEK293-CaSR cells were maintained in buffer at 22°C throughout the experiment. Treatment plates were designed to add $GdCl_2$ to a range of final concentrations. Lm1 (354/530nm) and Lm2 (415/530nm) fluorescence intensity was sampled at 4s intervals for a total time of 90s. Following automated background correction, ratiometric fluorescence values were calculated using a wavelength combination of Lm1/Lm2. Baseline fluorescence intensity was given by HEK293-CaSR mean fluorescence intensity in the first 16s seconds (4 data points) of the experiment, after which cells were inoculated with $GdCl_2$. Following $GdCl_2$ treatment, cells were monitored for a further 74s (17 data points) for $[Ca^{2+}]_i$ mobilisation. Four technical replicates were typically conducted for each condition and were averaged to give mean fluorescence intensity (Lm1/Lm2) ±SEM.

2.2 Molecular

2.2.1 Griess assay nitrite measurement

Nitrite concentration of conditioned cell media was quantified using the Griess assay kit (Invitrogen, #G7921) per manufacturer's protocol. In brief, 0.1% N-(1-naphthyl)ethylenediamine dihydrochloride and 1% Sulfanilic acid in 5% phosphoric acid was mixed in a 1:1 ratio to produce the Griess working solution. In a 96-well plate, Griess reactions were prepared in duplicate by mixing 150µL sample with 130µL dH_2O and 20µL working solution. Griess reactions were incubated at RT for 30min. Absorption was measured in duplicate at 550nm and recorded using the VictorX3 multilabel plate reader system (PerkinElmer, UK). Nitrite concentration was quantified in unknown samples by interpolating values from a standard curve ($NaNO_2$; 1-100µM) (Fig. 2-3). Nitrite concentration is provided as mean concentration (µM) ±SEM.

Figure 2-3

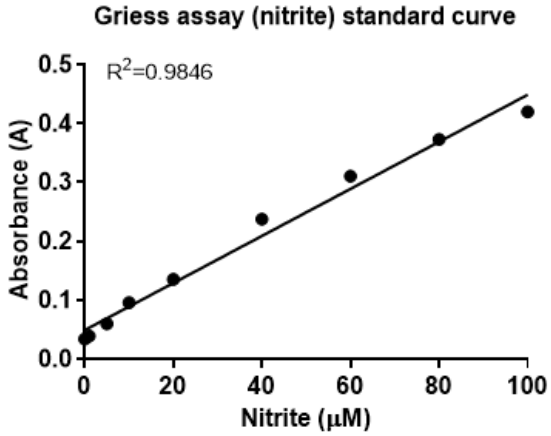

Figure 2-3: Griess assay standard curve.

Standard curves were generated for Griess reactions by calibrating with known concentrations of sodium nitrite ($NaNO_2$).

2.2.2 FFA Assay

Free fatty acid (FFA) content was quantified in mouse plasma samples using the Free Fatty Acid Quantitation Kit (Sigma, #MAK0044) in line with manufacturer's instructions. Absorption was measured at 570nm using the SPECTRAmax 190 Microplate Spectrophotometer system (Molecular Devices, UK). Concentrations were quantified in unknown samples by interpolating values from a standard

curve (Palmitic acid 0.02-0.1nmol/µl) (Fig. 2-4). Plasma FFA concentration is provided as mean concentration (nmol/µl) ±SEM.

Figure 2-4

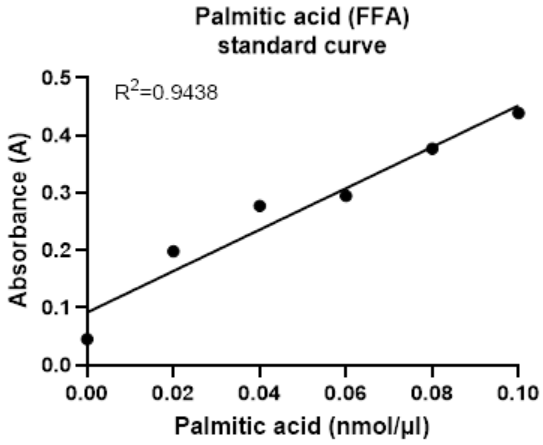

Figure 2-4: FFA assay standard curve.

Standard curves were generated for FFA reactions by calibrating with known concentrations of palmitic acid.

2.2.3 Triglyceride Assay

Plasma triglyceride content was assessed in mice using the Triglyceride Assay Kit (Abcam, #65336) in line with manufacturer's instructions. Absorption was measured in duplicate at 570nm using the SPECTRAmax 190 Microplate Spectrophotometer system (Molecular Devices, UK). Concentrations were quantified in unknown samples by interpolating values from a standard curve (Triglyceride standard 0.0025-0.1nmol/µl) (Fig. 2-5). Plasma triglyceride concentration is provided as mean concentration (nmol/µl) ±SEM.

Figure 2-5

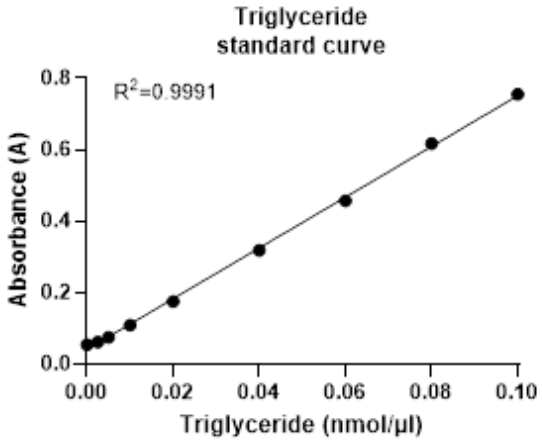

Figure 2-5: Triglyceride assay standard curve.

Standard curves were generated for triglyceride reactions by calibrating with known concentrations of solubilised triglyceride.

2.2.4 End-point PCR

End-point PCR was used to determine the genotypes of CaSR mice. Ear notches were lysed at 95°C for 1h with alkaline lysis reagent (25mM NaOH, 0.2mM disodium EDTA, pH 12). Ear notch digests were then diluted ½ with neutralising buffer (40mM Tris-HCl, pH5) and chilled to 4°C. PCR reactions contained 3µL of DNA sample, DreamTaq Hot Start Green PCR Master Mix (Thermo, #K9022) at ½ dilution, with forward and reverse primers at 500nM (Tb. 2-1). Specific thermal cycling protocols were performed according to the primer pair (Tb. 2-2).

Gel electrophoresis was used to separate PCR products. Gels containing 1.5% agarose gels with GelRed Nuclear Acid Stain (Merck, #SCT123) diluted 1/75,000 were cast in-house. Electrophoresis was performed in Tris-borate-EDTA buffer (TBE; 89 mM Tris, 89 mM boric acid, 2 mM EDTA) at 90v until adequate separation of PCR products was achieved. PCR products were visualised in UV using the ChemiDoc +XRS system (Biorad, UK) and molecular weight determined using the GeneRuler 100bp Plus DNA Ladder (Thermofisher, #10364280).

Table 2-1

Primer pair	Forward (5'→3')	Reverse (3'→5')
CaSR postneo	GACTTGCTATGTAGCCCAGAACTG	ACACCCCAAGTGCTCCTGATAACAG
CaSR floxed	TGTGTCAGTTTCATAGCCTGAAG	TGTCTATGGAAAGCCCCAGA
CaSR wildtype	CTTCAGAGGCCAGAGGTGTC	TGTCTATGGAAAGCCCCAGA
Cre recombinase	GCCTGCATTACCGGTCGATGCAACGA	GTGGCAGATGGCGCGGCAACACCATT

Table 2-1: PCR primers and sequences used in end-point PCR.

Primer pairs were used to determine mouse genotype by assessing the presence of mutant alleles. CaSR=Calcium sensing receptor.

Table 2-2

Protocol	Step	Temp (°C)	Duration
CaSR postneo primers	1	95	10min
	2	95	30sec
	3	55	45sec
	4	72	1min
	5	-	*Step 2-4 x30*
	6	72	1min
	7	4	∞
CaSR wildtype	1	94	2min
/floxed primers	2	94	20sec
	3	65 (-0.5 per cycle)	15sec
	4	68	10sec
	5	-	*Step 2-4 x10*
	6	94	15sec
	7	60	15sec
	8	72	10sec
	9	-	*Step 6-8 x24*
	10	72	2min
	11	10	∞
Cre primers	1	95	5min
	2	95	30sec
	3	60	40sec
	4	32	1min
	5	-	*Step 2-4 x40*
	6	72	10min
	7	4	∞

Table 2-2: PCR thermal cycling protocols.

Thermal cycling protocols are given for each primer pair used in the study. All protocols were performed using the MJ Research PTC-225 Gradient Thermal Cycler (MJ Research). CaSR=Calcium sensing receptor.

2.2.5 Reverse transcription quantitative PCR

All quantitative PCR (qPCR) experiments were performed and analysed by Miss Erin Higgins, with the exception of CaSR expression in $CaSR^{Ad-/-}$ adipocytes which was performed by Dr. Laura Dowsett (University of Glasgow). Cell cultures were prepared for mRNA analyses by washing twice in PBS and scraping adherent cells in the presence of RPL lysis buffer (Qiagen, #79216). Animal tissue or isolated primary adipocytes were thawed from -80°C. Tissues were mechanically homogenised by shaking with 5mm stainless steel beads at 30Hz for 60s

(TissueLyser II system. Qiagen, UK) in the presence of 700µL QIAzol Lysis Reagent (Qiagen, #79306). Homogenate was inoculated with 140mL 100% chloroform, shaken vigorously for 15s and incubated at RT for 2min. Samples were then centrifuged at 12,000rcf for 15min, 4°C. The clear aqueous supernatant fraction was aspirated and mixed with 1.5 volumes of 100% ethanol.

RNA was extracted from cell culture and tissue lysates using the RNeasy Mini Kit (Qiagen, #74106) and its concentration measured with the NanoDrop spectrophotometer system (ThermoFisher, UK). cDNA synthesis was performed using the High-Capacity cDNA Reverse Transcription Kit (Invitrogen, #4368814), according to the manufacturers' protocol. Primers (Tb. 2-3) were used at 200nM in combination with 10ng cDNA and Fast SYBR Green Mastermix (Invitrogen, #4385612) at ½ dilution. qPCR reactions were performed using the 7900T Fast Real-Time PCR System (Life Technologies, UK). Unless indicated otherwise, reagents were sourced from ThermoFisher (UK).

qPCR data was analysed using 2^{-ddCT} method (Eq. 1). 18S ribosomal RNA (18S), 60S ribosomal protein L13 (RPL13) or glyceraldehyde 3-phosphate dehydrogenase (GAPDH) were used reference genes; ΔCtrl=average control dCT, X=experimental sample dCT, C_TGOI=gene of interest C_T, C_TRef=reference gene C_T. The output from Eq. 1 was raised to the power of two to yield fold change in gene expression, relative to control.

Equation 1

$$ddCT = [X(C_TGOI - C_TRef)] - [\Delta Ctrl(C_TGOI - C_TRef)]$$

Table 2-3

Primer pair	Species	Forward (5'→3')	Reverse (3'→5')
ACC1	Ms	ATGGGCGGAATGGTCTCTTTC	TGGGGACCTTGCTTTCATCAT
ACE	Ms	CAGTTGCCCGGAATGAAACC	CTGGGCGGACTGGTAGATG
Adiponectin	Ms	CTTGTGCAGGTTGGATGGC	CAGCTCCTGTCATTCCAACA
Apelin	Ms	ATGAATCTGAGGCTCTGCGT	CTGGTCCAGTCCTCGAAGTT
CaSR E2-E4	Ms, Hu	ATGACTTCTGGTCCAATGAG	TGCGGAACTTGATAAACAC
CaSR	Ms	AGCACTGCGGCTCATGCTTTC	TCAGGGCCAGTGGTTGCTC
Catalase	Ms	ACATGGTCTGGGACTTCTGG	CAAGTTTTTGATGCCCTGGT
DDAH-1	Ms, Hu	GCCCTTTGTTGGGGATATTT	AGGCCCTTAAGATCATGCAA
DDAH-2	Ms	CCTGGTGCCACACCTTTCC	AGGGTGACATCAGAGAGCTTCTG
EDN-1	Ms	TCGTGACTTTCCAAGGAGCT	CCAGGTGGCAGAAGTAGACA
eNOS	Ms	AAGACAAGGCAGCGGTGG	GCAGGGGACAGGAAATAGTT
eNOS	Hu	GGGCAGCCTCACTCCTGTT	ACGGCGTTGGCCACTT
FABP4	Ms	TAAAAACACCGAGATTTCCTTCA	CCTTTCATAACACATTCCCACCA
FASN	Ms	TGCTCCCAGCTGCAGGC	GCCCGGTAGCTCTGGGTGTA
GAPDH	Ms, Hu	TGAACGGGAAGCTCACTGG	TCCACCACCCTGTTGCTGTA
iNOS	Hu	GAGGAAGTGGGCAGGAGAATG	GTAGTAGAAAGGGGACAGGAC
Leptin	Ms	AAGAAGATCCCAGGGAGGAA	TGATGAGGGTTTTGGTGTCA
MMP-2	Hu	CGTCTGTCCCAGGATGACATC	ATGTCAGGAGAGGCCCCATA
mTOR	Ms	GGCACATCTAGCAACGTGAG	CTGGTCATAGAAGCGAGTAG
NOX1	Ms	TCCCTTTGCTTCCTTCTTGA	CCAGCCAGTGAGGAAGAGTC
NOX2	Ms	CGCCCTTTGCCTCCATTCTC	CCTTTCCTGCATCTGGGTCTCC
NRF2	Ms	TGAGCCAAGCTATAAGCCATGA	AATGGTTCTTGTGCCTGTGAA
Omentin	Ms	GTCTCTATTTCCTGCGCACG	CTCTGTTGCCTTGCTGACTG
PGI_2	Ms	ATGCCTTGGAGTTTGGGAGA	TTCATCCTGGCCTTCTCCTC
PKG	Ms	TGTCCTCGAAGAGACCCACT	GCAACGCTTTCTCTCCAAAC
PPARγ	Ms	ATGCACTGCCTATGAGCACT	CAACTGTGGTAAAGGGCTTG
Resistin	Ms	TTCCTTGTCCCTGAACTGCT	TCTTCACGAATGTCCCACGA
RPL13	Ms, Hu	CTCATCCTGTTCCCCAGGAA	TGGGTGGCCAGCTTAAGTTC
sGC1a	Ms	CCCCTGGTCAGGTTCCTAAG	GGAGACTCCCTTCTGCATTCT
sGC1b	Ms	TGCTGGTGATCCGCAATTATG	GGTTGAGGACTTTGCTTGCAG
SOD	Ms	GAGACCTGGGCAATGTGACT	TTGTTTCTCATGGACCACCA
SREBP1	Ms	ACAAAAGCAAATCACTGAAGGACC	CGGGCTCAGAGTCACTACCACC
TGFβ	Hu	CTGCTGACCCCCACTGATAC	AGCCCTGTATTCCGTCTCCT
UCP-1	Ms	CGACTCAGTCCAAGAGTACTTCTCTTC	GCCGGCTGAGATCTTGTTTC
Visfatin	Ms	GCAGAGCACAGTACCATAACG	TGGTGCCTCTGTACTTCTCG
18S	Ms	GCTCAGCGTGTGCCTACC	GGCCTCACTAAACCATCCA

Table 2-3: Primers and primer sequences used in RT-qPCR analyses.

Primer sequences are given for each custom primer pair (ThermoFisher, UK) used in the study. RT-qPCR reactions were performed using 10ng cDNA and ½ dilution Fast SYBR Green Mastermix using the 7900T Fast Real-Time PCR System (Life Technologies, UK). ACC1=Acetyl coenzyme A; CaSR=Calcium sensing receptor; DDAH=Dimethylarginine dimethylaminohydrolase; EDN-1=Endothelin-1; eNOS=Endothelial nitric oxide synthase; FABP4=Fatty acid binding protein 4; FASN=Fatty acid synthase; GAPDH=Glyceraldehyde-3-Phosphate Dehydrogenase; iNOS=Inducible nitric oxide synthase; MMP-2=Matrix metalloproteinase-2; mTOR=Mammalian target of rapamycin; NOX1/2=NADPH oxidase; NRF2=Nuclear factor erythroid 2–related factor 2; PGI_2=Prostacyclin; PKG=Protein kinase G; PPARγ=Peroxisome proliferator-activated receptor gamma; RPL13=Ribosomal protein L13; sGC1a/1b=Soluble guanylate cyclase; SOD=Superoxide dismutase; SREBP-1= Sterol regulatory element-binding protein 1; TGFß=Transforming growth factor ß1; UCP-1=Uncoupling protein-1; 18S=Ribosomal subunit 18S.

2.2.6 Bradford assay

Protein concentration was determined using the Bradford protein assay (Biorad, #5000001) per the manufacturer's protocol. In brief, Bradford protein assay solution was diluted ⅕ with ddH_2O to produce a working solution. In a 96-well plate, Bradford reactions were prepared by mixing 200µL working solution with 10µL sample and incubated at RT for 20min. Absorption was measured in duplicate at 595nm and recorded using the VictorX3 multilabel plate reader system (PerkinElmer, UK). Protein concentration was quantified in unknown samples by interpolating values from a standard curve (BSA; 0.01-0.5mg/mL) (Fig. 2-6). Samples were standardised against the lowest protein concentration sample in each experimental set.

Figure 2-6

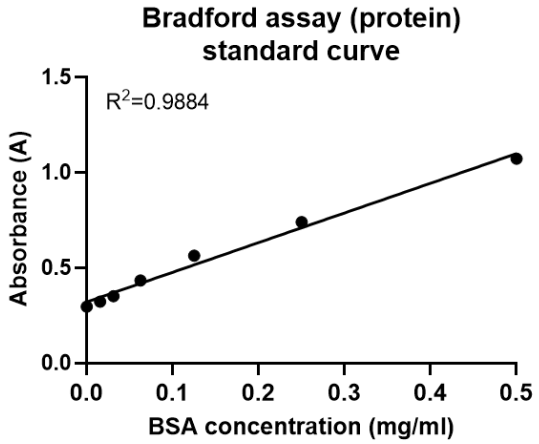

Figure 2-6: Bradford protein assay standard curve.

Standard curves were generated for Bradford reactions by calibrating with known concentrations of BSA. BSA=Bovine serum albumin.

2.2.7 ELISAs

Enzyme-linked immunosorbent assays (ELISAs) are a biochemical, plate-based method which is used to detect and quantify the concentration of soluble antigens within a sample. In brief, an ELISA uses a capture antibody to immobilise the target antigen to the plate surface; the capture antibody-antigen complex is then recognised and bound by a detection antibody cross-linked with the enzyme horseradish peroxidase (HRP). The addition of development solution

containing the HRP substrates hydrogen peroxide and tetramethylbenzidine (TMB) causes an oxidation reaction resulting in the formation of a soluble blue product. The ELISA stop solution acidifies this product producing a colorimetric shift from blue to yellow. This signal is proportional to the level of analyte present.

Adiponectin and leptin levels were assessed in plasma, adipocytes, PVAT-conditioned media and 3T3-L1 cell media using the Mouse Adiponectin ELISA Kit (Abcam, #226900) and Mouse Leptin ELISA Kit (Abcam, #199082) in line with manufacturer's instructions. Samples were assessed in duplicate where sample volume allowed. Absorption was measured at 450nm and recorded using the VictorX3 multilabel plate reader system (PerkinElmer, UK). Concentrations were quantified in unknown samples by interpolating values from a standard curve (Adiponectin 78-5000pg/mL; leptin 94-6000pg/ml) (Fig. 2-7). Adiponectin and leptin concentrations are expressed as a function of volume (µg/mL; ng/mL) ±SEM in plasma samples standardised to 1mg total protein in adipocyte lysates. Concentrations were expressed as change from control (%) ±SEM in 3T3-L1 media samples.

Figure 2-7

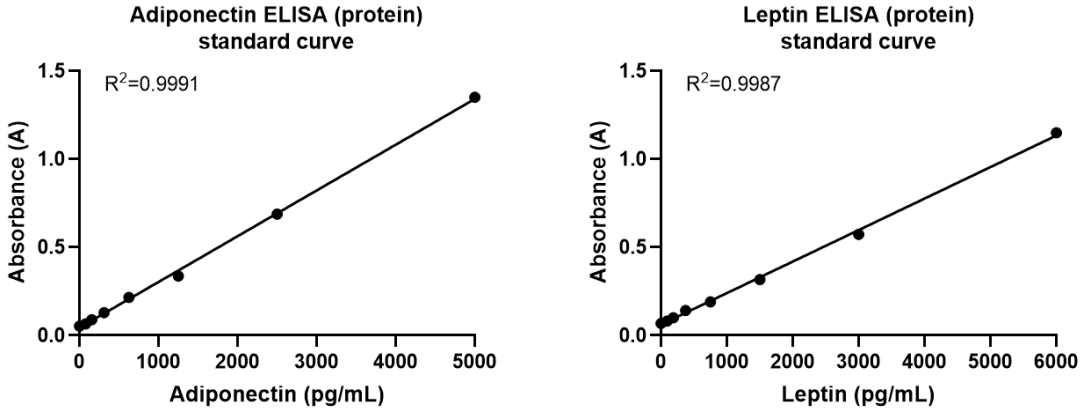

Figure 2-7: ELISA standard curves.

(a) Standard curves were generated for ELISA assays targeting adiponectin and **(b)** leptin. ELISA=Enzyme-linked immunosorbent assay.

2.2.8 Western blot

HEK293 or 3T3-L1 cells were washed twice in PBS and lysed with HEPES lysis buffer (50mM HEPES, 1mM EDTA, 1% Triton x-100 in dH2O), NP-40 lysis buffer (1% NP-40, 50mM Tris-HCl, 150mM NaCl in dH2O) or RIPA buffer (#R0278, Sigma, UK) at 4˚C for 5min. Cells were dislodged from wells by scraping or repeated pipetting. Lysates were centrifuged at 14,000rcf, 4˚C for 15min. Lysates were then mixed with 5X Laemmli buffer (5% ß-mercaptoethanol, 2.5mM Tris, 19mM glycine and 0.01% SDS and bromophenol blue in dH2O, pH8.6) to a final concentration of 1X and heated to 96˚C for 4min. Samples were chilled to 4˚C for same-day use, or stored at -20˚C.

Sodium dodecyl sulfate polyacrylamide gel electrophoresis (SDS-PAGE) was performed using 8-12% resolving gel and 5% stacking gel, cast in-house. Gels were loaded with 30-40µl sample and 10µl Precision Plus Protein Ladder (Biorad, #161-0373). Electrophoresis of samples was conducted in running buffer (0.025M Tris, 0.192M glycine and 0.1% SDS in dH2O) at 120V for 15min and then 160V until adequate separation of proteins had been achieved. Proteins were transferred to a methanol-activated Immobilon-P polyvinylidene difluoride membrane in transfer buffer (0.025M Tris, 0.092M glycine and 20% methanol in dH2O) at 100V, 4˚C for 1h. Membranes were blocked with milk (1-5%) or bovine serum albumin (BSA; 3-5%) dissolved in Tris-buffered saline (TBS; Thermo Fisher, #15440277) and 0.1% Tween20 (TBS-T), or with seablock (Thermofisher, #37527) at ½ dilution in TBS-T. Membranes were shaken in blocking buffer at 22˚C for 1h.

Membranes were incubated with primary antibodies diluted in antibody buffer at 4˚C overnight or at RT for 2h. Membranes were then incubated at RT for 1h in donkey anti-mouse or donkey anti-rabbit secondary antibodies at 1/10,000 dilution (Tb. 2-4). Three 10min washes using TBS-T were performed following each antibody incubation. Membranes were developed by scanning on the LI-COR system (LICOR, USA). Protein expression was quantified via densitometry analyses; median signal background was deducted, and expression normalised for loading against vinculin or actin (Image Studio Lite: v5.2). Protein expression

is given as relative expression normalised for loading (AU) ±SEM or change from control (%) ±SEM.

Table 2-4

Antibody	Dilution factor	Buffer	Manufacturer/ Product number
Primary antibodies			
Actin	1/10,000	5% BSA TBS-T	Abcam/#8226
Akt	1/1000	5% BSA TBS-T/1% milk TBS-T	Cell Signalling/#9272
Rb CaSR (aa151-376)	1/1000	5% BSA TBS-T	Abcam/#137408
Ms CaSR (aa200-300)	1/1000	5% BSA TBS-T	Abcam/#19347
p44/42 MAPK (Erk1/2)	1/2000	1% milk TBS-T	Cell Signalling/##9102L
Perilipin-1	1/1000	5% BSA TBS-T	Cell Signalling/#9349
Phospho-AKT (Ser473)	1/1000	5% BSA TBS-T/1% milk TBS-T	Cell Signalling/#9271
Phospho-p44/42 MAPK (Erk1/2) (Thr202/Tyr204)	1/2000	1% milk TBS-T	Cell Signalling/#9101
Phospho-p90RSK (Ser380)	1/2000	1% milk TBS-T/½ Seablock TBS-T	Cell Signalling/#12032
RSK1/RSK2/RSK3	1/2000	1% milk TBS-T	Cell Signalling/#9347
Vinculin	1/2000	5% BSA TBS-T	Thermo/#700062
Secondary antibodies			
Donkey anti-Rabbit IgG (H+L) Cross-Adsorbed, DyLight 800	1/10,000	*	Thermo Fisher/#SA5-10044
Donkey anti-Mouse IgG (H+L) Cross-Adsorbed, DyLight 680	1/10,000	*	Thermo Fisher/#SA5-10170

Table 2-4: Antibodies used in western blot analyses.

Unless otherwise stated, antibody incubations were conducted in TBS-Tween20 supplemented with milk, BSA or Seablock. *=buffer is the same as primary antibody buffer. AKT=Protein kinase B; BSA=Bovine serum albumin; CaSR=Calcium sensing receptor; ERK=Extracellular Signal-Regulated Kinase; p90RSK/RSK= p90 ribosomal S6 kinase; TBS-T=Tris-buffered saline-Tween20.

2.3 Animal

2.3.1 Mouse strains

All animal procedures were carried out in accordance with the Home Office Animals (Scientific Procedures) Act, 1986, under project licenses 70/9021 (University of Glasgow 2018-2021) and PP0895181 (University of Glasgow 2021-onwards). CaSR homozygous floxed mice were obtained from The Jackson Laboratory (stock #030647, $Casr^{tm1Mrpk}$). The adiponectin Cre mouse was a gift from Dr Dominic Withers, sourced originally from The Jackson Laboratory (stock #028020, B6.FVB-Tg(Adipoq-cre)1Evdr/J). CaSR homozygous floxed mice were paired with Cre+ mice to produce homozygous floxed/Cre- ($CaSR^{fl/fl}$) and homozygous floxed/Cre+ ($CaSR^{Ad-/-}$) offspring at a 1:1 ratio. Cre was maintained on a heterozygous background to avoid off-target effects. All mutant mice were maintained on a C57BL/6 background. Inbred C57BL/6 mice (strain OlaHsd) were obtained from Envigo (UK).

2.3.2 Housing and ear notch identification

Mice were caged with littermates of the same sex and stored in housing rooms with controlled humidity and temperature (22°C), operating under a 12-hour light/dark cycle. Mice accessed water and standard rodent chow *ad libitum*. Mice were ear notched at weaning for identification and genotyping.

2.3.3 Weight tracking, tissue isolation and mass

Following weaning, male and female $CaSR^{fl/fl}$ and $CaSR^{Ad-/-}$ mice aged 4-weeks were weighed weekly for a period of 15 weeks. Body weight is expressed as mean mass (g) ±SEM. At cull, the heart and both kidneys were collected and mass measured. Visceral gonadal adipose tissue (gAT) and subcutaneous inguinal adipose tissue (scAT) depots (Fig. 2-8) were carefully dissected and mass measured, expressed as mean mass (g) ±SEM. AT samples were immediately processed, or stored at -80°C for future analysis.

Figure 2-8

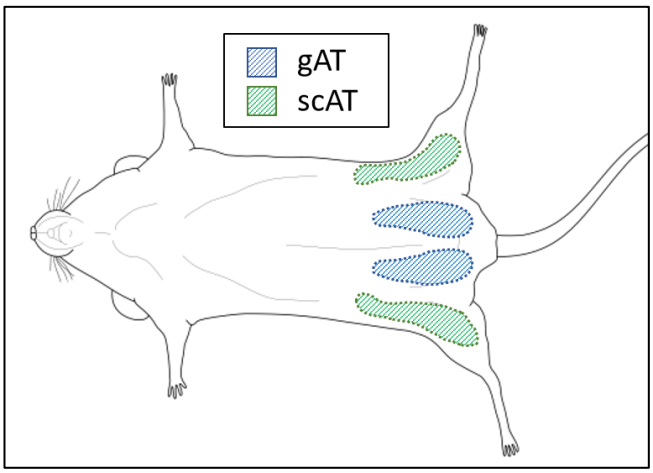

Figure 2-8: Anatomy of mouse adipose depots.

Mice were sacrificed by cervical dislocation. gAT is a visceral white adipose tissue depot found in the abdomen. gAT surrounds the ovaries and uterus in females or the testes and epididymis in males. scAT is located lateral to the hindlimb, between the skin and peritoneal wall. gAT=Gonadal white adipose tissue; scAT=Subcutaneous inguinal white adipose tissue.

2.3.4 Immunohistochemistry whole mount staining

gAT was excised from mice and immersed in 5% PFA. Following overnight fixation, gAT was rinsed with PBS and stored in 70% ethanol for a minimum of 24h. gAT was washed four times with PBS and minced finely into 1mm sections (Fig. 2-9). gAT segments were blocked in 5% donkey serum (Sigma, #D9663) in TBS with gentle agitation at 45RPM at 22°C for 2h. Tissue sections were incubated in 1/250 mouse anti-mouse CaSR primary antibody (Abcam, #137408) and 1/250 rabbit anti-mouse Perilipin-1 (PLN-1) primary antibody (Cell Signalling, #9349) overnight at 4°C, then 1/250 donkey anti-rabbit Alexa Fluor 594 secondary antibody (Thermofisher, #A-21207) and 1/250 donkey anti-mouse Alexa Fluor 488 secondary antibody (Thermofisher, #21202) at 22°C for 2.5h. Sections were stained with 1µg/mL DAPI in PBS at 22°C for 30min. Antibody incubations were conducted in 5% donkey serum in TBS, with three PBS washes between each incubation step. Finally, gAT segments were removed from PBS, blotted dry and mounted in ProLong Diamond Antifade Mountant (Thermofisher, #P36965). gAT samples were gently depressed under 1.5mm borosilicate coverslips and cured at RT overnight. gAT whole mount segments were imaged using the Zeiss Axio Imager A1 at 10x or 40x magnification. To quantify CaSR expression, three

images were collected from each mouse. Adipose tissue adipocytes were identified via adipocyte-specific PLN-1 staining. In each image, CaSR expression was evaluated by assessing mean CaSR staining intensity in 30 PLN-1 positive cells. Intensity was expressed as mean absolute intensity (AU) ±SEM.

Figure 2-9

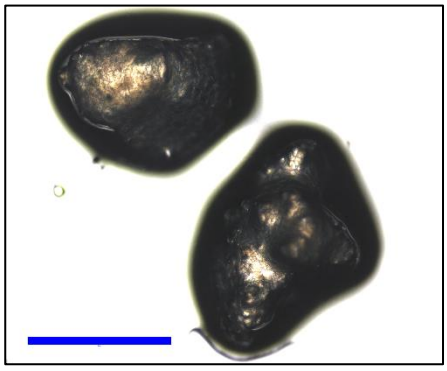

Figure 2-9: Whole mount gonadal adipose tissue sections.

Adipose was minced finely into 1mm sections. Scale bar=1mm.

2.3.5 Tissue dehydration and embedding

Adipose tissue was excised from mice and washed in PBS, placed immediately in ice-cold 4% PFA and incubated at 4°C for 48h. Tissues were washed three times in PBS and placed in 70% ethanol for short-term storage. Tissue processing was performed by Mrs. Nicola Britton (University of Glasgow). Tissue samples were dehydrated via an automated tissue processing protocol carried out by the Shandon Excelsior ES system (ThermoFisher, UK) as detailed (Tb. 2-5). Following dehydration, tissues were embedded in paraffin blocks using the Shandon Histocentre 3 (ThermoFisher, UK). Paraffin blocks were sectioned at 20µm until the tissue surface was revealed; thereafter, 5µm tissue sections were collected, mounted on silane-treated glass slides (#N/C260B, Dixon Science, UK) and cured at 60°C for 1h, then at 45°C for 12h. Slides were allowed to cool before staining.

Table 2-5

Step	Reagent	Time (min)
1	70% ethanol	30
2	95% ethanol	30
3	100% ethanol	30
4	100% ethanol	30
5	100% ethanol	45
6	100% ethanol	45
7	100% ethanol	60
8	100% xylene	30
9	100% xylene	30
10	100% xylene	30
11	Wax	30
12	Wax	30
13	Wax	45
14	Wax	45

Table 2-5: Tissue dehydration and paraffinization protocol.
Tissue samples were dehydrated and mounted in paraffin wax via an automated protocol carried out by the Shandon Excelsior ES system.

2.3.6 Haemotoxylin and eosin staining

Staining was performed by Lynn Stevenson (Histology service, University of Glasgow). Sections were deparaffinized and rehydrated using histoclear and cumulative concentrations of ethanol (Tb. 2-6a). Following deparaffinization, slides were then subjected to haemotoxylin and eosin staining, as per a standard protocol (Tb. 2-6b). Slides were mounted using DPX mountant (Sigma, #06522) and allowed to cure at 22˚C for 12h.

Image analysis was performed by assessing two tissue sections, separated by an interval of >30µm. Three images were collected from each section using the Olympus BX41 microscope system at x10 magnification. Cell size and number was measured manually (Image J: v1.52). In each image, 50 adjacent cells were measured and averaged to give mean cell area (AU) ±SEM in each condition. Cell number was assessed by counting the number of cells in a 500 pixel^2 area, expressed as mean cell number (AU) ±SEM.

Table 2-6

Protocol	Step	Reagent/procedure	Time (min)
(a) Deparaffinization & rehydration	1	Histoclear	7*
	2	100% ethanol	7
	3	95% ethanol	7
	4	70% ethanol	7
	5	dH_20	7
(b) Haemotoxylin & Eosin staining	1	Harris modified haemotoxylin	2
	2	dH_20/running	5
	3	70% ethanol/10 immersions	0.5
	4	Eosin Y solution	2
	5	95% ethanol	0.5*
	6	100% ethanol	1
	7	100% ethanol	7
	8	Histoclear	5*

Table 2-6: Histology protocols used to prepare adipose tissue sections.
Adipose tissue sections were prepared for cell sizing and counting experiments. **(a)** Slides were deparaffinized and rehydrated prior to the application of histological stains. *=step is repeated. **(b)** Cell dimensions were identified by staining adipose tissue with haemotoxylin and eosin. Slides remained in histoclear until coverslips could be mounted with DPX mountant.

2.3.7 Primary adipocyte isolation

Adipose pads were finely minced and incubated in serum-free DMEM supplemented with 1mg/mL collagenase A (Sigma, #10103578001) for 1h at 37°C. Adipocytes were mechanically dissociated by pipette aspiration at 10min intervals. Adipose digests were centrifuged at 800rcf for 5min at 22°C. Digests were washed in PBS and the centrifugation step repeated, causing fractional separation of adipocytes, stromal-vascular cells and lipid (Fig 2-10). Adipocytes, the stromal/vascular cell pellet and lipid fractions were collected and stored at -80°C for future analysis.

Figure 2-10

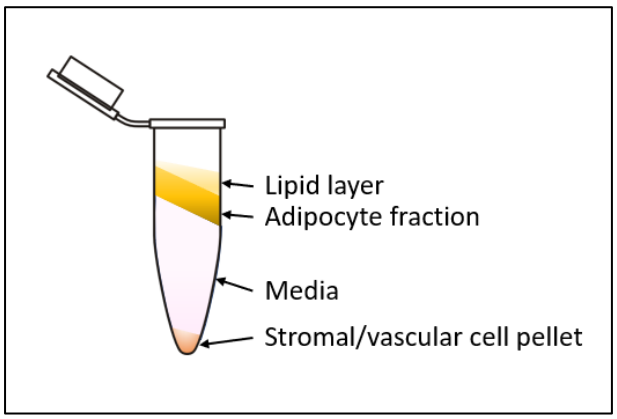

Figure 2-10: Fractional separation of adipose tissue digests.

Centrifugation at 800rcf for 5min causes fractional separation of the adipose tissue digest. The uppermost fraction is lipid. Following removal of the lipid layer, adipocytes were collected by gentle aspiration. The remaining stromal-vascular fraction was collected separately.

2.3.8 Primary BMSC isolation

Bone marrow stem cell (BMSC) isolation was performed in entirety by Mrs. Noha Alshuwayer (University of Glasgow). Femurs were dissected, placed in ice-cold PBS and carefully cleaned to remove muscle and tendon tissue. Femurs were sterilised using 70% ethanol and rinsed thoroughly with PBS. To release BMSCs femurs were cut at both ends and flushed of bone marrow using PBS and a 26G needle. The bone marrow suspension was passaged through a 70μM cell strainer and collected in 10mL PBS. BMSCs were centrifuged at 500rcf, 4°C for 10min and the cell pellet prepared for end-point PCR analysis as described previously.

2.3.9 Basic myography studies

Male C57BL/6 mice aged 8-12 weeks and transgenic mice aged 18-22 weeks were sacrificed by cervical dislocation. The thoracic aorta was excised and placed immediately in ice-cold PBS. Aortic segments were dissected to remove PVAT and cut into 2mm rings, as per standard myography protocol. Where there was a requirement for PVAT to be retained, aortic segments were dissected with minimal PVAT disruption (+PVAT) and compared to segments where PVAT was removed (-PVAT). Unless otherwise stated, experiments were carried out in aortic rings with intact (+E; >60% function preserved) endothelium. Denuded

aortic rings (-E; <20% function preserved) were used in experiments to assess the role of the vascular endothelium.

Technical assistance was provided by Mr. John McAbney (University of Glasgow). Aortic rings were mounted on 40µm wire in water baths (Danish Myo Technology) containing physiological salt solution (PSS; 130mM NaCl, 4.7mM KCl, 1.2mM $MgSO_4.7H_2O$, 24.9mM $NaHCO_3$, 1.2mM KH_2PO_4, 2.5mM $CaCl_2$ and 11.1mM glucose), gassed with 95% O_2 and 5% CO_2. Aortic ring preparations were warmed to 32°C and allowed to equilibrate for 30min. Vessels were normalised to 9.81mN to standardise vessel internal circumference and facilitate optimal maximum active tension. Following 15min equilibration, vessels were exposed to KPSS (PSS with 62.5mM KCl) to establish maximal vascular contraction. Vessels were washed three times in PSS, three times in reduced $CaCl_2$ (1mM) PSS and allowed to generate a steady baseline.

Cumulative concentration response curves conducted in series for the α_1-adrenoreceptor agonist phenylephrine (PE; $1x10^{-9}$M - $3x10^{-5}$M), the muscarinic $(M)_2$-receptor agonist acetylcholine (ACh; $1x10^{-9}$M - $3x10^{-5}$M) and the nitric oxide donor sodium nitroprusside (SNP; $1x10^{-10}$M - $3x10^{-6}$M). Aortic rings were pre-treated in some experiments (Tb. 2-7). In C57BL/6 PVAT preparations, control and treated PE cumulative concentration response curves were conducted in series in the same vessel segment. Myograph readouts were generated using PowerLab hardware (ADInstruments, UK) and recorded (LabChart: v8). PE vascular responses are expressed as mean contraction relative to KPSS contraction (%KPSS) ±SEM, while ACh and SNP responses are given as mean relaxation relative to PE pre-constriction (% $1x10^{-6}$M PE pre-constriction) ±SEM.

Table 2-7

Treatment	Concentration (M)
Standard/baseline $[Ca^{2+}]_o$	$1x10^{-3}$
High $[Ca^{2+}]_o$	$2.5x10^{-3}$
Cinacalcet	$1x10^{-6}$
NPS-2143	$1x10^{-6}$
L-Phe	$1x10^{-3}$
ADMA	$3x10^{-6}$

Table 2-7: Pre-treatment parameters of aortic rings.

Reagents were added to water baths 15min before PE dose-response curves were conducted on C57BL/6 aortic rings. 1mM $CaCl_2$ ($[Ca^{2+}]_o$) physiological salt solution was used to wash out vessel segments between subsequent dose-response curves. ADMA=Asymmetric dimethylarginine; PE=Phenylephrine; L-Phe=L-Phenylalanine.

2.3.10 Adipose transfer myography studies

To examine the ability of adipose tissue to mediate vascular tone, paired female $CaSR^{fl/fl}$ and $CaSR^{Ad-/-}$ mice aged 18-21 weeks were sacrificed. Gonadal adipose tissue was dissected and placed immediately in ice-cold PBS. Aortas were prepared for myography studies as in section 2.3.9. Isolated $CaSR^{fl/fl}$ and $CaSR^{Ad-/-}$ gonadal tissue was dissected to a final weight of 600mg and incubated at 37°C in 5mL reduced $CaCl_2$ (1mM) PSS gassed with 95% O_2 and 5% CO_2 for 4h. Gonadal adipose tissue was halved by weight and transferred along with 2mL of adipose-conditioned media and 3mL reduced $CaCl_2$ PSS to water baths containing $CaSR^{fl/fl}$ or $CaSR^{Ad-/-}$ aortas (Fig. 2-11). Vessel segments were equilibrised for 30min before performing phenylephrine cumulative concentration response curves (PE; 1x10-9M - 1x10-5M).

Figure 2-11

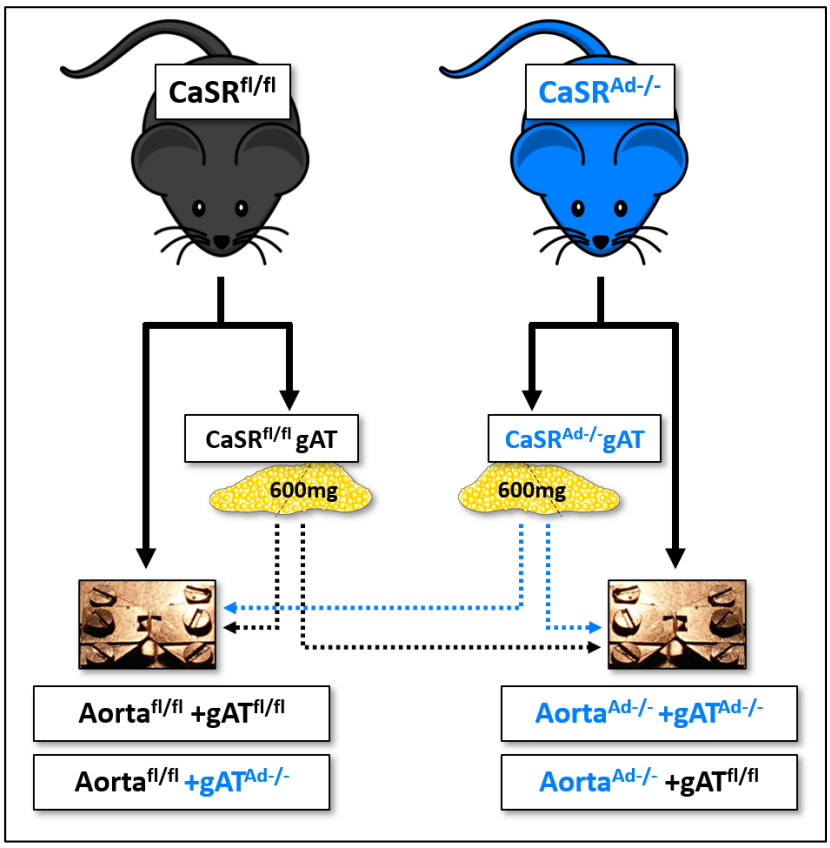

Figure 2-11: Adipose transfer myography studies.

$CaSR^{fl/fl}$ and $CaSR^{Ad-/-}$ were sacrificed in pairs on the day of the experiment. Aortas were prepared for vascular myography studies. Gonadal adipose tissue (gAT) was excised, weighed placed in water baths in reduced (1mM) $CaCl_2$ physiological salt solution (37°C; 95% O_2, 5% CO_2) for 4h. Gonadal AT and adipose-conditioned media derived from $CaSR^{fl/fl}$ mice was halved, with each half being transferred to a water bath containing either a $CaSR^{fl/fl}$ or $CaSR^{Ad-/-}$ vessel segment. The procedure was repeated for $CaSR^{Ad-/-}$ mice. CaSR=Calcium-sensing receptor.

2.3.11 Tail-cuff plethysmography

Blood pressure was measured in mice using non-invasive transmission photoplethysmography. In brief, the tail-cuff plethysmography system measures blood pressure by detecting the amount of light which is transmitted through the tail. Following a systolic heart contraction, the corresponding pulse wave travels through the vascular system, increasing pressure and dilation in tail blood vessels. During diastole, pressure and dilation is decreased in tail blood vessels. Since increased vessel pressure and dilation increases the amount of light which

is scattered by the blood vessels in the tail, measurement of light scatter allows systolic and diastolic pressure to be determined. As the tail-cuff inflates, it begins to occlude blood flow to the tail; diastolic pressure is identified when the mean signal begins to decay from baseline. Systolic pressure is identified when the mean signal falls and achieves a steady state (Fig. 2-12a).

Mice were gently captured using non-aversive handling and placed on the BP-2000 Blood Pressure Analysis System (Visitech Systems). Mice were restrained with magnetic holders, their tails fed through the inflatable occlusion cuff and secured with tape (Fig. 2-12b). Mice were preheated and held at 37°C throughout the procedure. To control stress, animals remained on the system for a maximum of 30min.

Systolic blood pressure (SBP), diastolic blood pressure (DBP), mean arterial blood pressure (MAP) and heart rate (HR) measurements were collected and recorded simultaneously (BP-2000 Blood Pressure analyst: vbeta, 2015). Mice received a minimum of four training sessions to allow habituation to the tail-cuff system. Mice were considered habituated when there was a reduction in faeces production and the standard deviation of measurement sets stabilised (Fig. 2-12c,d). After training completion, blood pressure was measured in mice aged 12-weeks, then every two weeks until cull at 18-weeks. At each time point, two blood pressure and HR measurement sets were performed on separate days and averaged. Each measurement set consisted of 10 preliminary and 15 definitive measurements, separated by 2.5s intervals. Measurement sets with <10 successful SBP measurements were excluded from analysis. SBP, DBP and MAP is given as mean blood pressure (mmHg) ±SEM. Heart rate is expressed as mean beats per minute (bpm) ±SEM.

Figure 2-12

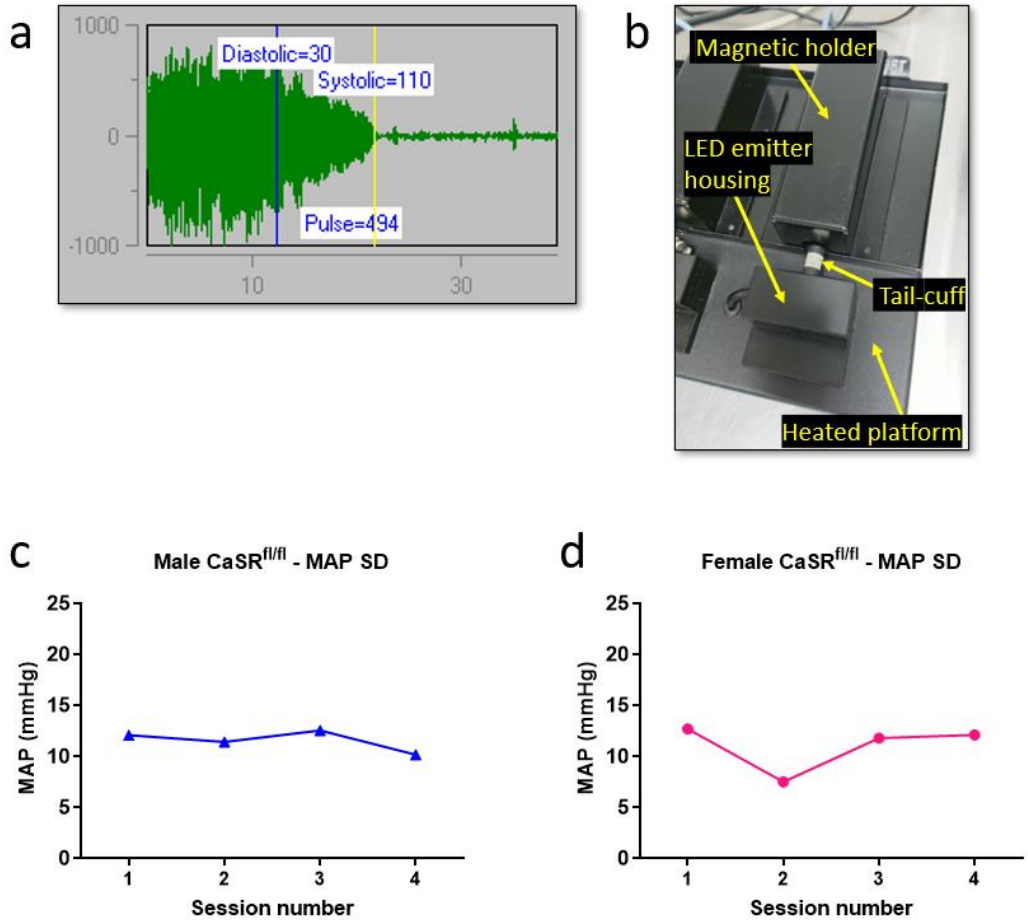

Figure 2-12: Tail-cuff plethysmography in mice.

The BP-2000 Blood Pressure Analysis System (Visitech) was used for all mouse blood pressure measurements in this study. **(a)** Increased vessel pressure and dilation increases light scatter. As the tail-cuff inflates, it begins to occlude blood flow to the tail. Decreased pressure and dilation reduces light scatter; diastolic pressure is identified when the mean signal decays from baseline blood pressure. Systolic pressure is identified with further tail-cuff inflation, where mean signal falls and achieves a steady state. **(b)** Mice were restrained using magnetic holders and their tail to be fed through the inflatable occlusion cuff. The platform was heated to 37°C to promote tail blood vessel dilation. An LED light source and reader is used to measure light scattered by tail blood vessels. **(c-d)** The standard deviation of MAP was monitored during habituation; stabilisation of standard deviation indicated that mice had acclimatised to the system.

2.3.12 Tail vein bleeds

Mice were warmed to 37°C for 10min to dilate tail blood vessels. Mice were then placed in a cylindrical holder and robustly secured to permit access to the tail and minimise movement during the procedure. Lateral tail veins were identified and venesection performed using a small scalpel. Blood was collected into lithium heparin polypropylene tubes (Teklab, #H10VPP) and placed immediately on ice. Blood samples were centrifuged at 14,000rcf, 4°C for 10min. Serum and blood pellet fractions were separated into new tubes and stored at -80°C for future use.

2.3 Statistical analysis

Students *t*-tests, one-way and two-way ANOVA analyses were performed where n≥3, with post-hoc tests where appropriate. Myography data were compared by extra sum of squares F-test, using EC_{50} and maximum response values of best fit, fitted to a nonlinear regression model. Weight gain data were compared by extra sum of squares F-test using EC_{50} and maximum response values of best fit, fitted to a third order polynomial regression model and adjusted for multiple comparisons (Graphpad Prism: v9). Breeding and litter data were assessed by test of proportion and test of two proportions (Minitab: v20.3).

Chapter Three

HEK293-CaSR cells

Chapter 3: HEK293-CaSR cells

3.1 Introduction

The calcium-sensing receptor (CaSR) is stimulated by a broad and varied range of ligands, including amino acids. At supraphysiological concentrations, 17 from the 20 common amino acid species sensitise intracellular Ca^{2+} ($[Ca^{2+}]_i$) signalling in response to stimulation by exogenous Ca^{2+} ($[Ca^{2+}]_o$) in CaSR transfected HEK293 cells (Conigrave, Quinn and Brown, 2000). In a very recent study, Liu *et al*. examined interactions between amino acids and CaSR using high sensitivity FRET-biosensor assays in isolated cell membranes (Liu *et al.*, 2020). Of the 17 CaSR-active amino acids proposed by Conigrave and colleagues, 15 acted to decrease the EC_{50} for $[Ca^{2+}]_o$-induced conformational changes in FRET-based CaSR biosensors, confirming their role as allosteric agonists. Interestingly, L-Arg was demonstrated as a CaSR-active amino acid in both cases. Given that the CaSR is broadly sensitive to L-amino acids and asymmetric dimethylarginine (ADMA) competes with L-Arg at NOS and amino acid transporters (Teerlink *et al.*, 2009), a potentially novel CaSR ligand may be realised in ADMA. In a HEK293 model of CaSR overexpression, our group has previously shown that $GdCl_2$ treatment leads to increased $[Ca^2]_i$. ADMA potentiates this response, while the ADMA effect is abolished by the calcilytic NPS-2143 (Dowsett *et al.*, 2022). Previously, L-amino acids have been shown to regulate key CaSR enzymes, such as extracellular signal-regulated kinase ($ERK_{1/2}$) (Lee *et al.*, 2007). Therefore, ADMA may act at CaSR to influence CaSR-dependent intracellular signalling in HEK293-CaSR cells.

Among several cell lines used to investigate CaSR signalling, CaSR transfected HEK293 cells have played a central role in delineating important features of CaSR signalling, such as $[Ca^{2+}]_o$ mobilisation, cyclic AMP (cAMP) inhibition and regulation of intracellular signalling cascades (Gerbino and Colella, 2018). Despite the utility of HEK293 cells in CaSR studies, accumulating evidence indicates that CaSR signalling is agonist-specific (Davey *et al.*, 2012) and is differentially regulated between cell types (Magno, Ward and Ratajczak, 2011). Accordingly, heterologous CaSR overexpression models must be characterised and carefully selected based on the objectives of the study. CaSR-induced $ERK_{1/2}$

signalling has been documented in many cell types, including HEK293 cells (Lee *et al.*, 2007; Magno, Ward and Ratajczak, 2011; Oh *et al.*, 2011; Peng *et al.*, 2014). On the other hand, descriptions of CaSR-mediated protein kinase B (AKT) activation are limited to native cell lines and CaSR transfected 786-O renal cells (Magno, Ward and Ratajczak, 2011; Frees *et al.*, 2018). It is not clear whether CaSR signalling implicates AKT in transgenic HEK293-CaSR cells. Considering that HEK293 cells are used extensively to model CaSR signalling, the effect of CaSR signalling on $ERK_{1/2}$ and AKT activation should be fully characterised.

CaSR-mediated intracellular signalling and its resulting biological effects have been intensively studied using heterologous and native cell systems (Conigrave and Ward, 2013) and animal models (Chang *et al.*, 2008; Toka *et al.*, 2012; Sundararaman *et al.*, 2021). However, the transcriptional consequences of CaSR signalling and thus genes linking CaSR signalling cascades with its effects on cell biology remains very poorly described. In HEK293 cells, the CaSR regulates key nuclear transcription factors Elk-1, Egr-1 and AP-1, suggesting that CaSR could potentially mediate an array of transcriptional responses in this model (Thiel, Lesch and Keim, 2012). If CaSR regulates transcription in HEK293-CaSR cells, then this system could be used to examine the effect of amino acids, such as ADMA, on CaSR-mediated transcription.

3.2 Aims

- To confirm that HEK293-CaSR cells express functional CaSR.
- To characterise $[Ca^{2+}]_o$- and CaSR agonist-induced intracellular signalling in HEK293-CaSR cells.
- To examine whether ADMA affects CaSR-dependent signalling cascades.
- To evaluate HEK293-CaSR cells as a model of CaSR-dependent gene transcription, in turning investigating whether ADMA regulates CaSR-dependent genes.

3.3 Results

3.3.1 CaSR overexpression

Image analysis and immunoblotting were used to validate CaSR expression in transfected HEK293 cells. To show that induced HEK293 cells express CaSR, HEK293 cells transfected with empty vector (vector control; HEK293-vec) and HEK293 cells transfected with vector containing human c-myc-tagged CaSR (HEK293-CaSR) were treated with doxycycline (DX) and monitored for c-myc expression using immunofluorescence analyses. HEK293-vec control cells which received media only demonstrated low signal intensity, corresponding to absent c-myc expression. Signal intensity in HEK293-CaSR cells (3.7±1.0) was unchanged by 0.01, 0.02, 0.1 and 0.2 µg/ml DX ($p>0.05$), but was significantly elevated by 0.5 µg/ml DX (12.7±3.4, $p=0.0408$). In contrast, c-myc signal intensity in HEK293-vec cells (2.8±0.4) was not enhanced by 0.5µg/ml DX (2.7±0.4, $p>0.05$). When signal intensity was compared in HEK293-vec and HEK293-CaSR cultures treated with 0.5 µg/ml DX, signal intensity was significantly enhanced in HEK293-CaSR cells ($p=0.0210$; Fig. 3-1a, b).

Next, HEK293-vec and HEK293-CaSR were treated with DX and CaSR examined with immunoblotting using a polyclonal rabbit CaSR-specific antibody. Densitometry analyses identified CaSR protein migrating at positions corresponding to two standard molecular masses; ~260kDa (upper band) and ~130kDa (lower band). These bands are consistent with the expected size of CaSR in its dimeric and monomeric form, respectively. CaSR expression in vector-only cells was not detectable in any experiments and was not quantified. The CaSR upper band in HEK293-CaSR controls was significantly raised following 0.1 µg/ml DX (13.5±1.1-fold, $p=0.0368$). Unexpectedly, this band was unchanged with 0.01, 0.02, 0.2 and 0.5 µg/ml DX, though densitometry analyses were highly variable ($p>0.05$; Fig. 3-2a, c). As with the higher density upper band, the CaSR lower band was not altered by 0.01 or 0.02 µg/ml DX ($p>0.05$). However, CaSR expression at 130kDa was significantly enhanced following treatment with 0.1 µg/ml (53.1±14.8-fold, $p=0.0170$), 0.2 µg/ml (49.8±10.1-fold, $p=0.0270$) and 0.5 µg/ml DX (53.3±15.5-fold, $p<0.0165$; Fig. 3-2b, c).

HEK293-CaSR cells treated with 0.1 µg/ml DX demonstrated marked expression of CaSR at both molecular masses. Under these conditions, expression of the 260kDa comprised 68±9% of the total immunoreactive protein. To confirm that these results were specific to CaSR expression, a second monoclonal mouse CaSR-specific antibody was used on HEK293-CaSR cells treated in the absence and presence of 0.1µg/ml DX. As seen before with c-myc-specific staining, control untreated HEK293-CaSR cells demonstrated low signal intensity (8.2±3.0) corresponding to low CaSR expression which was markedly elevated by 0.1 µg/ml DX (38.9±7.2, p=0.0169; Fig. 3-2d, e). CaSR expression in HEK293-CaSR cells was induced using 0.1µg/ml DX in subsequent experimentation.

Figure 3-1

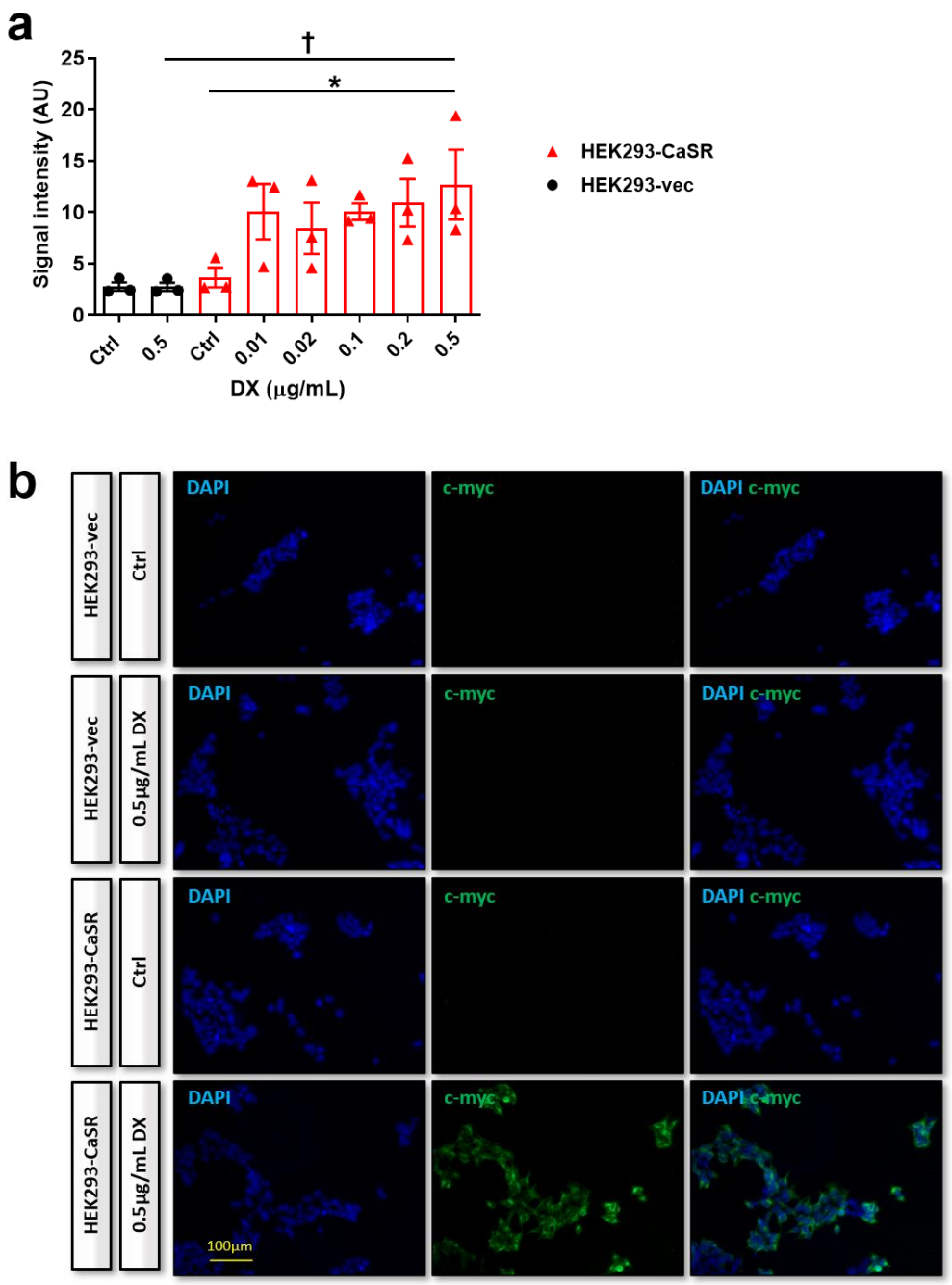

Figure 3-1: c-myc protein is expressed by induced HEK293-CaSR cells. **(a)** Immunofluorescent staining for c-myc is increased in CaSR overexpressing HEK293 (HEK293-CaSR) cells following doxycycline (DX) treatment. Signal intensity was low in vector-only control HEK293 (HEK293-vec) cells. **(b)** Representative image of positive immunofluorescent staining of c-myc in HEK293 cells. Mean±SEM. One-way ANOVA (a). *p<0.05 HEK293-CaSR Ctrl vs HEK293-CaSR +0.5µg/ml DX, †p<0.05 HEK293-vec +0.5µg/ml DX vs HEK293-CaSR +0.5µg/ml DX. Magnification 10X. Scale bar=100µm. CaSR=Calcium sensing receptor.

Figure 3-2

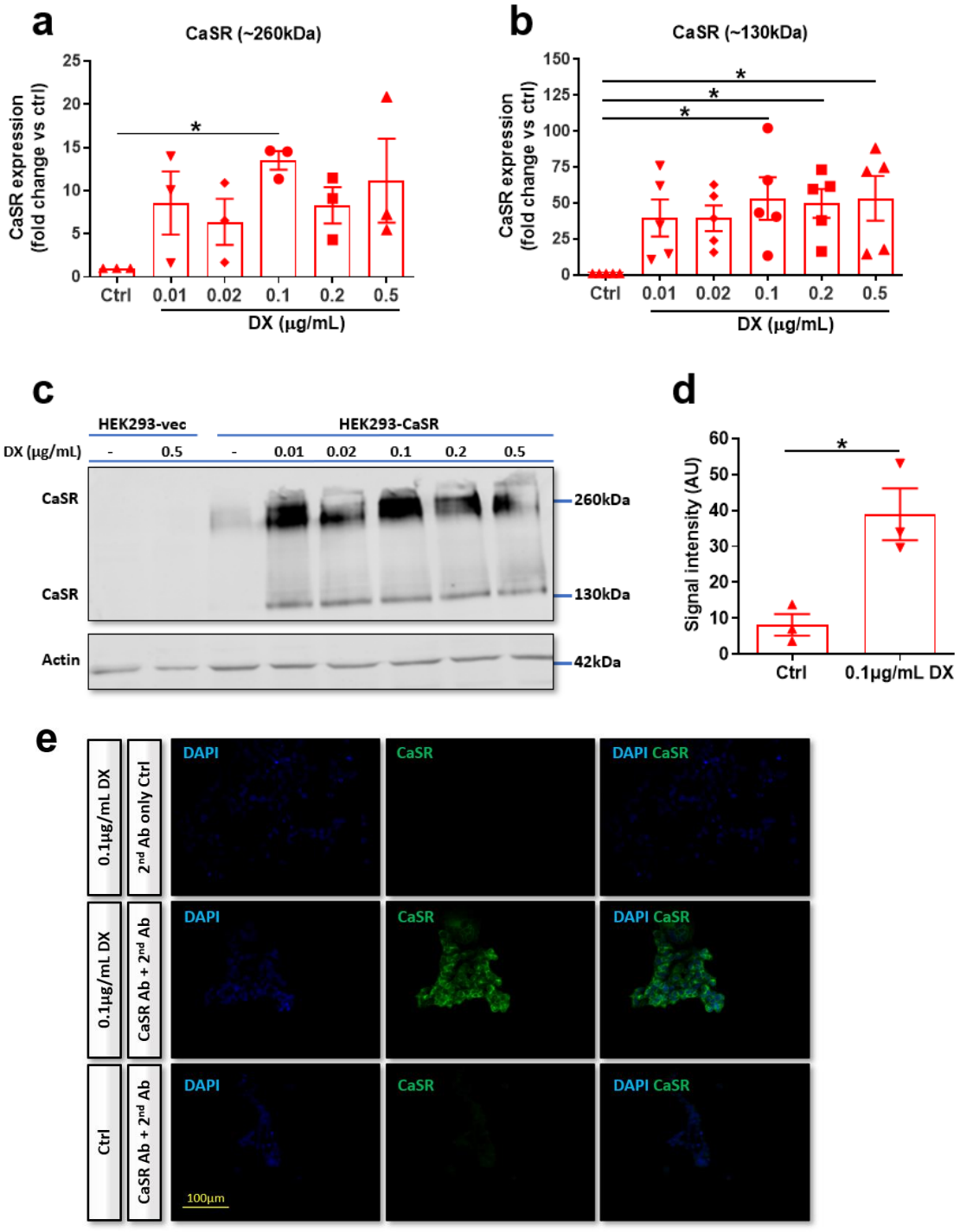

Figure 3-2: CaSR protein is expressed by induced HEK293-CaSR cells. **(a)** CaSR protein is identified at ~260kDa in CaSR overexpressing HEK293 (HEK293-CaSR) cells treated with 0.1µg/ml doxycycline (DX). **(b)** CaSR protein is identified at ~130kDa in HEK293-CaSR cells treated with 0.1, 0.2 and 0.5µg/ml doxycycline (DX). **(c)** Representative western blot image of CaSR protein in HEK293-CaSR and vector-only control HEK293 (HEK293-vec) cells

with and without DX treatment. CaSR was identified by two bands; an upper band and lower band migrating at 260kDa and 130kDa, respectively. CaSR protein is not detected in HEK293-vec cells. **(d)** Immunofluorescent staining for CaSR is increased in HEK293-CaSR cells following DX treatment. **(e)** Representative image of positive immunofluorescent staining of CaSR in HEK293-CaSR cells. Mean±SEM. One-way ANOVA (a,b). Unpaired t-test (d). *p<0.05 vs untreated Ctrl. Magnification 20X. Scale bar=100μm. CaSR=Calcium sensing receptor.

3.3.2 CaSR function

HEK293-CaSR cells showed robust CaSR expression following DX treatment. To examine CaSR function, HEK293-vec and HEK293-CaSR cells were exposed to $GdCl_2$, an orthosteric CaSR agonist, and monitored for $[Ca^{2+}]_i$ mobilisation using Flexstation plate reader analyses. HEK293-vec cells were insensitive to $GdCl_2$. Compared to HEK293-vec cells, increasing concentrations of $GdCl_2$ elicited a dose-dependent increase in $[Ca^{2+}]_i$ flux (E_{max}=4.5±0.1%, pEC_{50}=0.05±0.7, $p<0.0001$; Fig. 3-3a), showing that $GdCl_2$ stimulation in HEK293-CaSR cells stimulates CaSR-dependent $[Ca^{2+}]_i$ signalling.

In the literature, $GdCl_2$-induced $[Ca^{2+}]_i$ is reported in the μM range (Pearce *et al.*, 1996), so this study investigated the effect of differing physiological incubation buffers on $GdCl_2$-induced $[Ca^{2+}]_i$ signalling. The pEC_{50} for $GdCl_2$-induced $[Ca^{2+}]_i$ was 0.030±0.004 (0.94mM) in HBSS buffer. In HEPES buffer, the pEC_{50} for $GdCl_2$-induced $[Ca^{2+}]_i$ was 2.157±0.047 (7μM) and was significantly sensitised compared to HBSS ($p<0.0001$; Fig. 3-3b). As $GdCl_2$-mediated responses were detectable and reproducible in HBSS buffer, HBSS was used in subsequent experiments.

In the above experiments conducted in HBSS buffer, the pEC_{50} for $GdCl_2$-induced $[Ca^{2+}]_i$ release for HEK293-CaSR in HBSS buffer lies between 0.05 (0.89mM) and 0.03 (0.94mM). To confirm that $[Ca^{2+}]_i$ responses in HEK293-CaSR cell were regulated by CaSR, HEK293 cells were preincubated in the absence and presence of the CaSR inhibitor NPS-2143 and stimulated with $GdCl_2$ concentrations below (0.5mM) and above (1mM) the pEC_{50} for $GdCl_2$-induced $[Ca^{2+}]_i$ release. Following stimulation with 0.5mM $GdCl_2$, $[Ca^{2+}]_i$ responses were comparable in HEK293-vec cells (0.22±0.03) and HEK293-CaSR cells (0.25±0.06, $p>0.05$). Since 0.5mM $GdCl_2$ did not stimulate $[Ca^{2+}]_i$ in either HEK293-vec or HEK293-CaSR cells, there was no inhibitory effect of NPS-2143 ($p>0.05$; Fig. 3-3c).

Though 0.5mM $GdCl_2$ was unable to elicit $[Ca^{2+}]_i$ mobilisation, $[Ca^{2+}]_i$ was markedly increased in HEK293-CaSR cells stimulated with 1mM $GdCl_2$ (2.7±0.61) compared to HEK293-vec cells (0.19±0.03, $p=0.0027$). $[Ca^{2+}]_i$ flux was not stimulated with 1mM $GdCl_2$ in HEK293-vec cells, so NPS-2143 again had no effect

(p>0.05). However, $[Ca^{2+}]_i$ flux in HEK293-CaSR cells stimulated with 1mM $GdCl_2$ (2.7±0.61) was inhibited 76% with NPS-2143 (0.66±0.33, p=0.0092; Fig. 3-3d).

Figure 3-3

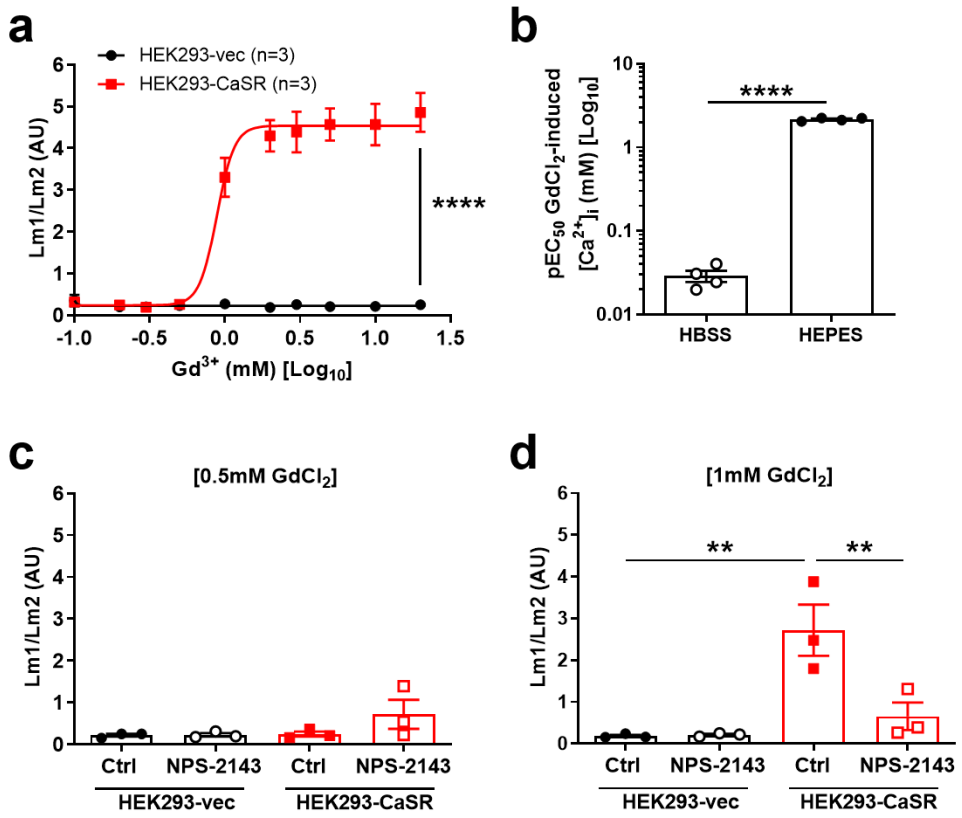

Figure 3-3: $GdCl_2$ stimulates CaSR-dependent $[Ca^{2+}]_i$ release in HEK293-CaSR cells.

(a) $GdCl_2$ stimulates intracellular Ca^{2+} release ($[Ca^{2+}]_i$) release in CaSR overexpressing HEK293 (HEK293-CaSR) cells. Control vector-only HEK293 (HEK293-vec) cells are insensitive to $GdCl_2$. **(b)** The pEC_{50} for $GdCl_2$-induced $[Ca^{2+}]_i$ signalling is significantly increased in the presence of HEPES buffer compared to HBSS buffer. **(c)** $[Ca^{2+}]_i$ mobilisation is comparable in HEK293-vec and HEK293-CaSR cells stimulated with 0.5mM $GdCl_2$. NPS-2143 does not influence $[Ca^{2+}]_i$ flux in HEK293-vec or HEK293-CaSR cells. **(d)** $[Ca^{2+}]_i$ mobilisation is greater in HEK293-CaSR cells stimulated with 1mM $GdCl_2$ when compared to HEK293-vec cells. NPS-2143 does not influence $[Ca^{2+}]_i$ flux in HEK293-vec cells, but attenuates $[Ca^{2+}]_i$ in HEK293-CaSR cells. Mean±SEM. Two-way ANOVA (a), t-test (b), One-way ANOVA (c,d). **p<0.01, ****p<0.0001. CaSR=Calcium sensing receptor. HEPES= 4-(2-hydroxyethyl)-1-piperazineethanesulfonic acid; HBSS=Hank's balanced salt solution.

3.3.3 $[Ca^{2+}]_o$-induced $ERK_{1/2}$ and AKT signalling

Agonist-induced CaSR stimulation activates a variety of downstream enzymes. Among the many mediators which are known to be targeted by CaSR, phospholipases, AKT, and mitogen-activated protein kinase cascade mediators such as $ERK_{1/2}$ are perhaps best described (Magno, Ward and Ratajczak, 2011). In this study, CaSR overexpressing HEK293 cells were used as a model to evaluate CaSR-dependent activation of two key CaSR signalling enzymes, $ERK_{1/2}$ and AKT. HEK293-CaSR cells were treated with $CaCl_2$ (0-10mM) for 10min and $[Ca^{2+}]_o$-dependent $ERK_{1/2}$ and AKT activation assessed using immunoblot analyses. Increasing $[Ca^{2+}]_o$ had a significant, dose-dependent effect on HEK293-CaSR $ERK_{1/2}$ signalling with an EC_{50} of 4.44±0.2mM ($p<0.0001$; Fig. 3-4a,c). Compared to HEK293-CaSR control cells without $[Ca^{2+}]_o$ (0.2±0.1), 10mM $[Ca^{2+}]_o$ induced a maximum 11-fold increase in $ERK_{1/2}$ activation (2.4±0.5, $p<0.0001$; Fig. 3-4b,c).

Though $[Ca^{2+}]_o$ caused robust $ERK_{1/2}$ activation, increasing $[Ca^{2+}]_o$ led to highly variable AKT activation; however, there was no overall relationship between $[Ca^{2+}]_o$ dose and AKT signalling ($p>0.05$; Fig. 3-4d,f). Compared to HEK293-CaSR control cells without $[Ca^{2+}]_o$ (0.6±0.5), 10mM $[Ca^{2+}]_o$ did not stimulate AKT activation (0.5±0.4, $p>0.05$; Fig. 3-4e,f).

Figure 3-4

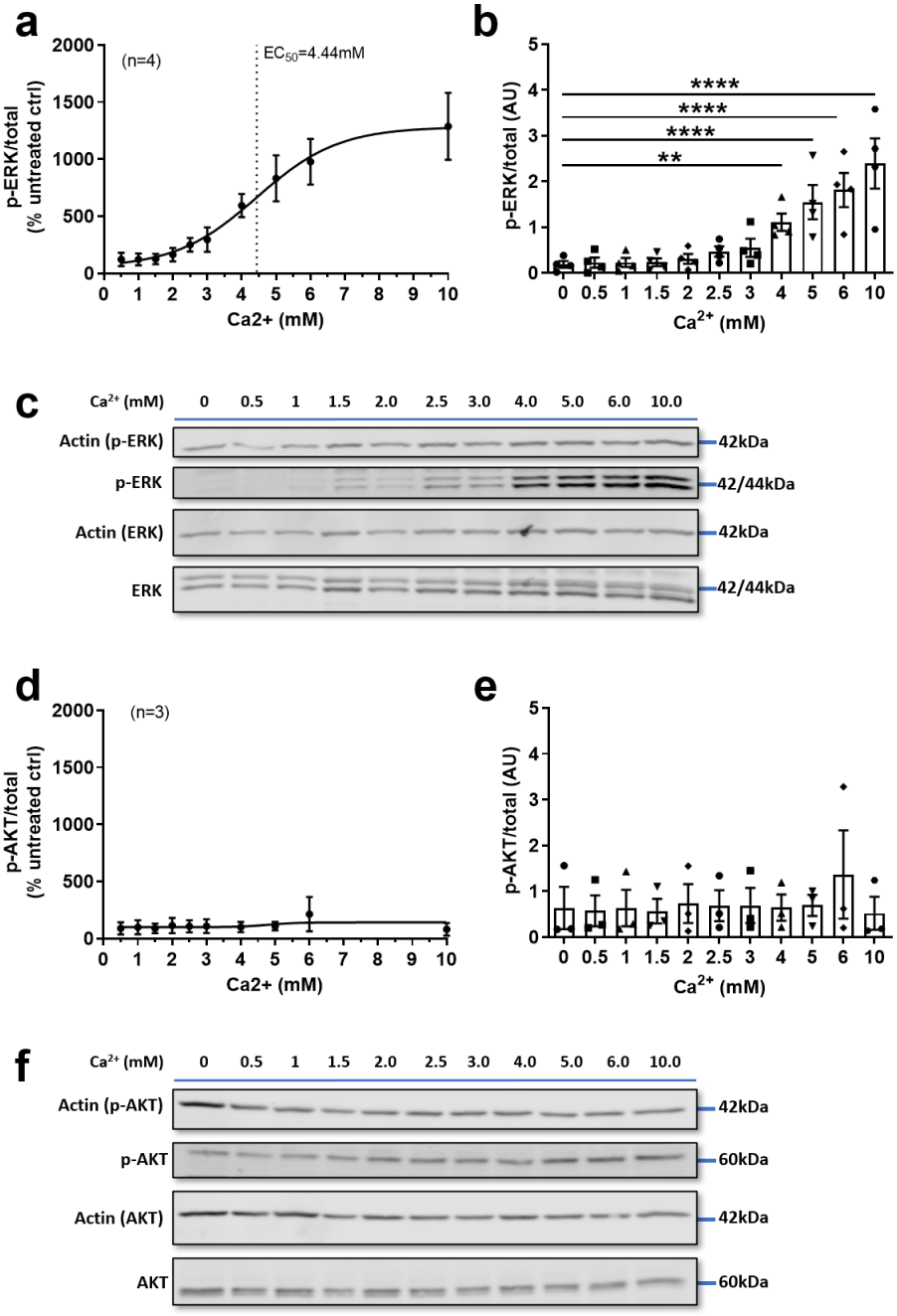

Figure 3-4: $[Ca^{2+}]_o$ stimulates $ERK_{1/2}$ in HEK293-CaSR cells.

(a) Curve fitting analyses demonstrate an EC_{50} of 4.44mM for $[Ca^{2+}]_o$-induced $ERK_{1/2}$ activation. **(b)** Extracellular $CaCl_2$ ($[Ca^{2+}]_o$) has a dose-dependent effect on $ERK_{1/2}$ activation in HEK293-CaSR cells. **(c)** Representative western blot image of total and phopho-$ERK_{1/2}$ protein (42/44kDa) demonstrating the effect of $[Ca^{2+}]_o$ in HEK293-CaSR cells. **(d)** Curve fitting analyses for $[Ca^{2+}]_o$-induced AKT activation. **(e)** $[Ca^{2+}]_o$ does not influence AKT activation in HEK293-CaSR cells. **(f)** Representative western blot image of total and phospho-AKT protein (60kDa demonstrating the effect of $[Ca^{2+}]_o$ in HEK293-CaSR cells. Mean±SEM.

One-way ANOVA (b,e), One-way ANOVA **p<0.01 vs Ctrl, ****p<0.0001 vs Ctrl. CaSR=Calcium sensing receptor.

3.3.4 CaSR-dependent $[Ca^{2+}]_o$-induced $ERK_{1/2}$ signalling

In the previous section, $ERK_{1/2}$ was induced by $[Ca^{2+}]_o$ in HEK293-CaSR cells. To investigate whether CaSR regulates $[Ca^{2+}]_o$-induced $ERK_{1/2}$ activation , HEK293-CaSR cells were treated with the CaSR type II (allosteric) agonist NPS R-568 (1μM) in the presence of variable (0-6mM) $[Ca^{2+}]_o$. As before, $[Ca^{2+}]_o$ had a significant effect on $ERK_{1/2}$ activation ($p<0.0001$). However, NPS R-568 acutely raised $ERK_{1/2}$ activation ($p<0.0001$). Multiple comparison analyses showed that there was no effect of NPS R-568 on $ERK_{1/2}$ activation in the absence of $[Ca^{2+}]_o$ ($p>0.05$), or when stimulated with low 0.5mM $[Ca^{2+}]_o$ ($p>0.05$). However, $ERK_{1/2}$ activation was significantly enhanced by NPS R-568 when HEK293-CaSR cells were stimulated with 1mM (Ctrl=0.3±0.1; +NPS R-568=1.5±0.0, p=0.0022), 2mM (Ctrl=0.3±0.1; +NPS R-568=2.0±0.1, $p<0.0001$) and 3mM $[Ca^{2+}]_o$ (Ctrl=0.8±0.1; +NPS R-568=2.2±0.3, p=0.0002), demonstrating that NPS R-568 sensitises $[Ca^{2+}]_o$-induced $ERK_{1/2}$ signalling. Unexpectedly, NPS R-568 did not elevate $ERK_{1/2}$ activation when cells were stimulated with high 6mM $[Ca^{2+}]_o$ ($p>0.05$; Fig. 3-5a,c).

NPS R-568 acutely stimulated $[Ca^{2+}]_o$-induced $ERK_{1/2}$ activation. To establish whether $[Ca^{2+}]_o$-induced responses were dependent on CaSR, HEK293-CaSR cells were treated with the CaSR inhibitor NPS-2143 (10μM) in the presence of variable (0-6mM) $[Ca^{2+}]_o$. $ERK_{1/2}$ activation was again raised by $[Ca^{2+}]_o$ ($p<0.0001$), but the effect was blunted by NPS-2143, which in contrast decreased $[Ca^{2+}]_o$-induced $ERK_{1/2}$ activation ($p<0.0001$). Post-hoc testing revealed no effect of NPS-2143 on $ERK_{1/2}$ activation when $[Ca^{2+}]_o$ was absent, following stimulation with 0.5mM or 1mM $[Ca^{2+}]_o$ ($p>0.05$). However, NPS-2143 significantly decreased $[Ca^{2+}]_o$-induced $ERK_{1/2}$ activation when HEK293-CaSR cells were stimulated with 2mM (Ctrl=1.0±0.2; +NPS-2143=0.3±0.1, p=0.0029), 3mM (Ctrl=1.6±0.1; +NPS-2143=0.4±0.1, $p<0.0001$) and 6mM $[Ca^{2+}]_o$ (Ctrl=3.5±0.3; +NPS-2143=0.6±0.1, $p<0.0001$; Fig. 3-5b, d), showing that NPS-2143 inhibits $[Ca^{2+}]_o$-induced $ERK_{1/2}$ responses.

Figure 3-5

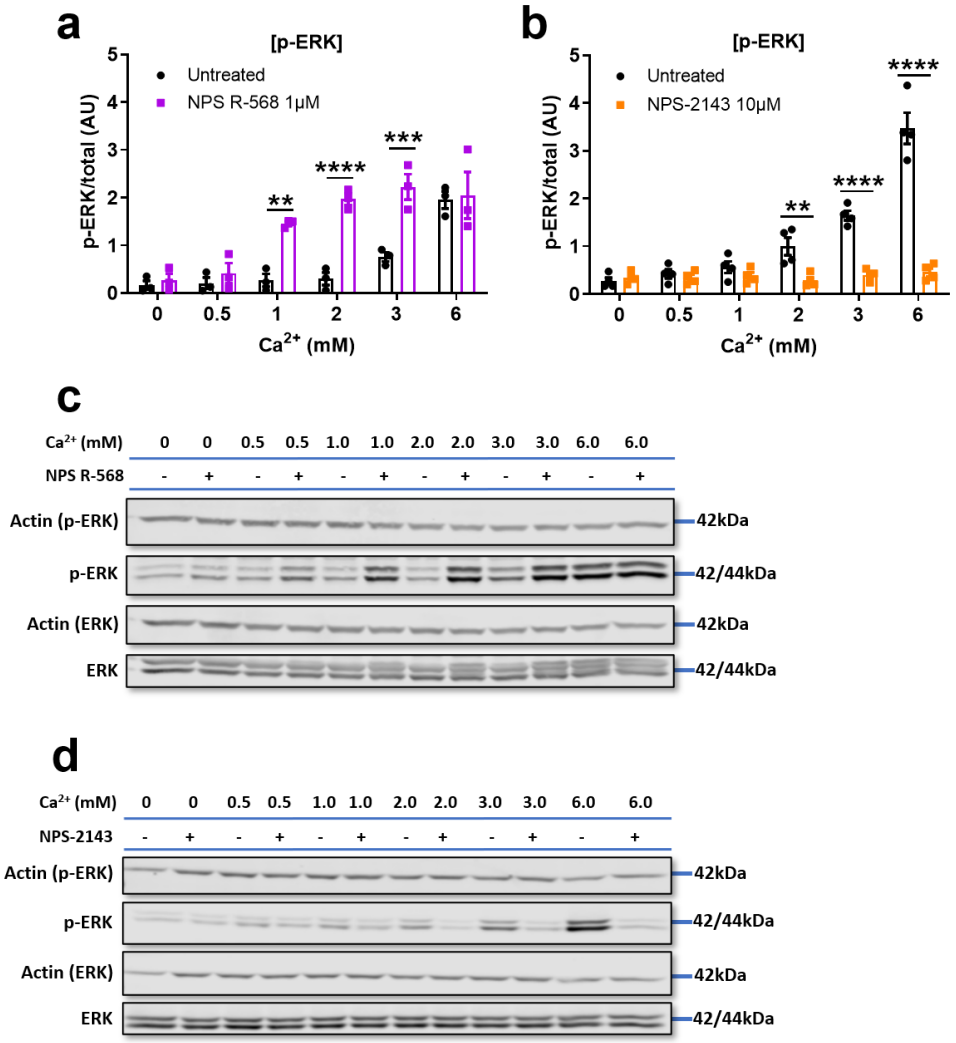

Figure 3-5: CaSR regulates $[Ca^{2+}]_o$-induced $ERK_{1/2}$ activation in HEK293-CaSR cells.

(a) NPS R-568 potentiates $ERK_{1/2}$ activation in HEK293-CaSR cells when stimulated with 1, 2 and 3mM extracellular $CaCl_2$ ($[Ca^{2+}]_o$). **(b)** NPS-2143 inhibits $ERK_{1/2}$ activation in HEK293-CaSR cells when stimulated with 2, 3 and 6mM $[Ca^{2+}]_o$. **(c)** Representative western blot image of total and phopho-$ERK_{1/2}$ protein (42/44kDa) demonstrating the effect of $[Ca^{2+}]_o$ and NPS R-568 in HEK293-CaSR cells. **(d)** Representative western blot image of total and phopho-$ERK_{1/2}$ protein (42/44kDa) demonstrating the effect of $[Ca^{2+}]_o$ and NPS-2143 in HEK293-CaSR cells. Mean±SEM. Two-way ANOVA (a,b). **p<0.01 vs Ctrl, ***p<0.001 vs Ctrl, ****p<0.0001 vs Ctrl. CaSR=Calcium sensing receptor; $ERK_{1/2}$=Extracellular signal-regulated kinase 1/2.

$ERK_{1/2}$ regulates cellular biology via activation of several downstream targets, such as s6 kinases (RSK) (Guo *et al.*, 2020). In heterologous 786-O renal cells, CaSR stimulation of $ERK_{1/2}$ coincides with p90RSK activation (Frees *et al.*, 2018). To establish whether $[Ca^{2+}]_o$ and CaSR regulates p90RSK in HEK293-CaSR cells, immunoblotting analyses were again performed following treatment with NPS R-568 or NPS-2143 in the presence of variable $[Ca^{2+}]_o$. As seen with $ERK_{1/2}$, P90RSK was significantly raised by both $[Ca^{2+}]_o$ ($p<0.0001$) and NPS R-568 ($p=0.0002$). Multiple comparison analyses showed that the effect reached significance at 3mM (Ctrl=1.2±0.2; +NPS R-568=3.4±0.3, $p=0.0003$; Fig. 3-6a, c), but surprisingly was not continued in the presence of high 6mM $[Ca^{2+}]_o$ ($p>0.05$).

Next, experiments were performed to assess whether $[Ca^{2+}]_o$-induced P90RSK signalling relies on CaSR activation. Once more, P90RSK was acutely stimulated by increasing $[Ca^{2+}]_o$ ($p<0.0001$). However, there was an inhibitory effect of NPS-2143 on $[Ca^{2+}]_o$-induced P90RSK activation ($p=0.0022$). Multiple comparison analyses did not detect an effect of NPS-2143 on p90RSK activation without $[Ca^{2+}]_o$ ($p>0.05$) or at $[Ca^{2+}]_o$ concentrations less than 3mM $[Ca^{2+}]_o$ ($p>0.05$). However, NPS-2143 significantly decreased p90RSK activation when HEK293-CaSR cells were stimulated with 6mM $[Ca^{2+}]_o$ (Ctrl=28.9±9.1; +NPS-2143=4.4±0.9, $p<0.0001$; Fig. 3-6b, d), showing that P90RSK signalling is sensitive to NPS-2143 at high $[Ca^{2+}]_o$ concentrations.

Figure 3-6

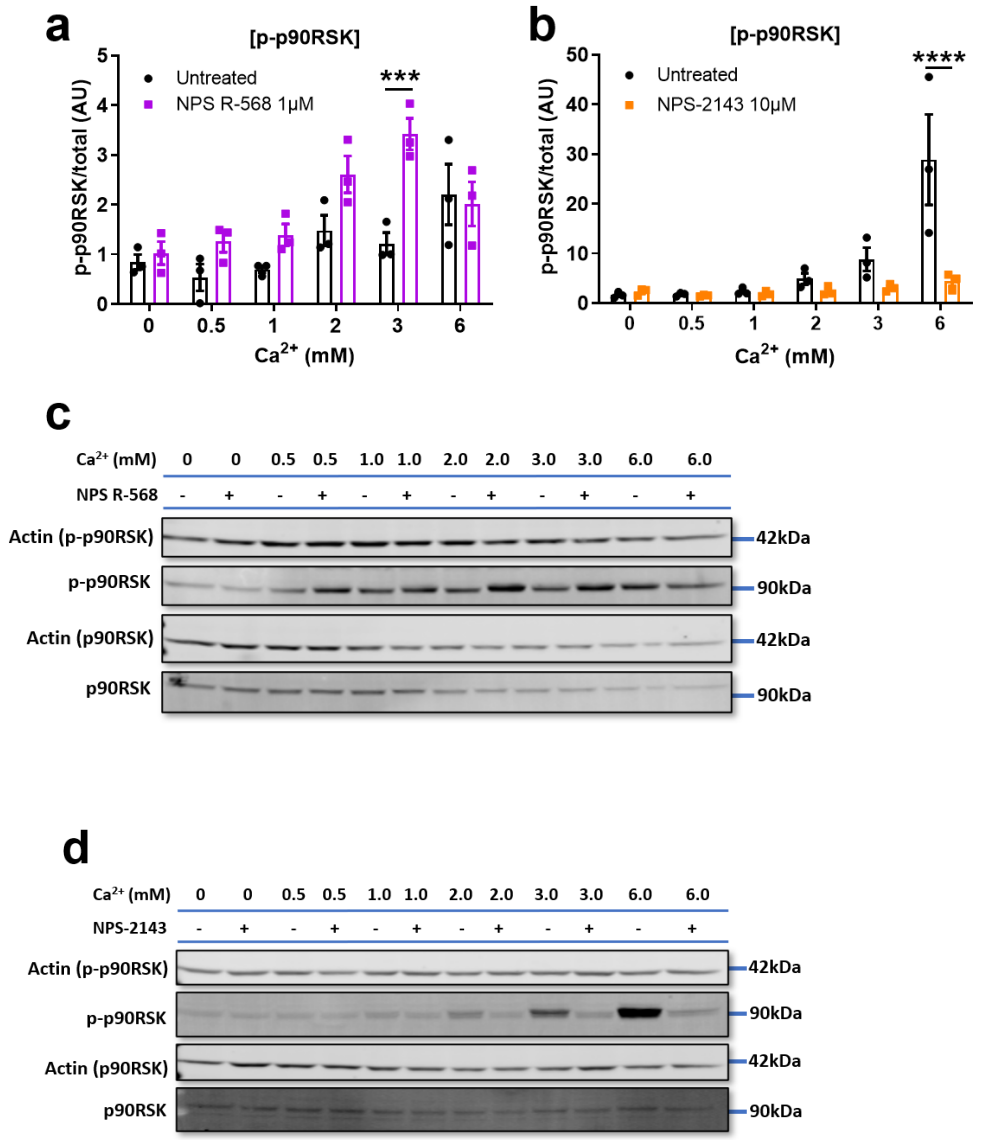

Figure 3-6: CaSR regulates $[Ca^{2+}]_o$-induced p90RSK activation in HEK293-CaSR cells.

(a) NPS R-568 potentiates $ERK_{1/2}$ activation in HEK293-CaSR cells when stimulated with 3mM extracellular $CaCl_2$ ($[Ca^{2+}]_o$). **(b)** NPS-2143 inhibits $ERK_{1/2}$ activation in HEK293-CaSR cells when maximally stimulated with 6mM $[Ca^{2+}]_o$. **(c)** Representative western blot image of total and phopho-p90RSK protein (90kDa) demonstrating the effect of $[Ca^{2+}]_o$ and NPS R-568 in HEK293-CaSR cells. **(d)** Representative western blot image of total and phopho-p90RSK protein (90kDa) demonstrating the effect of $[Ca^{2+}]_o$ and NPS-2143 in HEK293-CaSR cells. Mean±SEM. Two-way ANOVA (a,b). ***p<0.001 vs Ctrl, ****p<0.0001 vs Ctrl. CaSR=Calcium sensing receptor; p90RSK= p90 ribosomal S6 kinase.

Both NPS R-568 and NPS-2143 regulates the activation of $ERK_{1/2}$ and its downstream target p90RSK. To validate the role of CaSR in $[Ca^{2+}]_o$-induced $ERK_{1/2}$ and p90RSK signalling, CaSR-expressing (induced) and naïve (uninduced) HEK293-CaSR cells were treated with high (3mM) $[Ca^{2+}]_o$ and monitored for $ERK_{1/2}$ and p90RSK activation. $[Ca^{2+}]_o$ stimulation significantly increased $ERK_{1/2}$ activation in induced HEK293-CaSR cells (Ctrl=0.1±0.0; $[Ca^{2+}]_o$=2.0±0.4, p=0.0020). As expected, uninduced cells lacking transgenic CaSR expression were unable to reproduce this effect (Ctrl=0.1±0.0; $[Ca^{2+}]_o$=0.2±0.1, p>0.05). To confirm the role of CaSR in this response, $[Ca^{2+}]_o$-induced $ERK_{1/2}$ responses in induced and uninduced HEK293-CaSR cells were compared. $[Ca^{2+}]_o$-dependent $ERK_{1/2}$ activation in induced HEK293-CaSR was significantly enhanced relative to uninduced counterparts (p=0.0029; Fig 3-7a, b), suggesting that $[Ca^{2+}]_o$-induced $ERK_{1/2}$ responses rely on CaSR.

CaSR seemed to be important in $[Ca^{2+}]_o$-induced $ERK_{1/2}$ responses, so the role of CaSR on downstream p90RSK activation was also evaluated. As observed with $ERK_{1/2}$, $[Ca^{2+}]_o$ stimulation increased P90RSK activation in induced HEK293-CaSR cells (Ctrl=2.4±0.8; $[Ca^{2+}]_o$=15.0±3.1, p=0.0042), but had no effect in uninduced HEK293-CaSR cells (Ctrl=0.8±0.1; $[Ca^{2+}]_o$=1.0±0.2, p>0.05). When $[Ca^{2+}]_o$-induced P90RSK responses were compared between induced and uninduced HEK293-CaSR cells, p90RSK activation was markedly greater in induced cells (p=0.0024; Fig. 3-7c, d), showing that CaSR is required for $[Ca^{2+}]_o$-induced p90RSK activation.

$[Ca^{2+}]_o$-induced $ERK_{1/2}$ and downstream P90RSK activation in HEK293-CaSR cells depends on transgenic CaSR expression. To validate the involvement of CaSR in agonist-induced HEK293-CaSR signalling, a second series of experiments were performed to investigate the role played by CaSR in cinacalcet-induced $ERK_{1/2}$ signalling. As with $[Ca^{2+}]_o$, cinacalcet significantly increased $ERK_{1/2}$ activation in induced HEK293-CaSR cells (Ctrl=0.1±0.0; Cinacalcet=0.5±0.1, p=0.0010) and had no effect on $ERK_{1/2}$ activation in uninduced counterparts (Ctrl=0.2±0.0; Cinacalcet=0.2±0.0, p>0.05). In induced compared to uninduced cells, cinacalcet-mediated $ERK_{1/2}$ activation was increased (p=0.0045; Fig. 3-7e, f), suggesting cinacalcet-induced $ERK_{1/2}$ responses are regulated by CaSR.

Cinacalcet increased $ERK_{1/2}$ signalling in HEK293-CaSR cells, and these responses seemed to rely on CaSR. To validate the role of CaSR in $ERK_{1/2}$ signalling pathways, the effect of cinacalcet on p90RSK downstream of $ERK_{1/2}$ was interrogated. Cinacalcet tended to raise p90RSK activation in induced HEK293-CaSR cells, but the effect was variable and did not reach significance (Ctrl=0.3±0.3; Cinacalcet=1.5±0.9, p=0.0614). There was no effect of cinacalcet on p90RSK activation in uninduced HEK293-CaSR cells (Ctrl=0.5±0.4; Cinacalcet=0.5±0.4, p>0.05). Unexpectedly, cinacalcet-induced p90RSK signalling in induced and uninduced HEK293-CaSR cells was similar (p>0.05; Fig. 3-7g, h).

Figure 3-7

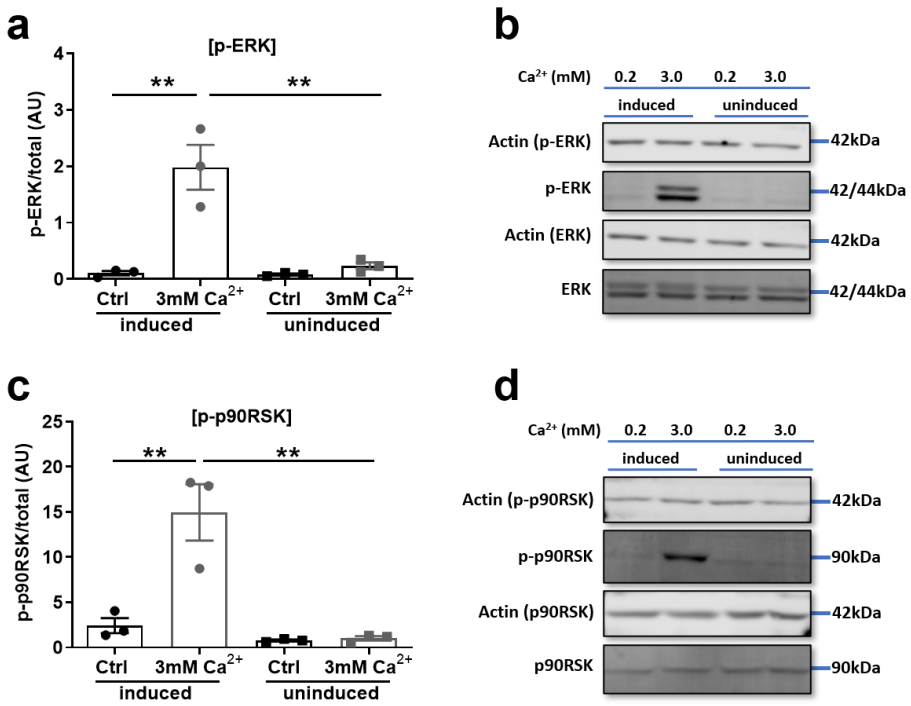

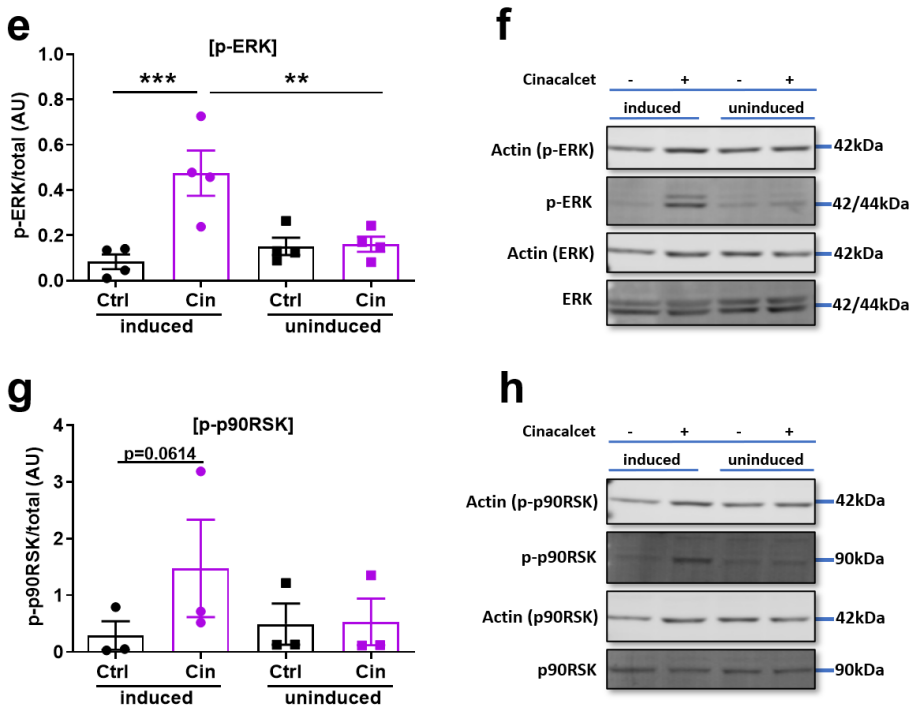

Figure 3-7: CaSR regulates $[Ca^{2+}]_o$-induced $ERK_{1/2}$ and p90RSK activation in DX-induced and uninduced HEK293-CaSR cells.

(a) $ERK_{1/2}$ activation is increased by extracellular $CaCl_2$ ($[Ca^{2+}]_o$) in doxycycline (DX)-induced HEK293-CaSR cells, but not in naïve uninduced cells. **(b)** Representative western blot image demonstrating the effect of $[Ca^{2+}]_o$ on $ERK_{1/2}$ activation in induced and uninduced HEK293-CaSR cells. **(c)** p90RSK activation is increased by $[Ca^{2+}]_o$ in induced HEK293-CaSR cells, but not in uninduced cells. **(d)** Representative western blot image demonstrating the effect of $[Ca^{2+}]_o$ on p90RSK in induced and uninduced HEK293-CaSR cells. **(e)** $ERK_{1/2}$ activation is increased by cinacalcet in induced HEK293-CaSR cells, but not uninduced cells. **(f)** Representative western blot image demonstrating the effect of cinacalcet on p90RSK in induced and uninduced HEK293-CaSR cells. **(g)** p90RSK activation is not modified by cinacalcet in induced or uninduced HEK293-CaSR cells. **(h)** Representative western blot image demonstrating the effect of cinacalcet on p90RSK in induced and uninduced HEK293-CaSR cells. Mean±SEM. One-way ANOVA (a,c,e,g). **p<0.01, ***p<0.001. CaSR=Calcium sensing receptor; $ERK_{1/2}$=Extracellular signal-regulated kinase 1/2; p90RSK= p90 ribosomal S6 kinase.

3.3.5 CaSR-dependent $[Ca^{2+}]_o$-induced AKT signalling

$[Ca^{2+}]_o$ stimulation in HEK293-CaSR cells increased $ERK_{1/2}$ but not AKT signalling. To confirm that AKT is not regulated by CaSR, HEK293-CaSR cells were treated with NPS R-568 or NPS-2143 in the presence of variable (0-6mM) $[Ca^{2+}]_o$ and AKT activation assessed. NPS R-568 had no influence on HEK293-CaSR AKT activation irrespective of $[Ca^{2+}]_o$ concentration ($p>0.05$; Fig. 3-8a, c). Similarly, AKT activation was unmodified by NPS-2143 at all $[Ca^{2+}]_o$ concentrations studied ($p>0.05$; Fig. 3-8b, d).

Figure 3-8

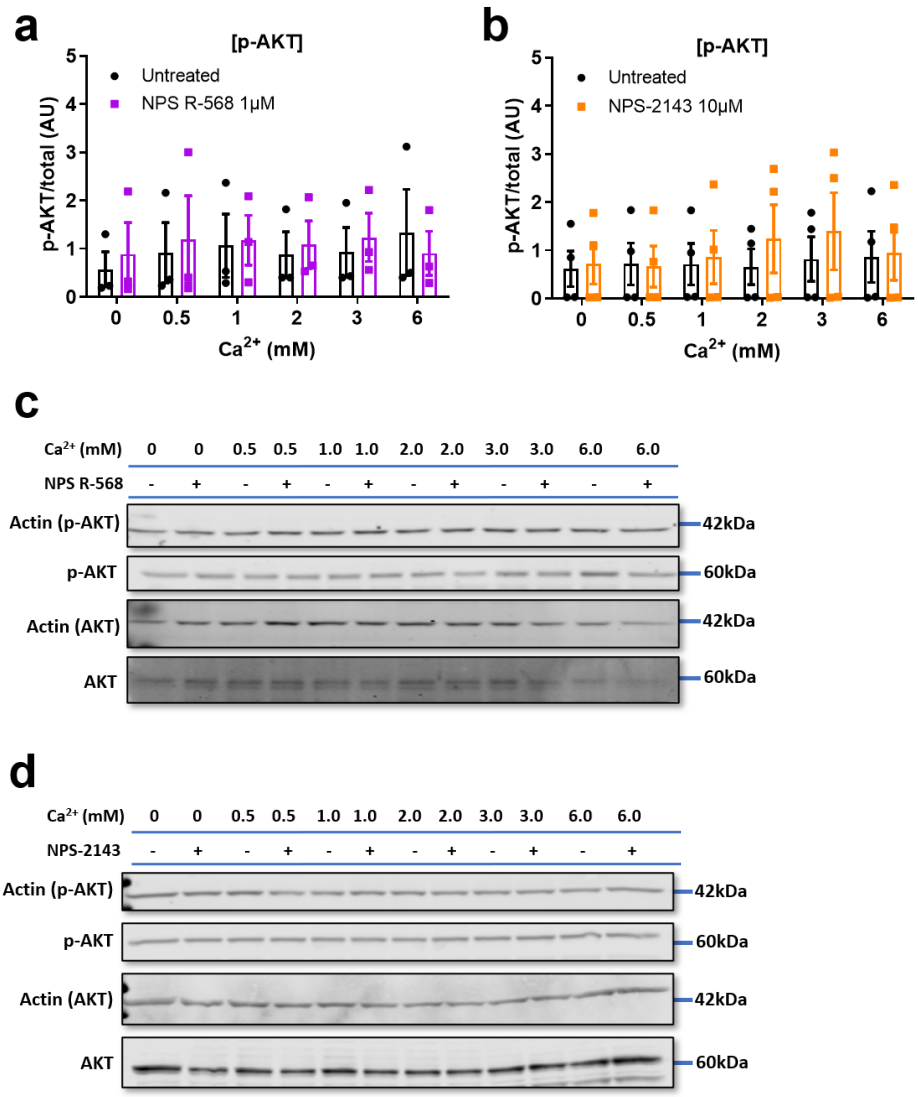

Figure 3-8: AKT activation is not regulated by $[Ca^{2+}]_o$ or CaSR in HEK293-CaSR cells.

(a) NPS R-568 does not alter AKT activation when stimulated with 0-6mM extracellular $CaCl_2$ ($[Ca^{2+}]_o$). **(b)** NPS-2143 does not alter AKT activation when stimulated with 0-6mM $[Ca^{2+}]_o$. **(c)** Representative western blot image of total and phospho-AKT protein (60kDa) demonstrating the effect of $[Ca^{2+}]_o$ and NPS R-568 in HEK293-CaSR cells. **(d)** Representative western blot image of total and phospho-AKT protein (60kDa) demonstrating the effect of $[Ca^{2+}]_o$ and NPS-2143 in HEK293-CaSR cells. Mean±SEM. Two-way ANOVA (a,b). AKT=Protein kinase B; CaSR=Calcium sensing receptor.

3.3.6 L-Phe-dependent $[Ca^{2+}]_o$-induced $ERK_{1/2}$ activation

L-Phenylalanine (L-Phe) is an allosteric modulator of CaSR which has been shown to enhance CaSR $[Ca^{2+}]_o$ sensitivity, leading to increased CaSR-dependent $ERK_{1/2}$ phosphorylation (Lee *et al.*, 2007). This study sought to recapitulate these data. HEK293-CaSR cells were treated with both physiological and pharmacological L-Phe, stimulated with variable $[Ca^{2+}]_o$ and $ERK_{1/2}$ signalling assessed with immunoblot analyses. In the presence of low 0.5mM $[Ca^{2+}]_o$, HEK293-CaSR cells showed no change in $ERK_{1/2}$ activation with 0.1mM (81±18%, $p>0.05$), 1mM (82±16%, $p>0.05$) or 10mM L-Phe (89±44%, $p>0.05$; Fig. 3-9a, c). Unexpectedly, L-Phe was also ineffective at higher $[Ca^{2+}]_o$ concentrations, HEK293-CaSR cells incubated in the presence of 2mM $[Ca^{2+}]_o$ showed no change in $ERK_{1/2}$ activation when treated with 0.1mM L-Phe (112±10%, $p>0.05$) 1mM (105±11%, $p>0.05$) or 10mM L-Phe (94±14%, $p>0.05$; Fig. 3-9b, c).

Figure 3-9

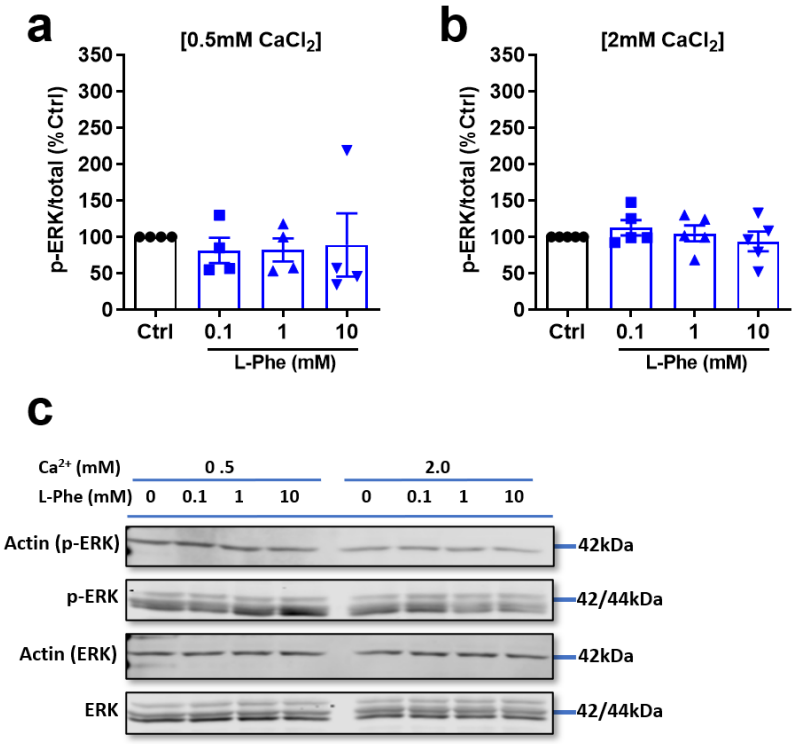

Figure 3-9: L-Phe does not regulate $ERK_{1/2}$ signalling in HEK293-CaSR cells. **(a)** L-Phenylalanine (L-Phe) does not alter $ERK_{1/2}$ activation when stimulated with 0.5mM extracellular $CaCl_2$ ($[Ca^{2+}]_o$). **(b)** L-Phe does not alter $ERK_{1/2}$ activation when stimulated with 2mM $[Ca^{2+}]_o$. **(c)** Representative western blot image of total and phopho-$ERK_{1/2}$ protein (42/44kDa) demonstrating the effect of L-Phe in HEK293-CaSR cells. Mean±SEM. One-way ANOVA (a,b). CaSR=Calcium sensing receptor; ERK1/2=Extracellular signal-regulated kinase 1/2.

3.3.7 ADMA-dependent $[Ca^{2+}]_o$-induced $ERK_{1/2}$ activation

Allosteric (type II) CaSR agonists NPS R-568 and cinacalcet enhanced $[Ca^{2+}]_o$-induced $ERK_{1/2}$ signalling in HEK293-CaSR cells. To investigate whether ADMA acts as an allosteric modulator of CaSR, HEK293-CaSR cells were treated with ADMA (0-100μM), stimulated for 10min using different concentrations of $[Ca^{2+}]_o$ and $ERK_{1/2}$ activation assessed. In the absence of $[Ca^{2+}]_o$, $ERK_{1/2}$ activation was not enhanced by ADMA at any concentration (1μM=93±12%; 3μm=102±11%; 10μM=80±8%; 30μM=104±11%; 100μM=90±13%, p>0.05; Fig. 3-10a, b). However, $ERK_{1/2}$ activation in HEK293-CaSR cells stimulated with low 0.5mM $[Ca^{2+}]_o$ was significantly enhanced by ADMA at physiologically relevant concentrations, in the presence of 1μM ADMA (159±15, p=0.0039) and also 3μM ADMA (144±18%, p=0.0458). $ERK_{1/2}$ activation was similarly enhanced when cells were treated

with 0.5mM $[Ca^{2+}]_o$ in higher 10μM ADMA concentrations (144±16%, p=0.0458). Interestingly, pharmacological ADMA levels had no effect on $ERK_{1/2}$ activation at this $[Ca^{2+}]_o$ concentration, as $ERK_{1/2}$ signalling was not similarly increased when cells were treated with low 0.5mM $[Ca^{2+}]$ alongside 30μM or 100μM ADMA ($p>0.05$; Fig. 3-10c, d). Following stimulation with 2mM $[Ca^{2+}]_o$, $ERK_{1/2}$ activation was again increased by 1μM ADMA (127±7%, p=0.0428). However, $ERK_{1/2}$ activation in the presence of 2mM $[Ca^{2+}]_o$ was not similarly augmented by 3-100μM ADMA ($p>0.05$; Fig. 3-10e, f). ADMA failed to modify $ERK_{1/2}$ activation when HEK293-CaSR cells were exposed to 3mM $[Ca^{2+}]_o$ ($p>0.05$; Fig. 3-10g, h).

Figure 3-10

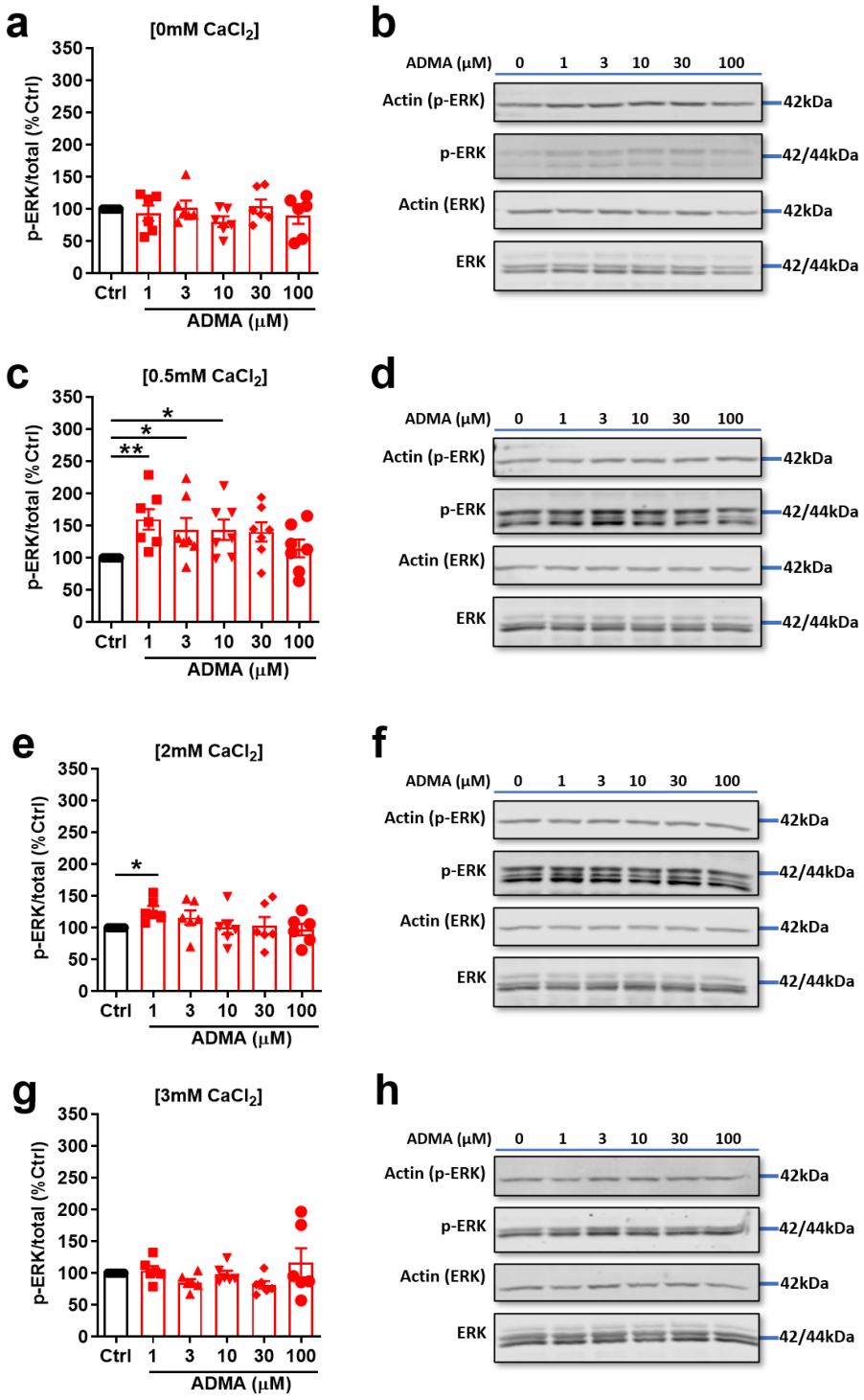

Figure 3-10: ADMA regulates $[Ca^{2+}]_o$-induced $ERK_{1/2}$ activation in HEK293-CaSR cells.

(a) $ERK_{1/2}$ activation is not affected by ADMA when extracellular $CaCl_2$ ($[Ca^{2+}]_o$) is absent. **(b)** Representative western blot image demonstrating the effect of ADMA on $ERK_{1/2}$ activation in HEK293-CaSR cells incubated without $[Ca^{2+}]_o$. **(c)** $ERK_{1/2}$ activation is enhanced by 1, 3 and 10μM ADMA when stimulated by 0.5mM $[Ca^{2+}]_o$. **(d)** Representative western blot image demonstrating the effect of ADMA

on $ERK_{1/2}$ activation in HEK293-CaSR stimulated with 0.5mM $[Ca^{2+}]_o$. **(e)** $ERK_{1/2}$ activation is enhanced by 1µM ADMA when stimulated by 2mM $[Ca^{2+}]_o$. **(f)** Representative western blot image demonstrating the effect of ADMA on $ERK_{1/2}$ activation in HEK293-CaSR stimulated with 2mM $[Ca^{2+}]_o$. **(g)** $ERK_{1/2}$ activation is unchanged by ADMA when stimulated by 3mM $[Ca^{2+}]_o$. **(h)** Representative western blot image demonstrating the effect of ADMA on $ERK_{1/2}$ activation in HEK293-CaSR stimulated with 3mM $[Ca^{2+}]_o$. Mean±SEM. One-way ANOVA (a,c,e,g). *p<0.05 vs Ctrl, **p<0.01 vs Ctrl. ADMA=Asymmetric dimethylarginine; CaSR=Calcium sensing receptor; $ERK_{1/2}$=Extracellular signal-regulated kinase 1/2.

To examine whether the effect of ADMA on $[Ca^{2+}]_o$-induced $ERK_{1/2}$ activation was mediated via CaSR, naïve (uninduced) HEK293-CaSR cells were treated for 10min with 0.5mM and 2mM $[Ca^{2+}]_o$ in the presence of ADMA (1-100μM) and $ERK_{1/2}$ activation assessed. In uninduced HEK293-CaSR cells lacking transgenic CaSR expression, ADMA had a highly variable effect on $ERK_{1/2}$ activation; ADMA at 1, 3 and 30μM concentrations had no significant effect on $ERK_{1/2}$ activation (1μM=66±17%; 3μM=75±21%; 30μM=74±26%, $p>0.05$), but interestingly $ERK_{1/2}$ activation was significantly decreased by 10μM ADMA (52±16%, $p=0.0090$) and 100μM ADMA (59±18%, $p=0.0286$; Fig. 3-11a, c). Despite these findings, $ERK_{1/2}$ activation was broadly unaltered by ADMA when cells were treated with 2mM $[Ca^{2+}]_o$ ($p>0.05$; Fig. 3-11b,c).

Figure 3-11

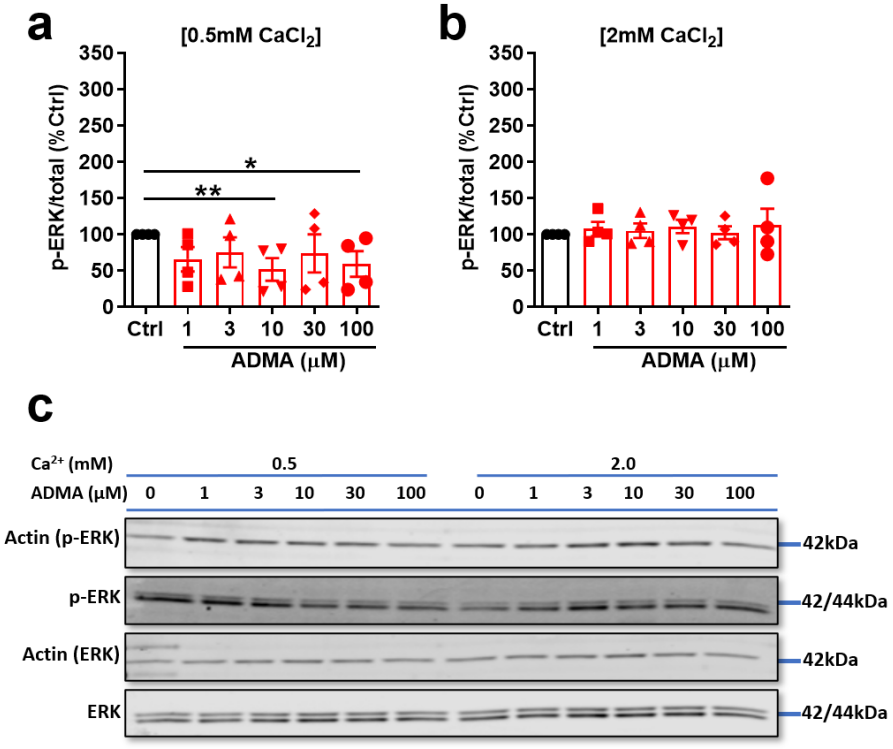

Figure 3-11: ADMA is unable to increase $[Ca^{2+}]_o$-induced $ERK_{1/2}$ activation in uninduced HEK293-CaSR cells.

(a) $ERK_{1/2}$ activation is reduced by 10 and 100μM ADMA in naïve (uninduced) HEK293-CaSR cells when stimulated with 0.5mM extracellular $CaCl_2$ ($[Ca^{2+}]_o$). **(b)** $ERK_{1/2}$ activation is unchanged by ADMA in uninduced HEK293-CaSR cells when stimulated with 2mM $[Ca^{2+}]_o$. **(c)** Representative western blot image demonstrating the effect of ADMA on $ERK_{1/2}$ activation in uninduced HEK293-CaSR stimulated with 0.5mM or 2mM $[Ca^{2+}]_o$. Mean±SEM. One-way ANOVA (a,b). *p<0.05 vs Ctrl, **p<0.01 vs Ctrl. ADMA=Asymmetric dimethylarginine; CaSR=Calcium sensing receptor; $ERK_{1/2}$=Extracellular signal-regulated kinase 1/2.

Earlier, NPS R-568-mediated CaSR stimulation caused activation of $ERK_{1/2}$ and the ERK cascade mediator p90RSK. To test whether ADMA-mediated $ERK_{1/2}$ activation similarly coincides with p90RSK recruitment, HEK293-CaSR cells were treated with 0.5mM and 2mM $[Ca^{2+}]_o$ in the presence of ADMA (1-100μM) and p90RSK activation assessed. In HEK293-CaSR cells, p90RSK activation was not altered by ADMA at any concentration following stimulation with 0.5mM $[Ca^{2+}]_o$ ($p>0.05$; Fig. 3-12a, b) or 2mM $[Ca^{2+}]_o$ ($p>0.05$; Fig. 3-12c, d).

Figure 3-12

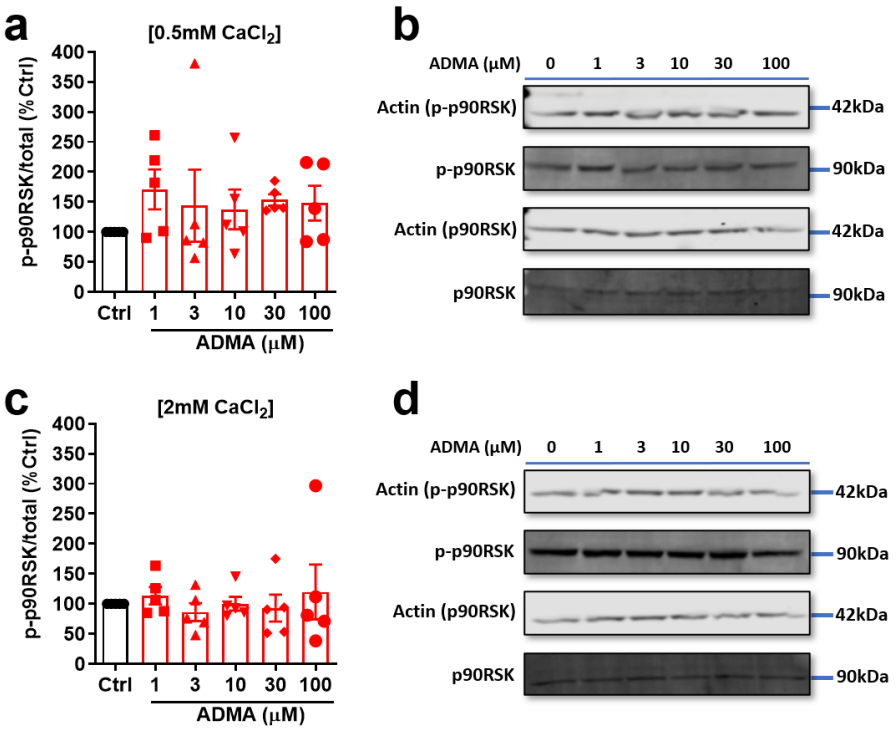

Figure 3-12: ADMA does not increase $[Ca^{2+}]_o$-induced p90RSK activation in HEK293-CaSR cells.

(a) p90RSK activation is unchanged by ADMA in HEK293-CaSR cells when stimulated with 0.5mM extracellular $CaCl_2$ ($[Ca^{2+}]_o$). **(b)** p90RSK activation is unchanged by ADMA in HEK293-CaSR cells when stimulated with 2mM $[Ca^{2+}]_o$. **(c)** Representative western blot image demonstrating the effect of ADMA on p90RSK activation in HEK293-CaSR stimulated with 0.5mM or 2mM $[Ca^{2+}]_o$. Mean±SEM. One-way ANOVA (a,b). ADMA=Asymmetric dimethylarginine; CaSR=Calcium sensing receptor; p90RSK= p90 ribosomal S6 kinase.

ADMA caused $ERK_{1/2}$ activation and this response appeared to rely on CaSR. To further explore ADMA-dependent CaSR signalling, HEK293-CaSR cells were stimulated for 10min with 0.5mM and 2mM $[Ca^{2+}]_o$ in the presence of 10μM SDMA, the structural analogue of ADMA, and $ERK_{1/2}$ activation assessed. Unlike ADMA, SDMA did not increase $ERK_{1/2}$ activation in cells stimulated with 0.5mM $[Ca^{2+}]_o$ (92±14%, $p>0.05$; Fig. 3-13a, c) or 2mM $[Ca^{2+}]_o$ (123±9%, $p=0.0784$; Fig 3-13b, c).

Figure 3-13

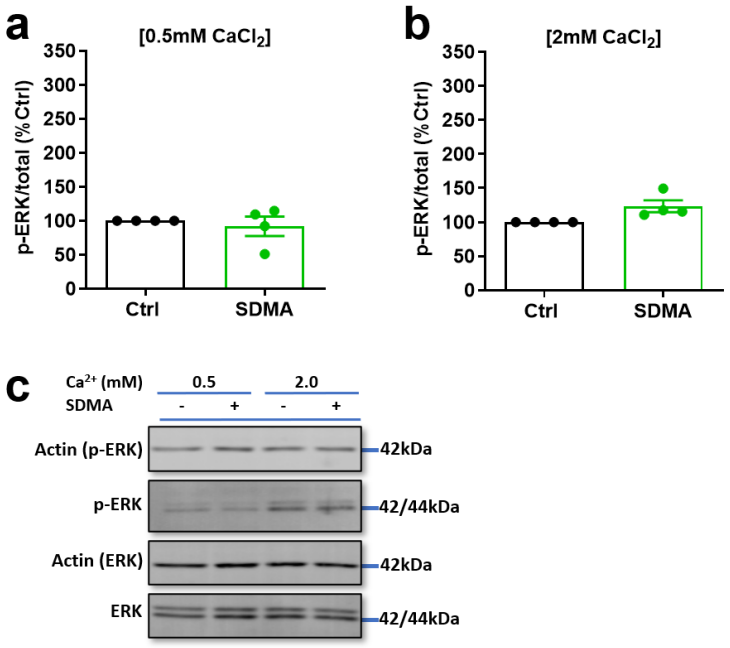

Figure 3-13: The effect of SDMA on $ERK_{1/2}$ signalling in HEK293-CaSR cells. **(a)** SDMA does not alter $ERK_{1/2}$ activation when stimulated with 0.5mM extracellular $CaCl_2$ ($[Ca^{2+}]_o$). **(b)** SDMA does not alter $ERK_{1/2}$ activation when stimulated with 2mM $[Ca^{2+}]_o$. **(c)** Representative western blot image of total and phopho-$ERK_{1/2}$ protein (42/44kDa) demonstrating the effect of SDMA in HEK293-CaSR cells. Mean±SEM. Paired t-test (a,b). CaSR=Calcium sensing receptor; ERK1/2=Extracellular signal-regulated kinase 1/2; SDMA=Symmetric dimethylarginine.

3.3.8 NOS signalling

To interrogate the mechanism(s) underpinning ADMA-mediated $ERK_{1/2}$ activation, this study examined whether ADMA regulates NOS signalling in HE293-CaSR cells. To validate the expression of NOS, qPCR was performed on HEK293-CaSR cells using eNOS- and iNOS-specific primers. The presence of transcript was confirmed via successful amplification of qPCR products (Fig. 3-14a). To evaluate the effect of ADMA on NOS-mediated NO production, HEK293-CaSR cells were treated with 1, 10 and 100μM ADMA in the presence of $[Ca^{2+}]_o$ (0.5, 2mM) for 24h and media nitrite concentration assessed via Griess assay. In some experiments, interpolation of unknown samples returned a negative value. Samples where nitrite concentrations were below the limit of detection were assigned a nitrite concentration of 0. In the presence of 0.5mM $[Ca^{2+}]_o$, nitrite concentration in

control HEK293-CaSR cells (2.0±0.9μM) was significantly elevated by 1μM ADMA (11.4±4.3μM, p=0.0400) but was unchanged by 10μM (5.7±2.2μM, p>0.05) or 100μM ADMA (2.2±1.2μM, p>0.05; Fig. 3-14b). However, nitrite concentration in HEK293-CaSR cells incubated with 2mM $[Ca^{2+}]_o$ (5.2±3.8μM) was not augmented by 1μM, 10μM or 100μM ADMA (p>0.05; Fig. 3-14c).

To explore the involvement of NO in ADMA-dependent CaSR signalling, HEK293-CaSR cells were stimulated for 10min with 0.5mM and 2mM $[Ca^{2+}]_o$ in the presence of the NOS inhibitor L-NAME and $ERK_{1/2}$ activation monitored. To ensure NOS was maximally inhibited, L-NAME was used at 1mM. Where ADMA increased $ERK_{1/2}$ signalling in cells stimulated with 0.5mM and 2mM $[Ca^{2+}]_o$, L-NAME was unable to modify $ERK_{1/2}$ signalling in the presence of 0.5mM $[Ca^{2+}]_o$ (128±23%, p>0.05; Fig. 3-15a, c) or when cells were stimulated with moderate 2mM $[Ca^{2+}]_o$ (114±27%, p>0.05; Fig. 3-15b,c).

Figure 3-14

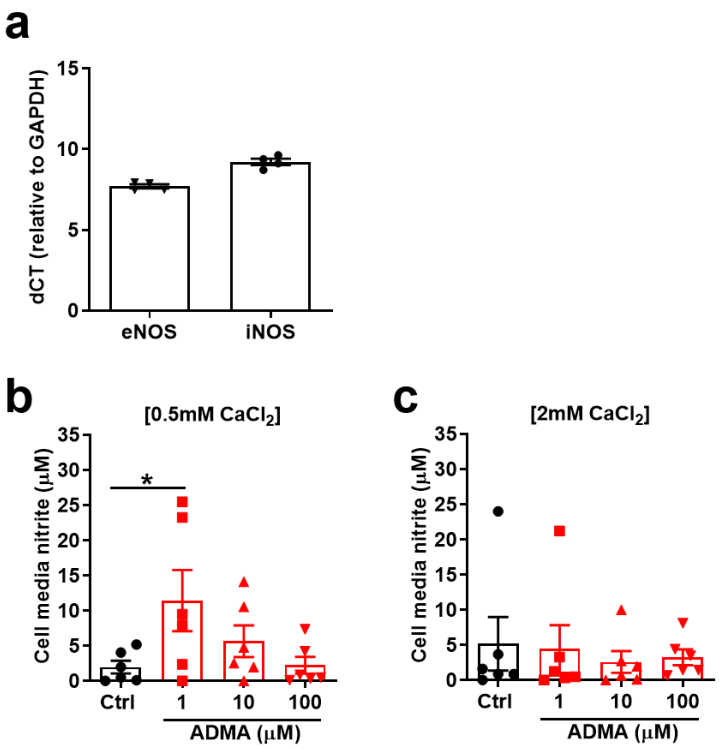

Figure 3-14: ADMA does not influence NOS signalling in HEK293-CaSR cells. **(a)** NOS mRNA expression is demonstrated HEK293-CaSR cells following qPCR analysis using primers against eNOS and iNOS. **(b)** Nitrite concentration in HEK293-CaSR cell media was increased by 1µM ADMA in the presence of with 0.5mM extracellular $CaCl_2$ ($[Ca^{2+}]_o$). ADMA had no effect on media nitrite concentration at 10 or 100µM. **(c)** Nitrite concentration in HEK293-CaSR cell media was unchanged by 1, 10 and 100µM in the presence of with 2mM $[Ca^{2+}]_o$. Mean±SEM. One-way ANOVA (b,c). *p<0.05. ADMA=Asymmetric dimethylarginine; eNOS=Endothelial nitric oxide synthase; iNOS=Inducible nitric oxide synthase.

Figure 3-15

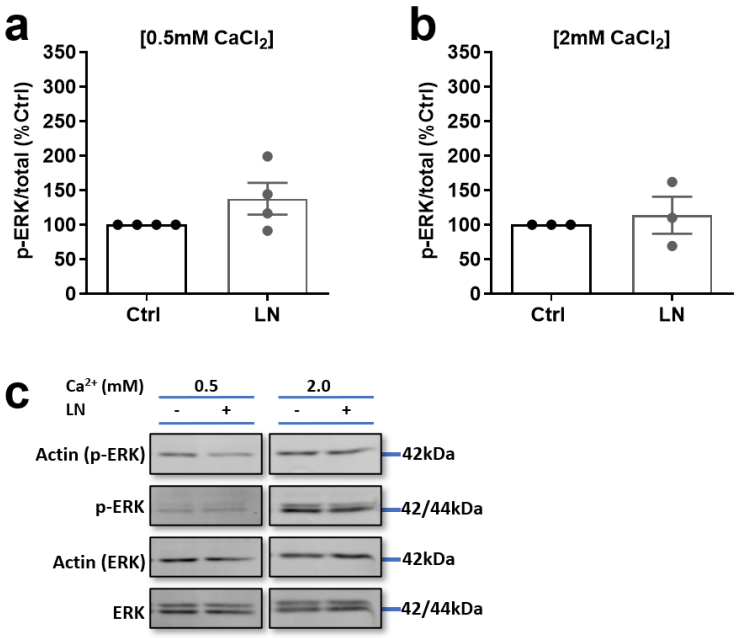

Figure 3-15: Acute 10min L-NAME NOS inhibition does not influence $[Ca^{2+}]_o$-induced $ERK_{1/2}$ signalling in HEK293-CaSR cells.

(a) L-NAME (LN) does not alter $ERK_{1/2}$ activation when stimulated with 0.5mM extracellular $CaCl_2$ ($[Ca^{2+}]_o$). **(b)** LN does not alter $ERK_{1/2}$ activation when stimulated with 2mM $[Ca^{2+}]_o$. **(c)** Representative western blot image of total and phopho-$ERK_{1/2}$ protein (42/44kDa) demonstrating the effect of LN in HEK293-CaSR cells. Mean±SEM. Paired t-test (a,b). CaSR=Calcium sensing receptor; ERK1/2=Extracellular signal-regulated kinase 1/2.

3.3.9 Chronic ADMA-dependent $[Ca^{2+}]_o$-induced $ERK_{1/2}$ activation

Given that $[Ca^{2+}]_o$-induced $ERK_{1/2}$ signalling was increased by ADMA following acute (10min) treatment, this study wanted to establish whether this effect was maintained in HEK293-CaSR cells following long-term ADMA treatment. To assess whether chronic ADMA exposure also regulates $ERK_{1/2}$ activation, HEK293-CaSR cells were treated for 24h with ADMA in the presence of 0.5 or 2mM $[Ca^{2+}]_o$. When stimulated with low 0.5mM $[Ca^{2+}]_o$, $ERK_{1/2}$ signalling was enhanced 154±22% by 10μM ADMA ($p=0.0212$), though there was no effect of 1μM or 100μM ADMA $ERK_{1/2}$ activation ($p>0.05$; Fig. 3-16a, b). Chronic ADMA treatment was unable to modify $ERK_{1/2}$ activation in the presence of 2mM $[Ca^{2+}]_o$ ($p>0.05$; Fig. 3-16c,d).

Figure 3-16

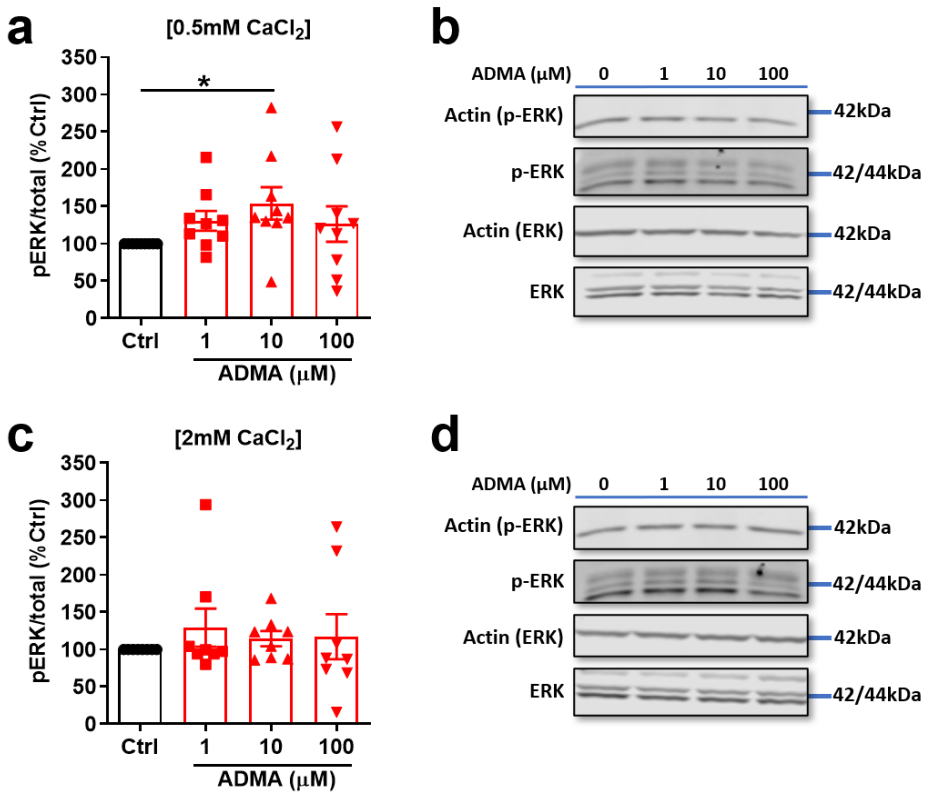

Figure 3-16: Chronic 24h ADMA increases $[Ca^{2+}]_o$-induced $ERK_{1/2}$ activation in HEK293-CaSR cells.

(a) $ERK_{1/2}$ activation is enhanced by 10μM ADMA when stimulated by 0.5mM extracellular $CaCl_2$ ($[Ca^{2+}]_o$). **(b)** Representative western blot image demonstrating the effect of chronic 24h ADMA on $ERK_{1/2}$ activation in HEK293-CaSR cells incubated with 0.5mM $[Ca^{2+}]_o$. **(c)** $ERK_{1/2}$ activation is unchanged by 1, 3 and 10μM ADMA when stimulated by 2mM $[Ca^{2+}]_o$. **(d)** Representative western blot image demonstrating the effect of chronic 24h ADMA on $ERK_{1/2}$ activation in HEK293-CaSR cells incubated with 0.5mM $[Ca^{2+}]_o$. Mean±SEM. One-way ANOVA (a,c). *$p<0.05$ vs Ctrl. ADMA=Asymmetric dimethylarginine; CaSR=Calcium sensing receptor; $ERK_{1/2}$=Extracellular signal-regulated kinase 1/2.

3.3.10 CaSR-dependent gene expression

Through regulating pleiotropic intracellular targets, $ERK_{1/2}$ signalling plays a key role in multiple biological processes including cell growth, proliferation, stress-responses and apoptosis (Guo *et al.*, 2020). CaSR mediates many biological functions, though its role in inflammation and fibrosis appears common among cardiovascular cells (Peng *et al.*, 2014; Sundararaman and van der Vorst, 2021)

and thus is of particular interest. To establish whether HEK293-CaSR cells could be used as a model of CaSR-induced gene expression, this study assessed whether CaSR regulates TGFβ, a principal mediator of fibrosis (Ruiz-Ortega *et al.*, 2007). HEK293-CaSR cells were treated with NPS R-568 in the presence of 0.5mM or 2mM $[Ca^{2+}]_o$ for 24h, then TGFβ expression assessed with qPCR. Compared to control cells, NPS R-568 tended to raise TGFβ mRNA levels when cells were incubated with 0.5mM $[Ca^{2+}]_o$, but the effect was not significant (1.6±0.2-fold, p=0.0680; Fig. 3-17a). Though unable to modify TGFβ expression in low 0.5mM $[Ca^{2+}]_o$ conditions, NPS R-568 markedly increased TGFβ expression in the presence of 2mM $[Ca^{2+}]_o$ (2.0±0.2-fold, p=0.0280; Fig. 3-17b), suggesting that NPS R-568 influences TGFβ gene expression under conditions of moderate, but not low $[Ca^{2+}]_o$.

TGFβ is activated by MMP2 in the vasculature (Ruiz-Ortega *et al.*, 2007), so this study investigated whether MMP2 could be similarly regulated by NPS R-568. As with TGFβ, MMP2 expression was not altered by NPS R-568 when HEK293-CaSR cells were stimulated with 0.5mM $[Ca^{2+}]_o$ (1.6±0.3-fold, p>0.05; Fig. 3-17c). However, NPS R-568 caused a small but significant increase in MMP2 expression when HEK293-CaSR cells were stimulated with moderate 2mM $[Ca^{2+}]_o$ (3.0±0.5-fold, p=0.0284; Fig. 3-17d), showing that NPS R-568 regulation of MMP2 expression is related to $[Ca^{2+}]_o$ concentration.

Figure 3-17

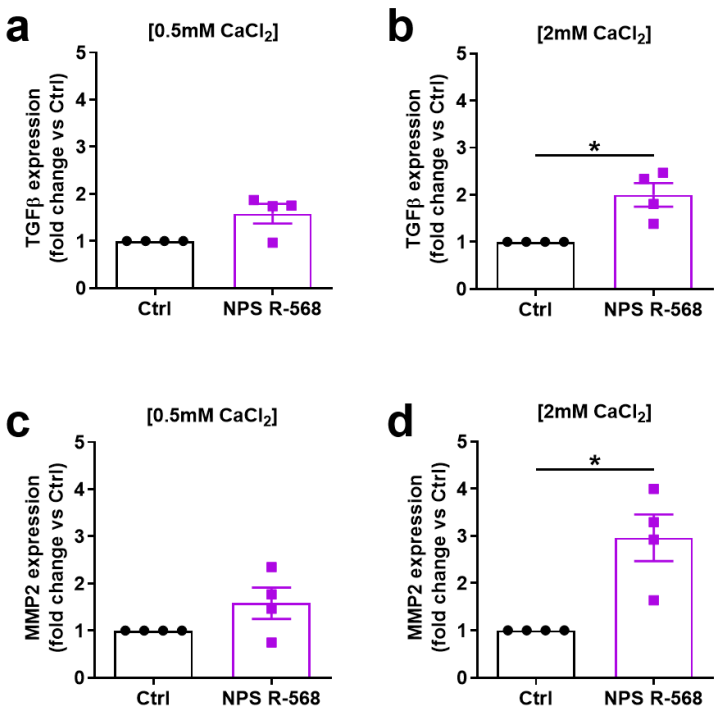

Figure 3-17: NPS R-568 increases pro-fibrotic gene expression HEK293-CaSR cells.

(a) NPS R-568 does not alter TGFß mRNA expression in HEK293-CaSR cells incubated with 0.5mM extracellular $CaCl_2$ ($[Ca^{2+}]_o$) for 24h. **(b)** NPS R-568 increases TGFß mRNA expression in HEK293-CaSR cells incubated with 2mM $[Ca^{2+}]_o$ for 24h. **(c)** NPS R-568 does not alter MMP2 mRNA expression in HEK293-CaSR cells incubated with 0.5mM $[Ca^{2+}]_o$ for 24h. **(d)** NPS R-568 increases MMP2 mRNA expression in HEK293-CaSR cells incubated with 2mM $[Ca^{2+}]_o$ for 24h. Mean±SEM. Paired t-test (a-d). *p<0.05. CaSR=Calcium sensing receptor; MMP2=Matrix metalloproteinase-2; TGFß=Transforming growth factor-beta.

3.3.11 ADMA-dependent gene expression

The pharmacological allosteric CaSR agonist NPS R-568 increases $ERK_{1/2}$ signalling alongside TGFß and MMP2 gene expression in a $[Ca^{2+}]_o$-dependent manner. To establish whether $[Ca^{2+}]_o$-dependent, ADMA-mediated $ERK_{1/2}$ signalling coincides with altered gene expression, HEK293-CaSR cells were incubated with 0.5mM or 2mM $[Ca^{2+}]_o$ in the absence or presence of ADMA (1-100µM) for 24h, then assessed for TGFß and MMP2 expression. Unexpectedly, ADMA did not influence TGFß mRNA expression in HEK293-CaSR cells stimulated with low 0.5mM $[Ca^{2+}]_o$

(p>0.05; Fig. 3-18a) or moderate 2mM $[Ca^{2+}]_o$ (p>0.05; Fig. 3-18b). Similarly, MMP2 expression was broadly unchanged by ADMA in the presence of 0.5mM $[Ca^{2+}]_o$ (p>0.05; Fig. 3-18c) and 2mM $[Ca^{2+}]_o$ (p>0.05; Fig. 3-18d).

Figure 3-18

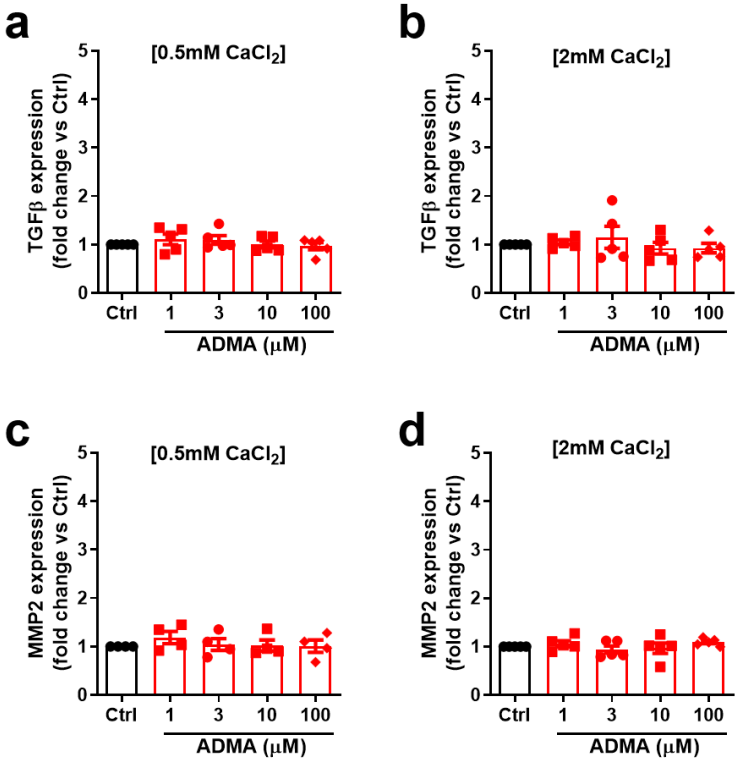

Figure 3-18: ADMA does not affect TGFß or MMP2 mRNA in HEK293-CaSR cells. **(a)** ADMA (1-100μM) does not alter TGFß mRNA expression in HEK293-CaSR cells incubated with 0.5mM extracellular $CaCl_2$ ($[Ca^{2+}]_o$) **(b)** or 2mM $[Ca^{2+}]_o$ for 24h. **(a)** ADMA (1-100μM) does not alter MMP2 mRNA expression in HEK293-CaSR cells incubated with 0.5mM $[Ca^{2+}]_o$ **(b)** or 2mM $[Ca^{2+}]_o$ for 24h. Mean±SEM. One-way ANOVA (a-d). ADMA=Asymmetric dimethylarginine; CaSR=Calcium sensing receptor; MMP2=Matrix metalloproteinase-2; TGFß=Transforming growth factor-beta.

3.4 Discussion

3.4.1 Expression of functional CaSR in HEK293-CaSR cells

ADMA- and CaSR-mediated intracellular signalling pathways were examined in HEK293 cells, a well-characterised cell line frequently used to model intracellular signal transduction. To confirm inducible expression of human c-myc-tagged CaSR in this model, c-myc was examined using immunofluorescence analyses. As anticipated, C-myc staining was absent in HEK293 cells transfected with empty vector (HEK293-vec). In contrast, c-myc was present and readily stimulated by the DX inducing agent in HEK293 cells transfected with CaSR (HEK293-CaSR), demonstrating inducible expression of the c-myc construct. These data were corroborated by CaSR immunoblotting analyses; immunoreactive bands were detected at ~130kDa and ~260kDa, consistent with the expected size of CaSR dimers (240-310kDa) and monomers with variable glycosylation (121, 138-169kDa) (Ward, Brown and Harris, 1998). This electrophoretic profile occurred specifically in HEK293-CaSR cells and like c-myc was markedly increased following DX exposure. Image analysis of CaSR immunoreactivity reproduced these findings, confirming robust and inducible CaSR expression in this model.

Among many cellular functions mediated by CaSR, $[Ca^{2+}]_i$ signalling has long been recognised as a hallmark of CaSR activation (Shoback *et al.*, 1983). In order to demonstrate that HEK293-CaSR cells express functional CaSR, agonist-induced $[Ca^{2+}]_i$ mobilisation was evaluated. The primary orthosteric CaSR agonist $GdCl_2$ imposed a marked dose-dependent effect on $[Ca^{2+}]_i$, illustrating that $GdCl_2$ sensitises $[Ca^{2+}]_i$ signalling in HEK293-CaSR cells. Interestingly, this response had an EC_{50} of 0.89mM, far higher than other HEK293-CaSR studies which observe $GdCl_2$-induced $[Ca^{2+}]_i$ signalling in the μM-range (Pearce *et al.*, 1996). However, the EC_{50} for $GdCl_2$-induced $[Ca^{2+}]_o$ was sensitised ~100-fold falling into this range when HEK293-CaSR cells were stimulated in HEPES compared to HBSS buffer. This observation was beneficial, as it demonstrated that the HEK293-CaSR cells used here could recapitulate orthostericCaSR agonist responses observed in earlier work. As shown in this study and others, untransfected HEK293 cells lack CaSR expression (Bai, Trivedi and Brown, 1998) and therefore control for CaSR-specific effects. In accordance, $GdCl_2$-induced $[Ca^{2+}]_i$ signalling was absent in

HEK293-vec cells and was effectively reduced with the CaSR inhibitor NPS-2143 in HEK293-CaSR cells. These data show that CaSR regulates $GdCl_2$-mediated responses, confirming expression of functional CaSR in HEK293-CaSR cells. Though buffers invoking greater $GdCl_2$ sensitivity would be preferred for investigating the detailed pharmacology of CaSR-mediated $[Ca^{2+}]_i$, these experimental conditions were adequate to demonstrate CaSR-dependent $GdCl_2$ effects in HEK293-CaSR cells here.

3.4.2 CaSR-mediated intracellular signalling

CaSR activation regulates a broad range of intracellular targets; these include phospholipases, AKT, filamin, Rho and MAPK cascade members (Magno, Ward and Ratajczak, 2011), though the latter is among the best described. In order to investigate the effect of ADMA on CaSR-dependent signalling pathways, initial studies characterised the effect of exogenous Ca^{2+} $[(Ca^{2+})_o]$ on $ERK_{1/2}$ activation. $[Ca^{2+}]_o$ imposed an acute, dose-dependent effect on $ERK_{1/2}$ activation with an EC_{50} of 4.4mM. Interestingly, this value was elevated compared to previous HEK293-CaSR studies, which report an EC_{50} of 2.6-2.9mM for $[Ca^{2+}]_o$-induced $ERK_{1/2}$ activation using western blot and ELISA-based approaches (Lee *et al.*, 2007), suggesting that HEK293-CaSR cells here are less responsive to $[Ca^{2+}]_o$. These disparate findings may be explained by differences between HEK293-CaSR overexpression models, as the study used transiently transfected cells compared to inducible HEK293-CaSR cells here.

Regarding CaSR pharmacology, $[Ca^{2+}]_o$-induced effects can be potentiated by synthetic allosteric CaSR agonists (calindol, cinacalcet, NPS R-568) which bind CaSR and enhance its sensitivity to $[Ca^{2+}]_o$. In contrast, calcilytics (NPS-2143, Calhex-231) allosterically inhibit CaSR activity, reducing $[Ca^{2+}]_o$ sensitivity (Ward and Riccardi, 2012). Aiming to explore the role played by CaSR in $[Ca^{2+}]_o$-induced $ERK_{1/2}$ activation in HEK293-CaSR cells, this study assessed the effect of pharmacological CaSR modulators, NPS R-568 and NPS-2143. As expected, $[Ca^{2+}]_o$-dependent $ERK_{1/2}$ activation was significantly enhanced in the presence of NPS R-568, suggesting that CaSR sensitises $[Ca^{2+}]_o$-induced $ERK_{1/2}$ signalling. Notably, $ERK_{1/2}$ activation was increased by NPS R-568 in the presence of ≥1mM $[Ca^{2+}]_o$, but not when cells were incubated in $[Ca^{2+}]_o$-free or 0.5mM $[Ca^{2+}]_o$ conditions. These data indicate that threshold $[Ca^{2+}]_o$ for NPS R-568-mediated

$ERK_{1/2}$ stimulation lies between 0.5-1mM, in alignment with previous work in HEK293-CaSR cells (Holstein *et al.*, 2004; Lee *et al.*, 2007). The role of CaSR in $[Ca^{2+}]_o$-induced $ERK_{1/2}$ activation was corroborated by inhibitor studies; NPS-2143 reduced $[Ca^{2+}]_o$-induced $ERK_{1/2}$ signalling by ~70-80%, implicating CaSR signalling as a predominant mechanism governing $[Ca^{2+}]_o$-induced $ERK_{1/2}$ signalling in HEK293-CaSR cells.

s6 kinase (RSK) is a well-recognised mediator of ERK signalling cascades (Guo *et al.*, 2020), so the effect of CaSR activation on p90RSK activation in HEK293-CaSR cells was also examined. As with $ERK_{1/2}$, p90RSK was strongly stimulated with increasing $[Ca^{2+}]_o$. These responses were potentiated by NPS R-568 and inhibited by NPS-2143, confirming that CaSR also regulates p90RSK. Investigations showing an effect of CaSR on p90RSK are scarce; those which describe CaSR-mediated p90RSK regulation use supraphysiological $[Ca^{2+}]_o$ concentrations (Frees *et al.*, 2018), while others reporting NPS R-568-induced p90RSK activation fail to state prevailing $[Ca^{2+}]_o$ levels (Oh *et al.*, 2011). Curiously, CaSR-mediated p90RSK signalling was not quantified statistically in either study, suggesting that the role played by in CaSR in $[Ca^{2+}]_o$-induced p90RSK signalling may be minor, or very variable in some models. Studies here comparing CaSR-expressing and uninduced HEK293-CaSR cells appeared to confirm this concept; $[Ca^{2+}]_o$ stimulation profoundly enhanced $ERK_{1/2}$ and p90RSK activation in induced cells. On the other hand, cinacalcet readily stimulated $ERK_{1/2,}$ but its effect on p90RSK was irregular and did not reach significance. Both effects were lacking in uninduced cells, demonstrating that $[Ca^{2+}]_o$ and cinacalcet responses rely on CaSR. However, it would appear that $ERK_{1/2}$ compared to p90RSK is more sensitive marker of allosteric CaSR stimulation.

CaSR-mediated AKT activation is evident in primary calvarial and kidney cells, as well as colonic myofibroblasts (Magno, Ward and Ratajczak, 2011) and 786-O renal cells overexpressing CaSR (Frees *et al.*, 2018), but this pathway had not been described in HEK293-CaSR overexpression models. Surprisingly, there was no effect of $[Ca^{2+}]_o$ or allosteric CaSR modulators on AKT activation, indicating that AKT is not regulated by CaSR in HEK293-CaSR cells. As aforementioned, HEK293-CaSR cells comprise a key tool in studying CaSR-dependent signal transduction. Given that CaSR-mediated AKT activation has been confirmed in

non-heterologous cells, these data demonstrate that HEK293-CaSR cells are not a comprehensive model of CaSR signalling. Consequentially, results from heterologous HEK293-CaSR systems should be interpreted cautiously when seeking to characterise the biological role of CaSR.

3.4.3 Amino acids and CaSR-mediated intracellular signalling

L-Phe is an amino acid allosteric modulator of CaSR. In HEK293-CaSR cells, L-Phe has previously been shown to increase $[Ca^{2+}]_o$ sensitivity, leading to increased CaSR-dependent $ERK_{1/2}$ phosphorylation (Lee *et al.*, 2007). The present study sought to establish whether ADMA can signal via the CaSR, so L-Phe was used as a positive control for amino acid mediated CaSR sensitisation. Surprisingly, L-Phe had no effect on $ERK_{1/2}$ signalling here, even at supraphysiological concentrations shown to mobilise $[Ca^{2+}]_o$ and reduce cAMP (Conigrave, Quinn and Brown, 2000; Broadhead et al., 2011). Interestingly, the effects mediated by L-Phe in previous studies are typically small; L-Phe reduces the EC_{50} for $[Ca^{2+}]_o$-induced $ERK_{1/2}$ activation by 15%, from 2.3 to 2mM (Lee *et al.*, 2007). Though other studies corroborate its positive allosteric effects in heterologous HEK293 systems, L-Phe effects are of similarly small magnitude, whereby L-Phe decreases the EC_{50} for $[Ca^{2+}]_o$-induced IP_3 by ~25% and $[Ca^{2+}]_o$-induced $[Ca^{2+}]_i$ accumulation by 11% (Liu *et al.*, 2020). As previously discussed, the EC_{50} for $[Ca^{2+}]_o$-induced $ERK_{1/2}$ activation here was 4.4mM, ~40% greater when compared to the Lee *et al.* (2007) study, suggesting that cells here may be less sensitive to CaSR stimulation. Accordingly, reduced $[Ca^{2+}]_o$ sensitivity may confound detection of small L-Phe-dependent $ERK_{1/2}$ effects in HEK293-CaSR cells here. Aside from the difficulties imposed by potentially small effect sizes, successful identification of amino acid effects is additionally complicated by the diverse range of ligands which are active at the CaSR, many of which are present in cell media and buffer formulations. For instance, the EC_{50} for $[Ca^{2+}]_o$-induced $[Ca^{2+}]_i$ signalling is 4.2mM in intact HEK293 cells. However, the EC_{50} rises to 4.5mM when determined by cell-free, nutrient-free assays studying isolated membranes and is further increased to 7.4mM in dialysed, disrupted membranes. These data suggest that ambient, structural amino acids contribute towards CaSR activation (Liu *et al.*, 2020), showing that even small deviations in experimental conditions can profoundly affect CaSR behaviour. Accordingly, investigations seeking to identify the effect of CaSR-active amino acids may be significantly influenced

by cell models, experimental approaches, and culture conditions. Possibly, variation in these factors may have confounded detection of L-Phe mediated CaSR effects in the present study.

Earlier work performed in HEK293-CaSR cells in our lab demonstrated that ADMA sensitises CaSR-mediated $[Ca^{2+}]_i$ mobilisation (Dowsett *et al.*, 2022), raising the possibility that ADMA acts as an allosteric agonist of CaSR. Seeking to explore how ADMA might impact on CaSR signalling, the effect of ADMA on $[Ca^{2+}]_o$-induced $ERK_{1/2}$ signalling was investigated. In the presence of low 0.5mM $[Ca^{2+}]_o$, ADMA caused a modest but significant increase in $ERK_{1/2}$ activation. Previous reports describe $ERK_{1/2}$ activation following ADMA treatment in kidney myofibroblasts (Jayachandran *et al.*, 2020) and endothelial cells *in vitro* (Jiang *et al.*, 2007). However, in both instances, $ERK_{1/2}$ activation occurred in response to chronic 24h stimulation with supraphysiological (≥30μM) ADMA concentrations. In contrast, the present study demonstrated that $ERK_{1/2}$ signalling can be stimulated with acute 10min exposure to ADMA at low (1-3μM) concentrations. Plasma ADMA concentration in healthy adults is ~0.5μM. However, levels are elevated in cardiovascular disease states, rising ~57% in hypercholesteremia and hypertension and ~2-fold in renal failure (Horowitz and Heresztyn, 2007). Therefore, this study shows that ADMA stimulates $ERK_{1/2}$ within a biologically relevant range. Despite these data, this study was surprised to find that there was no effect of ADMA following treatment with pharmacological (≥30μM) ADMA concentrations. Possibly, this finding suggests ADMA effects are concentration-dependent; however, the underlying reasons for this were not elucidated.

ADMA-mediated $ERK_{1/2}$ responses seemed closely related to prevailing $[Ca^{2+}]_o$ levels. ADMA was unable to stimulate $ERK_{1/2}$ signalling in the absence of $[Ca^{2+}]_o$, indicating that $[Ca^{2+}]_o$ is prerequisite in this response. This behaviour mimics that of NPS R-568 here, and L-amino acids acting at CaSR in HEK293-CaSR cells, which are typically inactive below 0.5mM $[Ca^{2+}]_o$ (Conigrave et al., 2004). Curiously, while 1μM ADMA enhanced $ERK_{1/2}$ activation by ~60% in low 0.5mM $[Ca^{2+}]_o$ conditions, the effect size was reduced to ~30% in moderate 2mM $[Ca^{2+}]_o$ and was absent in the presence of high 3mM $[Ca^{2+}]_o$. Consequentially, it would appear that $[Ca^{2+}]_o$ concentration is an important determinant of ADMA mediated $ERK_{1/2}$ activation. If ADMA acts to sensitise CaSR signalling, ADMA effects might

only be anticipated in conditions where $[Ca^{2+}]_o$-driven CaSR activation is submaximal. However, CaSR remains amenable to allosteric stimulation at 3mM $[Ca^{2+}]_o$, since earlier experiments showed a sensitising effect of NPS R-568 under these conditions. Though ADMA was unable to augment $ERK_{1/2}$ activation with 3mM $[Ca^{2+}]_o$, ADMA driven increases in $ERK_{1/2}$ activation are subtle compared to those mediated by NPS R-568. Considering that $ERK_{1/2}$ signal variability greatly increases with increasing $[Ca^{2+}]_o$ (Fig. 3-4a), amino acid-mediated $ERK_{1/2}$ effects may be masked or insignificant at higher $[Ca^{2+}]_o$ concentrations.

In this study, allosteric CaSR modulators were shown to influence $ERK_{1/2}$ as well as its downstream target p90RSK, so the effect of ADMA on p90RSK activation was also interrogated. Surprisingly, p90RSK was not similarly activated by ADMA, inconsistent with its effect on $ERK_{1/2}$ signalling. As previously discussed, p90RSK seems to be a less sensitive marker of CaSR activation compared to $ERK_{1/2}$. Therefore, it may be that small, ADMA-mediated increases in $ERK_{1/2}$ activation are unable to effectively trigger downstream p90RSK recruitment. Interestingly, CREB activation in HEK293-CaSR cells is regulated by synthetic CaSR modulators NPS 2143 and cinacalcet, but not L-Phe (Avlani *et al.*, 2013). Accordingly, amino acid modulators of CaSR may display signalling cascades which are distinct from those induced by calcimimetics or $[Ca^{2+}]_o$. Plausibly, p90RSK signalling may be differentially regulated by NPS R-568 and ADMA here. Future studies should determine whether NPS R-568-mediated p90RSK is dependent on $ERK_{1/2}$ signalling, and explore whether other $ERK_{1/2}$ cascade mediators (mitogen- and stress-activated protein kinases, MAP kinase-interacting serine/threonine-protein kinases and phospholipase A_2) (Guo *et al.*, 2020), could instead be regulated by ADMA.

Intending to understand whether ADMA enhances $[Ca^{2+}]$-dependent $ERK_{1/2}$ activation via a CaSR-dependent mechanism, this study examined how ADMA affects $ERK_{1/2}$ in uninduced HEK293-CaSR cells lacking CaSR expression. ADMA was unable to potentiate $ERK_{1/2}$ signalling in uninduced HEK293-CaSR cells irrespective of prevailing $[Ca^{2+}]_o$ concentrations, suggesting that ADMA-mediated $ERK_{1/2}$ effects rely on CaSR. Interestingly, ADMA effects would appear to be structurally specific, since SDMA could not reproduce ADMA-mediated $ERK_{1/2}$ activation in HEK293-CaSR cells. ADMA is thought to mediate its biological

effects by reducing NO production through inhibition of NOS (Caplin and Leiper, 2012), but studies examining methylarginine mediated NOS inhibition often use ADMA at supraphysiological concentrations. Electron paramagnetic resonance has demonstrated that pathological ADMA concentrations (10μM) produce 19% NOS inhibition, while physiological (<5μM) ADMA levels are predicted to inhibit NOS by 10% (Cardounel *et al.*, 2007). As such, ADMA concentrations shown to enhance $ERK_{1/2}$ signalling here (1-10μM) would not be expected to invoke significant inhibition of NOS. In alignment, there was no inhibitory effect of ADMA on cellular NO production here. In fact, ADMA modestly increased NO in some experiments, suggesting that NOS inhibition may not be a predominant mechanism underpinning ADMA-mediated $ERK_{1/2}$ activation. Supporting this view, $ERK_{1/2}$ activation was unaltered when NOS was maximally inhibited with L-NAME, demonstrating that NO is not an influential mediator of $ERK_{1/2}$ signalling in HEK293-CaSR cells. Taken together, it would appear that ADMA-mediated $ERK_{1/2}$ activation could be regulated by CaSR, independent of NO signalling.

Compared to the synthetic modulator NPS R-568, the effect of acute ADMA on $[Ca^{2+}]_o$-induced $ERK_{1/2}$ signalling was small. However, small shifts in CaSR sensitivity can manifest potentially significant effects on biological function. For instance, L-Phe reduces the IC_{50} for $[Ca^{2+}]_o$-induced parathyroid hormone inhibition by 0.1mM. Despite mediating a small shift in $[Ca^{2+}]_o$- sensitivity overall, L-Phe reduces parathyroid hormone secretion by 14-44% within a $[Ca^{2+}]_o$ range of 0.9-1.3mM (Conigrave *et al.*, 2004). Considering that circulating $[Ca^{2+}]_o$ concentrations are tightly regulated between 1.1-1.3mM (Zhang *et al.*, 2016), amino acid regulation of CaSR activity could have profound physiological implications. Here, acute $ERK_{1/2}$ activation was enhanced ~30% by 1μM ADMA in the presence of 2mM $[Ca^{2+}]_o$, rising to ~60% when $[Ca^{2+}]_o$ was lowered to 0.5mM. As ADMA enhances $ERK_{1/2}$ activation at $[Ca^{2+}]_o$ concentrations either side of the physiological range, this mechanism could prove significant in native cells *in vivo*. Future studies should examine the effect of ADMA on $ERK_{1/2}$ activation in a range of cell types, particularly parathyroid cells, to determine the biological significance of ADMA-mediated, $[Ca^{2+}]$-dependent $ERK_{1/2}$ activation.

3.4.4 CaSR-mediated gene expression

CaSR stimulation regulates key nuclear transcription factors Elk-1, Egr-1 and AP-1 in HEK293 cells, suggesting that CaSR may have pleiotropic effects on cellular gene expression (Thiel, Lesch and Keim, 2012). Among the many biological processes now known to be mediated by CaSR, its identified role in inflammation and fibrosis is common to several cells types, including cardiovascular cells (Peng *et al.*, 2014; Sundararaman and van der Vorst, 2021). To understand whether HEK293-CaSR cells could be used to model CaSR-dependent gene expression, this study examined whether NPS R-568 influences the transcriptional regulation of two key profibrotic genes, TGFß and MMP2 (Ruiz-Ortega *et al.*, 2007). Here, NPS R-568 increased the expression of both TGFß and MMP2, suggesting that these genes are positively regulated by CaSR. Notably, the transcriptional response to NPS R-568 was $[Ca^{2+}]_o$-dependent demonstrating a threshold between 0.5-2mM, reminiscent of the threshold $[Ca^{2+}]_o$ concentration for NPS R-568-mediated $ERK_{1/2}$ stimulation (0.5-1mM; Fig. 3-5a). Interestingly, previous work has linked CaSR activation with $ERK_{1/2}$ signalling, MMP2 expression and fibrosis in pulmonary arterial cells (Peng *et al.*, 2014). Plausibly, NPS R-568-induced $ERK_{1/2}$ activation may be similarly associated with TGFß and MMP2 mRNA expression in HEK293-CaSR cells; however, further work is required to examine this mechanism directly. Nonetheless, these data illustrate that HEK293-CaSR cells comprise a practical system for evaluating CaSR-dependent expression of two key profibrotic genes.

Replicating the results of acute treatment, chronic 24h stimulation with 10µM ADMA in the presence of 0.5mM $[Ca^{2+}]_o$ enhanced $ERK_{1/2}$ activation, raising the possibility that pathological perturbations in ADMA leading to chronically increased circulating levels may impact on cellular function. Though CaSR regulated TGFß and MMP2 mRNA expression, this effect was not reproduced by ADMA. Possibly, ADMA-mediated changes in gene expression may be lacking as a result of its modest effect on $ERK_{1/2}$ signalling. Future investigations should attempt to identify additional transcriptional targets of CaSR using a range of $[Ca^{2+}]_o$ concentrations to further examine how allosteric CaSR mediators and ADMA influence CaSR gene expression.

3.5 Conclusions

HEK293 cells overexpressing CaSR show $[Ca^{2+}]_o$-dependent $ERK_{1/2}$ and p90RSK activation in response to acute $[Ca^{2+}]_o$ and NPS R-568 stimulation. AKT was not similarly regulated, indicating that CaSR regulates $ERK_{1/2}$ cascades but not AKT signalling in HEK293-CaSR cells. In its physiological range, ADMA demonstrated $[Ca^{2+}]_o$-dependent $ERK_{1/2}$ activation. This effect was not recapitulated in uninduced HEK293 cells. Crucially, ADMA was unable to augment cell nitrite concentrations, and ADMA-mediated $ERK_{1/2}$ signalling was not replicated with the NOS inhibitor L-NAME. Collectively, these data suggest that ADMA-mediated $ERK_{1/2}$ activation relies on CaSR and does not implicate NO signalling. p90RSK activation and $[Ca^{2+}]_o$-dependent TGFβ and MMP2 mRNA expression were regulated by NPS R-568, but not ADMA, possibility due to the small effect of ADMA on $ERK_{1/2}$ activation. Future studies should explore how NPS R-568 and ADMA regulates $ERK_{1/2}$ signalling and identify additional CaSR-responsive gene targets to clarify the role of ADMA in CaSR signalling.

Chapter Four

3T3-L1 adipocytes

Chapter 4: 3T3-L1 adipocytes

4.1 Introduction

The relationship between adiposity and increased cardiovascular risk is well described, but changes in adipose distribution, inflammation, lipid storage and secretory function can also negatively impact cardiovascular homeostasis and aggravate cardiovascular disease (CVD) (Akoumianakis and Antoniades, 2017; Oikonomou and Antoniades, 2019). Adipose tissue (AT) is known to be disturbed in cardiometabolic pathologies such as obesity, diabetes and insulin resistance (Oikonomou and Antoniades, 2019). Asymmetrical dimethylarginine (ADMA) is elevated in these disease states (Abbasi *et al.*, 2001; Stühlinger *et al.*, 2002; Eid *et al.*, 2004) and increases cardiovascular risk in diabetes (Tarnow *et al.*, 2004). AT may therefore represent an important interface through which ADMA regulates cardiovascular (patho)physiology. As such, the effect of ADMA on AT is of considerable interest.

To date, few studies have sought to appraise the significance of ADMA in adipocytes. In humans, ADMA is increased in insulin-resistant, obese AT (El Assar *et al.*, 2016), suggesting that ADMA could be linked with AT dysfunction. When applied exogenously, ADMA stimulates lipid accumulation in HEPG2 hepatocyte cell lines; this effect is recapitulated in high-fat fed genetic murine models of ADMA accumulation, which are obese and insulin resistant (Li *et al.*, 2017). Our group has reported similar effects in adipocytes *in vitro*. In mature 3T3-L1 adipocytes, chronic ADMA stimulation results in enhanced lipid loading and cellular hypertrophy. This response is conserved *in vivo*, since mice with adipocyte-specific dimethylarginine dimethylaminohydrolase-1 (DDAH1) deficiency (reduced ADMA catabolism) demonstrate increased adipocyte lipid content and fat mass (Dowsett *et al.*, 2022). Together, these studies show that ADMA plays a role in both lipid metabolism and adipocyte physiology. ADMA (patho)physiology is thought to be mediated through its ability to perturb endogenous NO (Leiper and Nandi, 2011). However, our lab has recently demonstrated that ADMA-driven adipocyte hypertrophy is not emulated by L-NAME NOS blockade (Dowsett *et al.*, 2022). As such, the physiological effect of ADMA in adipocytes does not appear to be fully explained by the prototypical

ADMA/NO pathway, implying that other, NO-independent mechanism(s) could play a role.

The calcium-sensing receptor (CaSR) is expressed in preadipocytes, cell line adipocyte models and primary adipocytes (Cifuentes, Albala and Rojas, 2005; Cifuentes *et al.*, 2010; He, Zhang, *et al.*, 2011; He *et al.*, 2012; Xing *et al.*, 2019). Disturbances in CaSR signalling are linked to metabolic dysfunction (Vahe *et al.*, 2017) and there is some evidence to suggest that CaSR activation could be enhanced in obese individuals (Villarroel *et al.*, 2014). Moreover, animal models of increased CaSR activation demonstrate impaired glucose homeostasis characterised by hyperglycaemia and hypoinsulinemia (Babinsky *et al.*, 2017). Collectively, the CaSR is emerging as a mediator of metabolic derangement, though the mechanism(s) involved have not been fully clarified. CaSR activation regulates adipocyte lipid handling, inflammation and adipose expansion *in vitro*, suggesting that adipocyte CaSR mediates AT dysfunction and contributes toward obesity-related pathology (Bravo-Sagua *et al.*, 2016). Though CaSR is implicated in adipocyte dysfunction, these findings do not address whether adipocyte CaSR could be amenable to allosteric stimulation by amino acids, which have demonstrated bioactivity at CaSR in heterologous and native cell systems (Conigrave, Mun and Lok, 2007). Interestingly, plasma levels of potent CaSR-active amino acids such as L-Phenylalanine (L-Phe) and L-Tyrosine are negatively associated with insulin sensitivity in normoglycemic women (Wiklund *et al.*, 2016). These amino acids, in addition to CaSR-active L-Tryptophan, were also positively correlated with visceral adiposity in a very recent study (Muresan *et al.*, 2021). Though a causal role cannot be derived from these studies, these associations could be explained by interactions between amino acids and CaSR in AT. As the role of amino acids in CaSR signalling gains increasing recognition, the CaSR comprises a possible target through which ADMA mediates NO-independent effects on adipocyte biology.

To establish how CaSR and ADMA affects adipocyte function, this study utilised the murine embryonic fibroblast 3T3-L1 cell line. Previously, our lab has shown that cell size and lipid accumulation are positively regulated by extracellular ADMA in 3T3-L1 adipocytes (Dowsett *et al.*, 2022). As previously discussed, CaSR potentiates AT accumulation and inflammation in adipocyte cell lines. If ADMA

mediates adipocyte biology via a CaSR target, then CaSR stimulation would be expected to lead to adipocyte expansion. However, the effect of CaSR on adipocyte morphology is yet to be examined. Though ADMA potentiates cell size, the functional significance of this response has not been established. Considering that adipocyte size is related to adipokine secretion (Skurk *et al.*, 2007), ADMA-induced hypertrophy would predicted to influence adipokine signalling. Meanwhile, the effect of CaSR stimulation on adipokine production has not been evaluated. To understand the biological relevance of ADMA-mediated cellular hypertrophy and assess whether ADMA implicates CaSR signalling in adipocytes, this study examined lipogenic signalling pathways, as well as key adipokines adiponectin and leptin.

4.2 Aims

1. To demonstrate and characterise CaSR expression in 3T3-L1 adipocytes
2. To illustrate ADMA-mediated adipocyte hypertrophy and explore the molecular mechanism(s) underpinning ADMA responses in adipocytes.
3. To establish whether CaSR regulates adipocyte hypertrophy and characterise the effect of CaSR on adipocyte signalling.

4.3 Results

4.3.1 Mature adipocyte differentiation

3T3-L1 cells were differentiated from preadipocytes to mature adipocytes. To demonstrate adipocyte differentiation, lipid accumulation was assessed using oil-red-o neutral lipid staining in confluent, naive preadipocytes (d0) and in mature adipocytes following 10 days exposure to the differentiation induction cocktail (d10). Oil-red-O optical density in d0 cells was 0.085±0.004. Compared to d0 cells, optical density in d10 cells was increased to 0.151±0.016, corresponding to greater lipid content ($p=0.0147$; Fig 4-1a, b). To further demonstrate adipocyte development, the adipocyte maturation marker perilipin-1 (PLN-1) was assessed throughout the differentiation period (d0-d10). When compared to d0 cells, PLN-1 protein levels were not significantly increased at d3 or d6 ($p>0.05$). However, PLN-1 expression was markedly elevated 136.9± 7.9-fold by d8 ($p=0.0116$) and 136.2±47.2-fold by d10 ($p=0.0120$; Fig. 4-2a, b), indicating the acquirement of a mature adipocyte phenotype.

Figure 4-1

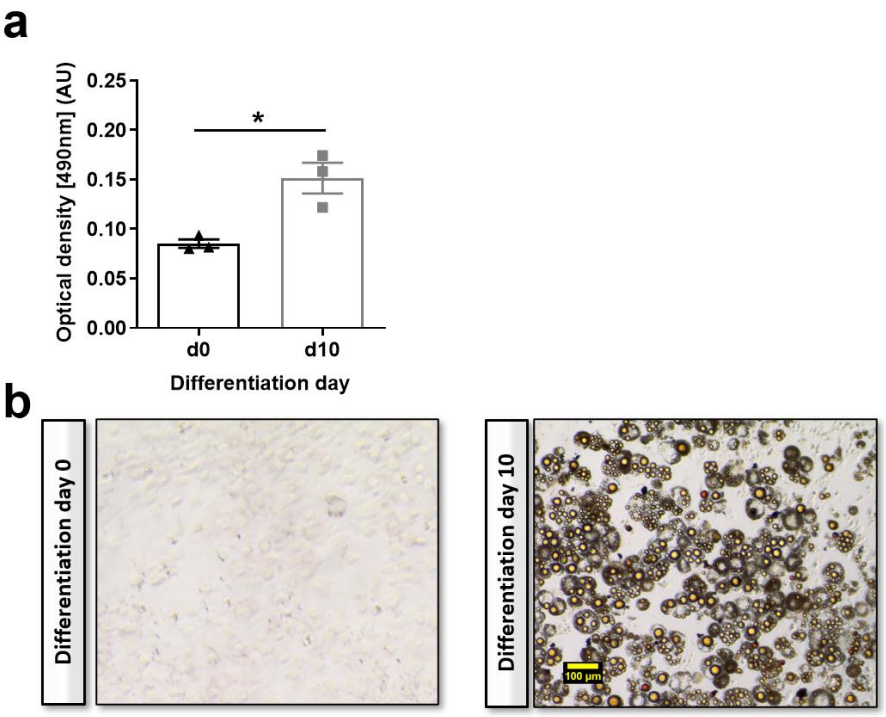

Figure 4-1: Lipid accumulation in differentiating 3T3-L1 adipocytes. **(a)** When compared to confluent, naïve preadipocytes (d0), oil-red-o neutral lipid staining is enhanced in 3T3-L1 adipocytes 10 days following differentiation induction (d10). **(b)** Representative images of oil-red-o neutral lipid staining in d0 and d10 3T3-L1 adipocytes. Mean±SEM. Unpaired t-test (a). *p<0.05. Magnification 10X. Scale bar=100µm.

Figure 4-2

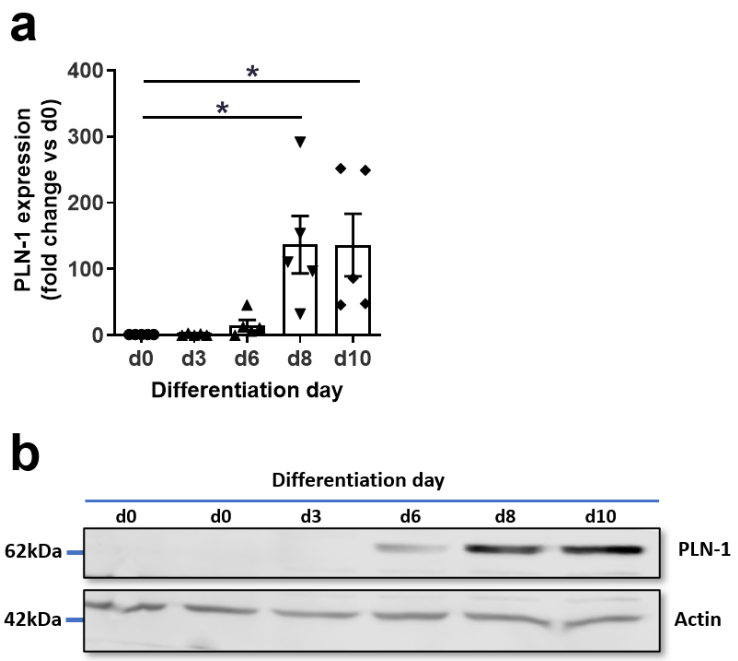

Figure 4-2: PLN-1 protein expression in differentiating 3T3-L1 cells.
(a) When compared to confluent, naïve preadipocytes (d0), PLN-1 protein levels are elevated through differentiation, becoming significantly raised by day 8 (d8) and d10 following differentiation induction **(b)** Representative western blot image of PLN-1 across the differentiation period in 3T3-L1 cells. Mean±SEM. One-way ANOVA (a). *p<0.05 vs d0. PLN-1=Perilipin-1.

4.3.2 CaSR expression

Previous studies have demonstrated CaSR expression in adipocyte models *in vitro* (Bravo-Sagua *et al.*, 2016). To show that 3T3-L1 adipocytes express CaSR, qPCR analyses were performed. CaSR qPCR products were successfully detected in 3T3-L1 lysates, showing that 3T3-L1 adipocytes produce CaSR transcript (Fig. 4-3). Before undertaking studies to assess how ADMA affects adipocyte signalling, qPCR analyses were used to probe the expression of ADMA-metabolising DDAH enzymes. Both DDAH1 and DDAH2 transcript was readily expressed by 3T3-L1 adipocytes, suggesting that ADMA undergoes catabolism and is regulated in adipocytes (Fig. 4-3).

Figure 4-3

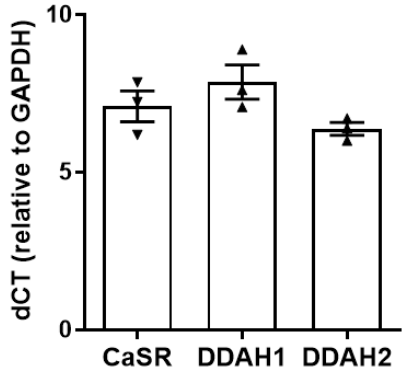

Figure 4-3: mRNA expression in 3T3-L1 adipocytes.
CaSR and DDAH mRNA expression is demonstrated in mature adipocytes following qPCR analysis using primers against CaSR, DDAH1 and DDAH2. Mean±SEM. CaSR=Calcium sensing receptor; DDAH=Dimethylarginine dimethylaminohydrolase.

CaSR transcript was detected in mature 3T3-L1 adipocytes. To confirm that 3T3-L1 adipocytes express CaSR at the protein level, western blot analyses were performed on 3T3-L1 cells throughout differentiation (d0-d10). The expression of CaSR protein in 3T3-L1 cell lysates was ascertained by the presence of two protein bands; a faint upper band migrating at ~260kDa and a lower band migrating at ~130kDa. The 260kDa upper band was present in all samples throughout differentiation. Compared to d0, the expression of CaSR protein migrating at 260kDa remained constant throughout differentiation ($p>0.05$; Fig. 4-4a, c). Similarly, the 130kDa lower band was present in 3T3-L1 fibroblasts and differentiating adipocytes. Expression of CaSR protein at 130kDa was constant through differentiation when compared to d0 fibroblasts ($p>0.05$; Fig. 4-4b, c), suggesting that CaSR is stably expressed throughout 3T3-L1 differentiation.

Western blot analysis demonstrating CaSR expression in 3T3-L1 adipocytes was validated using immunofluorescence imaging in mature 3T3-L1 adipocytes. Visualisation of 3T3-L1 cultures revealed successful CaSR staining, confirming CaSR protein expression. A faint signal was present following primary antibody only control staining, indicating low levels of autofluorescence in 3T3-L1 specimens. However, samples did not demonstrate fluorescence in response to

secondary antibody only control staining, illustrating that CaSR staining patterns are not due to non-specific secondary antibody interactions (Fig. 4-4d).

Figure 4-4

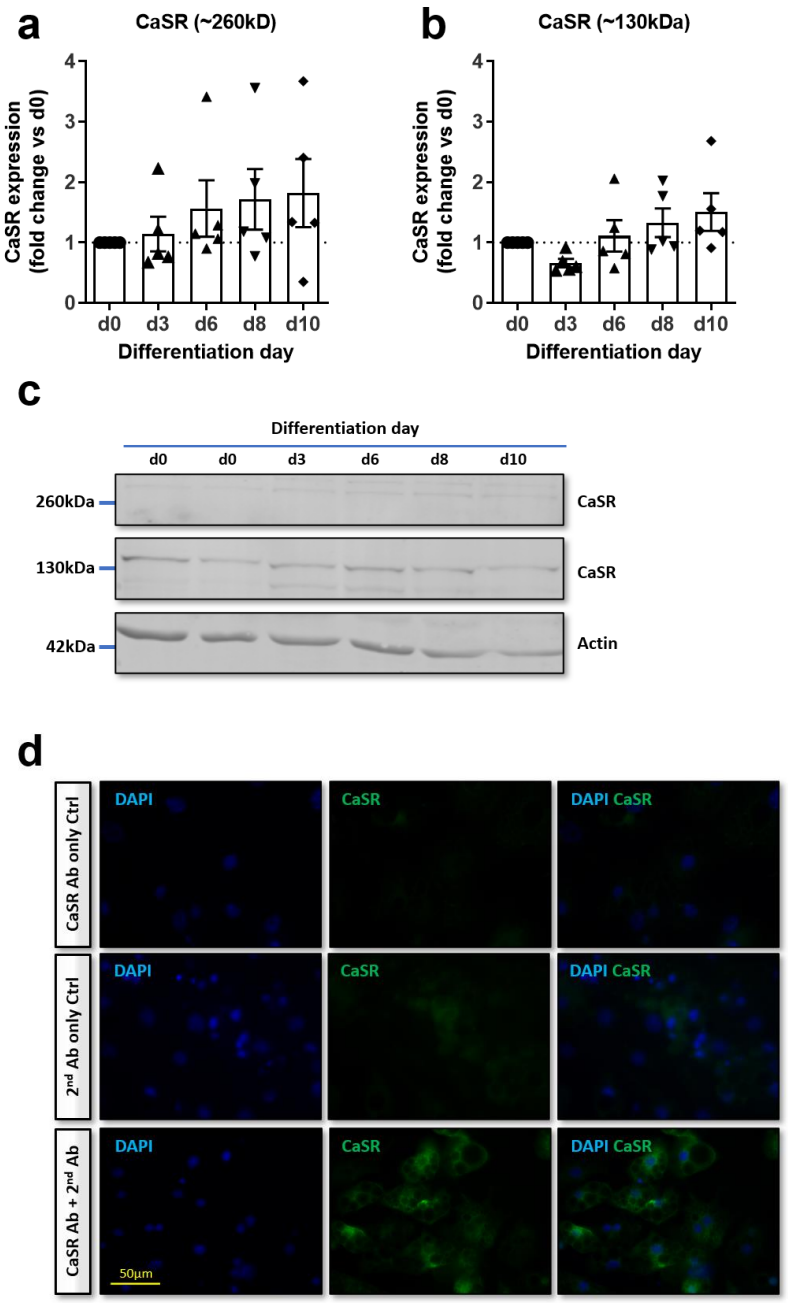

Figure 4-4: CaSR protein expression in 3T3-L1 cells.

(a) CaSR protein is present in naïve preadipocytes (d0) and throughout differentiation day (d)3-10, identified by bands migrating at ~260kDa **(b)** and ~130kDa. **(c)** Representative western blot image of CaSR protein across the differentiation period in 3T3-L1 cells. CaSR was identified by two bands; an upper band and lower band migrating at 260kDa and 130kDa, respectively. **(d)** Representative image of positive immunofluorescent staining of CaSR in 3T3-L1 adipocytes. Mean±SEM. One-way ANOVA (a,b). Magnification 40X. Scale bar=50µm. CaSR=Calcium sensing receptor.

4.3.3 Adipocyte hypertrophy

4.3.3.1 ADMA-induced adipocyte hypertrophy

Previous work by our lab showed that ADMA regulates adipocyte size. To reproduce the effect of ADMA on adipocyte size here, mature 3T3-L1 adipocytes were treated with exogenous ADMA. 3T3-L1 adipocytes were also exposed to the NOS inhibitor L-NAME (1mM) to assess how NO signalling affects adipocyte size. SDMA (10μM) was used as a structural control for ADMA. After 72h exposure, neutral lipid content was assessed in 3T3-L1 adipocytes using BODIPY staining. 3T3-L1 cells exhibited significant cellular hypertrophy when exposed to ADMA at all concentrations. The mean size of cells in untreated control cultures was 659.2±444.0μm^2. Compared to control specimens, treatment with 1μM ADMA increased cell size by 23% (813.9±572.2μm^2, $p<0.0001$) and 3μM ADMA increased cell size by 30% (859.7±556.6μm^2, $p<0.0001$). This effect was also observed following treatment with pathological ADMA levels. Cell size in 3T3-L1 cultures which were exposed to 10μM ADMA was increased by 28% compared to controls (843.9± 534.3μm^2, $p<0.0001$). In these experiments, cell size was not affected by SDMA (624.7± 420.8μm^2, $p>0.05$) or L-NAME (615.7± 397.4μm^2, $p>0.05$; Fig. 4-5a, b), suggesting that ADMA-mediated hypertrophy is structurally specific and is not perpetrated by NO inhibition. In this experimental set, technical and analytical work was performed in collaboration with Dr. Laura Dowsett (University of Glasgow).

Figure 4-5

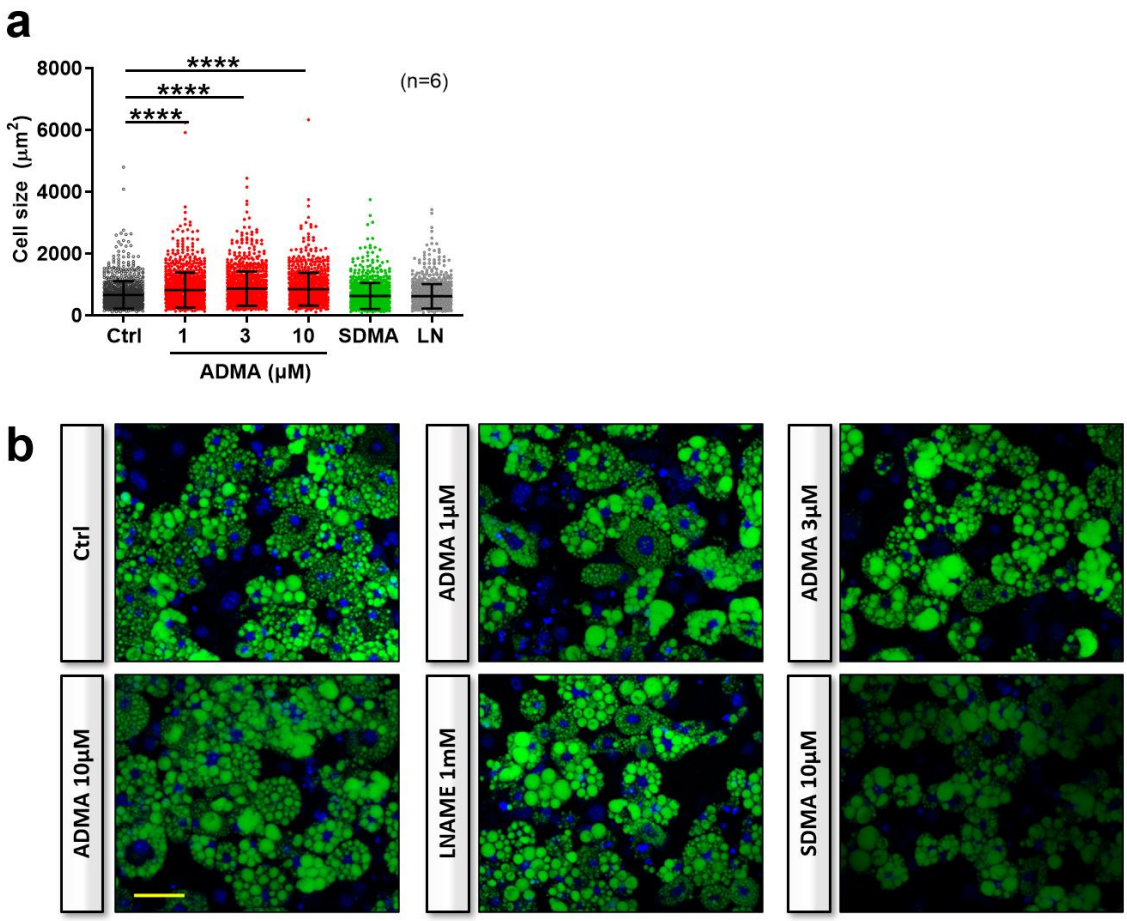

Figure 4-5: ADMA-induced hypertrophy in 3T3-L1 adipocytes.

(a) 3T3-L1 adipocytes with 1, 3 and 10µM ADMA are increased in size compared to control cultures. 10µM SDMA and 1mM L-NAME (LN) have no effect on cell size. **(b)** Representative images of 3T3-L1 BODIPY neutral lipid staining with DAPI counterstain. Mean±SD. One-way ANOVA (a). ****p<0.0001. Magnification 20X. Scale bar=50µm. ADMA=Asymmetric dimethylarginine; SDMA=Symmetric dimethylarginine.

ADMA caused adipocyte hypertrophy, but the response was not replicated by L-NAME. To investigate whether ADMA-mediated hypertrophy acts via inhibition of NO signalling, nitrite levels were examined in 3T3-L1 adipocyte media following 72h incubation with ADMA. Media nitrite levels from cells incubated in control media was 3.4±0.3 µM. ADMA was unable to influence media nitrite levels at all concentrations. Compared to control values, cell media nitrite concentrations were not reduced by 1µM ADMA (3.1±0.4 µM, p>0.05), 3µM ADMA (3.2±0.3 µM, p>0.05) or 10µM ADMA (5.2±0.5 µM, p>0.05; Fig. 4-6a).

As ADMA was unable to inhibit NO production in 3T3-L1 cultures, experiments were performed to demonstrate that NO could be inhibited pharmacologically *in vitro*. Cells were incubated with supraphysiological ADMA (100μM) or L-NAME (1mM) for 72h. In these experiments, media nitrite levels derived from untreated control cells was 3.4±0.2 μM. In comparison, 3T3-L1 cell media nitrites were not affected by 100μM ADMA (3.1±0.1 μM, $p>0.05$). However, cell media nitrites were significantly reduced by L-NAME, which were decreased 47% compared to those in control conditions (1.8±0.2μM, $p=0.0013$; Fig. 4-6b), showing that L-NAME inhibits NO in 3T3-L1 cultures.

ADMA does not influence NO production in 3T3-L1 cultures. To further explore whether ADMA affects adipocyte NO signalling, eNOS mRNA expression was investigated in 3T3-L1 adipocytes following 48h treatment with 10μM ADMA. Cells were also treated in the presence or absence of 10μM NPS-2143, a CaSR inhibitor, the evaluate how eNOS may be influenced by CaSR signalling. Compared to control conditions, ADMA tended to increase eNOS expression, but the effect was not statistically significant (1.7±0.1-fold, $p=0.0899$). CaSR inhibition did not influence eNOS mRNA levels, since expression was not modified with NPS-2143 (1.2±0.2-fold, $p>0.05$). Compared to ADMA or NPS-2143-only treatments, combined treatment with ADMA and NPS-2143 did not influence eNOS expression (1.7±0.2-fold, $p>0.05$; Fig. 4-6c).

Figure 4-6:

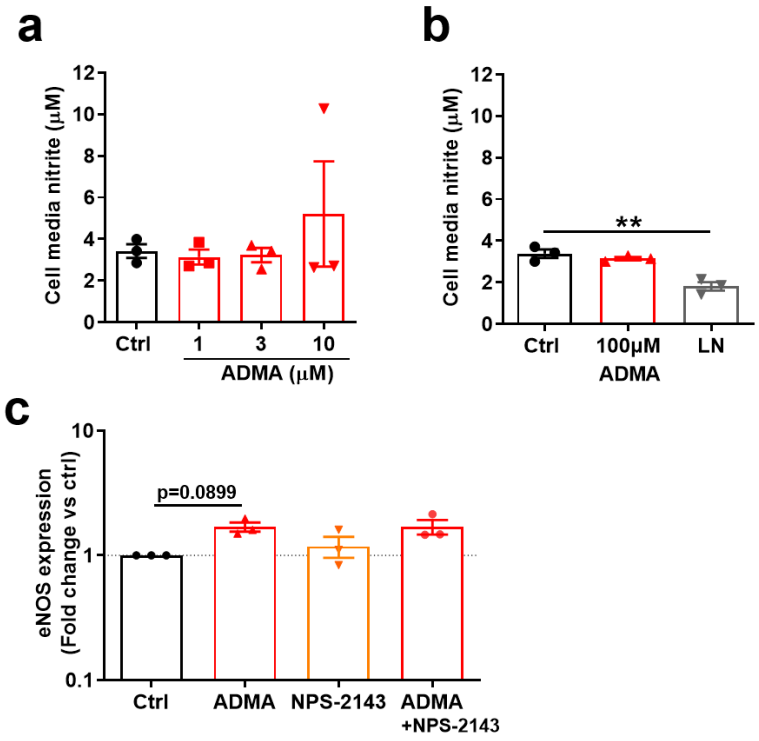

Figure 4-6: ADMA mediated NO signalling in 3T3-L1 adipocytes.

(a) Nitrite levels in 3T3-L1 cell media are unchanged by 72h physiological (1, 3 and 10µM) ADMA. **(b)** Nitrite levels in 3T3-L1 adipocyte media are not altered by 72h pharmacological (100µM) ADMA, but are significantly attenuated by 1mM L-NAME (LN). **(c)** eNOS mRNA expression is not significantly increased in adipocytes treated with ADMA (10µM) OR nps-2143 (10µm) for 48h. Mean±SEM. One-way ANOVA (a-c). **p<0.01. ADMA=Asymmetric dimethylarginine; SDMA=Symmetric dimethylarginine.

4.3.3.2 CaSR-induced adipocyte hypertrophy

ADMA potentiates adipocyte hypertrophy without impacting adipocyte NO production. To investigate whether ADMA-mediated adipocyte hypertrophy could be reproduced by CaSR stimulation, cells were treated with the CaSR type II (allosteric) agonist cinacalcet (0.1µM), ADMA (10µM) or SDMA (10µM) for 72h. The size of adipocytes incubated in control media was 394.9± 268.2µm^2. As with previous experiments, treatment with 10µM ADMA induced significant cellular hypertrophy, increasing cell size by 31% compared to controls (515.8±380.9µm^2, p<0.0001). Cinacalcet imposed a similar effect on 3T3-L1 cultures, which increased cell size by 23% (484.4± 386.3µm, p<0.0001). This was not replicated

by SDMA, which in these experiments significantly decreased cell size from control values (295.7±216.8μm^2, p<0.0001; Fig 4-7a, b).

Above, cinacalcet treatment causes hypertrophy in 3T3-L1 adipocytes. To further interrogate the effect of CaSR stimulation on 3T3-L1 adipocyte size, cells were incubated for 72h with NPS R-568 (1μM), a CaSR positive allosteric modulator. In these experiments, the size of cells in control conditions was 637.6± 566.2μm^2. As observed with cinacalcet, 3T3-L1 adipocytes treated with NPS R-568 exhibited significant cellular hypertrophy, where cell size was increased by 26% compared to control cultures (805.8± 586.3μm^2, p<0.0001; Fig. 4-8a, b), suggesting CaSR regulates adipocyte size.

Figure 4-7

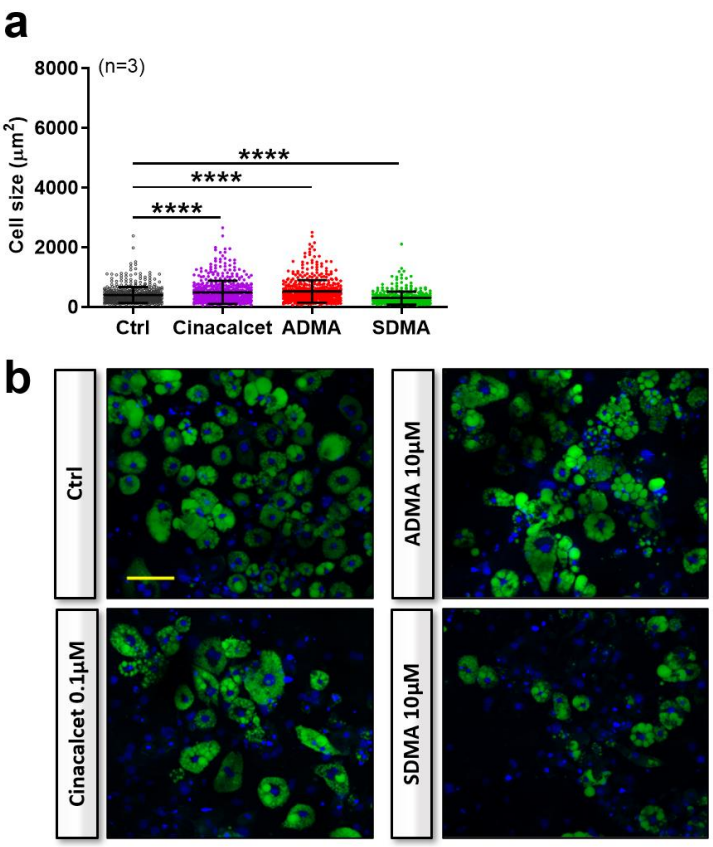

Figure 4-7: Cinacalcet-induced hypertrophy in 3T3-L1 adipocytes.
(a) Compared to control cultures, 3T3-L1 adipocyte size is increased by 10µM ADMA and 0.1µM cinacalcet, but decreased by 10µM SDMA. Mean±SD. **(b)** Representative images of 3T3-L1 BODIPY neutral lipid staining with DAPI counterstain. Mean±SD. One-way ANOVA (a). ****p<0.0001. Magnification 20X. Scale bar=50µm. ADMA=Asymmetric dimethylarginine; SDMA=Symmetric dimethylarginine.

Figure 4-8

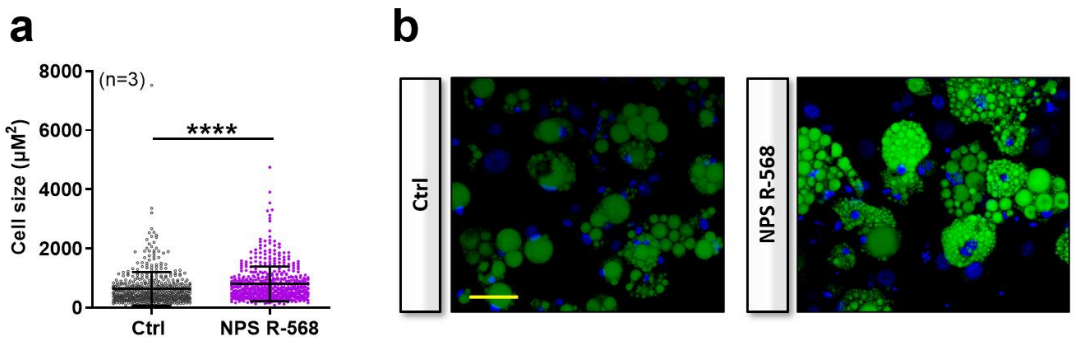

Figure 4-8: NPS R-568-induced hypertrophy in 3T3-L1 adipocytes.
(a) Compared to control cultures, 3T3-L1 adipocyte size is increased by 1μM NPSR-568. **(b)** Representative images of 3T3-L1 BODIPY neutral lipid staining with DAPI counterstain. Mean±SD. Unpaired t-test (a). ****p<0.0001. Magnification 20X. Scale bar=50μm.

The CaSR agonist cinacalcet and NPS R-568 caused adipocyte hypertrophy. In order to establish whether this response was associated with altered adipocyte NO signalling. cell media nitrite levels were examined following 72h treatment with cinacalcet. Control experiments demonstrated nitrite levels of 4.1±1.0μM. Compared to untreated cultures, media nitrite levels were not affected by 0.1μM cinacalcet (3.0±0.2μM, p>0.05) or 1μM cinacalcet (2.9±0.2μM, p>0.05; Fig. 4-9a). To confirm that CaSR stimulation did not lead to a change in 3T3-L1 adipocyte NO production, cells were treated with a second allosteric CaSR modulator, NPS R-568 (1μM). As with cinacalcet, nitrite levels in control cultures (1.1±0.3μM) were unchanged with 72h NPS R-568 incubation (1.6±0.1μm, p>0.05; Fig. 4-9b), indicating that adipocyte NO levels are unaffected by CaSR signalling.

To further demonstrate that CaSR stimulation does not affect adipocyte NO production, eNOS mRNA expression was assessed in 3T3-L1 adipocytes following 48h treatment with cinacalcet (0.1μM). Compared to control cultures, cinacalcet treatment did not alter adipocyte eNOS expression (1.1±0.2-fold, p>0.05; Fig. 4-9c). To confirm that eNOS expression is not regulated by CaSR signalling, 3T3-L1 adipocytes were treated with NPS R-568 (1μM). To ensure that CaSR would be amenable to allosteric stimulation and assess how CaSR activation affects the adipocyte response to allosteric stimulation, cells were exposed to NPS R-568 in the presence of a range of $[Ca^{2+}]_o$ concentrations (0.5, 1 and 2mM). Among these

conditions, there was no main effect of $[Ca^{2+}]_o$ (p=0.0929) or NPS R-568 alone (p>0.05), though interaction of these factors was a significant determinant of eNOS expression (p=0.0085; Fig. 4-9d). Multiple comparison analysis was performed to investigate the interplay between $[Ca^{2+}]_o$ or NPS R-568. In the presence of low 0.5mM $[Ca^{2+}]_o$, eNOS expression tended to be decreased with NPS R-568 treatment but did not reach significance (0.6±0.1-fold, p=0.0919). In contrast, eNOS expression was unchanged by NPS R-568 in the presence of 1mM and 2mM $[Ca^{2+}]_o$ (p>0.05; Fig. 4-9d), indicating that eNOS expression is not impacted by $[Ca^{2+}]_o$-mediated CaSR signalling.

Figure 4-9

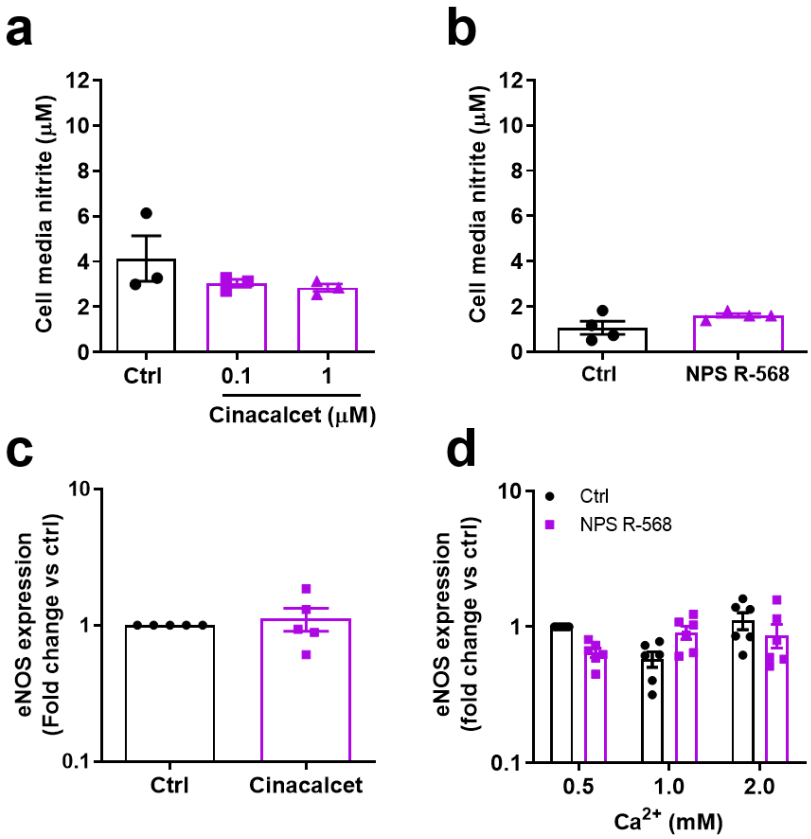

Figure 4-9: CaSR mediated NO signalling in 3T3-L1 adipocytes.
(a) Nitrite levels in 3T3-L1 cell media are unchanged by 72h cinacalcet. **(b)** Nitrite levels in 3T3-L1 cell media are unchanged by 72h 1µM NPS R-568. **(c)** eNOS mRNA expression is unaltered in 3T3-L1 adipocytes following 48h treatment with 0.1µM cinacalcet. **(d)** NPS R-568 (1µM) does not alter eNOS expression in the presence of 0.5, 1 or 2mM $[Ca^{2+}]_o$. Mean±SEM. One-way ANOVA (a). Unpaired t-test (b,c). Two-way ANOVA (d). ADMA=Asymmetric dimethylarginine; SDMA=Symmetric dimethylarginine.

4.3.4 Lipid accumulation

ADMA promoted 3T3-L1 adipocyte hypertrophy. To further explore how ADMA regulates lipid accumulation, mature adipocytes were treated for 72h with ADMA, SDMA (10μM) or L-NAME (1mM), then lipid droplet (LD) number and morphology were evaluated in 3T3-L1 adipocytes using BODIPY staining. In untreated control cultures, adipocytes demonstrated 16±2 LDs/cell. Unexpectedly, the number of LDs per adipocyte was broadly unaltered by ADMA. Compared to control adipocytes, LD number per cell was not influenced by 1μM ADMA (15±3 LDs/cell, $p>0.05$), 3μM ADMA (20±8 LDs/cell, $p>0.05$), or by higher, pathological 10μM ADMA concentrations (16±5 LDs/cell, $p>0.05$), suggesting that LD synthesis is not affected by ADMA. Likewise, the number of adipocyte LDs was not influenced by SDMA (17±6 LDs/cell, $p>0.05$) or by L-NAME (16±4 LDs/cell, $p>0.05$; Fig. 4-10a). ADMA similarly had no effect on other aspects of LD morphology. Mean LD area in control adipocytes was 33.8±5.7μm^2, but mean LD area was comparable following treatment with 1μM ADMA (30.7±2.5μm^2, $p>0.05$), 3μM ADMA (34.5±4.0μm^2, $p>0.05$) and also 10μM ADMA (35.0±2.3μm^2, $p>0.05$), showing no effect of ADMA on LD size. Again, LD area was not augmented by SDMA (32.0±3.0μm^2, $p>0.05$) or L-NAME (34.3±4.4μm^2, $p>0.05$; Fig. 4-10b).

Figure 4-10

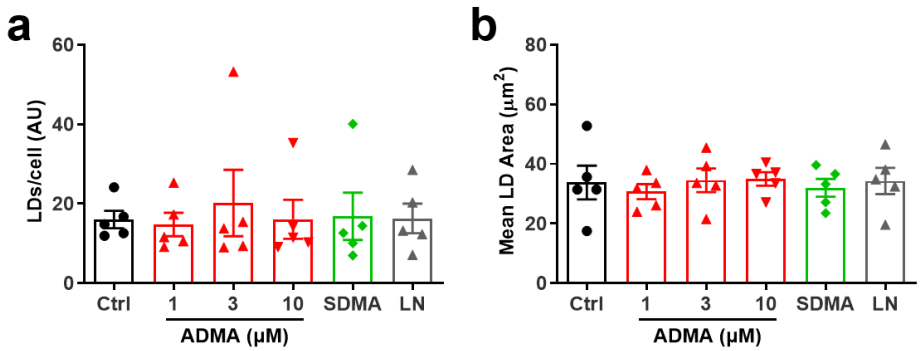

Figure 4-10: The effect of ADMA on LD morphology in 3T3-L1 adipocytes. **(a)** The number of lipid droplets (LDs) per cell is unchanged by 72h ADMA (1, 3 and 10μM), 10μM SDMA and 1mM L-NAME (LN). **(b)** LD area is unchanged by 72h ADMA (1, 3 and 10μM), SDMA and LN. Mean±SEM. One-way ANOVA (a, b). ADMA=Asymmetric dimethylarginine; SDMA=Symmetric dimethylarginine.

ADMA induces adipocyte hypertrophy without altering LD number or size. To understand whether ADMA affects molecular mediators of lipid handling, mRNA expression of key lipogenic mediators was probed in 3T3-L1 adipocytes following 48h treatment with ADMA (10μM), the CaSR inhibitor NPS-2143 (10μM) or combined ADMA and NPS-2143 treatment. Compared to control cultures, ADMA tended to increase peroxisome proliferator activated receptor gamma (PPARγ) expression, but was not statistically significant (1.6±0.2-fold, p=0.0545). PPARγ expression was unchanged with NPS-2143 treatment (1.0±0.2-fold, p>0.05). PPARγ expression in adipocytes which received combined ADMA and NPS-2143 treatment (1.1±0.1-fold) was similar to that observed in NPS-2143 treated cultures (p>0.05). Interestingly, PPARγ expression in cultures treated with ADMA and NPS-2134 was significantly decreased compared to ADMA alone (p=0.0046; Fig. 4-11a), showing that PPARγ in ADMA-treated 3T3-L1 cells is differentially regulated in the presence of NPS-2143. SREBP1 expression was not significantly altered by ADMA (1.5±0.2-fold, p>0.05) or NPS-2143 treatment (1.2±0.2-fold, p>0.05). Unlike PPARγ, sterol regulatory element-binding protein 1 (SREBP1) expression in adipocytes receiving combined ADMA and NPS-2143 treatment (1.1±0.1-fold) did not differ from ADMA or NPS-2143 alone (p>0.05; Fig. 4-11b). Acetyl coenzyme A (ACC1) expression in untreated cells was not augmented by ADMA (1.5±0.1-fold, p>0.05) or NPS-2143 (0.9±0.2-fold, p>0.05). Combined treatment (0.9±0.1-fold) tended to decrease ACC1 expression compared to ADMA treated cultures, but was non-significant (p=0.0537). ACC1 expression was comparable between NPS-2143 and combined ADMA/NPS-2143 treatment (p>0.05; Fig. 4-11c). The expression of fatty acid synthase (FASN) was not influenced by either ADMA (1.4±0.2-fold, p>0.05) or NPS-2143 (0.6±0.1-fold, p>0.05). FASN expression in cultures treated with combined ADMA/NPS-2143 (0.6±0.1-fold) was similar to those which received NPS-2143 treatment (p>0.05), but was significantly decreased compared to cultures which received ADMA (p=0.0128; Fig. 4-11d), suggesting that FASN expression in ADMA treated adipocytes is attenuated by NPS-2143. Fatty acid-binding protein 4 (FABP4) expression was not altered by ADMA (3.4±0.2-fold, p>0.05) or NPS-2143 (1.4±0.6-fold, p>0.05). Following combined treatment (0.9±0.1-fold), FABP4 expression was comparable to that in ADMA (p>0.05) and NPS-2143 treated cultures (p>0.05; Fig. 4-11e).

Figure 4-11

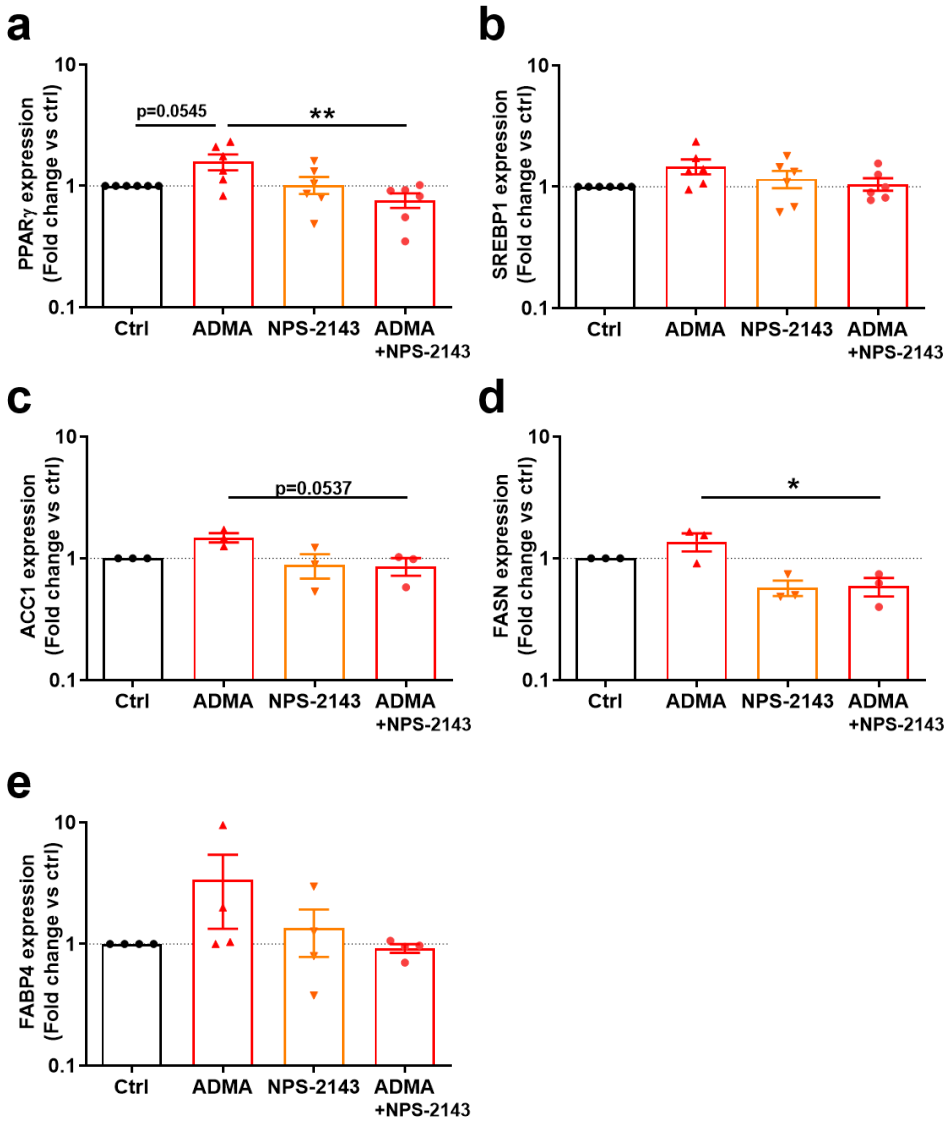

Figure 4-11: The effect of ADMA on lipogenic genes in 3T3-L1 adipocytes. **(a)** PPARγ mRNA expression is unchanged by ADMA (10μM) or NPS-2143 (10μM). Combined ADMA and NPS-2143 treatment results in decreased PPARγ expression compared to ADMA alone. **(b)** SREBP1 mRNA expression is unchanged by ADMA or NPS-2143. **(c)** ACC1 mRNA expression is unchanged by ADMA or NPS-2143. **(d)** FASN mRNA expression is unchanged by ADMA or NPS-2143. Combined ADMA and NPS-2143 treatment results in decreased FASN expression compared to ADMA alone. **(e)** ACC1 mRNA expression is unchanged by ADMA or NPS-2143. One-way ANOVA (a-e). *p<0.05, **p<0.01. ACC1=Acetyl coenzyme A; ADMA=Asymmetric dimethylarginine; FABP4=Fatty acid-binding protein 4; FASN=Fatty acid synthase; PPARγ=Peroxisome proliferator activated receptor gamma; SREBP1=Sterol regulatory element-binding protein 1.

ADMA hypertrophy was not associated with a significant induction of lipogenic enzymes, though PPARγ and FASN in ADMA-treated cultures were decreased by NPS-2143 treatment. To determine whether CaSR regulates lipogenic enzyme induction in adipocytes, mRNA expression was examined in 3T3-L1 adipocytes following 48h treatment with 0.1μM cinacalcet. Compared to control untreated cells, cinacalcet treatment increased PPARγ (1.5±0.1-fold, p=0.0036). FABP4 expression was also significantly elevated by cinacalcet compared to adipocytes in control cultures (1.7±0.2-fold, p=0.0028). Though cinacalcet elevated adipocyte PPARγ and FABP4 mRNA expression, expression of SREBP1, ACC1 and FASN was unchanged with cinacalcet exposure ($p>0.05$; Fig. 4-12a).

Cinacalcet increased mRNA expression of PPARγ and FABP4. To further evaluate the role of CaSR in regulating lipogenic gene expression, adipocytes were treated with NPS R-568 (1μM) for 48h. As before, adipocytes were exposed to NPS R-568 in the presence of varying concentrations of its primary agonist $[Ca^{2+}]_o$ (0.5, 1 and 2mM) to examine how allosteric CaSR responses could be impacted by CaSR activation. In these experiments, PPARγ mRNA expression was not altered by $[Ca^{2+}]_o$ ($p>0.05$) or NPS R-568 ($p>0.05$). Moreover, these factors did not interact to influence PPARγ expression ($p>0.05$). Multiple comparison analyses confirmed these findings; there was no effect of NPS R-568 on PPARγ mRNA expression when adipocytes were co-incubated with 0.5mM, 1mM or 2mM $[Ca^{2+}]_o$ ($p>0.05$; Fig. 4-12b).

Figure 4-12

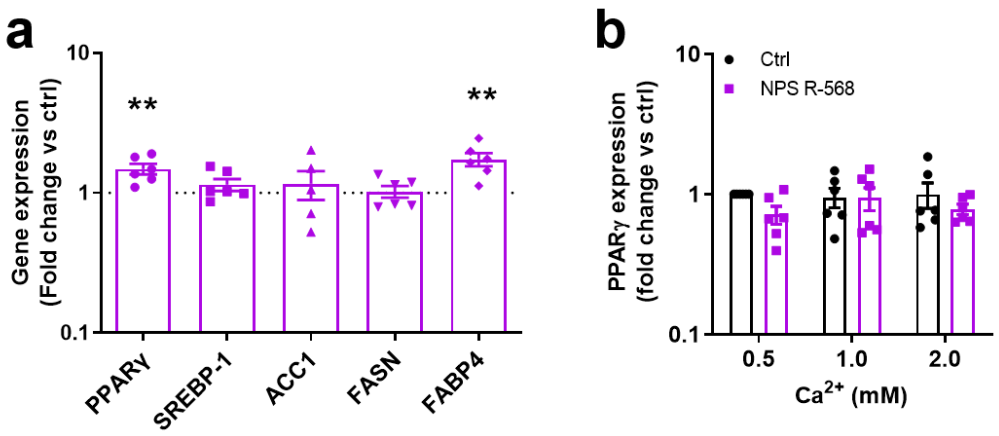

Figure 4-12: The effect of CaSR on lipogenic genes in 3T3-L1 cells.
(a) Cinacalcet (0.1μM) significantly increases mRNA expression of PPARγ and FABP4. Cinacalcet does not influence SREBP1, ACC1 or FASN expression. **(b)** NPS R-568 (1μM) does not alter PPARγ expression in the presence of 0.5, 1 or 2mM $[Ca^{2+}]_o$. Mean±SEM. Unpaired t-test (a). Two-way ANOVA (b). **p<0.01 vs Ctrl untreated. ACC1=Acetyl coenzyme A; FABP4=Fatty acid-binding protein 4; FASN=Fatty acid synthase; PPARγ=Peroxisome proliferator activated receptor gamma; SREBP1=Sterol regulatory element-binding protein 1.

4.3.5 Differentiation

ADMA stimulates 3T3-L1 adipocyte hypertrophy and ADMA-treated 3T3-L1 adipocytes show decreased PPARγ and FASN in the presence of NPS-2143, implying that ADMA supports lipogenic signalling. However, ADMA regulates lipid accumulation as well as PPARγ, FABP4 and C/EBP expression in differentiating 3T3-L1 preadipocytes, indicating that it can potentiate adipogenesis (Minakuchi *et al.*, 2016). To examine whether the effect of ADMA on cell size and lipogenic mediators could be attributed to increased adipogenesis, differentiation efficiency was studied in 3T3-L1 cells following 72h treatment with ADMA (1, 3 and 10μM), SDMA (10μM) and L-NAME (1mM). In untreated control cultures, differentiation efficiency was determined to be 45±7%. At all concentrations studied, the proportion of differentiated adipocytes in culture was not altered by ADMA. Compared to cultures which received control media, adipocytes which were conditioned with low 1μM ADMA showed no change in differentiation efficiency (43±8%, p>0.05). Relative numbers of differentiated adipocytes were also unmodified by 3μM ADMA (45±9%, p>0.05) and higher, 10μM ADMA levels

(45±12%, p>0.05). Differentiation efficiency was similarly unaltered with SDMA (39±3%, p>0.05) and L-NAME (40±9%, p>0.05; Fig. 4-13a).

To confirm that ADMA had no effect on differentiation efficiency and assess how CaSR may affect fibroblast differentiation, 3T3-L1 adipocytes were treated for 72h with ADMA (10μM), SDMA (10μM) and cinacalcet (0.1μM) and monitored for expression of PLN-1, a marker of adipocyte maturity. Compared to control adipocytes, PLN-1 expression was not augmented by ADMA (90±6%, p>0.05), SDMA (70±26%, p>0.05) or cinacalcet (59±28%, p>0.05; Fig. 4-13b, c), suggesting that the proportion of mature adipocytes in 3T3-L1 cultures remained stable in irrespective of treatment.

Figure 4-13

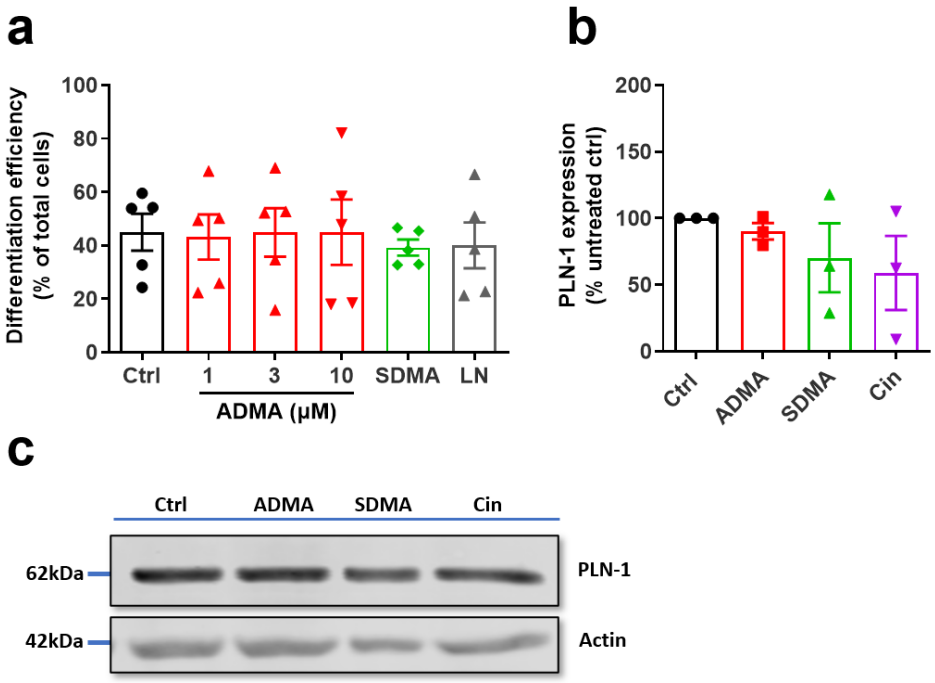

Figure 4-13: The effect of ADMA and CaSR on 3T3-L1 differentiation.
(a) The number of lipid positive adipocytes relative to total cell number is unchanged by 72h ADMA (1, 3 and 10μM), 10μM SDMA and 1mM L-NAME (LN). **(b)** The adipocyte maturity marker PLN-1 is unchanged by ADMA (10μM), SDMA (10μM) or cinacalcet (0.1μM). Mean±SEM. One-way ANOVA (a, b). ADMA=Asymmetric dimethylarginine; SDMA=Symmetric dimethylarginine.

4.3.6 Adipokines

ADMA increases 3T3-L1 adipocyte size. To assess whether ADMA-driven increased cell size coincides with altered function, the adipokines adiponectin and leptin were assessed in 3T3-L1 adipocytes following 48h treatment with ADMA (10μM), the CaSR inhibitor NPS-2143 (10μM) or combined ADMA and NPS-2143 treatment.

Adiponectin mRNA expression was not influenced when adipocytes were treated with ADMA or NPS-2143 alone. Compared to control cultures, adiponectin expression was not altered by ADMA (1.5±0.3-fold, $p>0.05$) or with NPS-2143 treatment (0.6±0.2-fold, $p>0.05$). Following combined ADMA and NPS-2143 treatment (0.5±0.1-fold), adiponectin expression was similar to NPS-2143 treated cultures ($p>0.05$). However, adiponectin expression in cultures which received combined ADMA and NPS-2143 treatment was significantly decreased compared to ADMA alone ($p=0.0218$; Fig. 4-14a). To assess whether adiponectin is augmented at the protein level, adiponectin concentration in 3T3-L1 cell media was determined via ELISA following 72h ADMA and L-NAME (1mM) treatment. Adiponectin protein levels were 1539±145μg/ml in control cultures. As with mRNA expression, ADMA was unable to alter adiponectin at the protein level. Compared to adipocytes treated with control media, adiponectin levels were not altered by 1μM ADMA (1875±355μg/ml, $p>0.05$), 3μM ADMA (1352±261 μg/ml, $p>0.05$) or 10μM ADMA (1560±417 μg/ml, $p>0.05$). Similarly, L-NAME NOS inhibition did not augment adiponectin levels compared to control values (1903±300μg/ml, $p>0.05$; Fig. 4-14b).

Leptin mRNA expression was also unaltered by exogenous ADMA and NPS-2143 treatment. Compared to control adipocytes, leptin mRNA expression was unchanged when cells were conditioned with ADMA (1.4±0.1-fold, $p>0.05$) or with NPS-2143 (1.3±0.4-fold, $p>0.05$). Leptin expression in adipocytes which received combined ADMA and NPS-2143 treatment (1.3±0.3-fold) was not different compared to those treated with ADMA or NPS alone ($p>0.05$; Fig. 4-14c). Leptin protein levels in 3T3-L1 cell media were determined via ELISA following 72h treatment with ADMA (1, 3 and 10μM) and L-NAME (1mM) treatment. Leptin protein levels were broadly unaltered by ADMA. In these experiments, leptin protein in untreated control cell media was 4480±1278pg/ml. Leptin protein concentrations in control media were not altered when adipocytes were exposed

to 1µM ADMA (7925±1616pg/ml, p>0.05), 3µM ADMA (3558±994 pg/ml, p>0.05) or pathological 10µM ADMA concentrations (2441±1265 pg/ml, p>0.05). L-NAME did not influence media leptin protein levels compared to controls (6767±1517pg/ml, p>0.05; Fig. 4-14d).

Figure 4-14

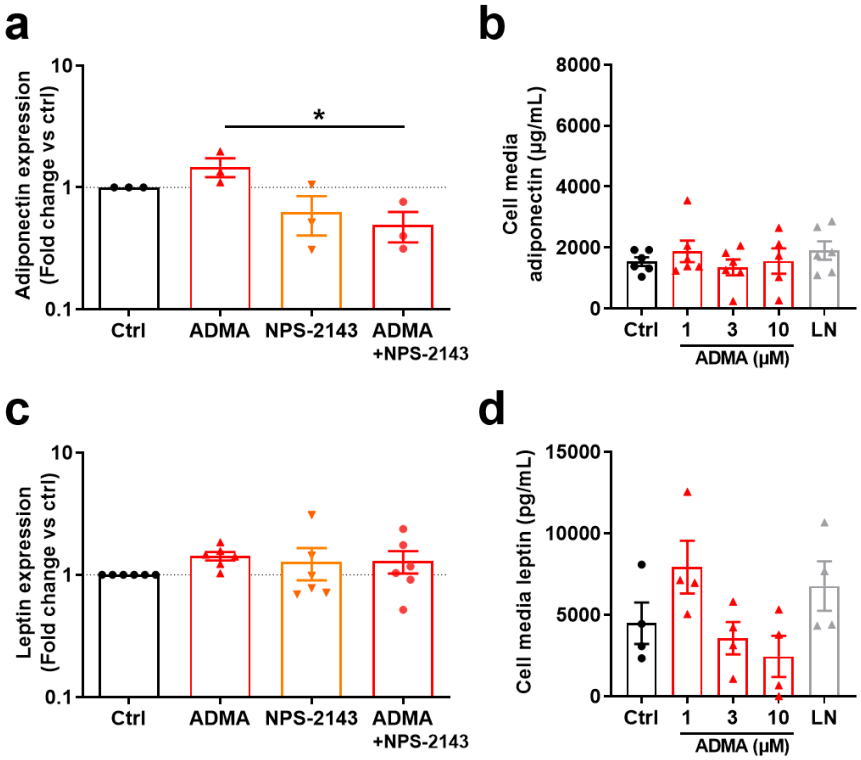

Figure 4-14: ADMA regulation of adipokines in 3T3-L1 adipocytes.
(a) Adiponectin mRNA expression is unchanged by 48h ADMA (10µM) or NPS-2143 (10µM). Combined ADMA and NPS-2143 treatment results in decreased adiponectin expression compared to ADMA alone. **(b)** Adiponectin protein levels in 3T3-L1 cell media are unchanged by 48h ADMA (1, 3 and 10µM) or 1mM L-NAME (LN). **(c)** Leptin mRNA expression is unchanged by 48h ADMA (10µM) or NPS-2143 (10µM). **(d)** Leptin protein levels in 3T3-L1 cell media in response to48h ADMA (1, 3 and 10µM) or L-NAME (1mM). Mean±SEM. One-way ANOVA (a-d). *p<0.05. ADMA=Asymmetric dimethylarginine.

ADMA did not regulate adiponectin or leptin secretion in 3T3-L1 cells, though adiponectin mRNA in ADMA-treated cultures were decreased by NPS-2143 treatment. To assess whether CaSR regulates adipocyte adipokine production, adiponectin mRNA expression and cell media protein levels were investigated in 3T3-L1 adipocytes following 72h treatment with cinacalcet. In comparison to control adipocytes, 0.1µm cinacalcet tended to increase adiponectin mRNA levels, though the effect was not statistically significant (1.5±0.3-fold, p=0.0851; Fig. 4-15a). Cinacalcet did not have any effect on cell media adiponectin levels. In control cultures, adiponectin concentrations were 1582±470µg/ml. Adiponectin protein concentrations in cell media were unchanged with 0.1µM cinacalcet (2992±686µg/ml, p>0.05) and 1µM cinacalcet (1597±336µg/ml, p>0.05; Fig. 4-15b), showing that adiponectin is not regulated by CaSR.

Next, this study investigated the effect of 72h cinacalcet treatment on adipocyte leptin production. Cinacalcet tended to increase leptin mRNA expression, though this increase was not determined to be significant (1.7±0.3-fold, p=0.0526; Fig. 4-15a). Whereas cinacalcet did not augment adiponectin secretion, cell media leptin levels were increased by low cinacalcet concentrations. In control conditions, cell media leptin levels were 2849±746pg/ml. Compared to these control values, low 0.1µM cinacalcet caused a 1.3-fold increase in cell media leptin levels (6431±819pg/ml, p=0.0129), suggesting that CaSR influences leptin signalling. Unexpectedly however, leptin levels were not similarly increased by 1µM cinacalcet (4503±769pg/ml, p>0.05; Fig. 4-15c).

Figure 4-15

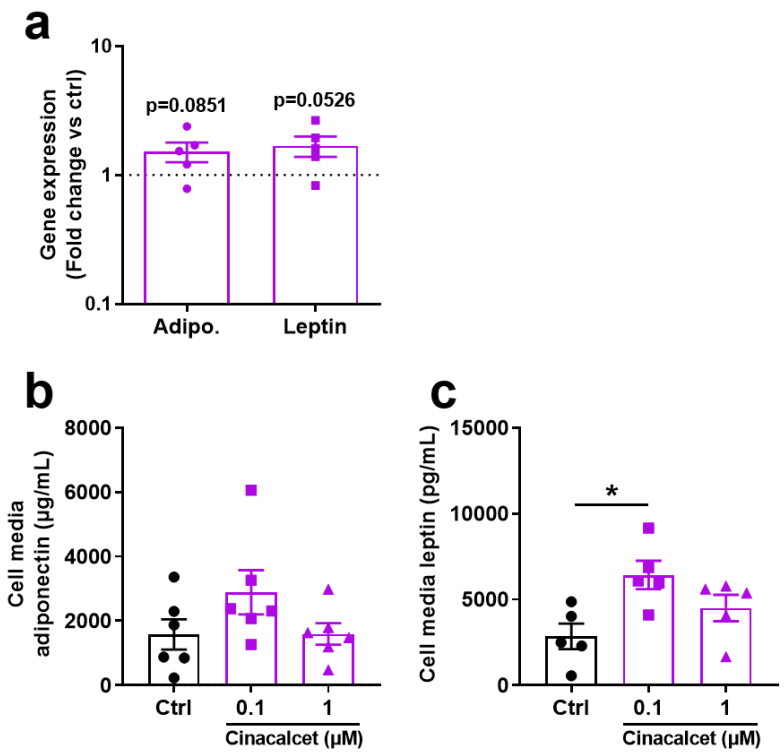

Figure 4-15: CaSR regulation of adipokines in 3T3-L1 adipocytes.
(a) Adiponectin (Adipo.) and leptin mRNA expression is unchanged by 48h cinacalcet (0.1µM). **(b)** Adiponectin protein levels in 3T3-L1 cell media are unchanged by cinacalcet (0.1 and 1µM). **(c)** Leptin protein levels are increased by 0.1µM, but not 1µM cinacalcet. Mean±SEM. Unpaired t-test (a). One-way ANOVA (b, c). *p<0.05. ADMA=Asymmetric dimethylarginine.

4.3.7 ERK signalling

$ERK_{1/2}$ regulates adipocyte hypertrophy (Ozaki *et al.*, 2016) and is induced by CaSR in numerous *in vitro* models (Magno, Ward and Ratajczak, 2011). In chapter 3, CaSR and ADMA were shown to regulate $[Ca^{2+}]_o$-induced $ERK_{1/2}$ activation in a HEK293 model of CaSR overexpression. To probe the mechanisms through which ADMA and CaSR regulate hypertrophy and lipogenic gene expression in 3T3-L1 adipocytes, $ERK_{1/2}$ activation was examined via western blot analyses.

4.3.7.1 $[Ca^{2+}]_o$-induced signalling

In initial experiments, 3T3-L1 adipocytes were treated with low (0.2mM) and high $[Ca^{2+}]_o$ (3mM) across several timepoints (5, 10, 15, 30, 60min) to evaluate $ERK_{1/2}$ activation in response to stimulation by $[Ca^{2+}]_o$, the primary endogenous agonist

of CaSR. Among these conditions, there was a main effect of both $[Ca^{2+}]_o$ ($p<0.0001$) and time ($p<0.0041$) on $ERK_{1/2}$ activation. Interaction of these factors was a significant determinant of $ERK_{1/2}$ activation ($p=0.0175$; Fig. 4-16a, b). To investigate the interplay between time and $[Ca^{2+}]_o$ concentration, multiple comparisons tests were performed. Compared to low $[Ca^{2+}]_o$, $ERK_{1/2}$ activation was not significantly altered by high $[Ca^{2+}]_o$ at 5min and 10min timepoints ($p>0.05$). However, $ERK_{1/2}$ activation was markedly increased by high $[Ca^{2+}]_o$ from 15min onwards. At 15min incubation, $ERK_{1/2}$ activation with low $[Ca^{2+}]_o$ (154±24%) was significantly increased with high $[Ca^{2+}]_o$ (1073±179%, $p=0.0013$). At 30min incubation, $ERK_{1/2}$ activation produced by stimulation with low $[Ca^{2+}]_o$ (253±95%) was again elevated by high $[Ca^{2+}]_o$ (1468±140%, $p<0.0001$). This effect remained evident at 60min incubation, where $ERK_{1/2}$ activation with low $[Ca^{2+}]_o$ (315±68%) was again raised in the presence of high $[Ca^{2+}]_o$ (1635±364%, $p<0.0001$). Given that $[Ca^{2+}]_o$ had a marked time-dependent effect on $ERK_{1/2}$ activation, subsequent treatment incubations in 3T3-L1 adipocytes were performed for 60min, which elicited the greatest activation of $ERK_{1/2}$.

Next, 3T3-L1 adipocytes were treated with varying $[Ca^{2+}]_o$ concentrations (0.2-3mM) for 60min to evaluate how $ERK_{1/2}$ activation is impacted by $[Ca^{2+}]_o$ concentration. There was a significant effect of increasing $[Ca^{2+}]_o$ on $ERK_{1/2}$ activation ($p=0.0070$). To further explore how $ERK_{1/2}$ activation was influenced by $[Ca^{2+}]_o$ concentration, multiple comparisons testing was employed. Compared to cultures treated with 0.2mM $[Ca^{2+}]_o$, $ERK_{1/2}$ activation was not significantly elevated by 1mM $[Ca^{2+}]_o$ (130±7%, $p>0.05$). However, $ERK_{1/2}$ activation was highly stimulated by 2mM $[Ca^{2+}]_o$ (276±43%, $p=0.0156$) and demonstrated further elevation with 3mM $[Ca^{2+}]_o$ (308±56%, $p=0.0082$; Fig. 4-16c, d), demonstrating concentration-dependent effects.

Figure 4-16

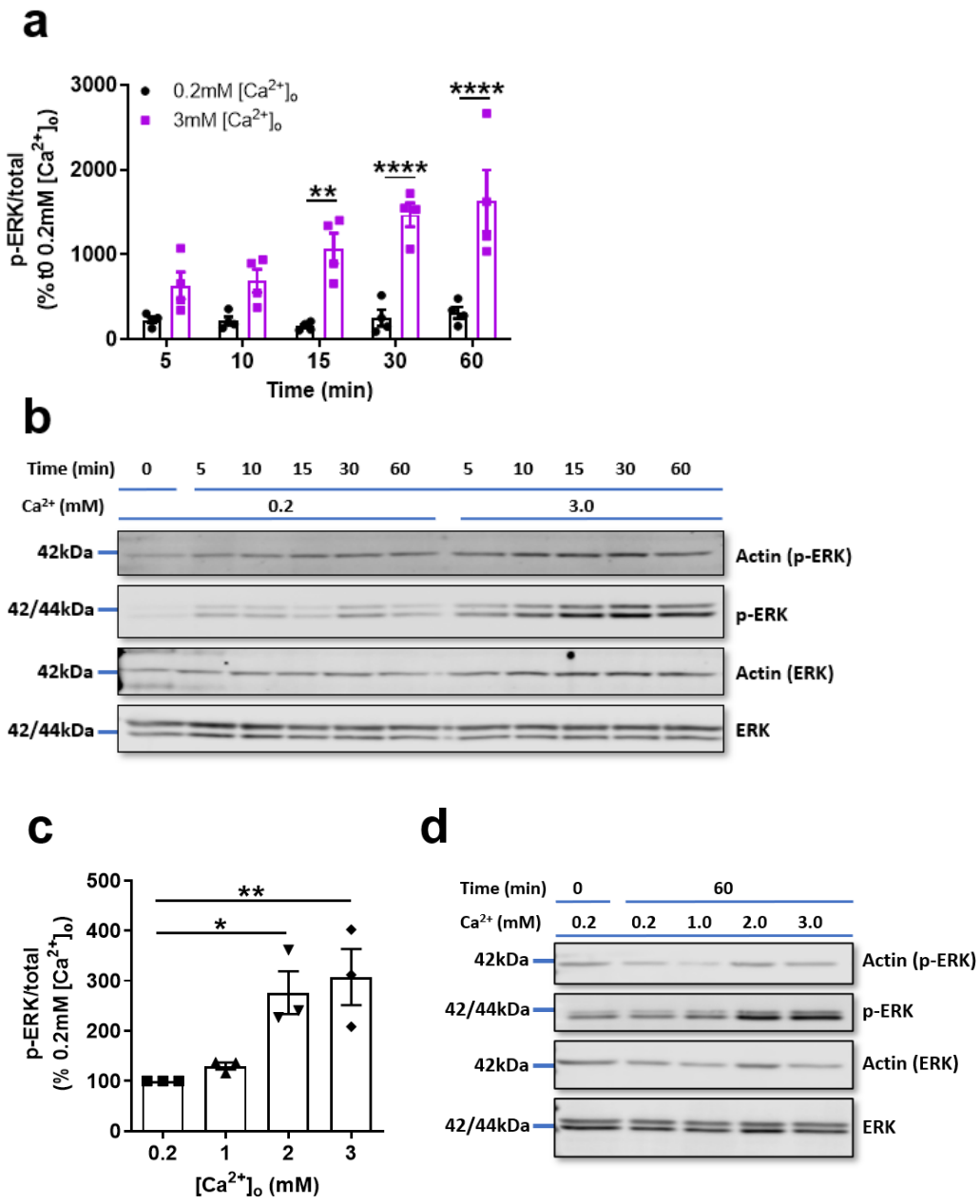

Figure 4-16: Time- and concentration-dependent effect of $[Ca^{2+}]_o$ stimulation on $ERK_{1/2}$ activation in 3T3-L1 adipocytes.

(a) $ERK_{1/2}$ activation is increased by 3mM (high) extracellular CaCl ($[Ca^{2+}]_o$) following 15, 30 and 60min treatment duration. $ERK_{1/2}$ activation is not significantly elevated by 3mM $[Ca^{2+}]_o$ after 5 or 10min incubation. **(b)** Representative western blot demonstrating the effect of time-dependent, $[Ca^{2+}]_o$-induced $ERK_{1/2}$ activation in 3T3-L1 adipocytes. **(c)** $ERK_{1/2}$ activation is not altered by 60min incubation with 1mM extracellular $CaCl_2$ ($[Ca^{2+}]_o$), but is significantly elevated following stimulation with 2mM and 3mM $[Ca^{2+}]_o$. **(d)** Representative western blot demonstrating the effect of dose-dependent,

$[Ca^{2+}]_o$-induced $ERK_{1/2}$ activation in 3T3-L1 adipocytes. Mean ±SEM. Two-way ANOVA (a), **p<0.01 vs 0.2mM $[Ca^{2+}]_o$, ****p<0.0001 vs 0.2 $[Ca^{2+}]_o$. One-way ANOVA (c), *p<0.05 vs 0.2mM $[Ca^{2+}]_o$, **p<0.01 vs 0.2 $[Ca^{2+}]_o$. ERK=Extracellular signal-regulated kinase.

4.3.7.2 CaSR-mediated signalling

$[Ca^{2+}]_o$ had significant time- and concentration dependent effects on $ERK_{1/2}$ activation in 3T3-L1 adipocytes. To investigate whether $ERK_{1/2}$ activation relies on CaSR, 3T3-L1 adipocytes were treated with the CaSR type II (allosteric) agonist cinacalcet (1μM) in the presence of 0.2mM $[Ca^{2+}]_o$. $ERK_{1/2}$ activation was monitored across time (5, 10, 15, 30, 60min). In these experiments, $ERK_{1/2}$ activation was not altered by cinacalcet ($p>0.05$), or incubation time ($p>0.05$). Additionally, there was no interaction between these factors to influence $ERK_{1/2}$ activation ($p>0.05$; Fig. 4-17a, b), demonstrating that cinacalcet does not influence adipocyte $ERK_{1/2}$ signalling.

Cinacalcet in the presence of low 0.2mM $[Ca^{2+}]_o$ was unable to stimulate adipocyte $ERK_{1/2}$ signalling. To overcome the possibility that adipocyte CaSR was insufficiently activated to observe a sensitising effect of allosteric CaSR stimulation, 3T3-L1 adipocytes were treated with 1μM NPS R-568 in the presence of variable $[Ca^{2+}]_o$ concentrations (0.2, 1, 3mM) and monitored for $ERK_{1/2}$ activation. Overall, NPS R-568 had no effect on $ERK_{1/2}$ activation ($p>0.05$). As before, $ERK_{1/2}$ activation was significantly enhanced by increasing $[Ca^{2+}]_o$ ($p<0.0001$). However, there was no interaction between $[Ca^{2+}]_o$ and NPS R-568 to influence $ERK_{1/2}$ activation ($p>0.05$; Fig. 4-17c, d).

As above $ERK_{1/2}$ activation was unaffected by cinacalcet and NPS R-568, suggesting that $ERK_{1/2}$ is not regulated by adipocyte CaSR. To confirm these findings, 3T3-L1 adipocytes were maximally stimulated with 3mM $[Ca^{2+}]_o$ in the presence and absence of the CaSR inhibitor NPS-2143 (10μM) and monitored for $ERK_{1/2}$ activation. Compared to 0.2mM $[Ca^{2+}]_o$ control cells, $ERK_{1/2}$ activation was raised by 3mM $[Ca^{2+}]_o$ (496±42%, $p<0.0001$). $ERK_{1/2}$ activation was similarly elevated by 3mM $[Ca^{2+}]_o$ in the presence of NPS-2143 (480±58%, $p<0.0001$), but this was comparable to 3mM $[Ca^{2+}]_o$ acting alone ($p>0.05$; Fig. 4-17e, f), showing that NPS-2143 does not modify $[Ca^{2+}]_o$-induced $ERK_{1/2}$ responses.

Figure 4-17

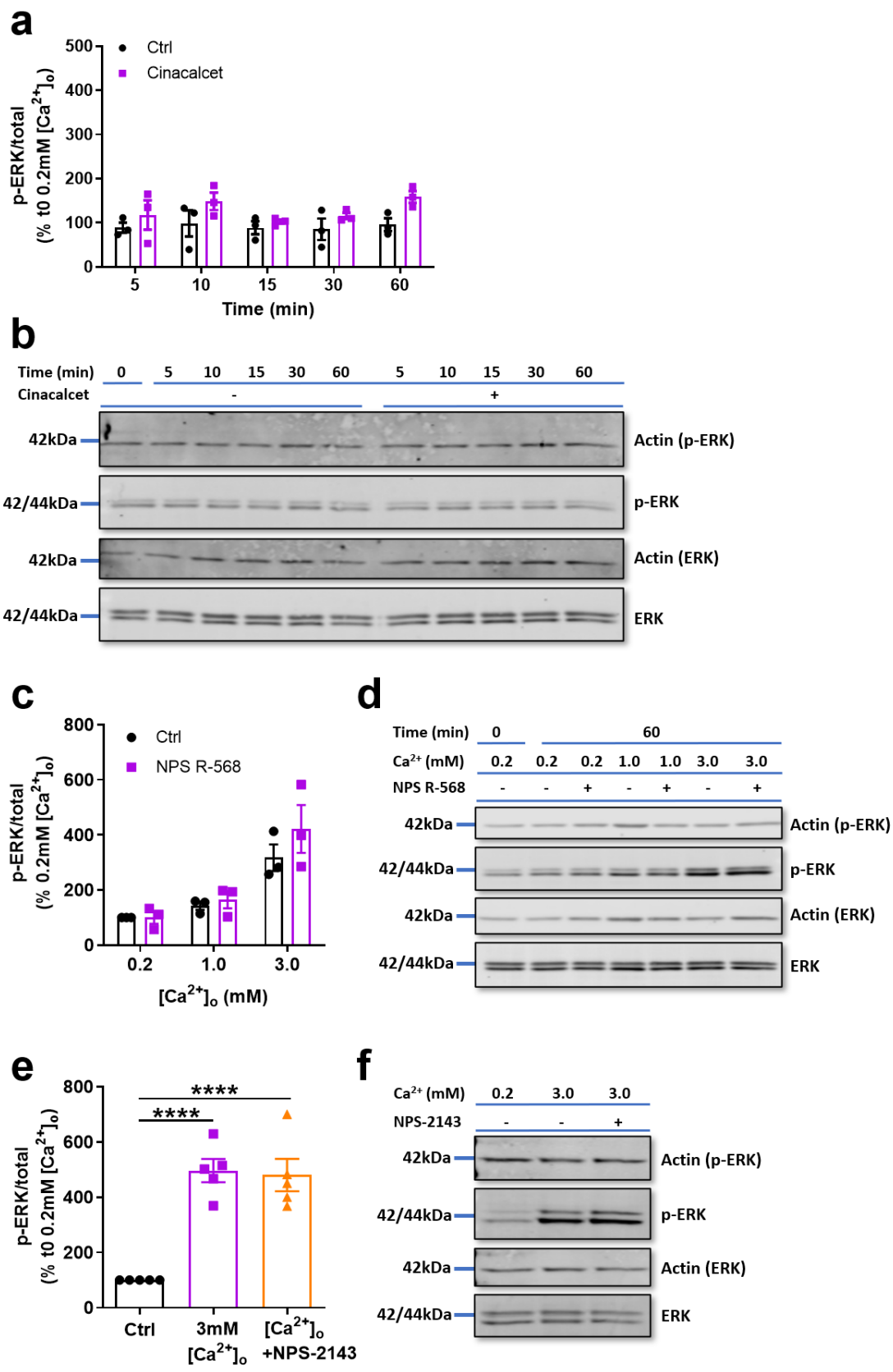
a
Ctrl
Cinacalcet
p-ERK/total
(% t0 0.2mM [Ca2+]o)
500
400
300
200
100
0
5
10
15
30
60
Time (min)
b
Time (min) 0 5 10 15 30 60 5 10 15 30 60
Cinacalcet - +
42kDa
Actin (p-ERK)
42/44kDa
p-ERK
42kDa
Actin (ERK)
42/44kDa
ERK
c
Ctrl
NPS R-568
p-ERK/total
(% 0.2mM [Ca2+]o)
800
600
400
200
0
0.2
1.0
3.0
[Ca2+]o (mM)
d
Time (min) 0 60
Ca2+ (mM) 0.2 0.2 0.2 1.0 1.0 3.0 3.0
NPS R-568 - - + - + - +
42kDa
Actin (p-ERK)
42/44kDa
p-ERK
42kDa
Actin (ERK)
42/44kDa
ERK
e
****
****
p-ERK/total
(% t0 0.2mM [Ca2+]o)
800
600
400
200
0
Ctrl
3mM [Ca2+]o
[Ca2+]o +NPS-2143
f
Ca2+ (mM) 0.2 3.0 3.0
NPS-2143 - - +
42kDa
Actin (p-ERK)
42/44kDa
p-ERK
42kDa
Actin (ERK)
42/44kDa
ERK

Figure 4-17: The effect of CaSR stimulation on $ERK_{1/2}$ activation in 3T3-L1 adipocytes.

(a) $ERK_{1/2}$ activation is unchanged by cinacalcet (1μM)-mediated CaSR stimulation following 15, 30 and 60min treatment duration. **(b)** Representative western blot demonstrating the effect of cinacalcet on $ERK_{1/2}$ activation in 3T3-L1 adipocytes. **(c)** $ERK_{1/2}$ activation is unchanged by 1μM NPS R-568 in the presence of 0.2 and 1mM $CaCl_2$ ($[Ca^{2+}]_o$). NPS R-568 increases $ERK_{1/2}$ activation in the presence of 3mM $[Ca^{2+}]_o$. **(d)** Representative western blot demonstrating the effect of NPS R-568 on $[Ca^{2+}]_o$-induced $ERK_{1/2}$ activation in 3T3-L1 adipocytes. **(e)** $ERK_{1/2}$ activation is increased by 60min treatment with 3mM $CaCl_2$ ($[Ca^{2+}]_o$). $ERK_{1/2}$ activation is also increased by 3mM $[Ca^{2+}]_o$ in presence of 10μM NPS-2143. **(f)** Representative western blot demonstrating the effect of NPS-2143 on $[Ca^{2+}]_o$-induced $ERK_{1/2}$ activation in 3T3-L1 adipocytes. Mean ±SEM. Two-way ANOVA (a, c). One-way ANOVA (e). ****$p<0.0001$ vs 0.2mM $[Ca^{2+}]_o$. CaSR=Calcium-sensing receptor; ERK=Extracellular signal-regulated kinase.

4.3.7.3 ADMA mediated-signalling

$ERK_{1/2}$ activation was increased by $[Ca^{2+}]_o$ but not CaSR agonists. However, ADMA is a mediator of $ERK_{1/2}$ signalling in multiple cell types (Jiang *et al.*, 2007; Zhou *et al.*, 2014; Jayachandran *et al.*, 2020). As shown section 4.3.7.1., $ERK_{1/2}$ activation is stimulated by 3mM $[Ca^{2+}]_o$, but lower (<2mM) concentrations are ineffective. To test whether ADMA regulates $[Ca^{2+}]_o$-independent $ERK_{1/2}$ signalling, 3T3-L1 adipocytes were treated for 60min with (subthreshold) 1mM $[Ca^{2+}]_o$ alone, 1mM $[Ca^{2+}]_o$ in the presence of ADMA (10μM), or 1mM $[Ca^{2+}]_o$ in the presence of ADMA (10μM) and NPS-2143 (10μM) and monitored for $ERK_{1/2}$ activation. Compared to 0.2mM $[Ca^{2+}]_o$ control cultures, $ERK_{1/2}$ activation was not significantly raised by 1mM $[Ca^{2+}]_o$ (168±74%, $p>0.05$). $ERK_{1/2}$ activation was similarly unchanged when adipocytes were treated with 1mM $[Ca^{2+}]_o$ in the presence of ADMA (118±23%, $p>0.05$), or treated with 1mM in the presence of both ADMA and NPS-2143 (194±65%, $p>0.05$; Fig. 4-18a, b). Since $ERK_{1/2}$ was not stimulated by 1mM $[Ca^{2+}]_o$ alone or by 1mM $[Ca^{2+}]_o$ in the presence of ADMA, these groups were not compared.

As ADMA does not stimulate $[Ca^{2+}]_o$-independent $ERK_{1/2}$ activation, the experiment above was repeated in the presence of 3mM $[Ca^{2+}]_o$ to evaluate whether ADMA influences $[Ca^{2+}]_o$-dependent $ERK_{1/2}$ signalling. $ERK_{1/2}$ When compared to adipocytes incubated in 0.2mM $[Ca^{2+}]_o$, 3mM $[Ca^{2+}]_o$ significantly increased $ERK_{1/2}$ activation (539±89%, p=0.0033). Compared to 0.2mM $[Ca^{2+}]_o$, $ERK_{1/2}$ activation was similarly raised with treatment with 3mM $[Ca^{2+}]_o$ in the presence of ADMA (494±77, p=0.0081), as well treatment with 3mM $[Ca^{2+}]_o$ in the presence of both ADMA and NPS-2143 (607±88%, p=0.0008). Adipocyte $ERK_{1/2}$ activation was not sensitive to ADMA or NPS-2143. $ERK_{1/2}$ activation was not elevated following treatment with 3mM $[Ca^{2+}]_o$ and ADMA when compared with 3mM $[Ca^{2+}]_o$ alone ($p>0.05$). Moreover, adipocytes treated with 3mM $[Ca^{2+}]_o$ and ADMA showed no reduction in $ERK_{1/2}$ activation when cells were additionally treated with NPS-2143 ($p>0.05$). Overall $[Ca^{2+}]_o$-mediated $ERK_{1/2}$ activation was insensitive to both ADMA and NPS-2143 (Fig. 4-18c, d).

Figure 4-18

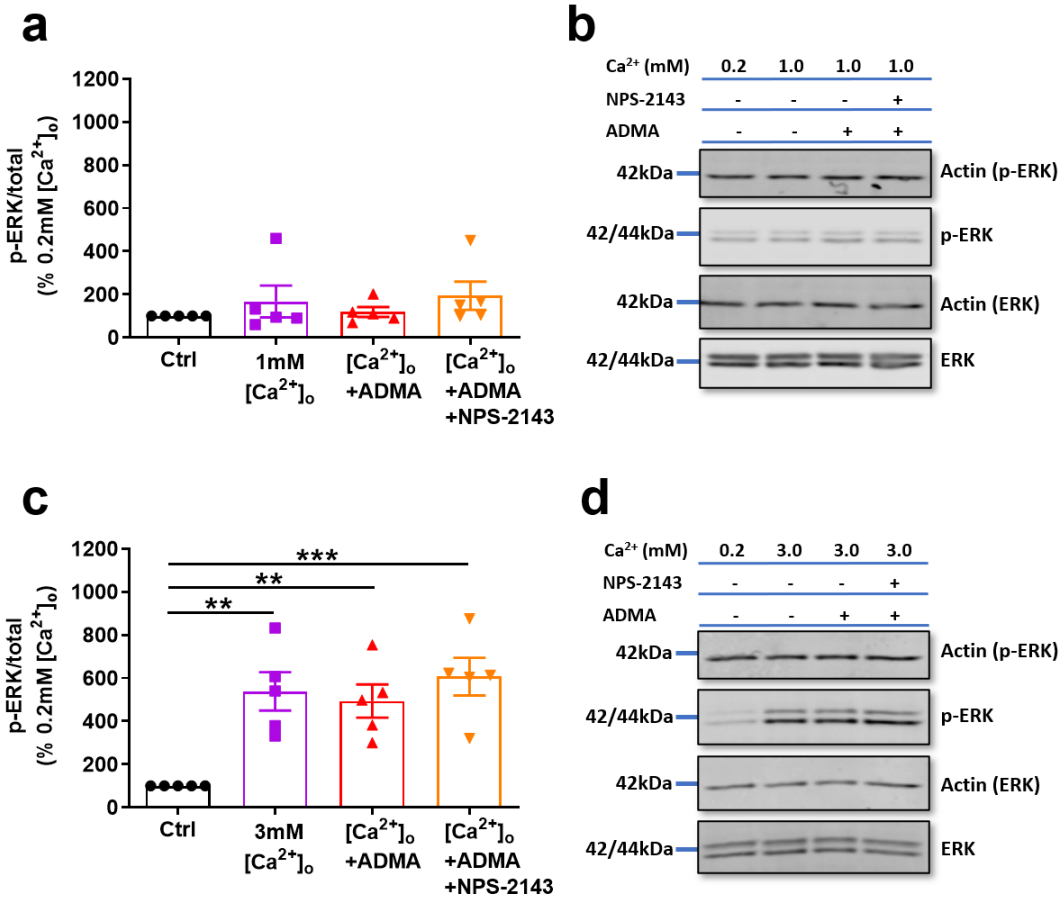

Figure 4-18: The effect of ADMA on $[Ca^{2+}]_o$-induced $ERK_{1/2}$ activation in 3T3-L1 adipocytes.

(a) $ERK_{1/2}$ activation is unchanged by 60min treatment with 3mM $CaCl_2$ ($[Ca^{2+}]_o$), 3mM $[Ca^{2+}]_o$ in the presence of ADMA (10μM) and by 3mM $[Ca^{2+}]_o$ in the presence of ADMA and NPS-2143. **(b)** Representative western blot demonstrating the effect of ADMA and NPS-2143 on 1mM $[Ca^{2+}]_o$-induced $ERK_{1/2}$ activation in 3T3-L1 adipocytes. **(c)** $ERK_{1/2}$ activation is increased by 60min treatment with 3mM $[Ca^{2+}]_o$, 3mM $[Ca^{2+}]_o$ in the presence of ADMA (10μM) and by 3mM $[Ca^{2+}]_o$ in the presence of ADMA and NPS-2143. Compared to 3mM $[Ca^{2+}]_o$ alone and 3mM $[Ca^{2+}]_o$ + ADMA conditions, treatment with 3mM $[Ca^{2+}]_o$ in the presence of ADMA and NPS-2143 does not altered $ERK_{1/2}$ activation. **(d)** Representative western blot demonstrating the effect of ADMA and NPS-2143 on 3mM $[Ca^{2+}]_o$-induced $ERK_{1/2}$ activation in 3T3-L1 adipocytes. Mean ±SEM. One-way ANOVA (a, c). **p<0.01 vs 0.2mM $[Ca^{2+}]_o$, ***p<0.001 vs 0.2mM $[Ca^{2+}]_o$ ERK=Extracellular signal-regulated kinase.

4.4 Discussion

4.4.1 3T3-L1 cells as an adipocyte model

To examine ADMA and CaSR signalling this study utilised 3T3-L1 cells, a well-characterised cell line model of adipogenesis. To initiate differentiation, 3T3-L1 cells were treated with an adipogenic cocktail containing insulin, dexamethasone, IBMX and troglitazone. Subsequent development of 3T3-L1 preadipocytes in differentiation medium over 10 days resulted in the formation of mature adipocytes, confirmed via the appearance of lipid droplets (LDs) and enhanced neutral lipid content. PLN-1 is an adipocyte-specific structural protein involved in LD formation. Its expression is significantly increased in 3T3-L1 cells by day 8 of the differentiation period (Jang, 2016), in alignment with observations here. 3T3-L1 cells were therefore considered to be mature adipocytes from post-differentiation day 8.

To justify the use of 3T3-L1 adipocytes to study ADMA and CaSR signalling, it was important to establish whether 3T3-L1 cells express CaSR. Previous studies report CaSR protein expression in a variety of adipocyte cell line models, such as differentiated SW872, LS14 and 3T3-L1 adipocytes (Cifuentes *et al.*, 2010; He, Zhang, *et al.*, 2011; He *et al.*, 2012; Xing *et al.*, 2019) and human adipocytes (Cifuentes, Albala and Rojas, 2005; Cifuentes *et al.*, 2010). In this study, primers targeted towards the CaSR gene sequence demonstrated the presence of CaSR mRNA in 3T3-L1 adipocyte lysates. This was validated with the identification of CaSR protein, since western blot analyses using CaSR-specific primary antibody (verified in CaSR-overexpressing HEK293 cells, chapter 3) produced two bands; a lower band migrating at ~130kDa and a faint upper band at ~260kDa. This immunoprecipitation pattern corresponds with the expected size of CaSR, which exists in dimeric (240-310kDa), monomeric glycosylated (138-169kDa) and monomeric unglycosylated (121kDa) forms (Ward, Brown and Harris, 1998). These data were confirmed by immunofluorescent analyses which demonstrated positive staining for CaSR in 3T3-L1 cultures, therefore confirming CaSR expression in 3T3-L1 adipocytes here.

CaSR was detected in both 3T3-L1 preadipocytes and adipocytes, but protein expression remained constant throughout differentiation. This implicates a role for CaSR in 3T3-L1 preadipocytes as well as differentiated 3T3-L1 adipocytes in the present study. Interestingly, previous studies have found that CaSR expression in differentiated adipocytes is elevated compared to their preadipocyte progenitors. For instance, CaSR mRNA and protein levels are increased in a time-dependent manner in differentiating SW872 cells (He *et al.*, 2012). CaSR is also elevated in d11 3T3-L1 adipocytes relative to fibroblast progenitors. Notably, CaSR was in fact absent in 3T3-L1 fibroblasts in this work (Xing *et al.*, 2019). These data suggest that CaSR plays a greater role in mature adipocyte physiology. Though these observations oppose those of the present study, Xing et al reported that CaSR expression in 3T3-L1 fibroblasts could be triggered by TNFα, whereas CaSR expression in 3T3-L1 adipocytes was reduced by TNFα. Considering that TNFα mediates opposing effects on 3T3-L1 cells depending on their developmental stage, the inflammatory state of this cell line at baseline could therefore modulate CaSR expression throughout differentiation, decreasing the likelihood that differences in CaSR would be detected. This is especially relevant when one considers the relative change in CaSR expression between 3T3-L1 fibroblasts and adipocytes. Though CaSR protein was raised ~5-fold in d11 adipocytes, d10 adipocytes showed a ~2.5-change in CaSR expression which did not reach significance (Xing *et al.*, 2019). In this study, CaSR protein was monitored using western blot analyses in 3T3-L1 cells through differentiation to d10. Therefore, the use of semiquantitative western blot analyses, or the cessation of 3T3-L1 monitoring after d10, may have prevented identification of small changes in CaSR expression during 3T3-L1 cell differentiation in the present study. Future work should assess CaSR expression in differentiating 3T3-L1 cells using more sensitive methods such as qPCR, perhaps examining CaSR expression for longer periods after adipocytes initially reach maturation.

Isolated human scAT adipocytes demonstrate mRNA expression of enzymes responsible for ADMA synthesis (protein arginine methyltransferase 1-4 and -6) and degradation (DDAH1 and -2) (Spoto *et al.*, 2007). In the present work, DDAH1 and DDAH2 mRNA expression was reproduced in 3T3-L1 adipocytes. Though not examined here, our lab has previously described adipocyte PRMT expression and

ADMA generation in 3T3-L1 cells (Dowsett, 2014). Accordingly, 3T3-L1 adipocytes represent a useful model in which to examine adipocyte-specific ADMA signalling as well as CaSR signalling.

4.4.2 Hypertrophy and lipid accumulation

Previously, our lab has shown that cell size and lipid accumulation are positively regulated by extracellular ADMA in 3T3-L1 adipocytes (Dowsett *et al.*, 2022). To investigate the mechanism(s) underpinning ADMA mediated hypertrophy in 3T3-L1 cells and establish whether these effects could be attributed to CaSR signalling, this study attempted to reproduce these findings. Here, 3T3-L1 adipocytes were enlarged 23-30% by physiological (1-3μM) ADMA levels and 28% by pathophysiological (10μM) ADMA levels. Though we previously reported greater ADMA-mediated adipocyte hypertrophy (>50%) (Dowsett *et al.*, 2022), 3T3-L1 adipocytes in control cultures here possessed a mean area of 659μM, nearly 3-fold larger than our previous study. Accordingly, the increased size of adipocytes at baseline may limit the hypertrophic capacity of 3T3-L1 adipocytes and thus their expansion in response to hypertrophic stimuli such as ADMA. Interestingly, SDMA did not exert a comparable effect on cell size, suggesting that dimethylarginine driven enlargement of 3T3-L1 adipocytes is structurally specific. The biological effects of ADMA are thought to be mediated through NO inhibition, however adipocyte hypertrophy was not recapitulated by the NOS inhibitor L-NAME. Considering that NO inhibition does not seem to be significant in 3T3-L1 adipocyte enlargement, ADMA may have alternative functional targets in adipocytes.

In order to establish the mechanism(s) underpinning ADMA-mediated hypertrophy, this study assessed adipocyte NO status via Griess assay and qPCR analysis in 3T3-L1 adipocytes. ADMA is thought to mediate is biological effects by inhibiting NOS and decreasing production of NO (Leiper and Nandi, 2011). Here, neither physiological (1 and 3μM) or pathophysiological (10μM) ADMA levels altered cell media nitrite concentrations. Indeed, cell media nitrite concentrations remained unchanged even after exposure to pharmacological (100μM) ADMA concentrations. L-NAME produced a measurable decline in cell media nitrite, confirming that adipocyte NO generation depends on NOS activity. However, this mechanism was not regulated by ADMA in 3T3-L1 cells here. mRNA

eNOS expression was also unaffected by ADMA. Collectively, these data indicate that ADMA does not modulate NO in adipocytes, and that ADMA-mediated adipocyte hypertrophy may involve NO-independent pathways.

To investigate whether ADMA mediates its effects on 3T3-L1 size via a CaSR pathway, this study compared cells treated cells with ADMA and the type II (allosteric) agonist cinacalcet. Again ADMA increased adipocyte size by ~30%, but the effect was reproduced by cinacalcet which enlarged 3T3-L1 adipocytes by ~23%. Adipocyte hypertrophy was similarly induced by NPS R-568, confirming the role of CaSR in adipocyte growth. These findings raise the possibility that ADMA and CaSR could have shared biological functions in adipocytes. Though unable to influence cell size in previous experiments, SDMA decreased cell size in this second experimental series. Accordingly, dimethylarginine mediated effects may be not only structurally specific, but possibly antagonistic in adipocytes. Collectively, these data demonstrate that adipocyte hypertrophy is positively regulated by both ADMA and CaSR. Adipocyte enlargement coincides with altered cellular lipolysis, cytokine secretion and insulin sensitivity in health (Stern *et al.*, 1972; Skurk *et al.*, 2007; Laurencikiene *et al.*, 2011), but is overwhelmed in the obese state leading to adipocyte dysfunction and AT pathology (Oikonomou and Antoniades, 2019). As such, ADMA and CaSR signalling may contribute to adipocyte dysregulation and hence obesity-related pathology.

ADMA is thought to inhibit NO signalling, but CaSR on the other hand stimulates NO in endothelial cells (Ziegelstein *et al.*, 2006; Greenberg, Shi, *et al.*, 2016). As such, the effect of CaSR stimulation on adipocyte NO generation was also examined. Neither cinacalcet or NPS R-568 altered cell media nitrite levels or eNOS mRNA expression, indicating that CaSR-induced NO signalling may not be relevant in adipocytes. Taken together, these data suggest that ADMA- and CaSR-induced hypertrophy may be regulated by NO-independent mechanism(s). Although Griess assay nitrite measurement is a reasonable surrogate marker for NO and was sufficient to detect L-NAME mediated NOS inhibition in adipocytes, this approach may not possess enough sensitivity to detect small changes in NO signalling. Further work should validate these data using other techniques.

4.4.3 Lipogenesis

3T3-L1 adipocytes were treated with ADMA and lipogenesis studied using immunofluorescent imaging and mRNA analyses to investigate whether the hypertrophic actions of ADMA were associated with altered lipid accumulation. Unlike our previous work (Dowsett *et al.*, 2022), LD morphology and lipogenic mediators were not significantly influenced by ADMA here, suggesting that ADMA does not affect lipogenesis under present conditions. However, ADMA-induced lipogenic effects may have been lacking in this study due to the image analysis method used to quantify LD morphology. During image analysis, very small LDs (<4μm) were difficult to resolve. LD number and diameter tend to vary inversely (Rizzatti *et al.*, 2013). If ADMA increased cell size by stimulating LD biogenesis, very small progenitor LDs may not have been identified or reliably measured by the image analysis pipeline used in the present investigation.

To establish the molecular mechanism(s) underpinning 3T3-L1 adipocyte hypertrophy, this study investigated the effect of ADMA on lipogenic gene expression. ADMA modestly increased PPARγ mRNA expression, but the effect was non-significant (p=0.0545) and there was no marked effect of ADMA on PPARγ downstream transcriptional targets ACC1, FASN and FABP4. Despite these data, adipocytes which received ADMA in addition to NPS-2143 demonstrated a small but significant reduction in PPARγ expression compared to cultures exposed to ADMA only. Though ADMA alone did not significantly influence lipogenic gene expression, the inhibitory effect of NPS-2143 on PPARγ and FASN appeared to be dependent on the presence of ADMA. This situation would not be expected unless ADMA was able to regulate PPARγ expression. In support of these findings, combined ADMA and NPS-2143 had the same effect on the downstream PPARγ target FASN. These data indicate a potential link between ADMA, CaSR and lipogenic gene expression in adipocytes. Though it is unclear why PPARγ and FASN could not be significantly elevated by ADMA alone, it may be that ADMA effects were not resolved in this instance due to allosteric CaSR activation occurring under control culture conditions. Standard cell media formulation contains several components which may interact with CaSR, such as free $CaCl_2$ ($[Ca^{2+}]_o$; 1.8mM) as well as amino acids. Notably, several amino acids identified in the media used here (L-Phe, -Try, -Ala, -His and -Glu) demonstrate activity at

CaSR (Conigrave, Mun and Lok, 2007), raising the possibility that adipocyte CaSR may be partially stimulated at baseline. Supporting this idea, the EC_{50} for $[Ca^{2+}]_o$-induced $[Ca^{2+}]_o$ release in falls from 2.6 to 1.6mM in the presence of amino acid mixtures comprising ≥0.5mM CaSR-activating amino acids (Conigrave *et al.*, 2004). Though 1.8mM $[Ca^{2+}]_o$ alone may not significantly activate CaSR (Conigrave *et al.*, 2004), the cumulative concentration of CaSR-active amino acids in cell media here exceeds 1mM, which is potentially sufficient to cause positive allosteric modulation of CaSR. As the effect of ADMA in this situation would be additive, it could be obscured by constituent CaSR activity resulting from ambient amino acids in cell culture media. Despite this prediction, gene expression in cultures which received the CaSR inhibitor NPS-2143 was comparable to untreated adipocytes, suggesting that the biological significance of CaSR in 3T3-L1 cells is negligible under control, non-stimulated conditions. Interestingly however, recent work conducted in HEK293-CaSR cells within our lab suggest that the potency of ADMA at CaSR may be greater than L-Phe, since 10μM ADMA and 100μM L-Phe exert a comparable sensitising effect on $[Ca^{2+}]_o$-induced $[Ca^{2+}]_i$ release (Dowsett *et al.*, 2022). If the potency of ADMA at CaSR is substantially greater than other amino acids, this model could explain why NPS-2143 inhibits PPARγ expression in the presence of small amounts of ADMA, but has no apparent effect on constituent CaSR activity which would be predicted under the conditions of the present study. A role for ADMA/CaSR signalling cannot be concluded from these data, though further examination of this pathway is warranted. A full series of experiments exploring the effect of ADMA, $[Ca^{2+}]_o$ and prevailing amino acid concentrations is required to further investigate a role for ADMA acting at CaSR in 3T3-L1 adipocyte gene expression.

To examine whether ADMA- and CaSR-induced adipocyte hypertrophy could be mediated via common transcriptional mechanism(s), lipogenic gene expression was studied following CaSR stimulation by cinacalcet and NPS R-568 in in 3T3-L1 adipocytes. In SW872 adipocytes, $GdCl_2$ causes CaSR-dependent induction of PPARγ and FABP4, increasing mRNA levels by ~2.5-fold and 3.5-fold, respectively (He *et al.*, 2012). These observations were recapitulated with cinacalcet in the present study, although the effect of cinacalcet on PPARγ (1.5-fold) and FABP4 (1.7-fold) were smaller. This disparity could be attributed to the difference in adipocyte cell line models between studies, differences between $GdCl_2$

(orthosteric) and cinacalcet (allosteric) agonism or differential effects mediated by cell medium $[Ca^{2+}]_o$, the latter of which was not referenced by He *et al*. Nonetheless, these data demonstrate that CaSR can be sensitised by synthetic allosteric CaSR modulators under the conditions of the present study. Experiments in bovine parathyroid cells using parathyroid hormone (PTH) inhibition as an index of CaSR activation report an IC_{50} of 28nM for cinacalcet (Nemeth *et al.*, 2004) and 27nM for NPS R-568 (Nemeth *et al.*, 1998), therein predicting similar bioactivity for both compounds acting at CaSR in native adipocytes. Though both cinacalcet and NPS R-568 elicited adipocyte enlargement in previous experiments, cinacalcet-induced PPARγ expression was not replicated by NPS R-568. Given that the widely understood mechanism of type II allosteric agonists acting at CaSR is to modulate the receptor's response to primary (orthosteric) agonists, 3T3-L1 cells were treated with NPS R-568 in the presence of variable $[Ca^{2+}]_o$. However, NPS R-568 was unable to augment PPARγ expression irrespective of prevailing $[Ca^{2+}]_o$ concentrations. In bovine parathyroid cells, NPS R-568 acts as a positive allosteric modulator with a functional $[Ca^{2+}]_o$ range of 0.5-1.5mM (Nemeth *et al.*, 1998). According to this work, NPS R-568 effects in native cells may be saturated by 2mM $[Ca^{2+}]_o$, but should be evident in the presence of 0.5 and 1mM $[Ca^{2+}]$. Therefore, it appears that PPARγ expression is not regulated by NPS R-568 in 3T3-L1 adipocytes. Considering that PPARγ and FABP4 expression were robustly stimulated by cinacalcet, CaSR activation in 3T3-L1 adipocytes may be agonist-specific; though, further studies are required to investigate potentially differing actions of cinacalcet and NPS R-568 on adipocytes.

PPARγ is a critical transcriptional regulator in adipocytes; though a variety of adipocyte functions are regulated by PPARγ, it plays a key role in lipogenesis and glucose uptake by targeting lipogenic genes, such as FABPs (Rosen, Eguchi and Xu, 2009). As discussed earlier, ADMA caused a non-significant elevation in PPARγ which was reduced by NPS-2143, suggesting that ADMA and CaSR may interact to regulate lipogenic gene expression. Supporting the view that CaSR activation stimulates lipogenesis, cinacalcet stimulated PPARγ expression coinciding with FABP4 induction. Collectively, these data raise the possibility that ADMA and CaSR drive adipocyte hypertrophy via a shared mechanism involving PPARγ. Though PPARγ activity is associated with lipogenesis in mature adipocytes, it is a key

mediator of preadipocyte proliferation and differentiation (i.e., adipogenesis) (Rosen, Eguchi and Xu, 2009). Consequentially, ADMA- and CaSR-mediated adipocyte hypertrophy and PPARγ modulation could arise due to adipogenic stimulation of preadipocyte populations. However, the proportion of mature adipocytes in culture remained stable following ADMA treatment, and there was no effect of ADMA or cinacalcet on PLN-1, the expression of which is closely linked with LD formation and thus 3T3-L1 differentiation (Jang, 2016). It is therefore likely that ADMA and CaSR regulate size and PPARγ in mature adipocytes, as opposed to upregulating lipogenic gene expression in preadipocytes and stimulating differentiation. Though this study focused primarily on the effect of CaSR on adipocyte growth and associated lipogenic pathways, adipocyte biology arises via the integration of both lipogenic and lipolytic pathways (Saponaro *et al.*, 2015). Accordingly, enhanced adipocyte size may reflect enhanced lipogenesis, decreased lipolysis, or both. Recent studies demonstrate CaSR involvement in adipocyte lipid handling via its role in lipolysis (He, Song, *et al.*, 2011; He, Zhang, *et al.*, 2011), which was not examined here. Accordingly, the effects of ADMA and CaSR on adipocyte growth here may be mediated, in part, by inhibition of lipolysis.

4.4.4 Adipocyte function

Among the various physiological functions mediated by adipocytes, regulation of tissue and plasma adipokine levels is of particular importance since adipocyte-derived adipokines can impact directly on cardiovascular function (Oikonomou and Antoniades, 2019). To examine whether ADMA- and CaSR-mediated adipocyte enlargement leads to altered adipokine secretory function, adiponectin and leptin signalling were investigated in 3T3-L1 adipocytes. Adiponectin and leptin were broadly unaffected by ADMA, both at the transcript and protein level. Enlarged adipocytes secrete increased proinflammatory cytokines, increased leptin and decreased adiponectin (Skurk *et al.*, 2007; Kwok, Lam and Xu, 2016). As such, ADMA-mediated adipocyte hypertrophy was expected to coincide with altered adipokine signalling; however, these data are inconsistent with the effect of ADMA on cell size in 3T3-L1 cells.

Previous work has demonstrated that cinacalcet increases adiponectin expression in LS14 preadipocytes (Villarroel et al., 2013). However, it was unclear whether altered transcript levels coincide with a biologically significant increase in adiponectin secretion, or whether CaSR regulates adipokine signalling in mature adipocytes specifically. To examine whether CaSR-induced hypertrophy and lipogenic gene expression coincides with altered adipokine secretion in mature adipocytes, this study investigated how cinacalcet regulates adiponectin and leptin. Though cinacalcet did not augment adiponectin, it had a profound effect on leptin secretion which was elevated ~128%. These data align with the effect of CaSR on cell size, since leptin mRNA expression and protein secretion are increased in large versus small cells (Skurk *et al.*, 2007). Interestingly, though Skurk et al. reported that leptin secretion was raised 5- to 10-fold in intermediate compared to small adipocytes, increased leptin mRNA expression was only evident in adipocyte fractions containing the largest adipocytes coinciding with the greatest leptin secretion. Here cinacalcet tended to increase leptin mRNA levels, but the effect was small and did not reach significance (1.7-fold, p=0.0526). Therefore, the link between adipocyte size and leptin secretion could be underpinned predominantly by mechanism(s) influencing post-translational regulation of leptin secretion. Notably in 3T3-L1 adipocytes, post-translational regulation of leptin secretion is mediated via decreased cAMP and activation of a P13K/AKT signalling pathway (Tsubai *et al.*, 2016). It could therefore be speculated that CaSR-mediated inhibition of cAMP may underpin cinacalcet-induced leptin secretion in 3T3-L1 adipocytes. During obesity, many adipokines become dysregulated. In particular, circulating leptin is raised and exerts pro-oxidant effects in the cardiovascular system (Oikonomou and Antoniades, 2019). Accordingly, activation of adipocyte CaSR and stimulation of leptin secretion could be important in obesity-related pathology. Though these data highlight a role for CaSR in leptin secretion, ADMA effects were lacking suggesting that CaSR and ADMA signalling impose differing effects on adipocyte secretory function, inconsistent with the idea that ADMA targets CaSR in adipocytes.

4.4.5 Enzyme signalling pathways

$ERK_{1/2}$ regulates adipocyte growth and lipogenesis (Ozaki *et al.*, 2016) and is stimulated by CaSR signalling (Magno, Ward and Ratajczak, 2011). In chapter 3, ADMA and CaSR stimulation enhanced $[Ca^{2+}]_o$-dependent $ERK_{1/2}$ activation in a HEK293-CaSR heterologous cell system. As such, $ERK_{1/2}$ activation represented a possible mechanism though which ADMA and CaSR could manifest adipocyte hypertrophy. To begin investigating whether ADMA acts as an allosteric modulator of CaSR signalling, this study first investigated $ERK_{1/2}$ activation in response to $[Ca^{2+}]_o$, the primary endogenous agonist of CaSR. In 3T3-L1 adipocytes, $[Ca^{2+}]_o$ had a marked time- and dose-dependent effect on $ERK_{1/2}$ activation. Interestingly, $ERK_{1/2}$ signalling was not significantly enhanced until prevailing $[Ca^{2+}]_o$ concentrations reached 2mM, suggesting that the activation threshold for this response lies between 1mM-2mM $[Ca^{2+}]_o$. Despite the clear effect of $[Ca^{2+}]_o$ on adipocyte $ERK_{1/2}$ activation, cinacalcet was unable to enhance $[Ca^{2+}]_o$-induced $ERK_{1/2}$ signalling, suggesting that this pathway is not regulated by CaSR in 3T3-L1 adipocytes. This was unexpected, as CaSR sensitises $[Ca^{2+}]_o$-induced $ERK_{1/2}$ signalling in CaSR-transfected HEK293 and 786-O cells (Davey *et al.*, 2012; Frees *et al.*, 2018), but also in non-heterologous systems such parathyroid cells (Avlani *et al.*, 2013), podocytes (Oh *et al.*, 2011) and vascular cells (Smajilovic *et al.*, 2006). Most curiously, CaSR-induced $ERK_{1/2}$ signalling has been observed in LS14 adipocytes *in vitro*. In this model, cinacalcet increases mRNA expression of IL-1ß and $ERK_{1/2}$ activation. Both responses were abolished with the MEK/ERK inhibitor U0126 (D'Espessailles *et al.*, 2018), suggesting that cinacalcet-mediated proinflammatory signalling is regulated via $ERK_{1/2}$ activation in adipocytes. However, compared to the present study which examined short-term (1h) CaSR signalling, D'Espessailles et al. in contrast studied greater durations (16h) of cinacalcet treatment. As such, $ERK_{1/2}$ activation may be more relevant in chronic versus acute CaSR signalling. Moreover, D'Espessailles et al. did not reference $[Ca^{2+}]_o$ conditions. Presumably, cells were exposed to typical concentrations in media (~1.8mM) and CaSR-active amino acids, the potential effect of which was not addressed. In chapter 3, cincacalcet was shown to sensitise $ERK_{1/2}$ activation in HEK293-CaSR cells exposed to 0.2mM $[Ca^{2+}]_o$, but this effect was not recapitulated in 3T3-L1 in adipocytes. This may be related to the threshold activation required for allosteric CaSR stimulation in adipocytes; threshold activation for L-amino acid stimulation of $[Ca^{2+}]_o$-induced $[Ca^{2+}]_i$ signalling is

0.2mM $[Ca^{2+}]_o$ in human parathyroid cells (Conigrave *et al.*, 2004), but bovine parathyroid cells models are insenstive to allosteric stimulation beneath $[Ca^{2+}]_o$ levels of 0.5mM (Nemeth *et al.*, 1998). Though insufficient prevailing $[Ca^{2+}]_o$ concentrations may have precluded an effect of cinacalcet acting upon $ERK_{1/2}$ activation in 3T3-L1 adipocytes, NPS R-568 was unable to stimulate $ERK_{1/2}$ activation irrespective of $[Ca^{2+}]_o$. In parathyroid cells, NPS R-568 sensitises $[Ca^{2+}]_o$-induced $[Ca^{2+}]_i$ signalling in the presence of 0.5-1.5mM $[Ca^{2+}]_o$ (Nemeth *et al.*, 1998). Thus, prevailing $[Ca^{2+}]_o$ seems suitably elevated to permit allosteric stimulation of CaSR by NPS R-568 in 3T3-L1 adipocytes. Collectively, the present data illustrate that cinacalcet and NPS R-568 are ineffectual in stimulating $[Ca^{2+}]_o$-induced $ERK_{1/2}$ activation, strongly suggesting that $[Ca^{2+}]_o$-induced $ERK_{1/2}$ signalling is not potentiated by CaSR in adipocytes. Reinforcing this view, $ERK_{1/2}$ activation in response to maximal $[Ca^{2+}]_o$ stimulation was completely insensitive to NPS-2143. Therefore, it seems that $ERK_{1/2}$ is not targeted by CaSR in 3T3-L1 adipocytes. Studies in other adipocyte models agree with this view; $[Ca^{2+}]_o$ stimulates $ERK_{1/2}$ in brown adipocytes, however the effect is independent of CaSR since $[Ca^{2+}]_i$ mobilisation, which is considered characteristic of CaSR signalling, was lacking (Pramme-Steinwachs, Jastroch and Ussar, 2017). Previous studies investigating CaSR pathways in adipocytes show that $GdCl_2$ inhibits cAMP leading to decreased PKA (He, Zhang, *et al.*, 2011). Future work testing ADMA/CaSR signalling in adipocytes should therefore examine whether allosteric CaSR agonists and ADMA affects CaSR/PKA signalling.

In chapter 3, ADMA enhanced $[Ca^{2+}]_o$-induced $ERK_{1/2}$ activation in HEK293-CaSR cells. Interestingly, ADMA modulates deleterious effects in ECs, VSMCs and renal cells via $ERK_{1/2}$ signalling (Jiang *et al.*, 2007; Zhou *et al.*, 2014; Jayachandran *et al.*, 2020), but its effect on $ERK_{1/2}$ in mature adipocytes was unknown. As CaSR did not regulate $[Ca^{2+}]_o$-induced $ERK_{1/2}$ activation in adipocytes, this study explored the effect of ADMA on both $[Ca^{2+}]_o$-independent -and dependent $ERK_{1/2}$ signalling in 3T3-L1 adipocytes. Confirming previous data here, 1mM $[Ca^{2+}]_o$ did not lead to $ERK_{1/2}$ activation. However, ADMA had no effect on $ERK_{1/2}$ activation under these conditions, suggesting that there is no specific effect of ADMA on $ERK_{1/2}$ activation in 3T3-L1 adipocytes. As with previous experiments, $ERK_{1/2}$ activation was maximally stimulated with 3mM $[Ca^{2+}]_o$. However, this response was unmodified by ADMA. Together, these observations indicate that ADMA does

not participate in adipocyte $ERK_{1/2}$ signalling. As discussed previously, CaSR does not appear to regulate $[Ca^{2+}]_o$-sensitive $ERK_{1/2}$ activation in adipocytes. Though the mechanism(s) involved remain unclear, these data preclude a role for $ERK_{1/2}$ signalling in ADMA- and CaSR-driven adipocyte hypertrophy.

4.5 Conclusions

Both ADMA and CaSR signalling drive hypertrophy in 3T3-L1 adipocytes with no change in adipocyte eNOS expression or NO production. The NOS inhibitor L-NAME did not alter adipocyte size, but significantly decreased adipocyte NO production, collectively indicating that NO may not be an important determinant of 3T3-L1 growth and suggesting that ADMA has alternative functional targets in adipocytes. ADMA did not significantly influence gene expression, but may interact with CaSR to regulate PPARγ. Cinacalcet increased PPARγ and FABP4 mRNA levels, confirming that lipogenic gene expression can be regulated by CaSR. NPS R-568 did not replicate these findings, indicating that adipocyte CaSR signalling could be agonist-specific. Neither ADMA or CaSR altered 3T3-L1 cell differentiation, suggesting that these mediators act upon mature adipocytes rather than preadipocytes. ADMA did not augment adiponectin or leptin signalling, but CaSR increased leptin secretion and this regulates adipokine signalling in 3T3-L1 adipocytes, suggesting that CaSR could contribute towards obesity-related pathology. Though $[Ca^{2+}]_o$ was a profound mediator of $ERK_{1/2}$ activation in 3T3-L1 adipocytes, neither ADMA or CaSR sensitised this effect, precluding a role for ADMA and CaSR in adipocyte $ERK_{1/2}$ activation.

Chapter Five

The role of CaSR and ADMA in the vasculature

Chapter 5: The role of CaSR and ADMA in the vasculature

5.1 Introduction

The importance of calcium in vascular function has been known since Bohr identified extracellular calcium ($[Ca^{2+}]_o$) as a key mediator of vasoreactivity, perpetrating dilatory as well as constrictive actions in isolated blood vessels (Bohr, 1963). Though later studies showed that dietary calcium lowers blood pressure in animal models of hypertension (Ayachi, 1979), the mechanisms involved were unclear. Much later, the discovery of a functional calcium sensing receptor (CaSR) in parathyroid tissue revealed a novel mechanism through which $[Ca^{2+}]_o$ regulated its biological effects (Brown *et al.*, 1993). The presence of CaSR in perivascular nerves, in addition to the observation that $[Ca^{2+}]_o$ stimulation in perivascular nerves triggers the release of vasodilator substance, led to the successful prediction that $[Ca^{2+}]_o$-induced CaSR stimulation in perivascular nerves could regulate vasodilation (Wang and Bukoski, 1998). It is now apparent that vascular CaSR expression is not limited to perivascular nerves; CaSR has been identified in blood vessel homogenate (Wonneberger, Scofield and Wangemann, 2000), and is confirmed to be specifically expressed in vascular smooth muscle cells (VSMCs), endothelial cells (ECs) and adventitia (Weston *et al.*, 2005; Smajilovic *et al.*, 2006). Given the robust expression of CaSR throughout the vascular wall, the role of CaSR in vascular function and its significance in haemodynamic regulation is of great interest.

Several studies have attempted to address the functional role of vascular CaSR, revealing both vasodilatory and contractile effects. In mesenteric arteries and aorta, increasing $[Ca^{2+}]_o$ causes vasodilation (Loot *et al.*, 2013; Greenberg, Shi, *et al.*, 2016). This response was shown to rely on CaSR activation in ECs since $[Ca^{2+}]_o$-mediated relaxation was abolished by the CaSR inhibitor Calhex-231, or endothelial denudation (Greenberg, Shi, *et al.*, 2016). In contrast to its effect in ECs, the CaSR can exert contractile effects in VSMCs since $[Ca^{2+}]_o$ stimulation in denuded vessels lacking endothelium results in vasoconstriction (Greenberg, Shi, *et al.*, 2016). The importance of VSMC CaSR in maintaining vascular tone is corroborated by studies performed in VSMC-specific CaSR deficient mice, since

this model demonstrates reduced vascular contractility and develops hypotension (Schepelmann *et al.*, 2016). Collectively, these data suggest that CaSR mediates dual effects in the vasculature; EC CaSR exerts vasodilatory effects, while VSMC CaSR in contrast is procontractile.

The role of CaSR in the vasculature is further complicated when considering other tissues which influence vasoreactivity, particularly those which are proximal and intrinsic to the vascular wall such as perivascular adipose tissue (PVAT). PVAT is recognised as a fundamental mediator of vascular health and biology (Szasz, Bomfim and Webb, 2013). As described previously, the CaSR is detected in adipose tissue (AT), cultured and native adipocytes (Cifuentes, Albala and Rojas, 2005; He, Zhang, *et al.*, 2011). The CaSR has been implicated in adipocyte biology (Bravo-Sagua *et al.*, 2016), confirmed here in chapter 4 using 3T3-L1 cells. Though it seems likely that CaSR is functionally expressed in PVAT, this has not been demonstrated to date. To gain a comprehensive understanding of vascular CaSR and its biological relevance, a full appraisal of CaSR signalling in VSMCs, ECs and essential ancillary tissues such as PVAT is warranted.

$[Ca^{2+}]_o$ is likely the main endogenous agonist of CaSR, but amino acids are also putative CaSR ligands, stimulating CaSR at physiologically relevant concentrations to modify the secretory function of parathyroid and gut cells (Conigrave *et al.*, 2004; Acar *et al.*, 2020). Very recently, dietary L-Phenylalanine (L-Phe) was shown to contribute to the development of pulmonary hypertension via a CaSR mechanism (Tan *et al.*, 2020). However, the effect of L-Phe acting at vascular CaSR specifically was not explored. As discussed in chapters 3 and 4, asymmetric dimethylarginine (ADMA) may comprise a novel amino acid ligand of CaSR. Interestingly, ADMA has also been implicated in vascular dysfunction and the development of cardiovascular disease (Dowsett *et al.*, 2020). To establish whether the cardiovascular actions of ADMA could be underpinned by ADMA/CaSR signalling, the effect of ADMA at vascular CaSR should also be investigated.

5.2 Aims

1. To evaluate PVAT function in the vasculature
2. To explore the effect of CaSR modulation in vascular and PVAT function
3. To establish the effect of amino acids L-Phe and ADMA in vascular and PVAT function.

5.3 Results

5.3.1 PVAT effects

PVAT plays an essential role in vasoreactivity, since substances secreted by PVAT confer both relaxing as well as contractile effects in the vasculature (Nava and Llorens, 2019). Physiological $[Ca^{2+}]_o$ levels are maintained within a narrow limit of 1.1-1.3mM (Zhang *et al.*, 2016), so vascular myography studies were conducted in the presence of 1mM (low) $[Ca^{2+}]_o$ to prohibit maximal activation of CaSR.

To investigate the significance of ADMA and CaSR signalling in PVAT, it was first necessary to characterise the effect of PVAT on vascular reactivity at baseline (Tb. 5-1a). In male C57BL/6 aortas, phenylephrine (PE) caused contraction (pEC_{50}=7.0±0.2, E_{max}=57.7±4.5%). When compared to this response, PVAT did not affect PE vascular contractility ($p>0.05$; Fig. 5-1a). As expected, acetylcholine (ACh) caused vasorelaxation in aortas (pEC_{50}=7.1±0.1, E_{max}=75.2±4.3%). ACh-mediated vasorelaxation with blunted by PVAT; the maximal ACh response was unchanged, but ACh sensitivity was reduced since the pEC_{50} for ACh was decreased (pEC_{50}=6.4±0.1, E_{max}=85.9±4.5%, p=0.0002; Fig. 5-1b). Sodium nitroprusside (SNP) also promoted vasorelaxation in C57BL/6 aortas (pEC_{50}=7.4±0.2, E_{max}=99.8±7.7%). However, PVAT did not alter SNP-mediated vasorelaxation ($p>0.05$; Fig. 5-1c).

PVAT secretory function affects vasoreactivity through two key mechanisms; firstly, by modulating VSMC contraction, and secondly by indirectly modulating VSMC tone by influencing EC function (Nava and Llorens, 2019). To establish the significance of EC activity in in PVAT-mediated vascular responses, this study performed experiments in aortic segments following endothelium removal (i.e., denudation) (Tb. 5-1b). In denuded aortas, again PE elicited vasoconstriction (pEC_{50}=7.2±0.2, E_{max}=116.0±6.4%). In contrast to intact vessels where PVAT had no effect, PVAT caused significant inhibition of PE contraction in denuded aortas (pEC_{50}=6.9±0.2, E_{max}=93.2±7.8%, p=0.0022; Fig. 5-1d). Curiously, PVAT reduced the maximal response to PE and pEC_{50} but neither effect was independently statistically significant, indicating PVAT inhibits PE contractility in aortic segments because of small, but cumulative effects on both PE efficacy and

potency. In denuded aortas, SNP caused vasorelaxation (pEC_{50}=7.5±0.2, E_{max}=101.6.0±4.8%, p=0.0022). SNP responses were significantly attenuated by PVAT in denuded aortas; maximum SNP responses were unaffected, though vascular sensitivity to SNP was reduced since the pEC_{50} for SNP fell in the presence of PVAT (pEC_{50}=6.9±0.2, E_{max}=116.4±16.6%, p=0.0035; Fig. 5-1e). PVAT decreased PE contraction in denuded vessels specifically so the vascular response to PVAT could be regulated by the endothelium. Subsequent experimentation focused on exploring the role of CaSR and ADMA in PE-mediated vascular responses.

Figure 5-1

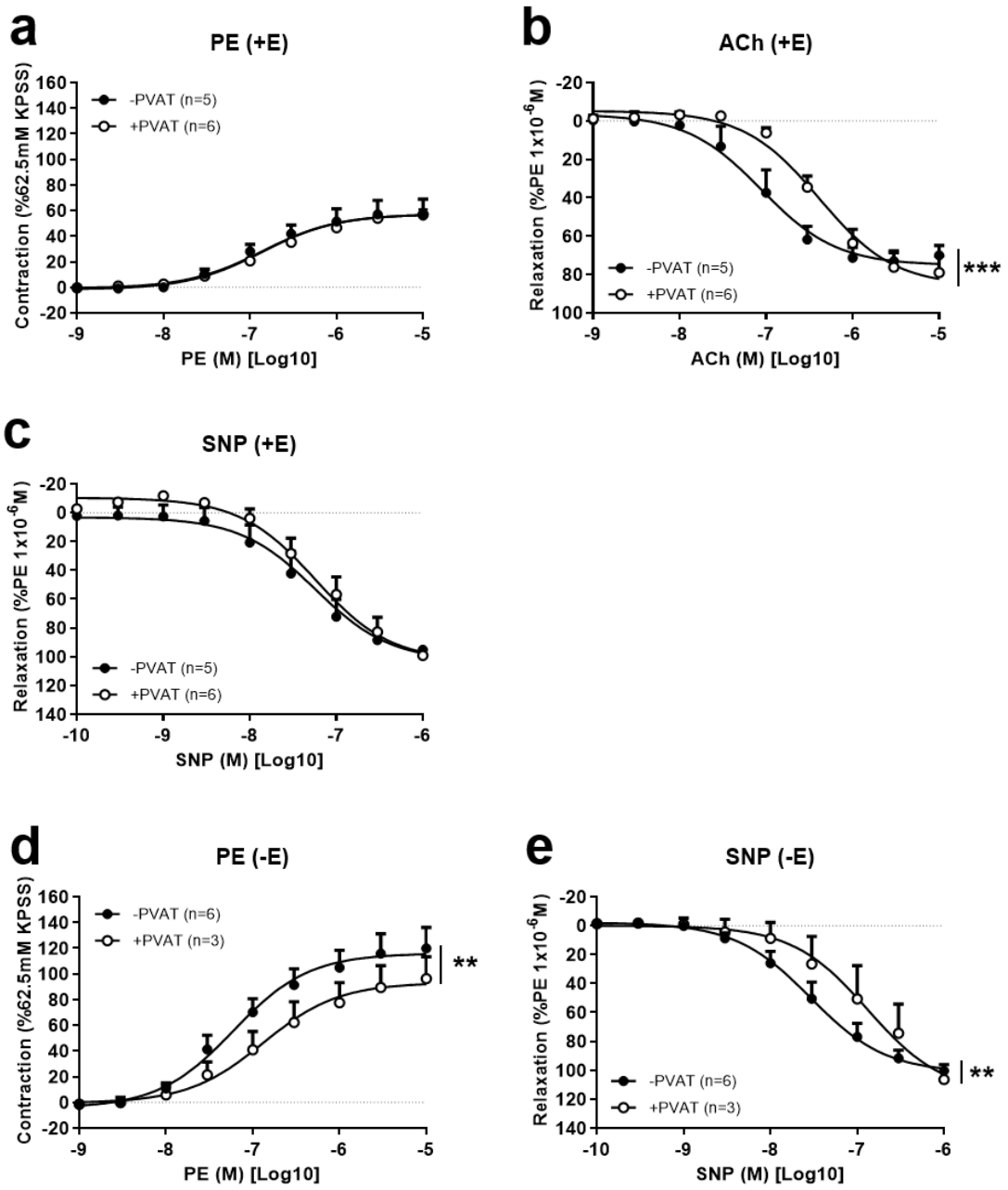

Figure 5-1: PVAT alters vascular reactivity.

(a) In C57BL/6 aorta with intact endothelium (+E), PVAT (+PVAT) does not influence PE-mediated vascular contraction. **(b)** PVAT reduces the pEC_{50} for ACh, but has no effect on maximal ACh responses. **(c)** PVAT does not influence SNP-mediated vascular relaxation. **(d)** In aortas lacking endothelium (-E), PE vasoconstriuction is signifcantly reduced by PVAT. **(e)** PVAT reduces pEC_{50} for SNP, but has no effect on maximal SNP responses. Mean ±SEM. F-test (a-e). **p<0.01, ***p<0.001, -PVAT vs +PVAT. ACh=Acetylcholine; PE=Phenylephrine; PVAT=Perivascular adipose tissue; SNP=Sodium nitroprusside.

Table 5-1

(a)

D-R Curve	PE (+E)			Ach (+E)			SNP (+E)		
Treatment	pEC_{50} ($-Log_{10}$)	E_{max} (%)	*p*	pEC_{50} ($-Log_{10}$)	E_{max} (%)	*p*	pEC_{50} ($-Log_{10}$)	E_{max} (%)	*p*
-PVAT	7.0±0.2	57.7±4.5		7.1±0.1	75.2±4.3		7.4±0.2	99.8±7.7	
+PVAT	6.7±0.1	57.1±2.0		6.4±0.1	85.9±4.5	***	7.1±0.1	105.9±7.3	

(b)

D-R Curve	PE (-E)			SNP (-E)		
Treatment	pEC_{50} ($-Log_{10}$)	E_{max} (%)	*p*	pEC_{50} ($-Log_{10}$)	E_{max} (%)	*p*
-PVAT	7.2±0.2	116.0±6.4		7.5±0.2	101.6.0±4.8	
+PVAT	6.9±0.2	93.2±7.8	**	6.9±0.2	116.4±16.6	**

Table 5-1: The effect of PVAT on vascular reactivity.

(a) Dose-response curves were conducted on C57BL/6 aorta segments with intact endothelium (+E; >60% function preserved) **(b)** or endothelium denuded (-E; <20% function preserved). Results are provided for PE, ACh and SNP dose-response curves in PVAT absence (-PVAT) and presence (+PVAT). PE response is expressed as % contraction relative to the mean KPSS contraction. ACh and SNP responses are expressed as % relaxation relative to PE $1x10^{-6}$M preconstriction. Mean ±SEM. F-test. **p<0.01, ***p=<0.001, -PVAT vs +PVAT. ACh=Acetylcholine; PE=Phenylephrine; PVAT=Perivascular adipose tissue; SNP=Sodium nitroprusside.

5.3.2 CaSR in the vasculature

In male C57BL/6 mice, PVAT had no effect on PE vasoconstriction in aortas with intact endothelium, but significantly reduced PE contractile responses in denuded aortas, suggesting that PVAT responses are regulated by the endothelium. To determine how CaSR might contribute to PVAT-mediated PE responses, a series of experiments were performed in endothelium-intact and denuded vessels to interrogate how the physiological CaSR ligand $[Ca^{2+}]_o$, the positive allosteric CaSR modulator cinacalcet and the CaSR inhibitor NPS-2143 influence vascular function.

5.3.1.1 CaSR expression in adipose

CaSR expression has been detected in white adipose tissue from rat (He, Song, *et al.*, 2011). To confirm the presence of CaSR in mouse white adipose tissue and investigate its expression in PVAT, mRNA analyses were conducted on gonadal adipose tissue (gAT), subcutaneous adipose (scAT) and PVAT isolated from C57BL/6 mice. In all tissue sampled, CaSR was present at the transcript level (Fig. 5-2). To further characterise CaSR expression in PVAT, mRNA levels were compared to gAT and scAT. PVAT CaSR levels were not altered compared to gAT ($p>0.05$) or scAT ($p>0.05$). However, further experiments should be performed since these data were highly variable.

Figure 5-2

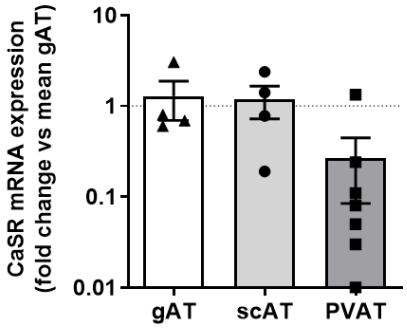

Figure 5-2: CaSR mRNA expression in murine adipose.

CaSR transcript is expressed by gAT, scAT and PVAT in adipose isolated from C57BL/6 mice. Compared to PVAT, there is no difference in CaSR gene expression in gAT or scAT. Mean±SEM. One-way ANOVA. CaSR=Calcium-sensing receptor; gAT=Gonadal adipose tissue; PVAT=Perivascular adipose tissue; scAT=Subcutaneous adipose tissue.

5.3.1.2 Vascular response to $[Ca^{2+}]_o$

To dissect the mechanism(s) underpinning PVAT responses in C57BL/6 aortas and investigate the role of CaSR in PVAT-mediated PE responses, aortas were stimulated with PE in the presence of variable $CaCl_2$ ($[Ca^{2+}]_o$; 1 and 2.5mM). PE caused contraction in aortas incubated with 1mM (low) $[Ca^{2+}]_o$ (pEC_{50}=6.8±0.1, E_{max}=57.0±3.1%). In comparison, the presence of 2.5mM (high) $[Ca^{2+}]_o$ led to enhanced PE contraction; maximal PE responses were increased, though PE sensitivity was unchanged since the pEC_{50} for PE was unaffected (pEC_{50}=6.7±0.1, E_{max}=76.4±3.2%, p=0.0001; Fig. 5-3a). To establish whether high $[Ca^{2+}]_o$ influences PVAT function, the effect of PVAT on PE contraction was assessed under low and high $[Ca^{2+}]_o$ conditions. When compared to their respective controls, preservation of PVAT did not change PE contraction in the presence of low 1mM $[Ca^{2+}]_o$ (pEC_{50}=6.7±0.1, E_{max}=63.4±3.5%, p>0.05; Fig. 5-3a) or high $[Ca^{2+}]_o$ (pEC_{50}=6.7±0.2, E_{max}=82.1±7.0%, p>0.05), showing that $[Ca^{2+}]_o$ alters vascular contraction but not PVAT function in intact vessels.

Earlier in section 5.3.1, PVAT decreased PE contractility specifically in denuded vessels, so the above experiments were repeated in denuded preparations. In these vessels, PE contraction was again profoundly increased by high $[Ca^{2+}]_o$ (1mM $[Ca^{2+}]_o$ pEC_{50}=7.1±0.1, E_{max}=100.2±4.8%; 2.5mM $[Ca^{2+}]_o$ pEC_{50}=7.1±0.1, E_{max}=120.4±5.8%, p=0.0044; Fig. 5-3b). To establish whether high $[Ca^{2+}]_o$ influences PVAT function in denuded vessels, the effect of PVAT on PE contraction was assessed under low and high $[Ca^{2+}]_o$ conditions. Compared to control denuded vessels incubated in low 1mM $[Ca^{2+}]_o$ buffer, PVAT attenuated PE contraction decreasing the maximum efficacy of PE by 14% (pEC_{50}=6.8±0.1, E_{max}=86.5±3.3%, p=0.0003; Fig. 5-3b). Interestingly however, PVAT was unable to reduce PE contraction in denuded vessels incubated with high 2.5mM $[Ca^{2+}]_o$ (pEC_{50}=7.0±0.1, E_{max}=109.9±5.0%, p>0.05; Fig. 5-3b). This shows that the inhibitory effect of PVAT in denuded vessels relies on prevailing $[Ca^{2+}]_o$ levels being held at low concentrations.

Figure 5-3

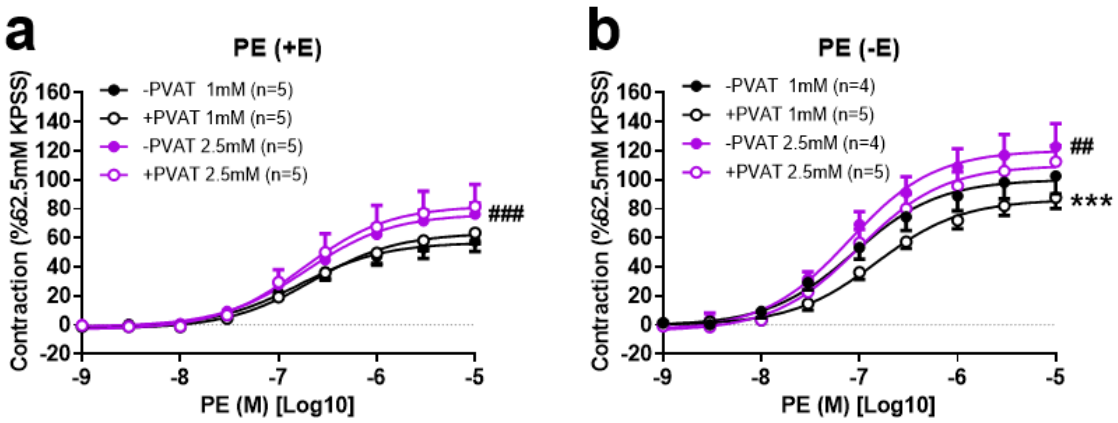

Figure 5-3: $[Ca^{2+}]_o$ increases PE-mediated vascular contraction.

(a) In vessels with intact endothelium (+E), PE contraction is increased by 2.5mM compared to 1mM CaCl ($[Ca^{2+}]_o$)). PVAT (+PVAT) does not influence PE-mediated vascular contraction when vessels are incubated in buffer containing 1mM or 2.5mM CaCl ($[Ca^{2+}]_o$)). **(b)** In vessels lacking endothelium (-E), PE contraction is increased by 2.5mM compared to 1mM $[Ca^{2+}]_o$. PVAT (+PVAT) decreases PE-mediated vascular contraction when vessels are incubated in buffer containing 1mM $[Ca^{2+}]_o$, but not when vessels are incubated in 2.5mM $[Ca^{2+}]_o$. Mean ±SEM. F-test (a,b). ***p<0.001 -PVAT 1mM vs +PVAT 1mM. ##p<0.001, ###p<0.0001 -PVAT 1mM vs -PVAT 2.5mM. PE=Phenylephrine; PVAT=Perivascular adipose tissue.

Table 5-2

D-R Curve	PE +E			PE -E		
Treatment	pEC_{50} ($-Log_{10}$)	E_{max} (%)	*p*	pEC_{50} ($-Log_{10}$)	E_{max} (%)	*p*
-PVAT						
1mM	6.8±0.1	57.0±3.1		7.1±0.1	100.2±4.8	
2.5mM	6.7±0.1	76.4±3.2	###	7.1±0.1	120.4±5.8	##
+PVAT						
1mM	6.7±0.1	63.4±3.5		6.8±0.1	86.5±3.3	***
2.5mM	6.7±0.2	82.1±7.0		7.0±0.1	109.9±5.0	

Table 5-2: The effect of $[Ca^{2+}]_o$ on PVAT-mediated vascular reactivity.
Dose-response curves were conducted on C57BL/6 aorta segments with intact endothelium (+E; >60% function preserved) or endothelium denuded (-E; <20% function preserved). Results are provided for PE in PVAT absence (-PVAT) and presence (+PVAT), with low $CaCl_2$ ($[Ca^{2+}]_o$; 1mM) or high $[Ca^{2+}]_o$ (2.5mM) buffer. PE response is expressed as % contraction relative to the mean KPSS contraction. Mean ±SEM. F-test. ***p<0.001 -PVAT 1mM vs +PVAT 1mM. ##p<0.001, ###p<0.0001 -PVAT 1mM vs -PVAT 2.5mM. PE=Phenylephrine; PVAT=Perivascular adipose tissue.

5.3.1.3 Vascular response to cinacalcet

In the previous section, $[Ca^{2+}]_o$ exacerbated PE vasoconstriction in intact and endothelium denuded vessels. $[Ca^{2+}]_o$ does not activate CaSR selectively, so vessels with and without PVAT were incubated with 1μM cinacalcet, an allosteric CaSR modulator, to determine whether CaSR activation produced similar effects on PVAT function (Tb. 5-2). Buffer $[Ca^{2+}]_o$ concentrations were held at 1mM to prohibit maximal stimulation of CaSR.

As before, PE caused vascular contraction in aortic vessel segments (pEC_{50}=6.6±0.2, E_{max}=51.9±4.7%). PE responses in these preparations were not altered with cinacalcet treatment (pEC_{50}=6.8±0.1, E_{max}=51.9±2.9%, p>0.05; Fig. 5-4a), suggesting that cinacalcet does not influence contraction in intact vessels. Next, the effect of cinacalcet on PVAT function was assessed. Although PVAT had no effect in previous experiments, here PVAT enhanced PE contraction in intact vessels which was increased through a cumulative effect on maximum PE contraction and PE sensitivity (pEC_{50}=6.6±0.1, E_{max}=63.9±4.1%, p=0.0417; Fig. 5-

4a). Compared to cinacalcet-treated vessels, PVAT preservation resulted in enhanced PE contraction, though in this case only maximal PE responses were increased (pEC_{50}=6.8±0.1, E_{max}=66.1±3.1%, p=0.0008; Fig. 5-4a). Broadly, cinacalcet does not seem to influence vascular reactivity or PVAT function in intact vessels.

In denuded vessels, high 2.5mM $[Ca^{2+}]_o$ blocked PVAT-mediated inhibition of PE contraction, indicating that PVAT function could be antagonised by CaSR stimulation. To test whether this effect could be attributed to CaSR specifically, this study examined whether $[Ca^{2+}]_o$-dependent PVAT responses in denuded vessels could be recapitulated by cinacalcet. Under control conditions, PE stimulated vasoconstriction in denuded vessels (pEC_{50}=7.0±0.1, E_{max}=105.9±3.5%). When compared to these responses, cinacalcet exacerbated PE contraction; maximal PE contraction was increased, with no change in pEC_{50} (pEC_{50}=7.1±0.1, E_{max}=124.3±5.4%, p=0.0044; Fig. 5-4b). This indicates that cinacalcet stimulates endothelial-independent vascular contraction in denuded vessels. To establish whether cinacalcet influences PVAT function in denuded vessels, PVAT responses were examined following cinacalcet stimulation. As before, PVAT significantly attenuated PE contraction in denuded vessels reducing maximum PE responses by 13% (pEC_{50}=6.8±0.1, E_{max}=91.2±3.2%, p<0.0001; Fig. 5-4b). However, PE responses in cinacalcet-treated vessels were decreased with PVAT preservation causing a 33% reduction in maximal PE responses (pEC_{50}=6.8±0.1, E_{max}=83.4±4.4%, p<0.0001; Fig. 5-4b). Though cinacalcet enhanced PE contractility, the PVAT inhibitory effect is preserved.

Figure 5-4

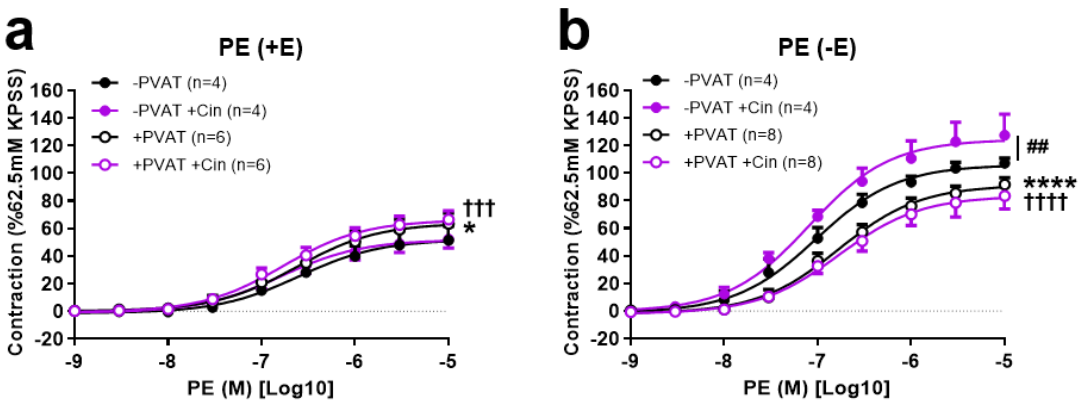

Figure 5-4: Cinacacet increases PE-mediated vascular contraction.

(a) In vessels with intact endothelium (+E), PE contraction is unaffected by 1μM cinacalcet. PVAT (+PVAT) increases PE-mediated vascular contraction in control and cinacalcet-treated vessels. **(b)** In vessels lacking endothelium (-E), PE contraction is increased by cinacalcet. PVAT (+PVAT) decreases PE-mediated vascular contraction in control and cinacalcet-treated vessels. Mean ±SEM. F-test (a,b). *p<0.05, ****p<0.0001 -PVAT vs +PVAT. †††p<0.001, ††††p<0.0001 -PVAT cinacalcet vs +PVAT cinacalcet. ##p<0.01 -PVAT vs -PVAT cinacalcet. PE=Phenylephrine; PVAT=Perivascular adipose tissue.

Table 5-3

D-R Curve	PE +E			PE -E		
Treatment	pEC_{50} ($-Log_{10}$)	E_{max} (%)	*p*	pEC_{50} ($-Log_{10}$)	E_{max} (%)	*p*
-PVAT						
Ctrl	6.6±0.2	51.9±4.7		7.0±0.1	105.9±3.5	
Cinacalcet	6.8±0.1	51.9±2.9		7.1±0.1	124.3±5.4	##
+PVAT						
Ctrl	6.6±0.1	63.9±4.1	*	6.8±0.1	91.2±3.2	****
Cinacalcet	6.8±0.1	66.1±3.1	†††	6.8±0.1	83.4±4.4	††††

Table 5-3: The effect of cinacalcet on PVAT-mediated vascular reactivity. Dose-response curves were conducted on C57BL/6 aorta segments with intact endothelium (+E; >60% function preserved) or endothelium denuded (-E; <20% function preserved). Results are provided for PE in PVAT absence (-PVAT) and presence (+PVAT), ±cinacalcet (1μM). PE response is expressed as % contraction relative to the mean KPSS contraction. Mean ±SEM. F-test. *p<0.05, ****p<0.0001 -PVAT ctrl vs +PVAT ctrl. †††p<0.001, ††††p<0.0001 -PVAT cinacalcet vs +PVAT cinacalcet. ##p<0.01 -PVAT ctrl vs -PVAT cinacalcet. PE=Phenylephrine; PVAT=Perivascular adipose tissue.

5.3.1.4 Vascular response to NPS-2143

In a third set of experiments, vessels with and without PVAT were incubated with 1μM NPS-2143 to establish whether inhibition of CaSR signalling could alter PVAT function (Tb. 5-3).

In control experiments, PE stimulated vascular contraction (pEC_{50}=6.9±0.1, E_{max}=72.4±1.6%). These PE responses were not altered by NPS-2143 treatment (pEC_{50}=7.0±0.0, E_{max}=76.9±1.1%, p>0.05; Fig. 5-5a), suggesting that NPS-2143 does not impact vascular contractility in intact vessels. Next, the effect of NPS-2143 on PVAT function was examined. Under control conditions, PVAT was unable to alter PE contraction (pEC_{50}=6.9±0.1, E_{max}=77.5±1.4%, p>0.05; Fig. 5-5a). Similarly, NPS-2143 treated vessels showed no change in PE responses with PVAT preservation (pEC_{50}=7.0±0.1, E_{max}=78.3±4.4%p>0.05; Fig 5-5a), suggesting that PVAT responses are unchanged by NPS-2143 in vessels with intact endothelium.

To investigate endothelial-independent vascular effects, the above experiments were repeated in denuded vessels. In these preparations, PE caused vasoconstriction (pEC_{50}=7.3±0.2, E_{max}=95.2±5.7%). Again, NPS-2143 treatment did not impact on PE responses (pEC_{50}=7.4±0.1, E_{max}=98.9±2.6%, p>0.05; Fig. 5-5b), indicating that NPS-2143 does not modify vascular responses in denuded vessels. To assess whether CaSR inhibition influences PVAT function, the effect of PVAT on PE contraction was assessed following NPS-2143 incubation. As seen in previous experiments, PE responses seen in control vessels were robustly decreased with PVAT preservation, which reduced the maximum response to PE by 17% (pEC_{50}=6.8±0.1, E_{max}=79.8±4.2%, p<0.0001; Fig. 5-5b). Compared to NPS-2143 treated vessels, PVAT inhibited maximal PE responses by 15% (pEC_{50}=6.9±0.2, E_{max}=83.9±5.1%, p<0.0001; Figure 5-5b). Thus PVAT function is unchanged by NPS-2143 treatment.

To avoid maximal stimulation of vascular CaSR and study how CaSR regulates vascular function, myography studies were conducted in the presence of low 1mM $[Ca^{2+}]_o$. Under these conditions, $[Ca^{2+}]_o$-mediated activation of vascular CaSR may not be sufficient to observe an inhibitory effect of NPS-2143. Therefore, another series of experiments were performed replicating those above in denuded vessels, but in contrast vessels were preincubated with high (2.5mM) $[Ca^{2+}]_o$ buffer (Tb. 5-4). In high $[Ca^{2+}]_o$ conditions, denuded vessels contracted in response to PE (pEC_{50}= 6.9±0.1, E_{max}= 119.7±4.7%). NPS-2143 tended to decrease PE-mediated vascular contraction in denuded vessels, though the effect did not reach significance (pEC_{50}= 6.9±0.1, E_{max}= 105.9±5.5%, p=0.0995; Fig. 5-5c). In this series of experiments, PVAT caused a small but significant reduction in PE contraction when compared to control vessels (pEC_{50}= 6.8±0.1, E_{max}= 107.3±5.2%, p=0.0137; Fig 5-5c). This response resulted from a combined reduction in maximal PE efficacy and PE sensitivity, since neither variable was significantly altered when tested independently. Surprisingly, NPS-2143 treated vessels showed unchanged PE responses with PVAT preservation (pEC_{50}= 6.7±0.1, E_{max}= 98.3±6.2%, p>0.05; Fig. 5-5c). Thus NPS-2143 inhibits the relaxing effect of PVAT, though this occurs specifically in high $[Ca^{2+}]_o$ conditions.

Figure 5-5

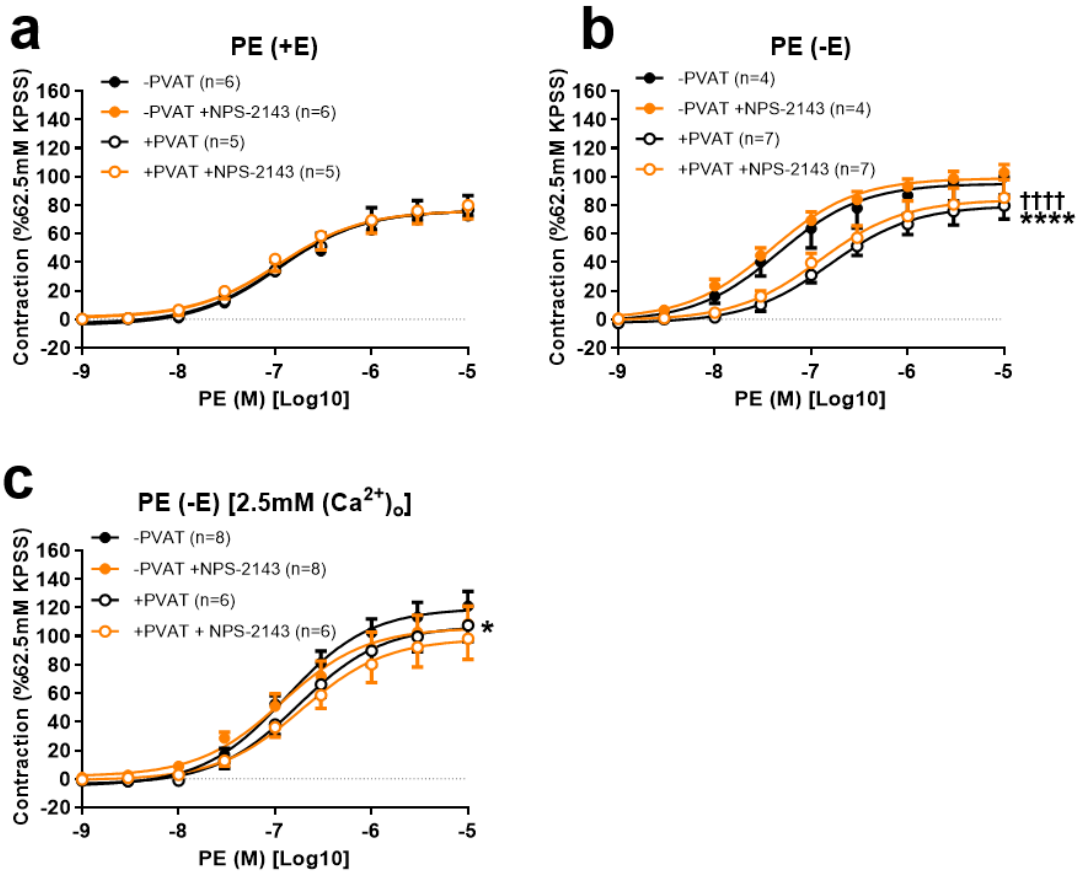

Figure 5-5: NPS-2143 does not alter PE-mediated vascular contraction.

(a) In vessels with intact endothelium (+E), PE contraction is unaffected by 1μM NPS-2143. PVAT (+PVAT) has no effect on PE contraction in control and NPS-2143-treated vessels. **(b)** In vessels lacking endothelium (-E), PE contraction is unaffected by NPS-2143. PVAT (+PVAT) reduces PE contraction in both control and NPS-2143-treated vessels. **(c)** In vessels lacking endothelium (-E) incubated in high (2.5mM) $CaCl_2$ buffer, PE contraction is not significantly affected by NPS-2143. PVAT (+PVAT) reduces PE contraction in control but not not NPS-2143-treated vessels. Mean ±SEM. F-test (a-c). *p<0.05, ****p<0.0001 -PVAT vs +PVAT. ††††p<0.0001 -PVAT NPS-2143 vs +PVAT NPS-2143. PE=Phenylephrine; PVAT=Perivascular adipose tissue.

Table 5-4

D-R Curve	PE +E			PE -E (1mM $[Ca^{2+}]_o$)			PE -E (2.5mM $[Ca^{2+}]_o$		
Treatment	pEC_{50} ($-Log_{10}$)	E_{max} (%)	*p*	pEC_{50} ($-Log_{10}$)	E_{max} (%)	*p*	pEC_{50} ($-Log_{10}$)	E_{max} (%)	*p*
-PVAT									
Ctrl	6.9±0.1	72.4±1.6		7.3±0.2	95.2±5.7		6.9±0.1	119.7±4.7	
NPS-2143	7.0±0.0	76.9±1.1		7.4±0.1	98.9±2.6		6.9±0.1	105.9±5.5	
+PVAT									
Ctrl	6.9±0.1	77.5±1.4		6.8±0.1	79.8±4.2	****	6.8±0.1	107.3±5.2	*
NPS-2143	7.0±0.1	78.3±4.4		6.9±0.2	83.9±5.1	††††	6.7±0.1	98.3±6.2	

Table 5-4: The effect of NPS-2143 on PVAT-mediated vascular reactivity.
Dose-response curves were conducted on C57BL/6 aorta segments with intact endothelium (+E; >60% function preserved) or endothelium denuded (-E; <20% function preserved). -E experiments were performed in low $CaCl_2$ ($[Ca^{2+}]_o$; 1mM) or high $[Ca^{2+}]_o$ (2.5mM) conditions. Results are provided for PE in PVAT absence (-PVAT) and presence (+PVAT), ±NPS-2143 (1μM). PE response is expressed as % contraction relative to the mean KPSS contraction. Mean ±SEM. F-test. *p<0.05, ****p<0.0001 -PVAT vs +PVAT. ††††p<0.0001 -PVAT NPS-2143 vs +PVAT NPS-2143. PE=Phenylephrine; PVAT=Perivascular adipose tissue.

5.3.3 Amino acids in the vasculature

5.3.3.1 L-Phenylalanine

Previously, PE-mediated vascular contraction in denuded vessels was significantly increased by high 2.5mM $[Ca^{2+}]_o$, in the absence and presence of PVAT. Cinacalcet recapitulated this effect in denuded vessels lacking PVAT, but not in vessels retaining PVAT. The amino acid L-Phenylalanine (L-Phe) is an allosteric modulator of CaSR which enhances CaSR $[Ca^{2+}]_o$ sensitivity in heterologous and native cell systems (Conigrave, Quinn and Brown, 2000; Conigrave *et al.*, 2004). To further elucidate the role of CaSR in vascular function, this study investigated how L-Phe (1mM) affects vasoreactivity and PVAT-mediated vascular responses in denuded vessels (Tb. 5-5; Fig. 5-6).

As before, PE caused vasoconstriction in denuded vessels (pEC_{50}=7.0±0.2, E_{max}=83.4±5.7%). L-Phe tended to enhance this response, though the effect was not statistically significant (pEC_{50}=7.1±0.1, E_{max}=94.2±4.4%, p=0.0826). This suggests that baseline vascular function is not modified by L-Phe, though further experiments are required to confirm these findings. To establish whether L-Phe influences the PVAT inhibitory function in denuded vessels, PVAT-mediated PE

contractility was assessed following L-Phe incubation. Compared to control vessels, PVAT reduced PE contraction; maximal PE contraction was unchanged, but pEC_{50} was reduced 9% (pEC_{50}=6.4±0.1, E_{max}=74.8±3.0%, p<0.0001; Fig. 5-6). Similarly, L-Phe-treated vessels showed reduced PE contraction with PVAT preservation; again, maximal PE contraction was unaffected, though the pEC_{50} for PE decreased by 7% (pEC_{50}=6.6±0.1, E_{max}=94.1±6.5%, p=0.0033; Fig. 5-6). Therefore L-Phe does not impact the anticontractile PVAT function.

Figure 5-6

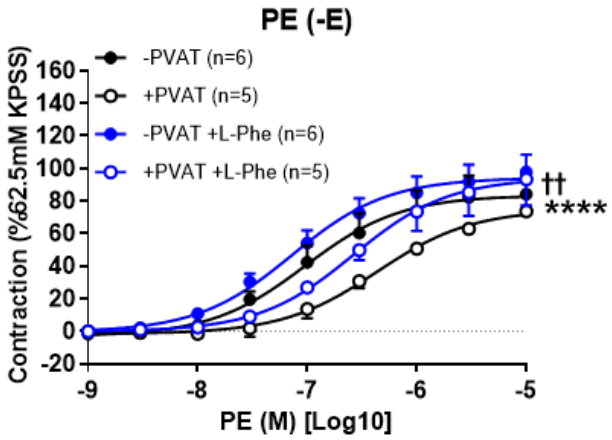

Figure 5-6: The effect of L-Phe in PE-mediated vascular contraction.
In vessels lacking endothelium (-E), PE contraction is unaffected by 1mM L-Phe. PVAT (+PVAT) decreases PE-mediated vascular contraction in control and L-Phe-treated vessels. Mean ±SEM. F-test. ****p<0.0001 -PVAT vs +PVAT. ††p<0.01 -PVAT +L-Phe vs +PVAT +L-Phe. L-Phe=L-Phenylalanine; PE=Phenylephrine; PVAT=Perivascular adipose tissue.

5.3.3.2 ADMA

This study wanted to assess whether ADMA may constitute a novel CaSR-amino acid. Before performing vascular myography studies, mRNA analyses were conducted on gAT, scAT and PVAT isolated from C57BL/6 mice to examine the expression of DDAH1, DDAH2 and eNOS, which regulate ADMA signalling (Leone *et al.*, 1992; J. Leiper and Vallance, 2006). In all sampled tissues, DDAH1, DDAH2 and eNOS were present at the transcript level (Fig. 5-7). As DDAH and eNOS were detected in all AT depots studied, expression of these mediators was further examined by comparing levels across the AT depots studied. PVAT compared to

gAT demonstrated significantly reduced levels of DDAH1 (0.2±0.1-fold, $p<0.0066$), DDAH2 (0.2±0.1-fold, $p<0.0015$) and eNOS (0.1±0.1-fold, $p<0.0075$). However, expression of these mediators in PVAT compared to scAT were similar ($p>0.05$).

Figure 5-7

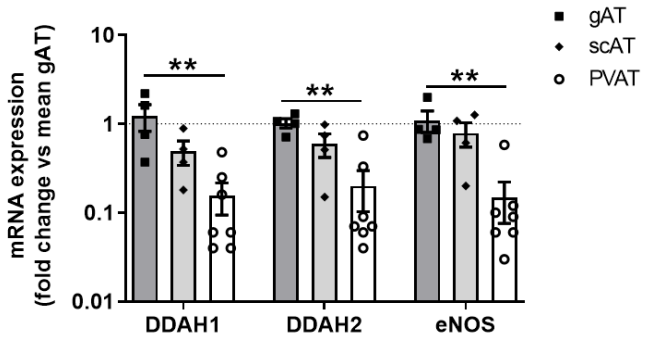

Figure 5-7: DDAH1, DDAH2 and eNOS mRNA expression in murine adipose. CaSR transcript is expressed by gAT, scAT and PVAT isolated from C57BL/6 mice. Compared to PVAT, there is no difference in CaSR gene expression in gAT or scAT. Mean±SEM. One-way ANOVA. **p<0.01 PVAT vs gAT. DDAH=Dimethylarginine dimethylaminohydrolase; eNOS=Endothelial nitric oxide synthase; gAT=Gonadal adipose tissue; PVAT=Perivascular adipose tissue; scAT=Subcutaneous adipose tissue.

In the sections previous, VSMC contractility was shown to be influenced by cinacalcet. Previous studies assessing the effect of ADMA on vascular function show that ADMA potentiates vascular contraction (Al-Zobaidy, Craig and Martin, 2010; Torondel *et al.*, 2010). To investigate whether ADMA acts as an allosteric modulator of CaSR in the vasculature, PE responses were assessed in denuded vessels incubated with physiological (3μM) ADMA concentrations (Tb. 5-5; Fig. 5-8). PE promoted contraction in denuded vessels (pEC_{50}=7.0±0.1, E_{max}=99.6±3.1%). However, there was no effect of ADMA on PE contractility (pEC_{50}=6.9±0.1, E_{max}=95.8±3.1%, $p>0.05$). Next, the effect of ADMA on PVAT function was assessed. Compared to control vessels, PVAT profoundly decreased PE contractility which showed a 16% reduction in maximal PE response (pEC_{50}=6.7±0.1, E_{max}=84.7±4.9%, $p<0.0001$; Fig. 5-8). Consistently, PVAT also reduced PE contraction in the presence of ADMA, inhibiting maximal PE

responses by 13% (pEC_{50}=6.7±0.1, E_{max}=83.5±5.0%, p=0.0004; Fig. 5-8). The PVAT inhibitory function is thus unaffected by ADMA.

Figure 5-8

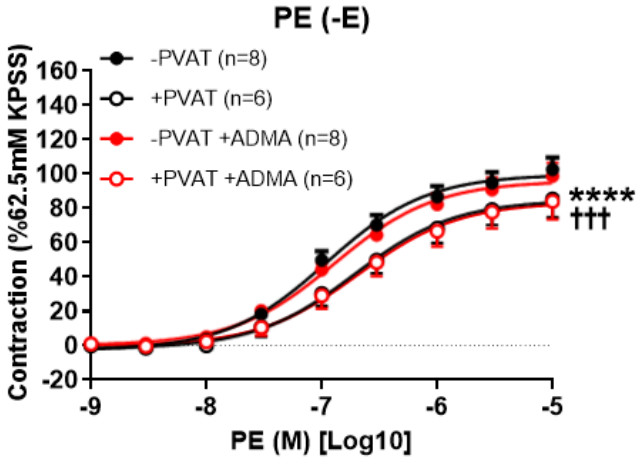

Figure 5-8: The effect of ADMA in PE-mediated vascular contraction.
In vessels lacking endothelium (-E), PE contraction is unaffected by 3μM ADMA. PVAT (+PVAT) decreases PE-mediated vascular contraction in control and ADMA-treated vessels. Mean ±SEM. F-test. ****p<0.0001 -PVAT vs +PVAT. †††p<0.001 -PVAT +ADMA vs +PVAT +ADMA. ADMA=Asymmetric dimethylarginine; PE=Phenylephrine; PVAT=Perivascular adipose tissue.

Table 5-5

D-R Curve	PE -E		
Treatment	pEC_{50} ($-Log_{10}$)	E_{max} (%)	*p*
-PVAT			
Ctrl	7.0±0.2	83.4±5.7	
L-Phe	7.1±0.1	94.2±4.4	
+PVAT			
Ctrl	6.4±0.1	74.8±3.0	****
L-Phe	6.6±0.1	94.1±6.5	††
-PVAT			
Ctrl	7.0±0.1	99.6±3.1	
ADMA	6.9±0.1	95.8±3.1	
+PVAT			
Ctrl	6.7±0.1	84.7±4.9	****
ADMA	6.7±0.1	83.5±5.0	†††

Table 5-5: The effect of amino acids on PVAT-mediated vascular reactivity. Dose-response curves were conducted on C57BL/6 aorta segments with denuded endothelium (-E; <20% function preserved). Results are provided for PE in PVAT absence (-PVAT) and presence (+PVAT), ±L-Phe (1mM) or ADMA (3µM). PE response is expressed as % contraction relative to the mean KPSS contraction. Mean ±SEM. F-test. ****p<0.0001 -PVAT vs +PVAT. ††p<0.01, †††p<0.001 -PVAT +treatment vs +PVAT +treatment. ADMA=Asymmetric dimethylarginine; L-Phe=L-Phenylalanine; PE=Phenylephrine; PVAT=Perivascular adipose tissue.

5.4 Discussion

5.4.1 PVAT anticontractile function

PVAT encapsulates blood vessels where it produces a broad panel of vasoactive molecules which profoundly influence vascular tone (Cheng *et al.*, 2018). In health, PVAT typically exerts vasodilatory effect by releasing a variety of substances (adiponectin, angiotensin 1-7, NO, H_2S, H_2O_2) which act within the vascular wall to promote vascular relaxation. However, several PVAT-derived mediators (O_2^-, angiotensin II, endothelin-1) are vasoconstrictive and thus PVAT has dual effects in the vasculature, conferring relaxation as well as contraction (Szasz, Bomfim and Webb, 2013; Nava and Llorens, 2019). To investigate the role of CaSR and ADMA signalling in PVAT regulated vascular function, the study first characterised vascular tone with and without PVAT in C57BL/6 wildtype mice. In denuded vessels, PVAT decreased maximal PE contraction by ~20%, consistent with previous studies which observe an inhibitory effect of PVAT on angiotensin, serotonin and PE-mediated vascular contraction (Löhn *et al.*, 2002). In denuded vessels, previous studies report comparable (18-30%) decreases in PE-mediated contraction when PVAT is retained, but the effect is preserved and in some cases potentiated in vessels with intact endothelium (Gao *et al.*, 2007; Victorio *et al.*, 2016). Interestingly, this effect was not evident in vessel segments with intact endothelium here. In fact, the inhibitory effect of PVAT on PE-mediated contraction was abolished in the presence of endothelium, suggesting that EC function opposes PVAT vasodilation in these experiments. These findings could potentially be attributed to the profound vasodilatory effect of ECs. When compared to control denuded vessels, an intact endothelium decreases maximal PE-mediated contraction by approximately 50%, much greater than the 20% reduction seen with PVAT. Plausibly, endothelial-dependent anticontractile function in vessels at rest masks the effect of PVAT on vascular relaxation in experiments here.

PVAT reduced the effective pEC_{50} for ACh in aortic segments, therein diminishing vasorelaxation. This finding conflicts with the reports of Gao and colleagues who describe the endothelial-dependent vasorelaxant effects exerted by PVAT extensively (Gao *et al.*, 2007; Lee *et al.*, 2009). Though PVAT is broadly considered to be a mediator of endothelial-dependent relaxation, PVAT reduces

endothelial-dependent relaxation in canine coronary arteries. Payne et al. ascribed these effects to protein kinase C ß-mediated alteration of endothelial eNOS at its inhibitory phosphorylation site Thr^{495}, indicating that PVAT can impair endothelial eNOS function and NO-mediated relaxation (Payne *et al.*, 2009). Additionally, recent work in human vascular ECs revealed that $[Ca^{2+}]_i$, eNOS Ser^{1177} phosphorylation and NO generation are increased by raised $[Ca^{2+}]_o$ (Horinouchi *et al.*, 2020). Together, these studies indicate important roles for PVAT as well as prevailing $[Ca^{2+}]_o$ levels in endothelial eNOS regulation and NO signalling. In many standard myography studies, vessels are incubated in PSS containing 2.5mM $[Ca^{2+}]_o$. To assess CaSR-dependent effects on the vasculature, the current study used 1mM $[Ca^{2+}]_o$. Accordingly, low $[Ca^{2+}]_o$ resulting in altered PVAT function and EC eNOS signalling may explain the unexpected effects of PVAT on ACh endothelial dependent relaxation. In vessel preparations, secretion of an unidentified perivascular adipose tissue relaxing factor (PVRF) is increased by $[Ca^{2+}]_o$ (Dubrovska *et al.*, 2004). It then follows that low $[Ca^{2+}]_o$ may act to modify PVAT-EC crosstalk and reduce PVAT-mediated endothelial relaxation. Though low $[Ca^{2+}]_o$ may have influenced the effect of PVAT on ACh responses, this does not explain why PE contraction generated by vessels with intact endothelium were insensitive to PVAT, since PVAT remained ineffectual in these vessels during subsequent experiments in high 2.5mM $[Ca^{2+}]_o$ buffer. Though the underpinning mechanism(s) are unclear, the robust inhibitory effect of PVAT on PE contraction in denuded vessels provided a suitable experimental system for evaluating the role of CaSR and ADMA in vasculature.

5.4.2 CaSR modulation

As an initial step to determine whether CaSR could be relevant in PVAT function, CaSR mRNA expression was assessed in scAT, gAT and PVAT isolated from male C57BL/6 mice. CaSR was robustly expressed all adipose depots studied, including PVAT, implicating CaSR in PVAT biology. To elucidate the significance of CaSR in PVAT, this study first investigated how $[Ca^{2+}]_o$ influences vascular and PVAT function. In intact vessels here, high $[Ca^{2+}]_o$ potentiated vascular contraction. However, earlier studies observe the opposite effect, since $[Ca^{2+}]_o$-mediated CaSR stimulation in aortic and mesenteric vessels with intact endothelium results in vasodilation (Thakore and Vanessa Ho, 2011; Loot *et al.*, 2013; Greenberg, Shi, *et al.*, 2016). Possibly, differences in experimental approach

may explain $[Ca^{2+}]_o$-mediated procontractile effects in endothelium-intact vessels. In work demonstrating $[Ca^{2+}]_o$-induced endothelial-dependent vasodilation, investigators precontracted vessels with PE or methoxamine, then assessed how increasing $[Ca^{2+}]_o$ (1-5mM) affects vascular tone. In contrast, this study incubated vessels in 1mM and 2.5mM $[Ca^{2+}]_o$ buffer conditions, before investigating the dose-dependent effect of PE. Therefore, the discordant results here may arise due to methodological differences. Interestingly, concentration-dependent $[Ca^{2+}]_o$ responses have been previously observed in studies examining CaSR function in rat mesenteric arteries. An initial stimulation with 0.5-2mM $[Ca^{2+}]_o$ causes vasoconstriction, but $[Ca^{2+}]_o$ increases beyond 2mM causes relaxation (Ohanian *et al.*, 2005). In this work, biphasic $[Ca^{2+}]_o$ responses were attributed to CaSR-dependent and independent mechanisms controlling $[Ca^{2+}]_o$ dynamics in the vascular microenvironment; since the CaSR activating aminoglycoside antibiotics consistently produce vasodilation, they propose that shifts in $[Ca^{2+}]_o$ within its physiological range stimulates $[Ca^{2+}]_o$ influx raising $[Ca^{2+}]_o$ and vascular tone, while further localised increases in $[Ca^{2+}]_o$ recruit CaSR and vasodilation, thereby functioning as negative feedback mechanism (Ohanian *et al.*, 2005). Accordingly, $[Ca^{2+}]_o$-mediated vasoconstriction here could be underpinned by a CaSR-independent mechanism. As discussed in the previous section, PVAT inhibits PE contraction in denuded but not intact vessels. Though $[Ca^{2+}]_o$ broadly increased vascular contractility in vessels with intact endothelium, the inhibitory PVAT mechanism remained absent irrespective of $[Ca^{2+}]_o$ treatment. As such, $[Ca^{2+}]_o$ in intact vessels mediates baseline contractility, but not PVAT function. In denuded vessels, vascular contraction was again potentiated by high $[Ca^{2+}]_o$, implicating CaSR in VSMC contraction. These findings align with previous studies which have examined endothelial-independent $[Ca^{2+}]_o$-mediated CaSR activation in mesenteric arteries (Greenberg, Jahan, *et al.*, 2016; Greenberg, Shi, *et al.*, 2016). Interestingly however, the PVAT anticontractile effect was attenuated in high $[Ca^{2+}]_o$ conditions. In addition to regulating VSMC contractility, this observation suggests that $[Ca^{2+}]_o$ concentration is an important determinant in endothelium-independent PVAT inhibitory function (Fig. 5-9).

Figure 5-9

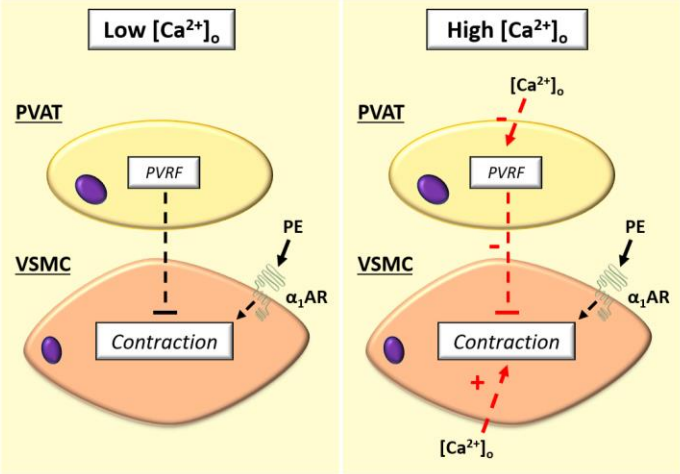

Figure 5-9: The effect of $[Ca^{2+}]_o$ on endothelial-independent PVAT function in denuded mouse aorta.

In conditions of low extracellular calcium ($[Ca^{2+}]_o$), PE exerts a contractile effect on VSMCs, which is opposed by the anticontractile effect of PVAT, presumably mediated by PVRF secretion. Under conditions of high $[Ca^{2+}]_o$, VSMC contractility is potentiated and the inhibitory effect of PVAT is abolished. α_1-AR=alpha-1 adrenoreceptor; PE=Phenylephrine; PVRF=Perivascular adipose tissue relaxing factor; PVAT=Perivascular adipose tissue; VSMC=Vascular smooth muscle cell.

In the context of CaSR pharmacology, synthetic allosteric CaSR agonists (calindol, cinacalcet, NPS R-568) are substances which bind CaSR and enhance its sensitivity to $[Ca^{2+}]_o$ stimulation (Ward and Riccardi, 2012). To test whether CaSR may mediate $[Ca^{2+}]_o$-induced VSMC contractility and attenuation of the PVAT inhibitory mechanism, the next stage of this study determined whether cinacalcet could reproduce the vascular effects of high $[Ca^{2+}]_o$ stimulation. Unlike $[Ca^{2+}]_o$, cinacalcet did not affect vascular contraction in endothelium intact vessels. In contrast, cinacalcet in denuded vessels elicited a distinct procontractile response suggesting that CaSR mediates endothelial-independent (i.e., VSMC) contraction. Despite $[Ca^{2+}]_o$ and cinacalcet imposing similar contractile effects in denuded vessels, $[Ca^{2+}]_o$-mediated attenuation of PVAT function was not replicated with cinacalcet. These observations suggest that CaSR modulates VSMC contraction without influencing PVAT function (Fig. 5-10). In previous work by Greenberg et al. (2016) and as demonstrated earlier here,

$[Ca^{2+}]_o$ stimulation in denuded vessels perpetrates vasoconstriction, linking CaSR activation with VSMC contraction. However, this field lacks uniformity. Vascular myography studies examining the effect of allosteric CaSR agonists in isolated mesenteric and aortic arteries have found that cinacalcet and calindol causes VSMC relaxation (Thakore and Vanessa Ho, 2011; Loot *et al.*, 2013). As such, $[Ca^{2+}]_o$ compared to allosteric activation of CaSR may impose differing effects on vascular function. Interestingly, subsequent studies examining the vascular actions of calcimimetics have shown that calindol and cinacalcet inhibit voltage-gated $[Ca^{2+}]_o$ channels (VGCCs) and reduce cellular $[Ca^{2+}]_o$ permeation. Consequentially, calcimimetics target VGCCs as well as CaSR in the vasculature (Thakore and Vanessa Ho, 2011; Greenberg, Jahan, *et al.*, 2016). Though the vascular responses produced by cinacalcet here were vasoconstrictive rather than dilatory, VGCCs effects cannot be excluded. It is possible that off-target pharmacological effects may have contributed towards the differences observed in $[Ca^{2+}]_o$- and cinacalcet-mediated vascular responses.

Figure 5-10

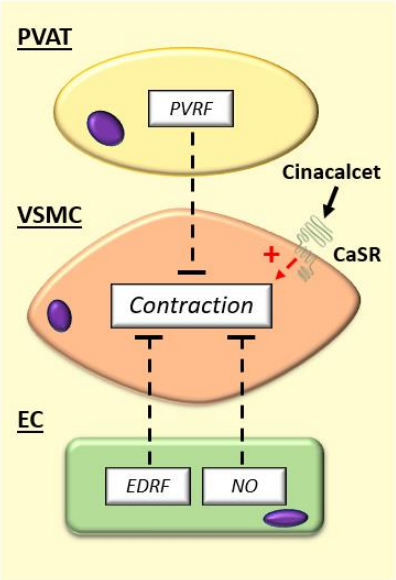

Figure 5-10: CaSR-induced vasoconstriction in mouse aorta.
CaSR activation by cinacalcet causes VSMC contraction. VSMC contraction is constituently opposed by EC and PVAT vasodilatory function. Procontractile cinacalcet effects are abolished when EC or PVAT in vessels is preserved. EC=Endothelial cell; EDRF=Endothelium derived relaxing factor; PVAT=Perivascular adipose tissue; PVRF=Perivascular adipose tissue relaxing factor; VSMC=Vascular smooth muscle cell.

To further explore the role of CaSR in the vasculature, the next step in this study sought to examine the effect of the CaSR inhibitor NPS-2143 on vascular tone and PVAT function. In the presence of 1mM $[Ca^{2+}]_o$, NPS-2143 had no effect on vascular reactivity in endothelium intact or denuded vessels, opposing other work which shows that NPS-2143 potentiates contractility in intact vessels, and reduces contractility in denuded vessels derived from rat (Zhang *et al.*, 2019). In contrast to the Zhang et al. study, the present investigation tested the effect of NPS-2143 in vessels without (acute) CaSR stimulation. Considering that PVAT function was broadly unaltered by NPS-2143 in intact and denuded vessel preparations, it may be that CaSR is not particularly relevant in blood vessels under resting conditions. To overcome the possibility that vascular CaSR was insufficiently activated to observe an inhibitory effect of NPS-2143, prevailing $[Ca^{2+}]_o$ levels were increased to 2.5mM. In these preparations, NPS-2143 tended to decrease PE contractility, though the effect was non-significant (p=0.0995).

As this study previously showed that vascular contractility was greatly enhanced by high $[Ca^{2+}]_o$, these data confirm that $[Ca^{2+}]_o$-induced VSMC responses are predominantly mediated by CaSR-independent mechanisms. Interestingly, NPS-2143 appeared to abolish the inhibitory function of PVAT in the presence of high $[Ca^{2+}]_o$. However, PVAT behaviour in control experiments differed from that observed previously; PVAT decreased PE-mediated contraction in studies examining NPS-2143 effects under 2.5mM $[Ca^{2+}]_o$ conditions (Fig. 5-5c), but the inhibitory PVAT mechanism was blocked by high 2.5mM $[Ca^{2+}]_o$ in a prior data series investigating the effect of $[Ca^{2+}]_o$ in the vasculature (5.3b). In addition to the inconsistency of this response, the PVAT effect size in 2.5mM $[Ca^{2+}]_o$ buffer (10%) was noticeably smaller compared to the mean PVAT effect size observed reliably in 1mM $[Ca^{2+}]_o$ conditions (16%, n=6 data sets; Fig. 5-1d, 5.3b, 5.4b, 5.5b, 5.6 and 5.7). Since anticontractile PVAT effects demonstrate decreased reproducibility and magnitude in higher prevailing $[Ca^{2+}]_o$ concentrations, it remains likely that high $[Ca^{2+}]_o$ acts to abbreviate the anticontractile actions of PVAT. In this light, NPS-2143-mediated attenuation of PVAT function in 2.5mM $[Ca^{2+}]_o$ conditions could be an erroneous result arising from the incomplete inhibition of PVAT function by high 2.5mM $[Ca^{2+}]_o$ in this experimental series. Moreover, these findings are likely to be confounded by the tendency for NPS-2143 to decrease contraction in vessels lacking PVAT, since the anticontractile actions of PVAT would be less pronounced when compared to vessels with decreased baseline vascular tone. Collectively, the CaSR does not appear to be a major regulator of vascular or PVAT function in vessels at rest, or when stimulated with high $[Ca^{2+}]_o$. Overall, these conclusions in addition to those from previous studies are highly contradictory. Possibly, the pharmacological agents used in this study and others do not possess the required selectively to reliably discern the role of CaSR in the vasculature. As such, targeting of CaSR in vascular tissue using a genetic approach would be useful in defining the true role of vascular CaSR.

5.4.3 Amino acids

To assess the importance of allosteric amino acid CaSR sensitisation in vasculature, this study examined how L-Phe affects vascular tone. L-Phe tended to increase contraction in denuded vessels, but the effect was not statistically significant (p=0.0826). PVAT function was similarly unaffected. Interestingly, L-

Phe stimulation of CaSR has been implicated in the development of pulmonary hypertension in rat (Tan *et al.*, 2020). Though vascular reactivity was not directly assessed, subjects demonstrated raised pulmonary blood pressure and vascular resistance, which could be attributed to procontractile effects in the vasculature. Here, the tendency for L-Phe to increase contractility was observed in response to supraphysiological (1mM) L-Phe concentrations, far greater than plasma levels in the fasted (50μM) and fed (100μM) state (Conigrave *et al.*, 2004). Curiously however, studies investigating long-term dietary L-Phe administration in rat report that L-Phe modifies blood pressure despite no change in plasma L-Phe content (Heikal *et al.*, 2018; Tan *et al.*, 2020), suggesting that L-Phe dysregulation can manifest biological effects without a corresponding increase in plasma levels. Though L-Phe treatment is unable to affect circulating measures, levels become raised in the lung (Tan *et al.*, 2020), indicating that systemic L-Phe may be sequestered by tissues leading to accumulation at discrete sites. Therefore, future studies are required to establish typical L-Phe levels in the vasculature and clarify the biological mechanism underpinning L-Phe-mediated vascular effects. The CaSR is sensitised by amino acids, particularly L-Phe (Conigrave, Quinn and Brown, 2000). Though this study and those previous suggest L-Phe as a possible vasoconstrictive factor, the mechanism(s) involved remain outstanding.

To determine whether ADMA may constitute a novel CaSR-active amino acid, this study first sought to confirm the relevance of ADMA in PVAT by assessing transcript levels of ADMA metabolising enzymes DDAH-1 and -2 in addition to NOS, a putative ADMA target (Leone *et al.*, 1992; J. Leiper and Vallance, 2006). mRNA levels of each enzyme were lower in PVAT compared to gAT but were nonetheless robustly detected. The identification of ADMA regulatory mediators suggest that ADMA signalling is likely pertinent in PVAT. Next, the effect of ADMA was examined in the vasculature. ADMA had no effect on aortic vascular reactivity, inconsistent with previous studies which report that ADMA potentiates PE-mediated contraction in aorta (Al-Zobaidy, Craig and Martin, 2010) and acts as independent procontractile factor in carotid (Torondel *et al.*, 2010). However, it is worth noting that these effects are elicited by supraphysiological (>100μM) ADMA levels, whereas more modest concentrations (3μM) were used here. Therefore, although pharmacological ADMA levels are

vasoconstrictive, ADMA does not manifest significant vascular effects in its physiological range. Consistently, the PVAT anticontractile response was unmodified by ADMA, indicating that low ADMA concentrations do not regulate PVAT function. Following studies should assess the vascular effects of ADMA at a range of concentrations to establish a system in which in the dependence of ADMA on CaSR can be evaluated.

5.5 Conclusions

High 2.5mM $[Ca^{2+}]_o$ and cinacalcet increase endothelial-independent VSMC contraction. High $[Ca^{2+}]_o$ blocks PVAT-mediated inhibition of PE contraction, though these effects are not recapitulated by cinacalcet or inhibited by NPS-2143, suggesting that $[Ca^{2+}]_o$-mediated effects are CaSR-independent. L-Phe tends to potentiate VSMC contraction but does not affect the inhibitory PVAT mechanism. CaSR comprises a possible target for L-Phe in the vasculature, though further studies are required to establish whether L-Phe interacts with vascular CaSR. There was no effect of ADMA in the vasculature.

Chapter Six

Generation of a $CaSR^{Ad-/-}$ Mouse

Chapter 6: Generation of a CaSR$^{Ad-/-}$ Mouse

6.1 Introduction

Adipocyte CaSR expression was originally detected in human visceral adipose tissue (Cifuentes, Albala and Rojas, 2005). It has since been described in primary adipocyte lineages, as well as cell lines LS14 and SW872 modelling human adipocytes (He, Zhang, *et al.*, 2011; Cifuentes *et al.*, 2012), indicating that CaSR would likely play a role in adipocyte biology. Indeed, CaSR mediates a variety of adipocyte functions, including lipid loading (Cifuentes and Rojas, 2008; He, Zhang, *et al.*, 2011) and inflammation (Cifuentes et al., 2012). Given that lipid accumulation and proinflammatory signalling are considered detrimental in adipocytes, these studies underpin a growing consensus that dysregulation of adipocyte CaSR invokes dysfunction (Bravo-Sagua *et al.*, 2016). Adipocyte-driven adipose tissue expansion and derangement plays a key role in the development of cardiometabolic disorders, such as obesity and insulin resistance (Oikonomou and Antoniades, 2019). As such, the significance of adipocyte CaSR in adipose health is of considerable interest. At present, our understanding of adipocyte CaSR signalling is mostly derived from its identified roles *in vitro*. To further understand the importance of adipocyte CaSR, its activity and its significance in adipocyte dysregulation, adipocyte CaSR must be studied in intact animals.

Following its initial description in parathyroid tissue (Brown *et al.*, 1993), the functional significance of CaSR *in vivo* has been explored using genetic manipulation of CaSR in murine models. The systemic importance of CaSR was first demonstrated by Ho and colleagues, who generated mice with global CaSR deletion via disruption of CaSR exon 5. CaSR$^{-/-}$ mice demonstrated severe hypercalcemia, malformation of the skeletal structure and premature death. Heterozygous CaSR knockouts thrived in contrast, though serum $[Ca^{2+}]_o$, parathyroid hormone and Mg^{2+} levels remained elevated (Ho *et al.*, 1995). Later studies demonstrated that this model was not a true representation of CaSR deletion, since CaSR exon 5 disruption lead to alternatively spliced CaSR retaining some functionality in keratinocytes and chondrocytes (Oda *et al.*, 2000; Rodriguez *et al.*, 2005). Improved deletion of CaSR was later achieved by targeting exon 7, which produced non-functional CaSR protein while maintaining

exon 1-6 expression. Using this approach, Chang and colleagues determined a definitive role for CaSR in parathyroid tissue (Chang *et al.*, 2008). More recently, CaSR deletion was produced in murine models via excision of exon 3, which encodes the CaSR transmembrane region and $[Ca^{2+}]_o$ binding sites (Toka *et al.*, 2012). Though excision of exon 7 and exon 3 both produce non-functional proteins, exon 3 targeting is arguably superior since CaSR disruption is far more extensive resulting in the disturbance of all Ca^{2+} binding sites (Riccardi, 2012).

The Cre (recombinase)-LoxP gene editing system, first pioneered in mammalian cells (Sauer and Henderson, 1988), has been used to investigate cell-specific gene deletion in a variety of tissues. To achieve targeted manipulation of genes in adipocytes, Eguchi and colleagues inserted Cre into the Adipoq (adiponectin) locus. These mice demonstrated Cre expression selectively in adipose tissues, therein providing an effective mechanism to perform adipocyte-targeted LoxP-mediated gene editing (Eguchi *et al.*, 2011). In a very recent study, the adiponectin Cre-LoxP recombination reagent developed by Eguchi et al. was utilised to achieve targeted deletion of CaSR exon 3 specifically in adipocytes. To examine the effect of adipocyte CaSR on cardiovascular pathogenesis, Sudararaman and colleagues studied adipocyte-specific CaSR deletion in $ApoE^{-/-}$ mice. In this model, CaSR did not influence body weight, adipose cytokine expression or circulating triglyceride levels (Sundararaman *et al.*, 2021), suggesting that CaSR does not play a role in adipose phenotype or function. However, murine ApoE deficiency reduces fat mass, adipocyte size and confers obesity resistance (Kypreos *et al.*, 2018). As genetic deletion of adipocyte CaSR was investigated in atherosclerosis-prone $ApoE^{-/-}$ mice, the phenotype of adipocyte CaSR deletion alone is unclear.

To appraise the role of adipocyte CaSR *in vivo*, this study generated an adipocyte-specific CaSR knockout mouse ($CaSR^{Ad-/-}$), based on the CaSR flox and Adipoq-Cre murine models developed by Toka et al. (2012) and Eguchi et al. (2011). The beginning of this chapter validates adipocyte-specific CaSR deletion in this model. In preadipocyte and adipocyte cell lines, CaSR activation stimulates expression of critical adipocyte growth and biology mediators, such as peroxisome proliferator-activated receptor gamma (PPARγ) (He *et al.*, 2012; Villarroel *et al.*, 2013). PPARγ controls a variety of key adipocyte processes, such as lipogenesis, differentiation, lipid accumulation

and adipokine secretion (Rosen, Eguchi and Xu, 2009). Therefore, CaSR may act to regulate adipocyte phenotype and thus adipose biology in an intact system. Indeed, functional studies *in vitro* suggest that CaSR stimulates adipocyte lipid loading (Cifuentes and Rojas, 2008; He, Zhang, *et al.*, 2011), suggesting that CaSR deletion *in vivo* could influence systemic lipid handling. More recently, the role of CaSR has been investigated in vascular tissue. This work has established that vascular function can be controlled by endothelial cell (EC) and vascular smooth muscle cell (VSMC)-specific CaSR, possibly regulating antagonistic effects (Greenberg et al., 2016; Schepelmann et al., 2016). Adipose phenotype is a known determinant of vascular function (Oikonomou and Antoniades, 2019). Plausibly, adipocyte-specific CaSR could also act to augment vascular function, though this has not been investigated to date. To examine how adipocyte CaSR influences adipocyte phenotype, function and vascular reactivity, this study performed a phenotypic evaluation of $CaSR^{Ad-/-}$ mice. Sex-dependent differences in cardiometabolic health are mediated by adipose tissue (AT) biology and locale (Kwok, Lam and Xu, 2016), therefore $CaSR^{Ad-/-}$ mice of both sexes were examined.

6.2 Aims

1. To demonstrate and characterise adipocyte-specific CaSR deletion in $CaSR^{Ad-/-}$ mice.
2. To determine if adipocyte-specific CaSR deletion influences body fat mass and adipocyte phenotype in male and female mice.
3. To determine whether adipocyte-specific CaSR deletion influences systemic lipid and adipokine balance.
4. To determine whether adipocyte-specific CaSR deletion influences vascular function and haemodynamic homeostasis.

6.3 Results

6.3.1 CaSR$^{Ad-/-}$ Mouse genotyping

CaSR mice were obtained from The Jackson Laboratory (stock #030647, Casr^{tm1Mrpk}). Genomic DNA PCR analysis of ear clips was used to assess the status of CaSR alleles. CaSR wildtype (wt; lane 1) and CaSR homozygous floxed mice (hom; lane 3) produced single bands migrating at 239bp and 206bp, respectively. CaSR heterozygous floxed mice (het; lane 2) produced two bands, migrating at 239bp and 206bp (Fig. 6-1a).

CaSR hom mice were crossed with transgenic mice expressing CRE recombinase operating under the adiponectin promotor. Cre was maintained on a heterozygous background to reduce off-target effects. CaSR hom (Cre-) mice were mated with CaSR hom/Cre+ mice to produce CaSR hom/Cre- and CaSR hom/Cre+ offspring. Through genomic DNA PCR analysis, the presence of Cre was ascertained via identification of a single band migrating at 720bp (lane 2) (Fig. 6-1b).

In this study, CaSR hom/Cre+ (CaSR$^{Ad-/-}$) mice were used to examine the effects of adipocyte-specific CaSR deletion. CaSR hom/Cre- (CaSR$^{fl/fl}$) mice were taken as controls.

Figure 6-1

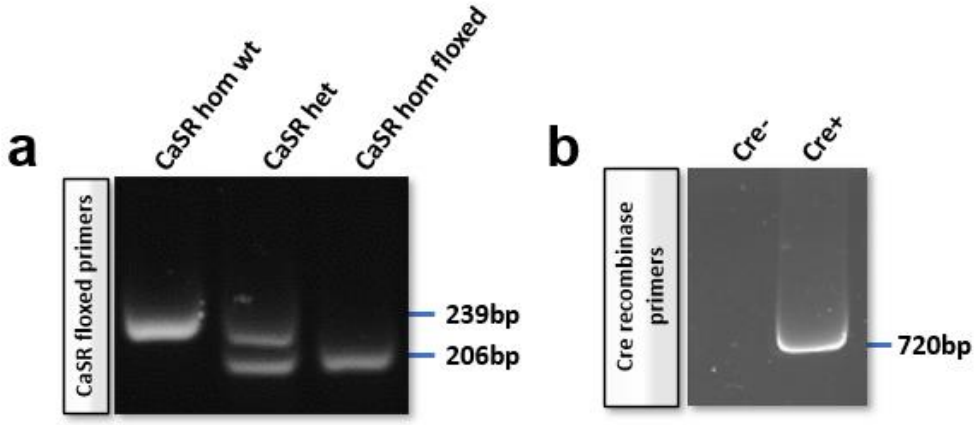

Figure 6-1: PCR analysis of CaSR floxed alleles and Cre recombinase expression in mice.

(a) Genomic DNA PCR analysis validates expression of homozygous (hom) CaSR floxed alleles by the appearance of a single band migrating at 206bp. Homozygous CaSR wildtype (wt) alleles migrate at 239bp. Mice which are heterozygous (het) carry both floxed and wt alleles, confirmed by the appearance of two bands migrating at 206bp and 239bps. **(b)** Genomic DNA PCR validates Cre recombinase expression via the appearance of a single band migrating at 720bp.

6.3.2 CaSR exon 3 and neomycin cassette expression

To demonstrate successful excision of CaSR exon 3 and genomic recombination of CaSR exon 2-exon 4, PCR primers were designed to target CaSR exon 2 and the post-neomycin cassette region (CaSR F-postneo R; Fig. 6-2a) (Toka *et al.*, 2012). CaSR hom/Cre- (lane 2) and CaSR het/Cre- mice (lane 4) demonstrated no amplification of CaSR-postneo products in subcutaneous or gonadal adipocyte homogenate. However, CaSR hom/Cre+ (lane 3) and CaSR het/Cre+ mice (lane 5) produced CaSR-postneo PCR products from adipocyte homogenate, identified via a single band migrating at ~350bp. To assess to specificity of CaSR deletion, CaSR-postneo PCR products were also characterised in non-targeted tissue. CaSR-postneo PCR amplification was absent in the lung tissue of all mice (Fig. 6-2b).

To further interrogate adipocyte-specific CaSR deletion in floxed mice, generation of CaSR-postneo PCR products were examined in perivascular adipose tissue (PVAT). Both CaSR hom/Cre+ and CaSR het/Cre+ demonstrated single bands migrating at ~350bp. These bands were absent in mice lacking Cre (Fig. 6-3a).

Recent reports indicate that adiponectin is expressed by bone marrow mesenchymal stem cells (BMSCs) (Mukohira *et al.*, 2019). It was therefore important to establish whether CaSR deletion was evident in other cell types where Cre recombinase expression could be driven under an adiponectin promotor. Neither CaSR hom/Cre- and CaSR hom/Cre+ mice demonstrated CaSR-postneo amplification in isolated BMSCs (Fig. 6-3b). Isolation of BMSCs was performed by Miss Noha Alshuwayer (University of Glasgow).

Figure 6-2

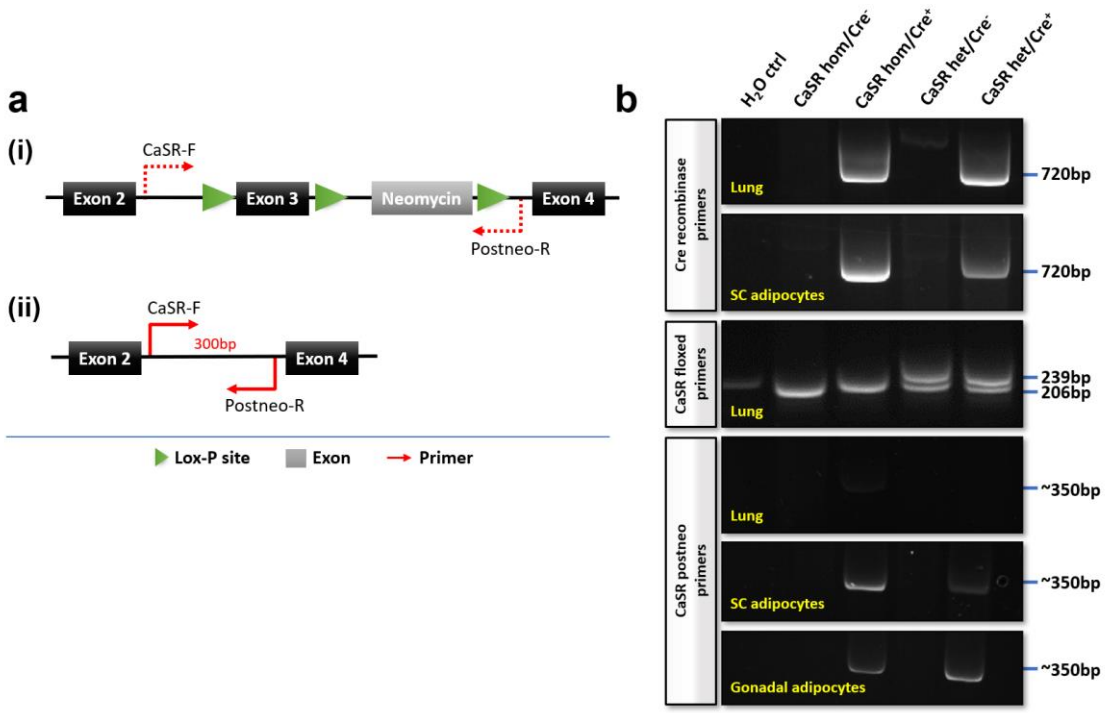

Figure 6-2: PCR analysis of the CaSR floxed construct in adipose.
(a, i) CaSR hom floxed mice possess a construct targeted towards CaSR exon 3 deletion. The CaSR hom floxed construct consists of CaSR exon 2, exon 3, a neomycin resistance gene and CaSR exon 4. Primers targeting exon 3 (CaSR-F) and the post-neomycin cassette region (postneo-R) are used to demonstrate excision of CaSR exon 3. Exon 3 is intact in CaSR hom/Cre- mice; CaSR-postneo PCR products are absent due to large amplicon size. **(a, ii)** Excision of exon 3 and the neomycin cassette region is predicted in CaSR hom/Cre+ mice. CaSR-postneo PCR products are expected due to short (350bp) amplicon size. **(b)** CaSR-postneo PCR confirms excision of CaSR exon 3 and the neomycin cassette via a single band migrating at ~350bp. CaSR-F/Postneo-R products are present in adipocyte homogenates of Cre+ mice only. Cre expressing CaSR hom and het mice show CaSR-postneo amplification in subcutaneous (SC) and gonadal adipocytes, but not lung tissue. CaSR hom and CaSR het lacking Cre demonstrate no amplification of CaSR-postneo products in SC adipocytes, gonadal adipocytes or lung tissue. Figure 2a adapted from Toka *et al.* (2012).

Figure 6-3

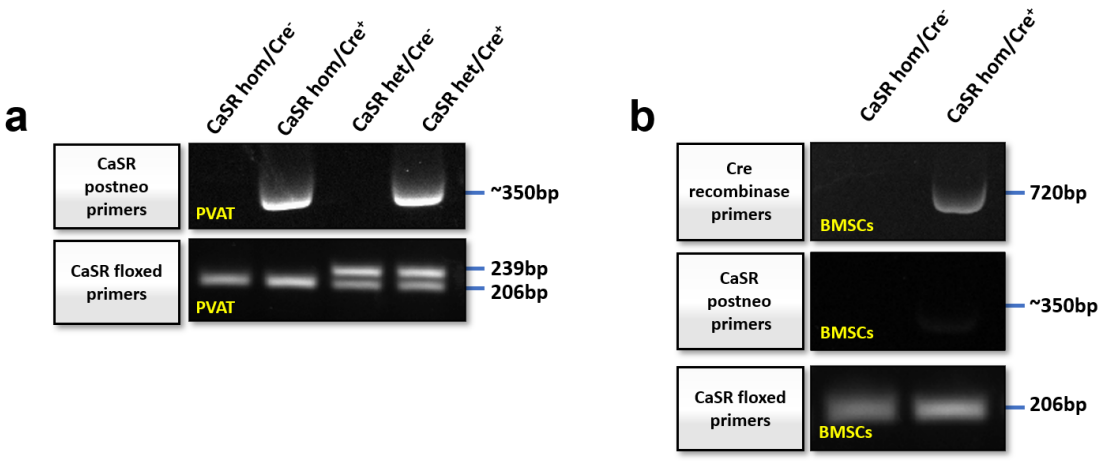

Figure 6-3: PCR analysis of the CaSR floxed construct in PVAT and BMSCs. **(a)** Cre expressing CaSR hom and het mice show CaSR-postneo amplification in perivascular adipose tissue (PVAT) homogenate, confirming recombination of CaSR exon2-exon 4. **(b)** CaSR hom floxed mice do not demonstrate CaSR-postneo amplification in isolated bone marrow derived stem cells (BMSCs) irrespective of Cre recombinase expression.

6.3.3 Adipocyte-specific CaSR deletion

To investigate adipocyte-specific CaSR deletion in $CaSR^{Ad-/-}$ mice, CaSR immunofluorescent staining was first developed in gonadal adipose tissue (gAT) isolated from C57BL/6 control mice. The specificity of mouse anti-CaSR antibody staining was previously confirmed in chapter 3 using DX-induced CaSR overexpressing HEK293 cells. Visualisation of C57BL/6 gAT revealed positive staining for CaSR. This signal was not evident following primary antibody only and secondary antibody only control staining, illustrating a negligible level of autofluorescence and non-specific secondary antibody interactions in this system (Fig. 6-4).

To demonstrate adipocyte-specific CaSR deletion, CaSR protein expression was assessed in gAT isolated from mixed sex $CaSR^{fl/fl}$ and $CaSR^{Ad-/-}$ mice. Adipose tissue contains multiple cell types, so gAT was counter-stained with the adipocyte-specific marker perilipin-1 (PLN-1); CaSR staining intensity was assessed in PLN-1 positive cells. Positive CaSR labelling in $CaSR^{Ad-/-}$ adipocytes (111.6±11.7) tended to be decreased compared to $CaSR^{fl/fl}$ controls, though the difference did not reach statistical significance (160.5±22.9, p=0.0760; Fig. 6-

5a, b). Aiming to evaluate whether CaSR is reduced at the mRNA level, CaSR transcript was also examined in isolated gAT adipocytes. CaSR mRNA expression in $CaSR^{Ad-/-}$ adipocytes (0.4±0.1-fold) was significantly reduced compared to $CaSR^{fl/fl}$ controls (1.2±0.3-fold, p=0.0208; Fig. 6-5c), demonstrating deletion of CaSR in $CaSR^{Ad-/-}$ adipocytes. This qPCR experiment was performed by Dr. Laura Dowsett (University of Glasgow).

Figure 6-4

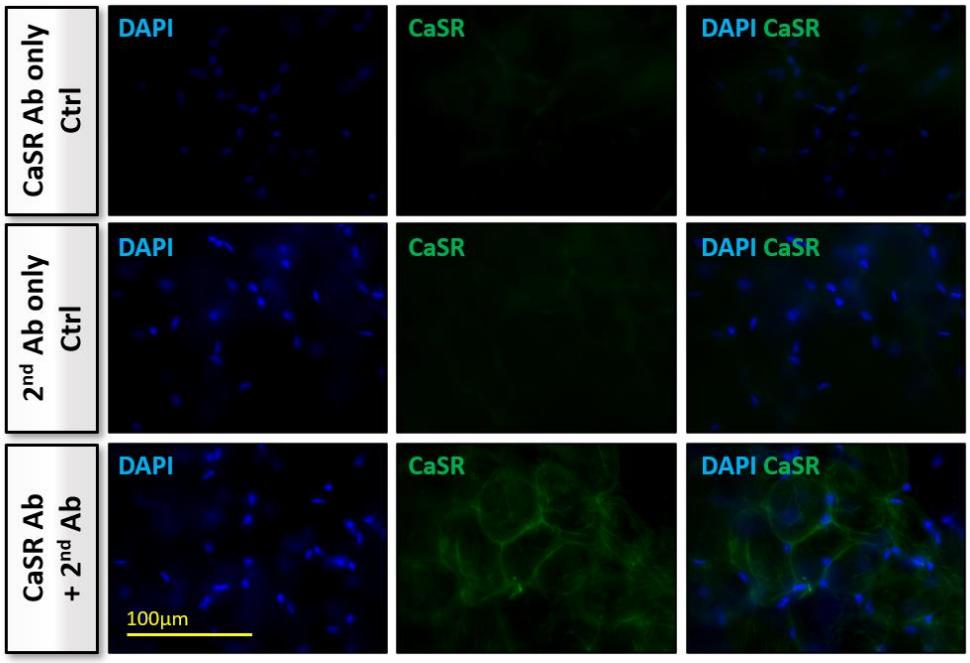

Figure 6-4: CaSR is expressed in murine adipose tissue.

Gonadal adipose tissue isolated from C57BL/6 mice shows positive CaSR staining following incubation with CaSR primary and anti-mouse secondary antibodies. Positive staining was not apparent in the absence of primary or secondary antibodies. Magnification 40X. Scale bar=100µm.

Figure 6-5

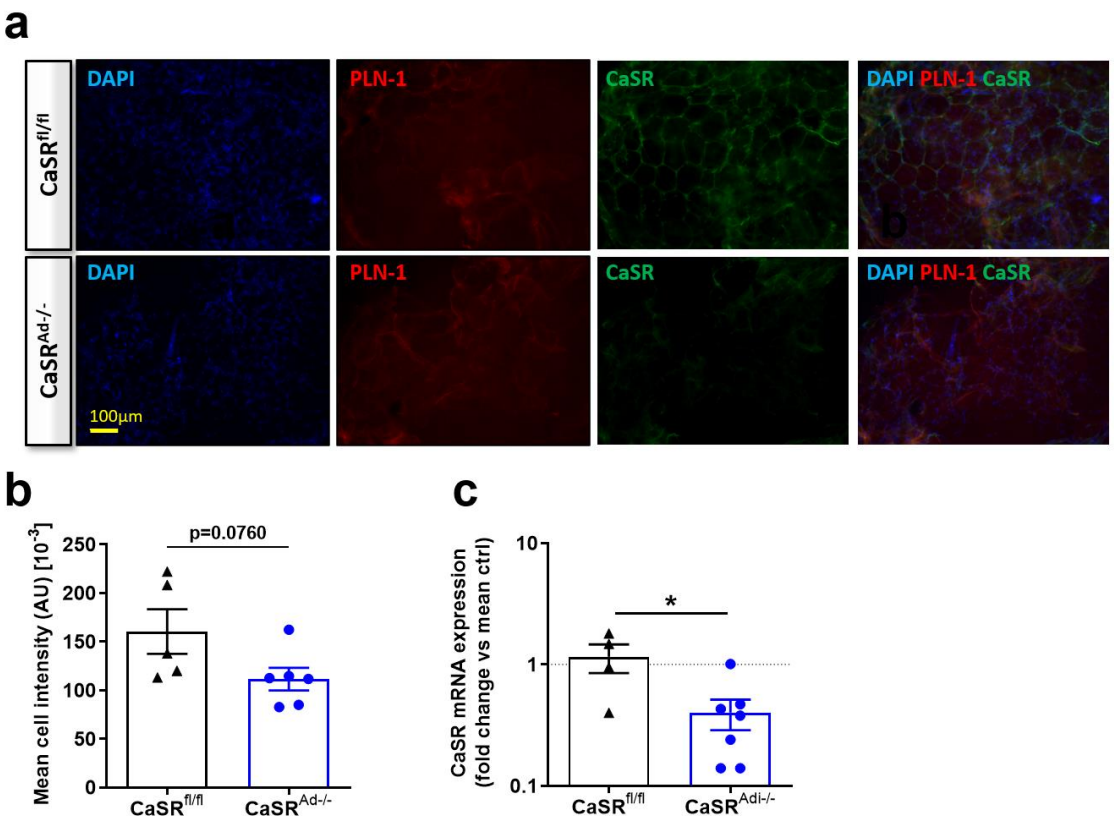

Figure 6-5: Adipocyte-specific CaSR deletion in CaSR$^{Ad-/-}$ mice.
(a-b) Adipocyte-specific CaSR staining tends to be reduced in CaSR$^{Ad-/-}$ compared to control CaSR$^{fl/fl}$ mice. **(c)** CaSR mRNA levels are decreased in CaSR$^{Ad-/-}$ versus CaSR$^{fl/fl}$ adipocytes. PLN-1 was used as an adipocyte-specific marker. Mean±SEM. Unpaired t-test (b,c). *p<0.05. Magnification 10X. Scale bar=100µm. CaSR=Calcium-sensing receptor; gAT=Gonadal adipose tissue; PLN-1=Perilipin-1.

6.3.4 CaSR$^{Ad-/-}$ breeding and viability

To assess whether adipocyte-specific CaSR deletion influences offspring viability, sex, genotype distribution and mortality were examined in CaSR$^{fl/fl}$ x CaSR$^{Ad-/-}$ matings.

Unexpectedly, CaSR$^{fl/fl}$ x CaSR$^{Ad-/-}$ matings produced greater numbers of female pups (60%) relative to male pups (40%, n=106, p=0.041; Fig. 6-6a). To establish whether genotype influenced this skewed distribution, this study compared the number of CaSR$^{fl/fl}$ relative to CaSR$^{Ad-/-}$ genotype occurrences in female and male offspring. Despite the birth of more female pups, the genotype

distribution of offspring was unchanged. Among female pups, the number of $CaSR^{fl/fl}$ mice (52%) and $CaSR^{Ad-/-}$ counterparts (48%) were consistent with the expected proportion of 0.5 (n=27, $p>0.05$; Fig. 6-6c). In male offspring, again the number of $CaSR^{fl/fl}$ mice (43%) and $CaSR^{Ad-/-}$ mice (57%) aligned with an expected 0.5 genotype distribution (n=26, $p>0.05$; Fig. 6-6b).

Next, offspring mortality (stillborn and postnatal deaths) was assessed and grouped according to whether Cre was expressed by father ($CaSR^{Ad-/-}$ father) or mother ($CaSR^{Ad-/-}$ mother). Mortality was not influenced by which parent expressed Cre. Matings with $CaSR^{Ad-/-}$ fathers resulted in 20% offspring mortality (n=49). In comparison, matings with $CaSR^{Ad-/-}$ mothers showed 25% offspring mortality (n=88), comparable to $CaSR^{Ad-/-}$ fathers (p=0.534).

Figure 6-6

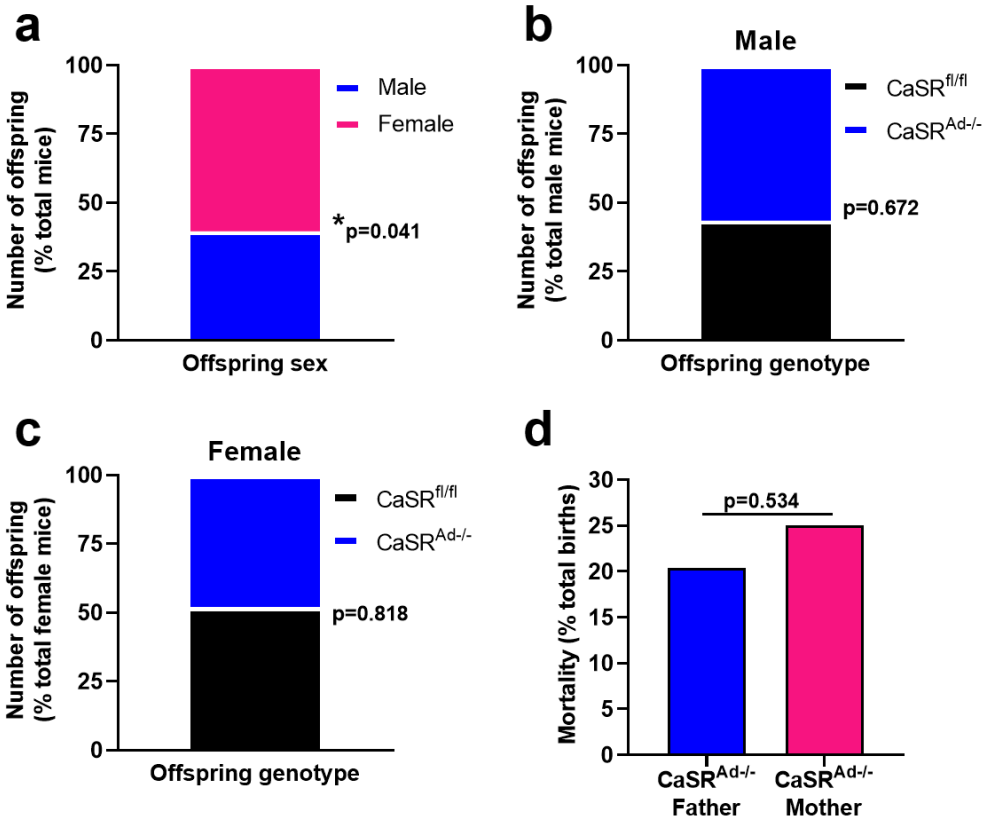

Figure 6-6: CaSR$^{Ad-/-}$ offspring genotype and viability.

(a) CaSR$^{Ad-/-}$ mice produce a greater number of female than male offspring (n=106). **(b)** The distribution of CaSR$^{fl/fl}$/CaSR$^{Ad-/-}$ genotypes produced by CaSR hom floxed matings was comparable in male (n=26) **(c)** and female mice (n=27). **(d)** Offspring mortality arising from CaSR hom floxed matings was comparable irrespective of whether Cre was expressed by the male (CaSR$^{Ad-/-}$ father, n=49) or female (CaSR$^{Ad-/-}$ mother, n=88) parent. Test of proportions, 0.5 (a-c). Test of two proportions (d). *p<0.05.

6.3.5 Systemic phenotype

To assess whether adipocyte-specific deletion leads to prominent differences in systemic cardiovascular phenotype, kidney and heart mass were measured in CaSR$^{fl/fl}$ and CaSR$^{Ad-/-}$ mice aged 18-22 weeks. Male CaSR$^{fl/fl}$ and CaSR$^{Ad-/-}$ mice showed no difference in kidney weight (p>0.05; Fig. 6-7a) or heart weight (p>0.05; Fig. 6-7b). Similarly, female CaSR$^{fl/fl}$ and CaSR$^{Ad-/-}$ mice showed no change in kidney weight (p>0.05; Fig. 6-7c) or heart weight (p>0.05; Fig. 6-7d).

Figure 6-7

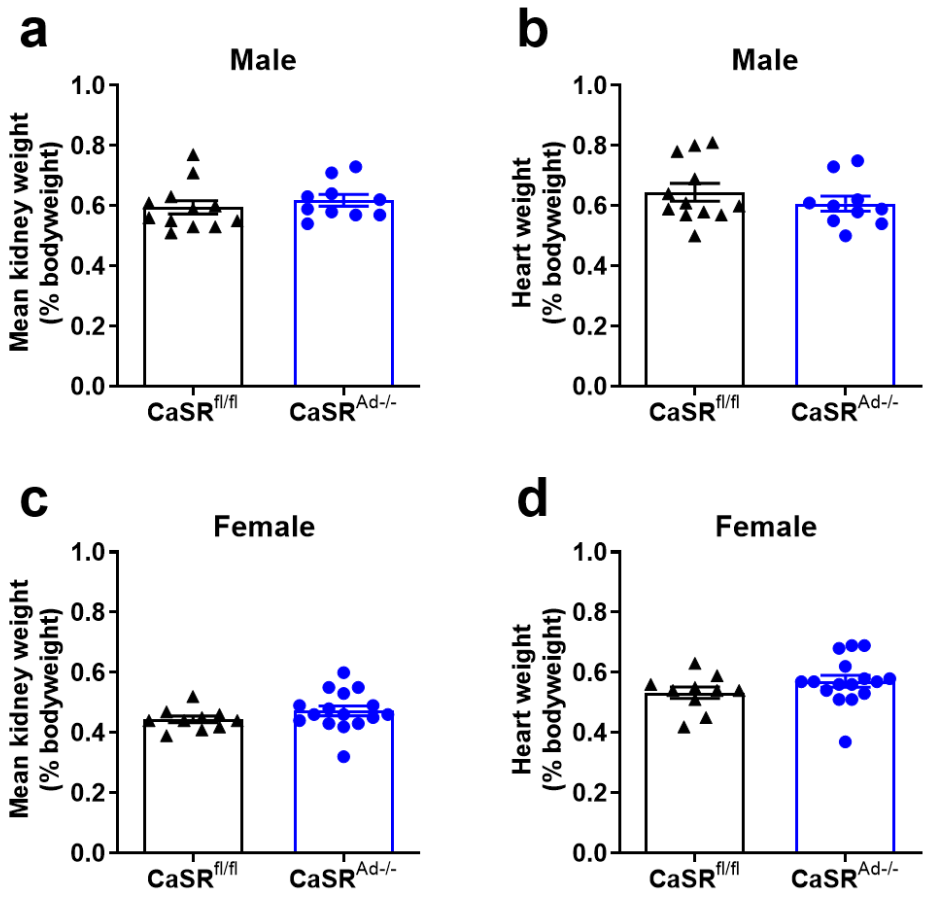

Figure 6-7: Heart and kidney mass in CaSR$^{Ad-/-}$ mice.

(a) Male CaSR$^{fl/fl}$ and CaSR$^{Ad-/-}$ mice (18-22 weeks) showed no difference in kidney **(b)** or heart mass. **(c)** Female CaSR$^{fl/fl}$ and CaSR$^{Ad-/-}$ mice showed no difference at cull in kidney weight **(d)** or heart weight. Mean±SEM. Unpaired t-test (a-d).

6.3.6 Body composition

Adipocyte CaSR signalling is linked with adipocyte dysregulation *in vitro* (Bravo-Sagua *et al.*, 2016). To establish the importance of adipocyte CaSR signalling *in vivo*, the effect of adipocyte-specific CaSR deletion on body weight and fat pad mass was assessed in CaSR$^{Ad-/-}$ mice. Both male and female mice were weighed from 5 until 18 weeks of age. Fat pad mass measurements were made at 18-22 weeks of age.

6.3.6.1 Male body composition

At the beginning of the study, male $CaSR^{fl/fl}$ mice weighed 17.6±0.5g and $CaSR^{Ad-/-}$ 17.7±0.4g. Male $CaSR^{fl/fl}$ and $CaSR^{Ad-/-}$ mice, which achieved final weights of 29.5±0.3g and 29.8±0.4g respectively, did not show differing body weight across time ($p>0.05$; Fig. 6-8a). To control for weight differences established before the study onset, mouse weight was assessed relative to their initial 5-week weight. As with body weight, % growth from initial 5-week weight in $CaSR^{fl/fl}$ mice (169.6±5.4%) was unchanged in $CaSR^{Ad-/-}$ mice (169.0±4.5%, $p>0.05$; Fig. 6-8b).

When fat pad mass was studied, male $CaSR^{fl/fl}$ and $CaSR^{Ad-/-}$ mice showed no difference in adipose tissue mass, as both subcutaneous adipose tissue (scAT) weight and gAT weight was comparable ($p>0.05$; Fig. 6-8c). Fat pad weight remained comparable between groups when normalised for body weight ($p>0.05$; Fig. 6-8d). To assess whether adipocyte-specific deletion could impact body size, tibia length was also assessed. Tibia length in male $CaSR^{fl/fl}$ mice (19.5± 0.3mm) relative to $CaSR^{Ad-/-}$ mice (20.7± 0.6mm) was also comparable ($p>0.05$; Fig. 6-8e).

Figure 6-8

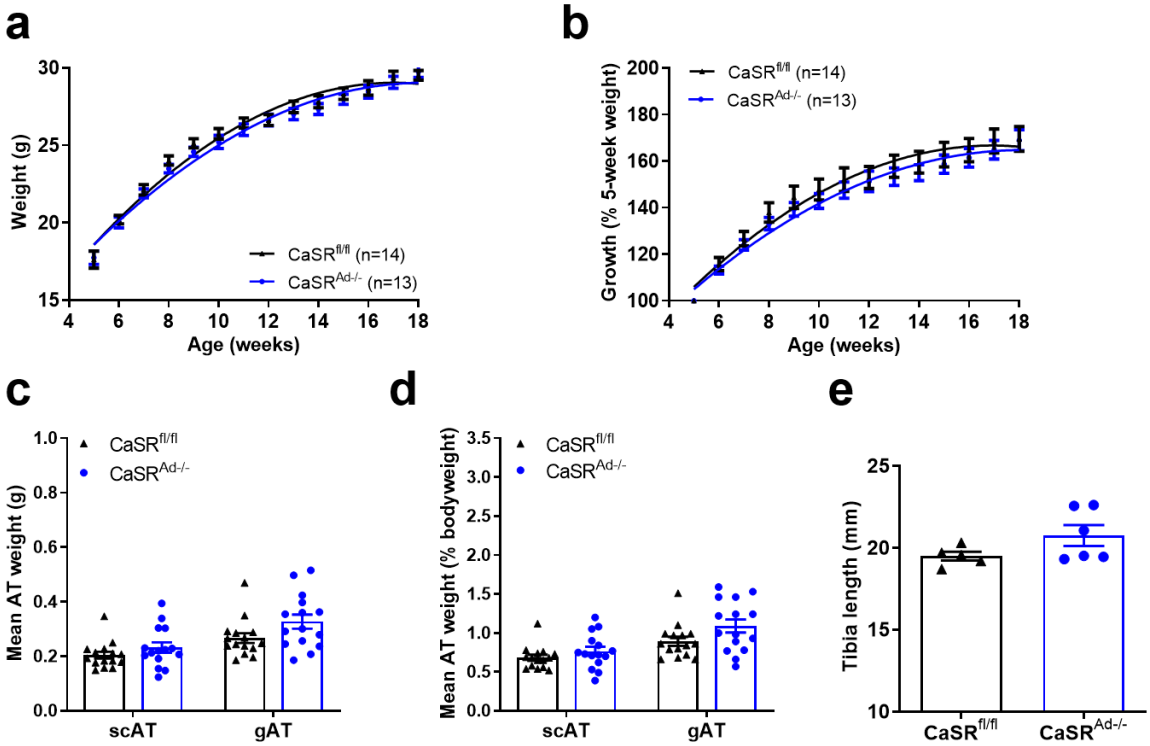

Figure 6-8: Body weight and fat pad mass in male CaSR$^{Ad-/-}$ mice

(a) Body weight across time is comparable between male CaSR$^{fl/fl}$ and CaSR$^{Ad-/-}$ mice. **(b)** % growth from 5-week weight across time is comparable between male CaSR$^{fl/fl}$ and CaSR$^{Ad-/-}$ mice. **(c)** scAT and gAT weight is unchanged between male CaSR$^{fl/fl}$ and CaSR$^{Ad-/-}$ mice. **(d)** Bodyweight normalised scAT and gAT weight is unchanged between male CaSR$^{fl/fl}$ and CaSR$^{Ad-/-}$ mice. **(e)** Tibia length is similar between male CaSR$^{fl/fl}$ and CaSR$^{Ad-/-}$ mice. Mean±SEM. F-test (a,b). Unpaired t-test (c-e). scAT=Subcutaneous adipose tissue; gAT=Gonadal adipose tissue.

6.3.6.2. Female body composition

In females, body weight in CaSR$^{fl/fl}$ and CaSR$^{Ad-/-}$ mice was determined as 16.1±0.3g and 15.2±0.4g respectively at the study outset, reaching a final weight of 23.9±0.4g in CaSR$^{fl/fl}$ mice and 22.9±0.5g in CaSR$^{Ad-/-}$ mice. Comparison of body weight across time revealed a small but consistent reduction in CaSR$^{Ad-/-}$ when compared to CaSR$^{fl/fl}$ controls ($p<0.0001$; Fig. 6-9a). Though body weight differed between groups, % growth from initial 5-week weight was unaltered in female CaSR$^{fl/fl}$ mice (148.9±3.2%) relative to CaSR$^{Ad-/-}$ mice (151.7±3.5%, $p>0.05$; Fig. 6-9b).

Although body weight was reduced in female $CaSR^{Ad-/-}$ mice, this did not coincide with reduced fat pad mass. scAT mass in $CaSR^{fl/fl}$ mice (0.361±0.022g) was unchanged compared to $CaSR^{Ad-/-}$ mice (0.333±0.022g, $p>0.05$; Fig. 6-9c). Similarly, $CaSR^{fl/fl}$ gAT weight (0.388±0.019g) was comparable to $CaSR^{Ad-/-}$ gAT weight (0.346±0.026g, $p>0.05$; Fig. 6-9c). Both scAT and gAT remained similar between groups when normalised against body weight ($p>0.05$; Fig. 6-9d). Though female $CaSR^{Ad-/-}$ mice showed reduced body weight with no significant change in fat pad mass, the relative size of $CaSR^{fl/fl}$ and $CaSR^{Ad-/-}$ mice was unchanged; $CaSR^{fl/fl}$ tibia length (19.0±0.1mm) was similar to $CaSR^{Ad-/-}$ tibia length (19.9±0.5mm, $p>0.05$; Fig. 6-9e).

Figure 6-9

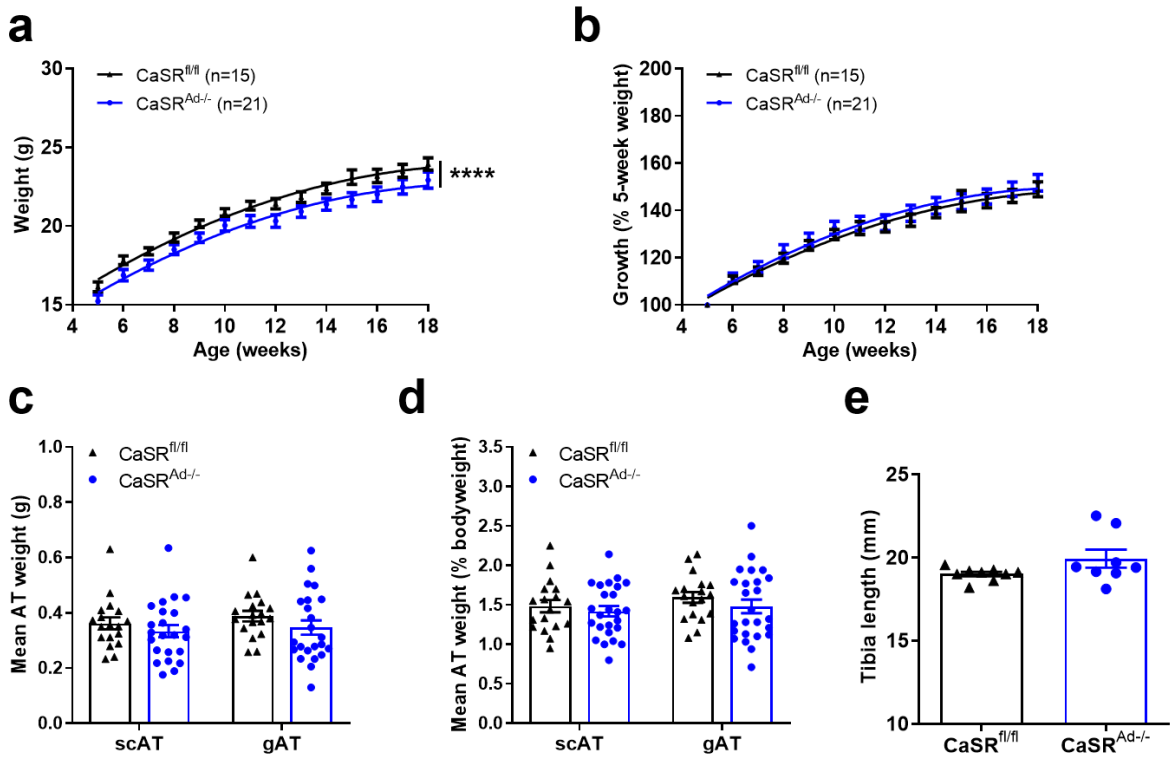

Figure 6-9: Body weight is decreased in female CaSR$^{Ad-/-}$ mice.

(a) Body weight across time is decreased in female CaSR$^{Ad-/-}$ mice compared to CaSR$^{fl/fl}$ controls. **(b)** % growth from 5-week weight across time is comparable between female CaSR$^{fl/fl}$ and CaSR$^{Ad-/-}$ mice. **(c)** scAT and gAT weight is unchanged between female CaSR$^{fl/fl}$ and CaSR$^{Ad-/-}$ mice. **(d)** Bodyweight normalised scAT and gAT weight is unchanged between female CaSR$^{fl/fl}$ and CaSR$^{Ad-/-}$ mice. **(e)** Tibia length is similar between female CaSR$^{fl/fl}$ and CaSR$^{Ad-/-}$ mice. Mean±SEM. F-test (a,b), Unpaired t-test (c-e). ****p=0.0001. scAT=Subcutaneous adipose tissue; gAT=Gonadal adipose tissue.

6.3.6.3. Baseline body composition in CaSR$^{fl/fl}$ mice

Body weight was decreased in female CaSR$^{Ad-/-}$ mice, but unaltered in male CaSR$^{Ad-/-}$ mice. To understand how differences in male and female mice at baseline may contribute to the sex-dependent effect of adipocyte-specific CaSR deletion, body weight and fat pad mass was compared in male and female CaSR$^{fl/fl}$ control mice. Relative to males, female CaSR$^{fl/fl}$ mice demonstrated reduced absolute body weight and body weight growth over time. At the study outset, male CaSR$^{fl/fl}$ mice weighed 17.6±0.5g and reached a final weight of 29.5±0.3g. The initial weight of female CaSR$^{fl/fl}$ mice was 16.1±0.3g and reached

23.9±0.4g, significantly less than male counterparts ($p<0.0001$; Fig. 6-10a). Similarly, % growth from initial 5-week weight was increased across time in male $CaSR^{fl/fl}$ mice (169.6±5.4%) compared to females (148.9±3.2%, $p<0.0001$; Fig. 6-10b).

Body weight and body weight growth were increased in male compared to female $CaSR^{fl/fl}$ mice. To establish whether decreased weight in female $CaSR^{fl/fl}$ mice correlated with lower AT weights, fat pad mass was assessed. Interestingly, fat pad mass in female $CaSR^{fl/fl}$ mice was significantly greater than males, despite decreased body weights in female mice. Compared to scAT isolated from male $CaSR^{fl/fl}$ mice (0.204±0.013g), the mass of female $CaSR^{fl/fl}$ scAT was significantly increased (0.361±0.022g, $p<0.0001$; Fig. 6-10c). A similar trend was observed with gAT mass, which was increased in female $CaSR^{fl/fl}$ mice (0.388±0.019g) relative to male $CaSR^{fl/fl}$ mice (0.267±0.018g, $p=0.0002$; Fig. 6-10c). When these data were normalised for body weight, the trend for scAT and gAT to be increased in females relative to males was conserved ($p<0.0001$; Fig. 6-10d).

As body weight differed significantly between male and female $CaSR^{fl/fl}$ mice, tibia length was assessed to evaluate whether body weight varied as a function of body size. Though tibia length tended to be greater in male $CaSR^{fl/fl}$ mice (19.5±0.3mm) compared to female $CaSR^{fl/fl}$ mice (19.0±0.1mm), the difference was not statistically significant ($p=0.0855$; Fig. 6-10e).

Figure 6-10

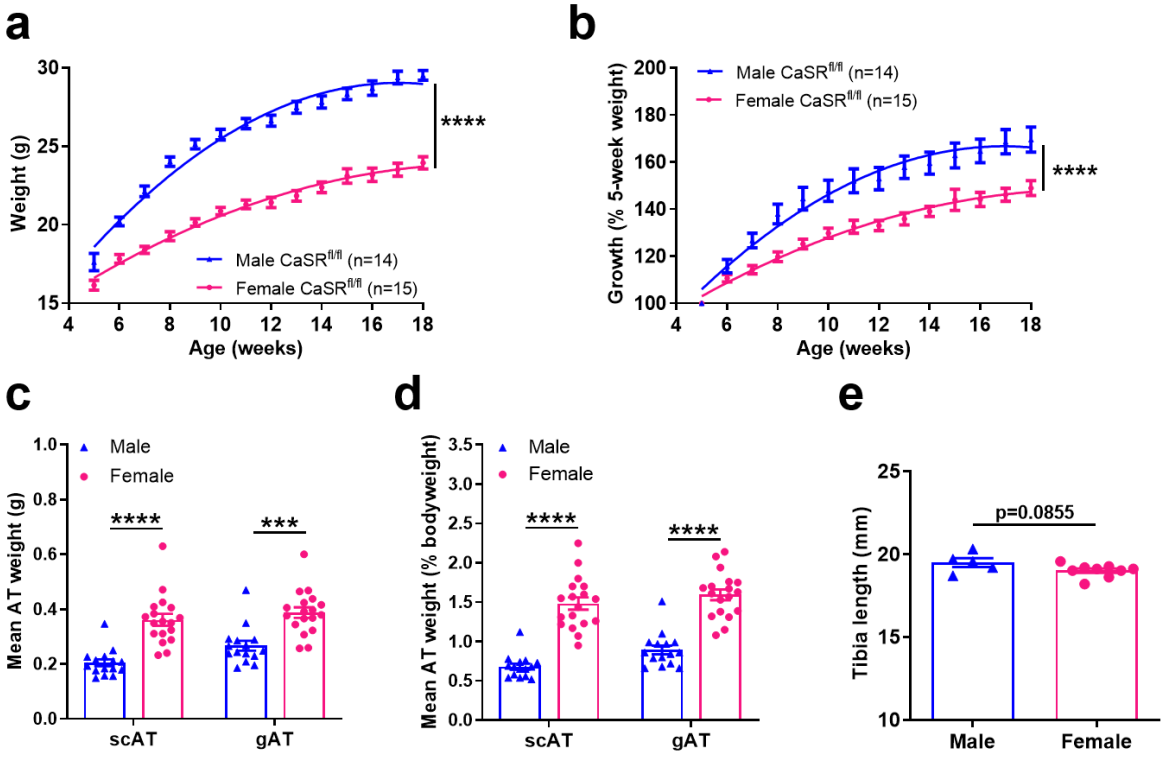

Figure 6-10: Body weight is decreased and fat pad mass is increased in female versus male CaSR$^{fl/fl}$ mice.

(a) Body weight across time in male CaSR$^{fl/fl}$ mice is greater compared to females. **(b)** % growth from 5-week weight across time is greater in male CaSR$^{fl/fl}$ mice than females. **(c)** scAT and gAT weight is greater in male CaSR$^{fl/fl}$ compared to females. **(d)** scAT and gAT weight normalised to total bodyweight is greater in male CaSR$^{fl/fl}$ compared to females. **(e)** Tibia length is comparable in male CaSR$^{fl/fl}$ mice when compared to females. Mean±SEM. F-test (a,b), Unpaired t-test (c-e). *p<0.05, **p<0.01, ***p<0.001, ****p<0.0001. scAT=Subcutaneous adipose tissue; gAT=Gonadal adipose tissue.

6.3.7 Adipocyte size

In chapter 4, 3T3-L1 cell size was increased following stimulation with pharmacological CaSR agonists. Female CaSR$^{Ad-/-}$ mice have reduced body weight compared to CaSR$^{fl/fl}$ controls with no change in tibia length. To evaluate whether body weight differences in CaSR$^{Ad-/-}$ mice are linked with altered adipocyte phenotype *in vivo*, CaSR$^{fl/fl}$ and CaSR$^{Ad-/-}$ adipocytes were examined in gAT using H&E staining. Tissue embedding was carried out by Nicola Britton

(University of Glasgow) and staining was performed by Lynn Stevenson (Histology service, University of Glasgow).

6.3.7.1. Male adipocyte size

In males, mean adipocyte size in $CaSR^{fl/fl}$ gAT was 1609±143μm^2. Mean adipocyte size in $CaSR^{Ad-/-}$ gAT was 1758±99μm^2, comparable to $CaSR^{fl/fl}$ controls ($p>0.05$; Fig. 6-11a, d). In line with unchanged adipocyte size, male $CaSR^{fl/fl}$ and $CaSR^{Ad-/-}$ mice did not differ in adipocyte size frequency ($p>0.05$; Fig. 6-11b) or mean cell number ($p>0.05$; Fig. 6-11c).

Figure 6.11

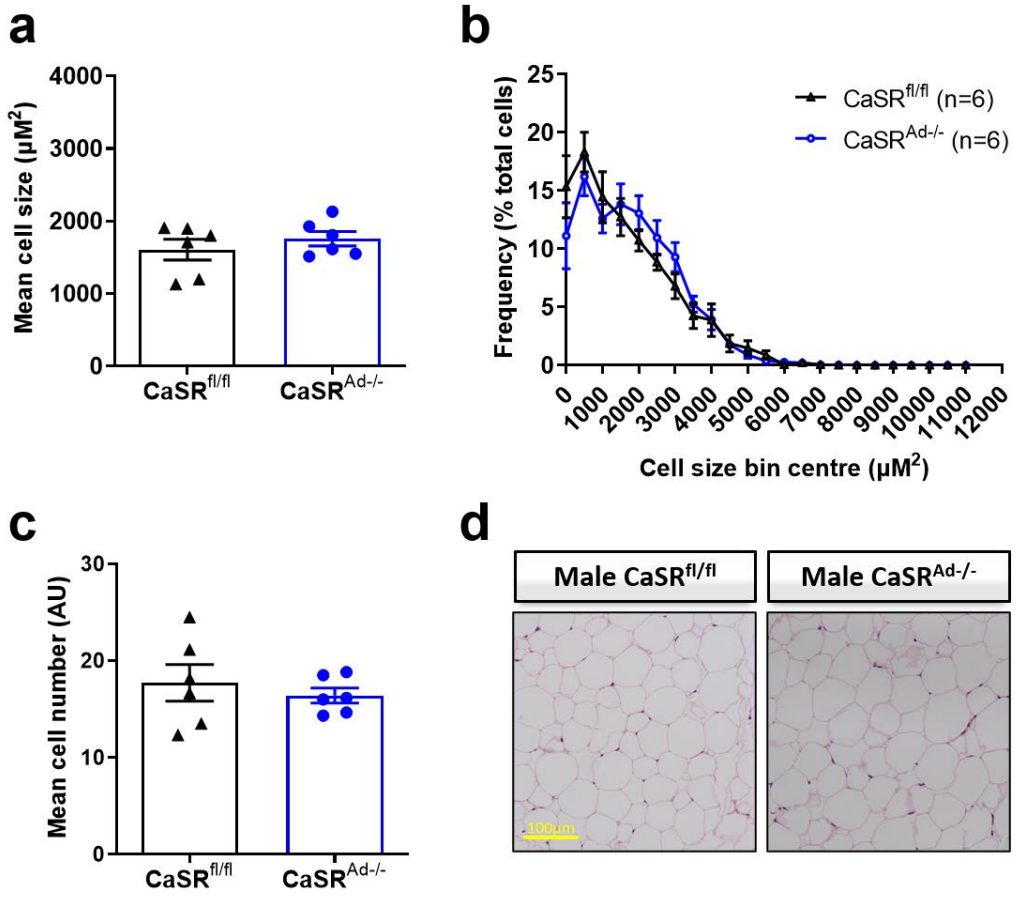

Figure 6-11: Adipocyte size in male $CaSR^{Ad-/-}$ gAT.

(a) Mean adipocyte size per mouse is comparable between $CaSR^{fl/fl}$ and $CaSR^{Ad-/-}$ mice. **(b)** Adipocyte size frequency is similar between $CaSR^{fl/fl}$ and $CaSR^{Ad-/-}$ mice. **(c)** Mean adipocyte number of $CaSR^{fl/fl}$ and $CaSR^{Ad-/-}$ mice is unaltered. **(d)** Representative images of H&E stained male $CaSR^{fl/fl}$ and $CaSR^{Ad-/-}$ gAT adipocytes. Mean±SEM. Unpaired t-test (a,c). Two-way ANOVA (b). Magnification 10X. Scale bar=100μm. gAT=Gonadal adipose tissue.

6.3.7.2. Female adipocyte size

In females, $CaSR^{fl/fl}$ gAT demonstrated a mean adipocyte size of 2732±124μm^2. When compared to $CaSR^{fl/fl}$ gAT adipocytes, the mean size of $CaSR^{Ad-/-}$ gAT adipocytes was reduced by 30% to 1920±128μm^2 (p=0.0009; Fig. 6-12a,d). Cell size frequency analysis reflected these findings; relative to $CaSR^{fl/fl}$ gAT, $CaSR^{Ad-/-}$ gAT demonstrated an increased number of adipocytes which were classed within the two smallest size bins 0μm^2 (p<0.0001) and 500μm^2 (p<0.01). In concert with an increased number of small adipocytes, the number of $CaSR^{Ad-/-}$ gAT adipocytes which fell into larger adipocyte size classifications 4000μm^2 (p<0.05) and 4500μm^2 (p<0.05) was decreased compared to $CaSR^{fl/fl}$ gAT (Fig. 6-12b). In $CaSR^{Ad-/-}$ gAT, reduced adipocyte size coincided with an increased adipocyte number. Cell number per unit area in $CaSR^{fl/fl}$ gAT (10±1) was increased by 40% in $CaSR^{Ad-/-}$ gAT (14±1, p=0.0152; Fig. 6-12c).

To interrogate the mechanism unpinning reduced adipocyte size in female $CaSR^{Ad-/-}$ mice, mRNA levels of several lipogenic and metabolic mediators were examined in isolated female gAT adipocytes. Lipogenic genes acetyl-CoA carboxylase (ACC1), fatty acid binding protein (FABP4), fatty acid synthase (FASN), PPARγ and sterol regulatory element-binding protein 1 (SREBP1), as well as the cell metabolism mediator mammalian target of rapamycin (mTOR), were unchanged in $CaSR^{Ad-/-}$ mice when compared to $CaSR^{fl/fl}$ controls (p>0.05; Fig. 6-13; Tb. 6-1). Interestingly, uncoupling protein-1 (UCP-1) was highly variable in $CaSR^{Ad-/-}$ adipocytes, which was increased greatly in several subjects. Though UCP-1 expression was overall not significantly altered in $CaSR^{Ad-/-}$ adipocytes compared to $CaSR^{fl/fl}$ controls (p>0.05; Fig. 6-13; Tb. 6-1), further experiments are required to fully elucidate the status of UCP-1 in $CaSR^{Ad-/-}$ adipocytes.

Figure 6-12

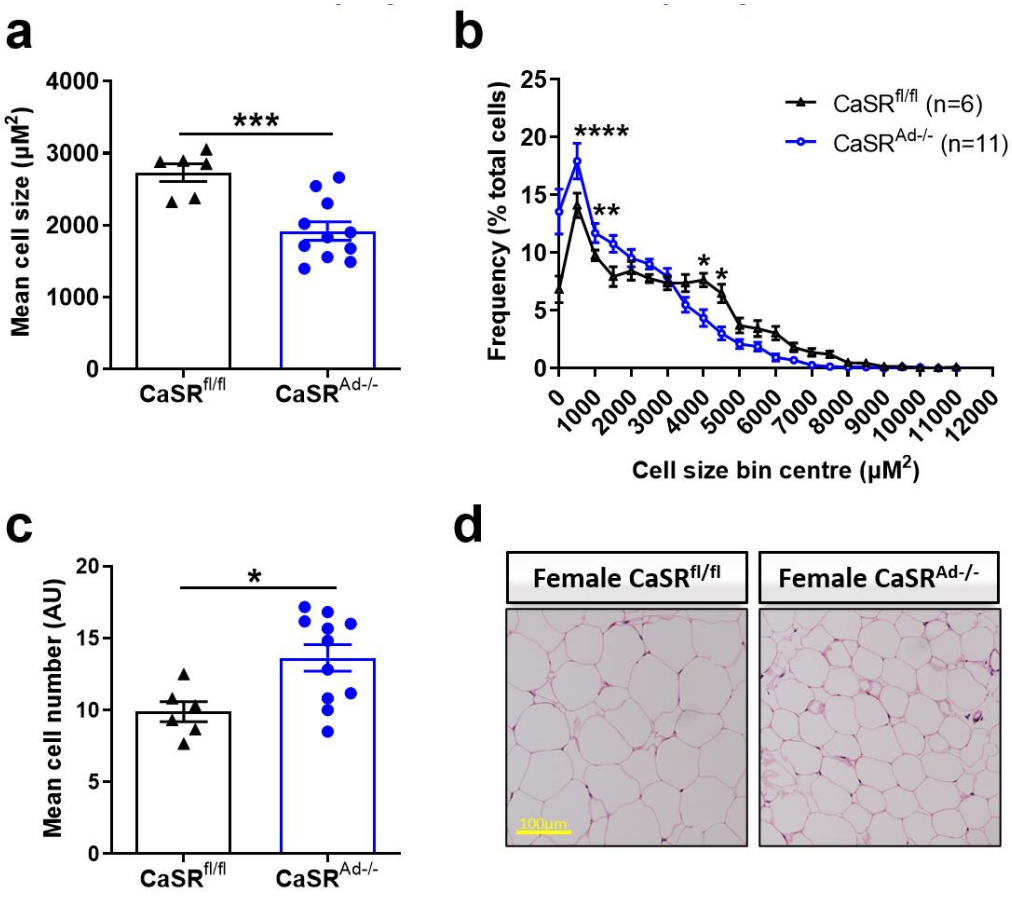

Figure 6-12: Adipocyte size is increased in female CaSR$^{Ad-/-}$ gAT.

(a) Mean adipocyte size per mouse is reduced in CaSR$^{Ad-/-}$ mice compared to CaSR$^{fl/fl}$. **(b)** Adipocyte size frequency is altered in CaSR$^{Ad-/-}$ when compared to CaSR$^{fl/fl}$ controls. **(c)** Mean adipocyte number in CaSR$^{Ad-/-}$ mice is greater than CaSR$^{fl/fl}$ controls. **(d)** Representative images of H&E stained female CaSR$^{fl/fl}$ and CaSR$^{Ad-/-}$ gAT adipocytes. Mean±SEM. Unpaired t-test (a,c). Two-way ANOVA (b). *p<0.05, **p<0.01, ***p<0.001, ****p<0.0001. Magnification 10X. Scale bar=100μm. gAT=Gonadal adipose tissue.

Figure 6-13

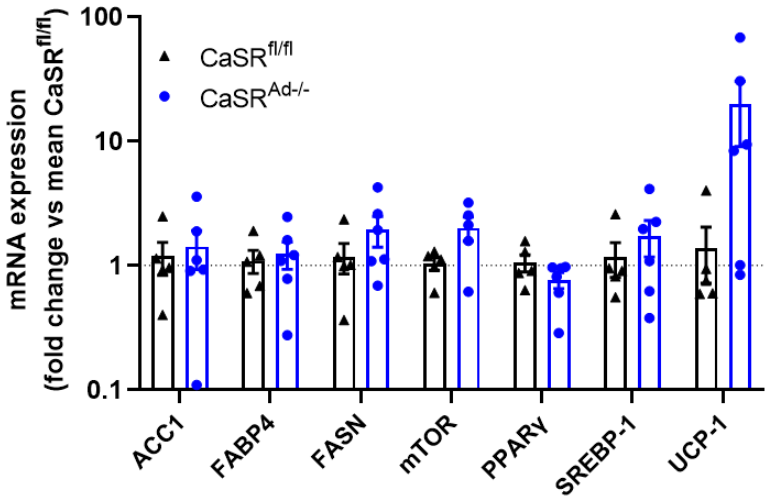

Figure 6-13: Gene expression in female CaSR$^{Ad-/-}$ adipocytes.

Genes responsible for adipocyte growth and lipid handling in adipocytes are unaltered in CaSR$^{Ad-/-}$ mice when compared to CaSR$^{fl/fl}$ controls. UCP-1 tends to be increased in female CaSR$^{Ad-/-}$ mice, though the effect is non-significant. Mean±SEM. Unpaired t-test (a,b). ACC1=Acetyl-CoA; FABP4=Fatty acid-binding protein 4; FASN= Fatty acid synthase; gAT=Gonadal adipose tissue; mTOR=Mammalian target of rapamycin; PPARγ=Peroxisome proliferator-activated receptor γ; SREBP1=Sterol regulatory element-binding protein 1; UCP-1=Uncoupling Protein 1.

Table 6-1

Gene target	$CaSR^{fl/fl}$	$CaSR^{Ad-/-}$	*P*-value
	(Mean fold change±SEM)		(*t*-test)
ACC1	1.2±0.3	1.4±0.5	>0.05
FABP4	1.1±0.2	1.2±0.3	>0.05
FASN	1.2±0.3	1.9±0.5	>0.05
mTOR	1.0±0.1	2.0±0.4	>0.05
PPARγ	1.0±0.2	0.8±0.1	>0.05
SREBP-1	1.2±0.4	1.7±0.6	>0.05
UCP-1	1.4±0.7	19.6±10.6	>0.05

Table 6-1: Gene expression in female $CaSR^{Ad-/-}$ adipocytes.
Genes responsible for adipocyte growth and lipid handling in adipocytes is unaltered in $CaSR^{Ad-/-}$ mice when compared to $CaSR^{fl/fl}$ controls. ACC1=Acetyl-CoA; FABP4=Fatty acid-binding protein 4; FASN= Fatty acid synthase; gAT=Gonadal adipose tissue; mTOR=Mammalian target of rapamycin; PPARγ=Peroxisome proliferator-activated receptor γ; SREBP-1=Sterol regulatory element-binding protein 1; UCP-1=Uncoupling Protein 1.

6.3.7.3. Baseline adipocyte characteristics in $CaSR^{fl/fl}$ mice

Adipocyte phenotype was altered in female $CaSR^{Ad-/-}$ mice, but unchanged in male $CaSR^{Ad-/-}$ mice. To understand how baseline differences in male and female adipocytes may lead to sex-dependent differences in $CaSR^{Ad-/-}$ adipocyte phenotype, adipocyte size and CaSR expression was compared in male and female control $CaSR^{fl/fl}$ gAT. In male $CaSR^{fl/fl}$ gAT, mean adipocyte size was 1609±143μm^2. Mean adipocyte size in male gAT $CaSR^{fl/fl}$ was considerably decreased when compared to female counterparts, which demonstrated a mean adipocyte size of 2732±124μm^2 ($p=0.0001$; Fig. 6-14a). Analysis of cell size frequency confirmed these findings. Compared to males, female $CaSR^{fl/fl}$ gAT possessed fewer adipocytes classified into bins representing the smallest adipocytes 0μm^2 ($p<0.0001$), 500μm^2 ($p<0.01$), 1000μm^2 ($p<0.01$) and 1500μm^2 ($p<0.05$). Where female $CaSR^{fl/fl}$ gAT possessed fewer small (<2000μm^2) adipocytes, the number of large adipocytes was increased in females compared to males; female $CaSR^{fl/fl}$ gAT showed an increased number of adipocytes which were classed within bins attributed to larger adipocyte sizes 4000μm^2 ($p<0.05$) and 4500μm^2 ($p<0.01$; Fig. 6-14b).

To further examine the factors which may contribute to sex-dependent effect of adipocyte-specific CaSR deletion on adipocyte size, it was important to establish whether CaSR expression differed between sexes at baseline in CaSR$^{fl/fl}$ control mice. Despite demonstrating differences in adipocytes size, CaSR mRNA expression was similar between male CaSR$^{fl/fl}$ gAT adipocytes (1.1±0.2-fold) and female CaSR$^{fl/fl}$ gAT adipocytes (1.1± 0.1-fold, p>0.05; Fig. 6-14c).

Figure 6-14

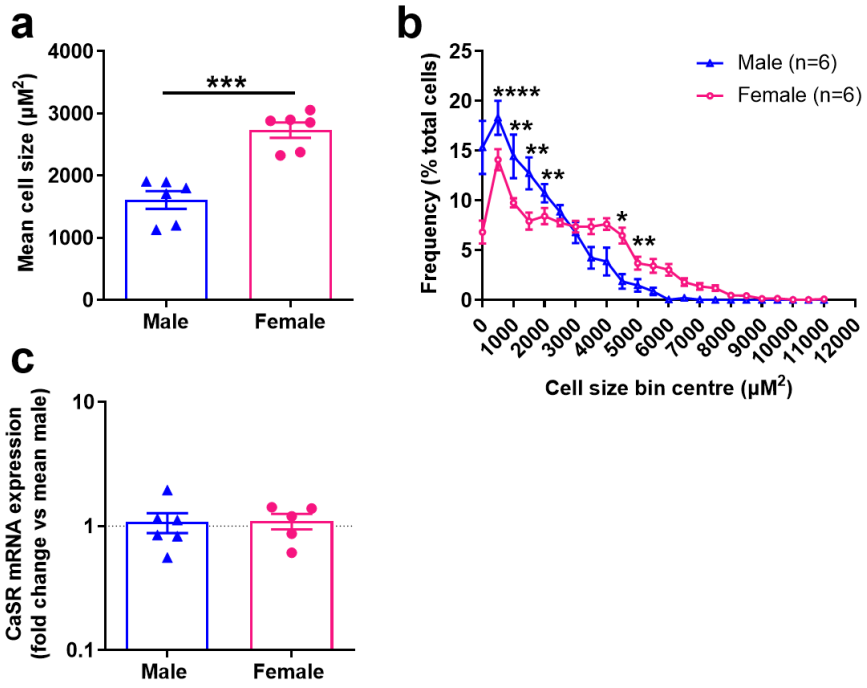

Figure 6-14: Adipocyte size is increased in female versus male CaSR$^{fl/fl}$ gAT. **(a)** Mean adipocyte size per mouse is reduced in male CaSR$^{fl/fl}$ controls compared to females. **(b)** Adipocyte size frequency is altered between male and female CaSR$^{fl/fl}$ mice. **(c)** CaSR mRNA expression is comparable between male and female CaSR$^{fl/fl}$ gAT adipocytes. Mean±SEM. Unpaired t-test (a, b). Two-way ANOVA (c). *p<0.05, **p<0.01, ***p<0.001, ****p<0.0001. gAT=Gonadal adipose tissue.

6.3.8 ERK signalling

In chapter 3, stimulation of CaSR lead to increased $ERK_{1/2}$ signalling in HEK293-CaSR cells. In rat, $ERK_{1/2}$ activation is positively associated with cell size (Farnier *et al.*, 2003). To establish whether CaSR-mediated $ERK_{1/2}$ signalling is conserved *in vivo* and if the reduced size of $CaSR^{Ad-/-}$ adipocytes was linked with $ERK_{1/2}$ signalling, western blot analyses were performed on isolated $CaSR^{Ad-/-}$ gAT adipocytes. In $CaSR^{fl/fl}$ adipocytes, total ERK protein was 1.8±1.3. Compared to $CaSR^{fl/fl}$ adipocytes, total $ERK_{1/2}$ protein in $CaSR^{Ad-/-}$ adipocytes was not significantly changed (5.0±1.6, $p>0.05$; Fig. 6-15a,c). As with total ERK protein, there was no difference in $ERK_{1/2}$ activation between $CaSR^{fl/fl}$ and $CaSR^{Ad-/-}$ adipocytes, determined as 0.51±0.04 and 0.59±0.04 respectively ($p>0.05$; Fig. 6-15b,c).

Figure 6-15

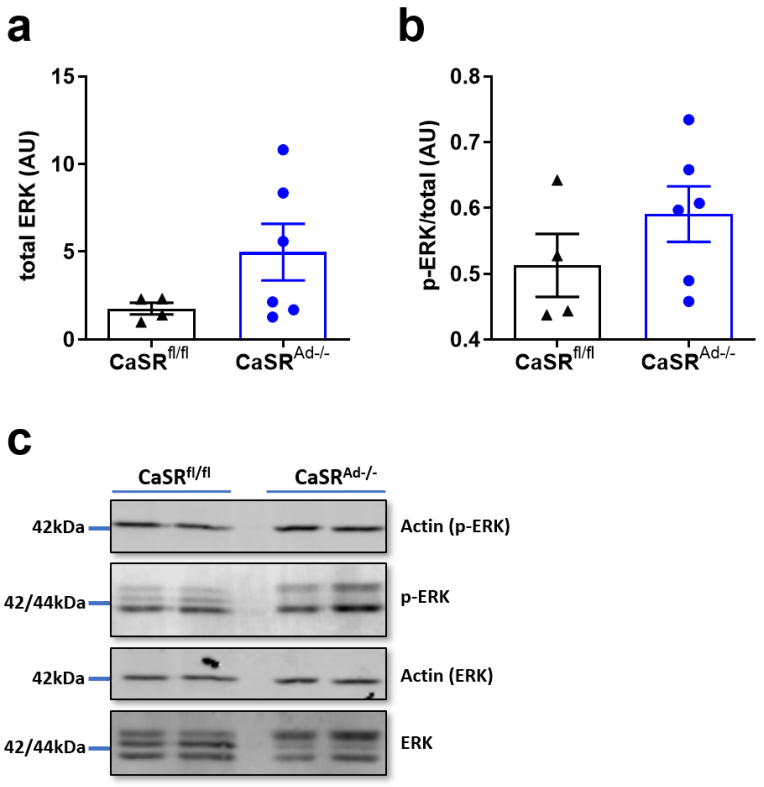

Figure 6-15: ERK signalling in female $CaSR^{Ad-/-}$ adipocytes.

(a) There is no difference in total ERK between $CaSR^{fl/fl}$ or $CaSR^{Ad-/-}$ gAT adipocytes. **(b)** There is no difference in p-ERK activation between $CaSR^{fl/fl}$ or $CaSR^{Ad-/-}$ gAT adipocytes. **(c)** Representative western blot images of p-ERK, ERK and ß-actin housekeeping protein. Mean±SEM. Unpaired t-test (a,b). gAT=Gonadal adipose tissue.

6.3.9 Systemic lipid content

To examine whether reduced adipocyte size leads to altered lipid handling in female $CaSR^{Ad-/-}$ mice, plasma free fatty acid (FFA) and triglyceride (TG) levels were interrogated. Compared to FFA levels in $CaSR^{fl/fl}$ plasma (0.053±0.003nmol/µl), FFAs in $CaSR^{Ad-/-}$ plasma were unaltered (0.065±0.009nmol/µl, $p>0.05$; Fig. 6-16a). Though FFAs were unchanged, TG levels in $CaSR^{Ad-/-}$ plasma (1.1±0.1nmol/µl) were lowered by 27% compared to $CaSR^{fl/fl}$ plasma (1.5±0.2nmol/µl; $p=0.0487$; Fig. 6-16b).

Figure 6-16

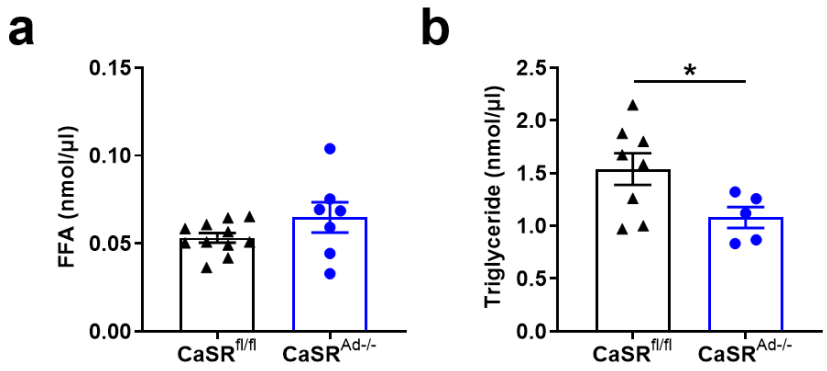

Figure 6-16: Systemic lipids are altered in female $CaSR^{Ad-/-}$ mice.
(a) Circulating FFA levels are comparable in $CaSR^{fl/fl}$ and $CaSR^{Ad-/-}$ mice. **(b)** Circulating TG levels are decreased in $CaSR^{Ad-/-}$ mice compared to $CaSR^{fl/fl}$ controls . Mean±SEM. Unpaired t-test (a. b). *$p<0.05$. FFA=Free fatty acid. TG=Triglyceride.

6.3.10 Adipokines

To investigate whether reduced adipocyte size leads to altered adipokine signalling in female $CaSR^{Ad-/-}$ mice, circulating plasma adipokine levels were interrogated. Circulating adiponectin was unchanged between $CaSR^{fl/fl}$ plasma (12.5±0.9µg/ml) and $CaSR^{Ad-/-}$ plasma (13.3±1.5µg/ml, $p>0.05$; Fig. 6-17a). Similarly, $CaSR^{fl/fl}$ plasma leptin levels (10.2±1.9ng/ml) were comparable to those in $CaSR^{Ad-/-}$ plasma (11.8±2.0ng/ml, $p>0.05$; Fig. 6-17b).

Adipokine and endothelial nitric oxide synthase (eNOS) signalling was also assessed at the cellular level in isolated $CaSR^{Ad-/-}$ gAT adipocytes. First, mRNA transcript levels of eNOS, adiponectin and leptin were examined in $CaSR^{fl/fl}$ and $CaSR^{Ad-/-}$ adipocytes. Between groups, there was no significant difference found in eNOS ($p>0.05$), adiponectin ($p>0.05$) or leptin mRNA levels ($p>0.05$; Fig. 6-18a). Though adiponectin and leptin mRNA expression was unchanged, adiponectin and leptin protein expression was also interrogated to determine whether post-translational regulation is affected by reduced adipocyte CaSR. Adiponectin protein expression in $CaSR^{fl/fl}$ adipocytes (218.3±53.1ng/mg) was not altered in $CaSR^{Ad-/-}$ adipocytes (171.5±53.1ng/mg, $p>0.05$; Fig. 6-18b). Leptin expression in $CaSR^{fl/fl}$ adipocytes (1107.0±342.0pg/mg) was similarly unchanged in $CaSR^{Ad-/-}$ adipocytes (737.4±251.2pg/mg, $p>0.05$; Fig. 6-18c).

Figure 6-17

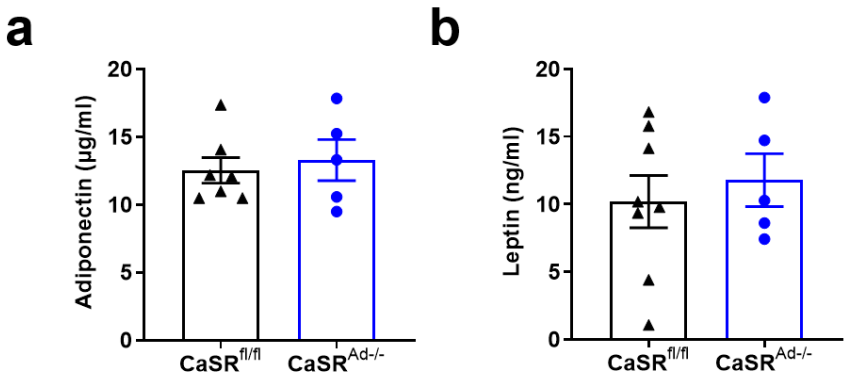

Figure 6-17: Plasma adipokines in female $CaSR^{Ad-/-}$ mice.

(a) Circulating adiponectin levels are comparable in $CaSR^{fl/fl}$ and $CaSR^{Ad-/-}$ mice.

(b) Circulating leptin levels are similar in $CaSR^{fl/fl}$ and $CaSR^{Ad-/-}$ mice.

Mean±SEM. Unpaired t-test (a. b).

Figure 6-18

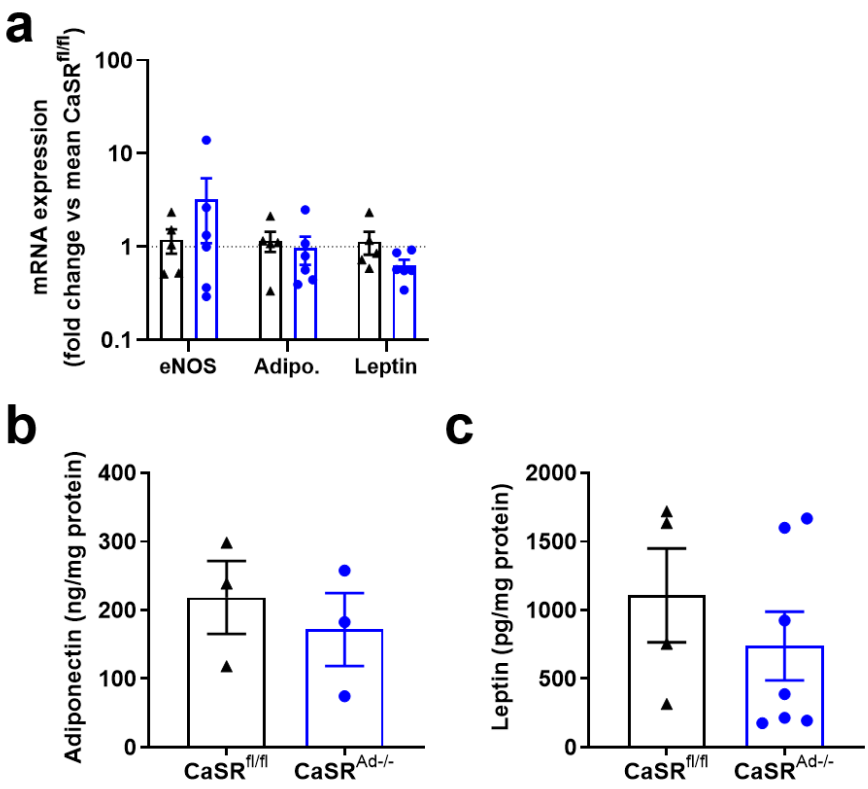

Figure 6-18: NO and adipokine signalling in female CaSR$^{Ad-/-}$ adipocytes.
(a) CaSR$^{fl/fl}$ and CaSR$^{Ad-/-}$ gAT adipocytes show comparable levels of eNOS, adiponectin (Adipo) and leptin mRNA transcript levels. **(b)** Adiponectin protein levels are similar in CaSR$^{fl/fl}$ and CaSR$^{Ad-/-}$ gAT adipocytes. **(c)** Leptin protein levels are similar in CaSR$^{fl/fl}$ and CaSR$^{Ad-/-}$ gAT adipocytes. Mean±SEM. Unpaired t-test (a-c). eNOS=Endothelial nitric oxide synthase. gAT=Gonadal adipose tissue.

6.3.11 PVAT and vascular function *ex vivo*

To test whether adipocyte-specific CaSR deletion affects PVAT-mediated vascular function *in vivo*, the effect of PVAT on aortic contraction and relaxation was studied in CaSR$^{Ad-/-}$ mice aged 18-22 weeks. As physiological $[Ca^{2+}]_o$ levels are regulated within a narrow limit of 1.1-1.3mM (Zhang *et al.*, 2016), vascular myography studies were conducted in the presence of 1mM $[Ca^{2+}]_o$ to prevent maximal stimulation of CaSR.

6.3.11.1. Male vascular responses

In males, phenylephrine (PE) promoted contractile responses in $CaSR^{fl/fl}$ aortas (pEC_{50}=6.8±0.2, E_{max}=41.3±3.7%). Contractile responses in $CaSR^{fl/fl}$ aortas were significantly increased by the presence of PVAT, which raised maximum PE contractions with no alteration in pEC_{50} (pEC_{50}=6.4±0.1, E_{max}=69.1±4.0%; p<0.0001; Fig. 6-19a). PE also caused contraction in male $CaSR^{Ad-/-}$ aortas (pEC_{50}=6.7±0.2, E_{max}=48.9±4.5%). PVAT enhanced PE-mediated contractility in $CaSR^{Ad-/-}$ aortas, where it again acted to increase maximum PE contractions with no change in pEC_{50} (pEC_{50}=6.4±0.1, E_{max}= 74.6±2.7%; p<0.0001; Fig. 6-19a). Although both $CaSR^{fl/fl}$ and $CaSR^{Ad-/-}$ aortas demonstrated markedly increased PE-mediated contraction in the presence of PVAT, the effect of PVAT was comparable in male $CaSR^{fl/fl}$ and $CaSR^{Ad-/-}$ aortas (p>0.05; Fig. 6-19a; Tb. 6-2a).

In $CaSR^{fl/fl}$ aortas lacking PVAT, ACh stimulated vasorelaxation (pEC_{50}=7.0±0.1, E_{max}=78.0±4.4%). Though maximum relaxation was unaltered in the presence of PVAT, the pEC_{50} for ACh-mediated relaxation was decreased, demonstrating that PVAT significantly reduces ACh sensitivity in $CaSR^{fl/fl}$ aortas (pEC_{50}= 6.1±0.1, E_{max}=95.8±5.2%; p<0.0001; Fig. 6-19b). ACh-mediated relaxation in $CaSR^{Ad-/-}$ aortas (pEC_{50}= 7.2±0.1, E_{max}= 80.0±3.5%) was similarly attenuated in the presence of PVAT; when compared to baseline $CaSR^{Ad-/-}$ aorta responses, PVAT again reduced the pEC_{50} for ACh, thus blunting ACh sensitivity (pEC_{50}= 6.3±0.1, E_{max}= 93.6±7.3%; p<0.0001; Fig. 6-19b). Where PVAT reduced the pEC_{50} for ACh in both $CaSR^{fl/fl}$ and $CaSR^{Ad-/-}$ aortas, these effects were comparable (p>0.05; Fig. 6-19b; Tb 6-2a).

SNP elicited relaxation in $CaSR^{fl/fl}$ aortas (pEC_{50}= 7.5±0.2, E_{max}= 103.1±7.5%). In the presence of PVAT, $CaSR^{fl/fl}$ aortas showed decreased SNP sensitivity, demonstrated by a reduced pEC_{50} for SNP without any change in maximum relaxation (pEC_{50}= 6.8±0.1, E_{max}= 113.1±10.0%, p<0.0005; Fig. 6-19c). SNP also caused vasorelaxation in $CaSR^{Ad-/-}$ aortas (pEC_{50}= 7.9±0.1, E_{max}= 91.8±3.7%). In $CaSR^{Ad-/-}$ aortas, PVAT again decreased the pEC_{50} for SNP. However, maximum SNP relaxations were also increased (pEC_{50}= 6.6±0.1, E_{max}= 119.2±6.4%, p<0.0001; Fig. 6-19c). Collectively, PVAT acted to decrease the pEC_{50} in both $CaSR^{fl/fl}$ and $CaSR^{Ad-/-}$ aortas, but PVAT caused an additional increase in maximum SNP-mediated relaxation in $CaSR^{Ad-/-}$ aortas. Despite this difference, PVAT-mediated

SNP responses remained comparable between $CaSR^{fl/fl}$ and $CaSR^{Ad-/-}$ aortas ($p>0.05$; Fig. 6-19c; Tb. 6-2a).

In the vasculature, adipocyte-derived secretions influence vasoreactivity directly by modulating VSMC contraction, but also indirectly by acting upon the endothelium to regulate release of vasoactive substances (Nava and Llorens, 2019). To examine the role of the endothelium in PVAT-mediated vascular responses, a second set of experiments were performed in $CaSR^{fl/fl}$ and $CaSR^{Ad-/-}$ aortas following endothelial denudation (Tb. 6-2b). As with intact aortas, denuded $CaSR^{fl/fl}$ aortas contracted in response to PE (pEC_{50}= 7.0±0.2, E_{max}= 107.7±7.7%). PVAT decreased the pEC_{50} for PE in denuded $CaSR^{fl/fl}$ aortas, though maximum PE contractions were unchanged (pEC_{50}= 6.4±0.2, E_{max}=98.6±9.5%, $p<0.0017$; Fig. 6-19d). As with $CaSR^{fl/fl}$ control counterparts, PE caused contraction in denuded $CaSR^{Ad-/-}$ aortas (pEC_{50}= 7.2±0.1, E_{max}= 114.5±4.3%). In presence of PVAT, denuded $CaSR^{Ad-/-}$ vessels demonstrated decreased pEC_{50} for PE and reduced maximum PE contractions (pEC_{50}= 6.4±0.2, E_{max}=91.5±7.2%, $p<0.0001$; Fig. 6-19d). Collectively, PVAT acted to decrease the pEC_{50} in both $CaSR^{fl/fl}$ and $CaSR^{Ad-/-}$ aortas, but these responses were similar ($p>0.05$; Fig. 6-19d; Tb. 6-2b).

SNP caused relaxation in denuded $CaSR^{fl/fl}$ aortas (pEC_{50}= 7.6±0.1, E_{max}= 114.7±4.7%). Though maximal SNP relaxation was unchanged, PVAT decreased the pEC_{50} for SNP in denuded $CaSR^{fl/fl}$ aortas, indicating that PVAT reduces SNP sensitivity (pEC_{50}= 6.7±0.2, E_{max}=131.2±19.4%, $p<0.0001$; Fig. 6-19e). SNP also elicited vasorelaxation in denuded $CaSR^{Ad-/-}$ aortas (pEC_{50}= 7.6±0.1, E_{max}= 115.8±4.6%). PVAT potentiated SNP-mediated relaxation in denuded $CaSR^{Ad-/-}$ aortas, though the pEC_{50} for SNP was decreased (pEC_{50}= 6.1±0.2, E_{max}=200.0±37.0%, $p<0.0001$; Fig. 6-19e). Though PVAT imposed a differential effect on maximum SNP contractions, PVAT-mediated SNP relaxation in denuded $CaSR^{fl/fl}$ and $CaSR^{Ad-/-}$ aortas was comparable ($p>0.05$; Fig. 6-19e; Tb 6-2b).

Figure 6-19

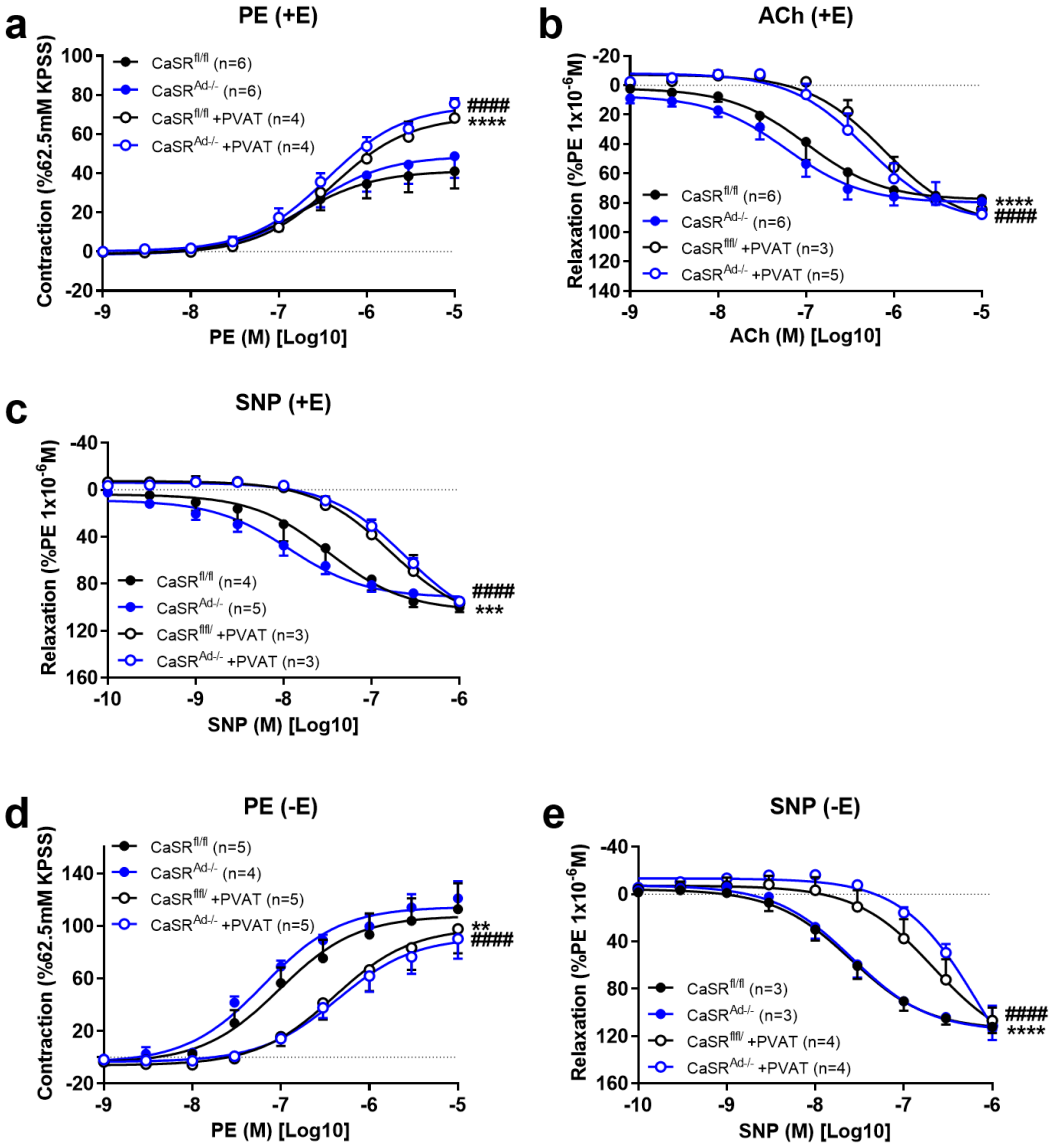

Figure 6-19: PVAT-mediated vascular reactivity in male CaSR$^{Ad-/-}$ mice.

(a) In vessels with intact endothelium (+E), maximum PE-mediated contraction is potentiated in the presence of PVAT (+PVAT) in both CaSR$^{fl/fl}$ and CaSR$^{Ad-/-}$ aortas. **(b)** PVAT-mediated ACh relaxation EC_{50} is reduced with PVAT in CaSR$^{fl/fl}$ and CaSR$^{Ad-/-}$ aortas. **(c)** PVAT-mediated SNP relaxation EC_{50} is reduced in CaSR$^{fl/fl}$ and CaSR$^{Ad-/-}$ aortas. **(d)** In aortas lacking endothelium (-E), PVAT-mediated maximum PE-mediated contraction and EC_{50} is reduced in CaSR$^{Ad-/-}$ mice and EC_{50} reduced in CaSR$^{fl/fl}$ mice. **(e)** SNP relaxation EC_{50} is reduced in denuded CaSR$^{fl/fl}$ and CaSR$^{Ad-/-}$ aortas. Mean ±SEM. F-test (a-e). **p<0.01, ***p<0.001, ****p<0.0001 CaSR$^{fl/fl}$ vs CaSR$^{fl/fl}$ +PVAT. ####p=<0.0001 CaSR$^{Ad-/-}$ vs CaSR$^{Ad-/-}$ +PVAT. ACh=Acetylcholine; PE=Phenylephrine; PVAT=Perivascular adipose tissue; SNP=Sodium nitroprusside.

Table 6-2

(a)

D-R Curve (+E)	PE (+E) pEC_{50} ($-Log_{10}$)	PE (+E) E_{max} (%)	PE (+E) *p*	Ach (+E) pEC_{50} ($-Log_{10}$)	Ach (+E) E_{max} (%)	Ach (+E) *p*	SNP (+E) pEC_{50} ($-Log_{10}$)	SNP (+E) E_{max} (%)	SNP (+E) *p*
Male									
$CaSR^{fl/fl}$	6.8±0.2	41.33±3.64		7.0±0.1	78.04±4.36		7.5±0.2	103.1±7.54	
$CaSR^{Ad-/-}$	6.7±0.2	48.89±4.47		7.2±0.1	80.03±3.52		7.9±0.1	91.76±3.68	
$CaSR^{fl/fl}$ +PVAT	6.4±0.1	69.08±4.02	****	6.1±0.1	95.81±5.18	****	6.8±0.1	113.1±10.03	***
$CaSR^{Ad-/-}$ +PVAT	6.4±0.1	74.58±2.69	####	6.3±0.1	93.55±7.26	####	6.6±0.1	119.2±6.38	####
Female									
$CaSR^{fl/fl}$	6.9±0.2	41.97±3.61		7.3±0.1	92.70±4.54		7.5±0.1	105.3±3.00	
$CaSR^{Ad-/-}$	6.8±0.2	48.63±4.01		7.2±0.1	83.76±3.07		8.0±0.1	98.42±2.78	
$CaSR^{fl/fl}$ +PVAT	6.7±0.1	74.00±4.86	****	6.4±0.2	93.19±10.46	****	6.7±0.1	120.3±8.72	****
$CaSR^{Ad-/-}$ +PVAT	6.5±0.1	54.60±3.14	§§§§	6.6±0.1	96.55±4.18	###	6.7±0.2	108.2±16.40	####

(b)

D-R Curve (-E)	PE (-E) pEC_{50} ($-Log_{10}$)	PE (-E) E_{max} (%)	PE (-E) *p*	SNP (-E) pEC_{50} ($-Log_{10}$)	SNP (-E) E_{max} (%)	SNP (-E) *p*
Male						
$CaSR^{fl/fl}$	7.0±0.2	107.70±7.71		7.6±0.1	114.65±4.68	
$CaSR^{Ad-/-}$	7.2±0.1	114.50±4.27		7.6±0.1	115.82±4.60	
$CaSR^{fl/fl}$ +PVAT	6.4±0.2	98.56±9.46	**	6.7±0.2	131.17±19.44	****
$CaSR^{Ad-/-}$ +PVAT	6.4±0.2	91.49±7.24	####	6.1±0.2	199.98±37.01	####
Female						
$CaSR^{fl/fl}$	7.0±0.1	127.40±4.13		7.8±0.2	99.97±6.33	
$CaSR^{Ad-/-}$	6.9±0.1	102.30±3.83		8.5±0.1	116.20±3.65	
$CaSR^{fl/fl}$ +PVAT	6.8±0.2	113.50±12.00		7.0±0.1	125.30±6.79	***
$CaSR^{Ad-/-}$ +PVAT	6.5±0.1	96.78±4.30	####, §	6.9±0.2	120.10±12.00	####

Table 6-2: The effect of PVAT on vascular reactivity in $CaSR^{Ad-/-}$ mice.

Dose-response curves were conducted on aorta segments with intact endothelium (+E; >60% function preserved) **(b)** or endothelium denuded (-E; <20% function preserved). Results are provided for PE, ACh and SNP dose-response curves in PVAT absence and presence (+PVAT). PE response is expressed as % contraction relative to the mean KPSS contraction. ACh and SNP responses are expressed as % relaxation relative to PE $1x10^{-6}$M preconstriction. Mean ±SEM. **p<0.01, ***p=<0.001, ****p=<0.0001 $CaSR^{fl/fl}$ vs $CaSR^{fl/fl}$ +PVAT. ###p<0.001, ####p=<0.0001 $CaSR^{Ad-/-}$ vs $CaSR^{Ad-/-}$ +PVAT. §p<0.05, §§§§p<0.0001 $CaSR^{fl/fl}$ +PVAT vs $CaSR^{Ad-/-}$ +PVAT. ACh=Acetylcholine; PE=Phenylephrine; PVAT=Perivascular adipose tissue; SNP=Sodium nitroprusside.

6.3.11.2. Female vascular responses

Vascular reactivity was also assessed in female $CaSR^{Ad-/-}$ mice. As with male mice, PE had a procontractile effect in female $CaSR^{fl/fl}$ aortas (pEC_{50}=6.9±0.2, E_{max}=42.0±3.6%). Compared to $CaSR^{fl/fl}$ aortas at baseline, PVAT enhanced the maximum PE contraction, with no alteration in the pEC_{50} for PE (pEC_{50}=6.7±0.1, E_{max}=74.0±4.9, p<0.0001; Fig. 6-20a). Although PE caused contraction in $CaSR^{Ad-/-}$ aortas (pEC_{50}=6.8±0.2, E_{max}=48.6±4.0%), PVAT did not similarly enhance PE responses $CaSR^{Ad-/-}$ aortas, since maximum PE contraction and the pEC_{50} for PE were unchanged (pEC_{50}=6.5±0.1, E_{max}=54.6±3.1, p>0.05; Fig. 6-20a). When PVAT-mediated PE contractile responses were compared between groups, maximum responses were significantly decreased in $CaSR^{Ad-/-}$ aortas compared to $CaSR^{fl/fl}$ controls (p<0.0001; Fig. 6-20a; Tb 6-2a)

ACh induced relaxation in female $CaSR^{fl/fl}$ aortas (pEC_{50}=7.3±0.1, E_{max}=92.7±4.5%). Compared to baseline ACh responses in $CaSR^{fl/fl}$ aortas, PVAT caused a reduction in ACh sensitivity, as the pEC_{50} for ACh fell significantly (pEC_{50}=6.4±0.2, E_{max}=93.2±10.5, p<0.0001; Fig. 6.20b). In $CaSR^{Ad-/-}$ aortas, ACh again induced relaxation (pEC_{50}=7.2±0.1, E_{max}= 83.8±3.1%). In the presence of PVAT, the pEC_{50} for ACh was decreased in $CaSR^{Ad-/-}$ aortas. Despite reducing ACh sensitivity, there was a small but significant effect on maximum ACh relaxation, which was increased by PVAT in $CaSR^{Ad-/-}$ aortas (pEC_{50}=6.6±0.1, E_{max}=96.6±4.2, p=0.0004; Fig. 6.20b). While PVAT caused slightly differing effects in $CaSR^{fl/fl}$ and $CaSR^{Ad-/-}$ aortas, PVAT-mediated responses in $CaSR^{fl/fl}$ and $CaSR^{Ad-/-}$ aortas were comparable overall (p>0.05; Fig. 6.20b; Tb 6.2a).

SNP promoted vasorelaxation in In $CaSR^{fl/fl}$ aortas (pEC_{50}=7.5±0.1, E_{max}=105.3±3.0%). Compared to baseline responses, PVAT decreased the pEC_{50} for SNP in $CaSR^{fl/fl}$ aortas (pEC_{50}=6.7±0.1, E_{max}=120.3±8.7, p<0.0001; Fig. 6.20c). Like $CaSR^{flf/fl}$ aortas, $CaSR^{Ad-/-}$ aortas demonstrated vasorelaxation in response to SNP (pEC_{50}=8.0±0.1, E_{max}= 98.4±2.8%). SNP sensitivity was decreased with PVAT, which reduced the pEC_{50} for SNP (pEC_{50}=6.7±0.2, E_{max}=108.2±16.4, p<0.0001; Fig. 6.20c). PVAT-mediated SNP relaxation was equivalent between $CaSR^{fl/fl}$ and $CaSR^{Ad-/-}$ aortas (p>0.05; Fig. 6.20c; Tb 6.2a).

To investigate the role of the endothelium in female mice, vascular function was also examined in denuded aortas. PE induced contraction in denuded $CaSR^{fl/fl}$ aortas (pEC_{50}=7.0±0.1, E_{max}=127.4±4.1%). These responses were not altered by PVAT, since PE sensitivity and maximum responses were unchanged (pEC_{50}=6.8±0.2, E_{max}=113.5±12.0%, p>0.05; Fig. 6.20d). As with $CaSR^{fl/fl}$ counterparts, PE had a procontractile effect in denuded $CaSR^{Ad-/-}$ aortas at baseline (pEC_{50}=6.9±0.1, E_{max}=102.3±3.8%). In contrast to the effect of PVAT in denuded $CaSR^{fl/fl}$ aortas, PVAT reduced PE sensitivity in denuded $CaSR^{Ad-/-}$ aortas, as the pEC_{50} for PE fell in the presence of PVAT (pEC_{50}=6.5±0.1, E_{max}=96.8±4.3%, p<0.0001; Fig. 6.20d). When compared to denuded $CaSR^{fl/fl}$ aortas, PVAT-mediated PE contraction responses in $CaSR^{Ad-/-}$ aortas were significantly decreased. The difference in maximum PE mediated contraction and pEC_{50} were not independently significant, so altered responses in $CaSR^{Ad-/-}$ aortas were due to the cumulative effect of both (p=0.0185; Fig. 6-20d; Tb. 6-2b).

SNP induced vascular relaxation in denuded $CaSR^{fl/fl}$ aortas (pEC_{50}= 7.8±0.2, E_{max}=100.0±6.3%). Baseline SNP responses in $CaSR^{fl/fl}$ aortas were altered by PVAT, which increased the maximum SNP relaxation but decreased SNP sensitivity, as PVAT reduced the pEC_{50} for SNP (pEC_{50}= 7.0±0.1, E_{max}= 125.3±6.8%, p<0.0002; Fig. 6-20e). Relaxation was also mediated by SNP in denuded $CaSR^{Ad-/-}$ aortas (pEC_{50}= 8.5±0.1, E_{max}= 116.2±3.7%). Like denuded $CaSR^{fl/fl}$ aortas, PVAT acted to decrease the pEC_{50} for SNP in denuded $CaSR^{Ad-/-}$ aortas, though in this case there was no effect of PVAT on the maximum SNP relaxation (pEC_{50}= 6.9±0.2, E_{max}= 120.1±12.0%, p<0.0001; Fig. 6-20e). PVAT decreased the pEC_{50} for SNP in both denuded $CaSR^{fl/fl}$ and $CaSR^{Ad-/-}$ aortas. Though PVAT had additional effects in denuded $CaSR^{fl/fl}$ aortas where it acted to increase maximum SNP relaxation, PVAT-mediated SNP responses were ultimately comparable between denuded $CaSR^{fl/fl}$ and $CaSR^{Ad-/-}$ aortas (p>0.05; Fig. 6-20e; Tb. 6-2b).

Figure 6-20

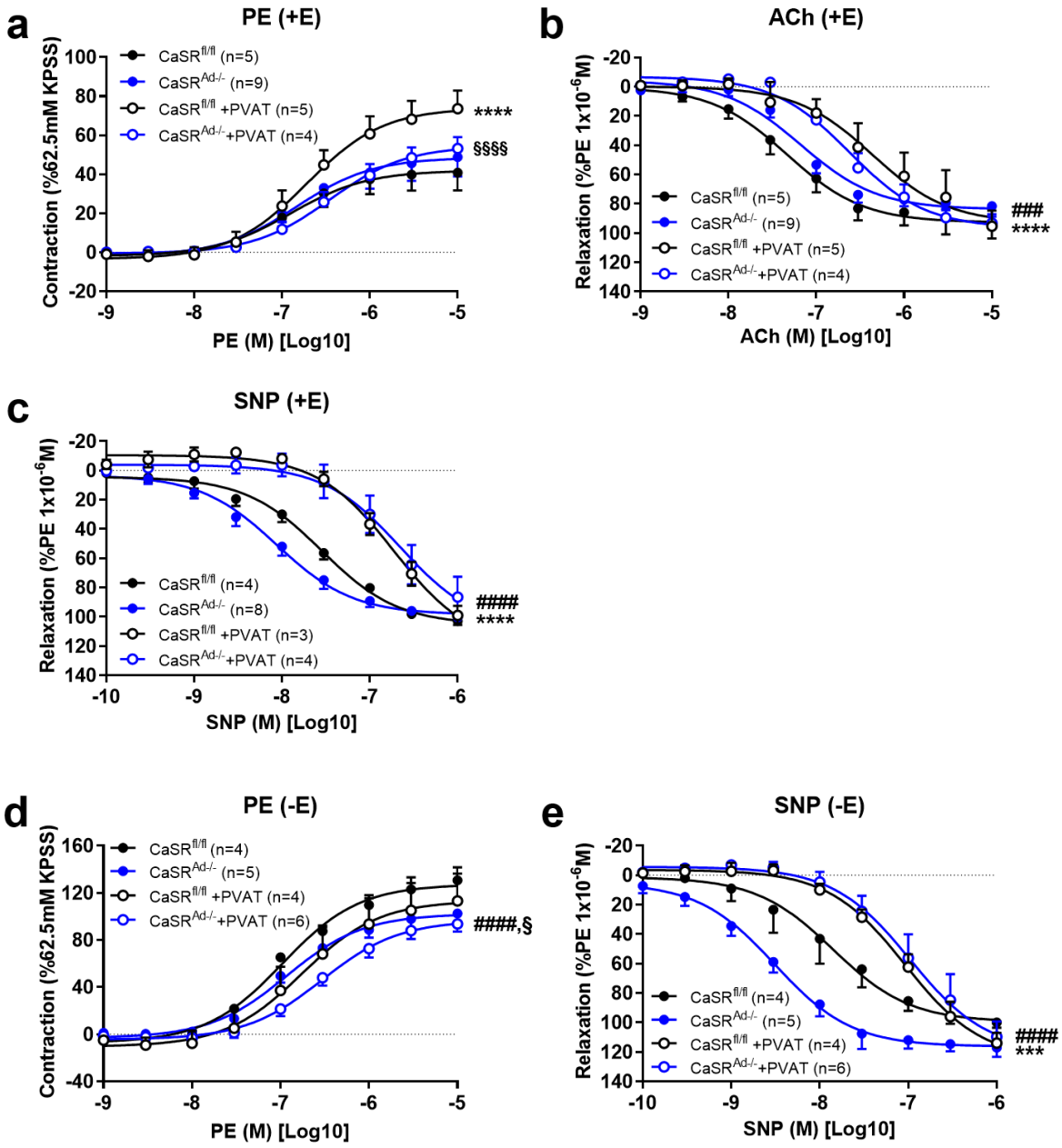

Figure 6-20: PVAT-mediated vascular reactivity is attenuated in female CaSR$^{Ad-/-}$ mice.

(a) In vessels with intact endothelium (+E), maximum PE-mediated contraction is potentiated in the presence of PVAT (+PVAT) in CaSR$^{fl/fl}$ but not CaSR$^{Ad-/-}$ aortas. PVAT mediated responses are signficantly reduced in CaSR$^{Ad-/-}$ aortas when compared to CaSR$^{fl/fl}$ controls. **(b)** ACh relaxation EC_{50} is reduced with PVAT in both CaSR$^{fl/fl}$ and CaSR$^{Ad-/-}$ aortas. **(c)** PVAT-mediated SNP relaxation EC_{50} is reduced with PVAT in both CaSR$^{fl/fl}$ and CaSR$^{Ad-/-}$ aortas. **(d)** In aortas lacking endothelium (-E), PVAT has no effect on PE-mediated contraction in CaSR$^{fl/fl}$

aortas, but reduces EC_{50} in $CaSR^{Ad-/-}$ aortas. PVAT-mediated PE contraction is attenuated in $CaSR^{Ad-/-}$ aortas compared to $CaSR^{fl/fl}$ controls. **(e)** SNP relaxation EC_{50} is reduced in denuded $CaSR^{fl/fl}$ and $CaSR^{Ad-/-}$ aortas. Mean ±SEM. F-test (a-e). ***p=<0.001, ****p=<0.0001 $CaSR^{fl/fl}$ vs $CaSR^{fl/fl}$ +PVAT. ###p<0.001, ####p=<0.0001 $CaSR^{Ad-/-}$ vs $CaSR^{Ad-/-}$ +PVAT. §p<0.05, §§§§p<0.0001 $CaSR^{fl/fl}$ +PVAT vs $CaSR^{Ad-/-}$ +PVAT. ACh=Acetylcholine; PE=Phenylephrine; PVAT=Perivascular adipose tissue; SNP=Sodium nitroprusside.

6.3.12 PVAT biology

In intact aortas, PVAT caused a significant increase in PE contraction in male $CaSR^{Ad-/-}$ aortas, but female $CaSR^{Ad-/-}$ aortas were insensitive to PVAT stimulation. To understand the mechanism(s) which may underpin altered vascular responses specifically in female $CaSR^{Ad-/-}$ mice, baseline CaSR mRNA expression was compared in male and female control $CaSR^{fl/fl}$ PVAT. CaSR mRNA levels in male mice (1.1±0.2-fold) were not altered compared to female counterparts (2.2±0.8-fold, p>0.05; Fig. 6-21a). To validate these findings, CaSR mRNA in were also investigated in male and female C57BL/6 mice. Again, CaSR mRNA expression in male PVAT (0.8±0.5-fold) was similar to that of females (1.5±0.6-fold, p>0.05; Fig. 6-21b).

As CaSR mRNA expression was unchanged between male and female $CaSR^{fl/fl}$ PVAT, mRNA expression of PVAT endocrine products were determined to see if these signalling pathways might explain altered PVAT-mediated PE contraction in female $CaSR^{Ad-/-}$ mice. PVAT regulates contractile vascular effects via a variety of bioactive substances including adipokines, prostanoids and reactive oxygen species (ROS), among others (Nava and Llorens, 2019), so mRNA expression of these mediators were investigated in the PVAT of female $CaSR^{Ad-/-}$ mice. eNOS and Angiotensin-converting enzyme (ACE), which regulate NO and angiotensin-II signalling respectively, were assessed along with non-adipokine mediators endothelin-1 (EDN-1) and prostacyclin (PGI_2). mRNA expression of eNOS, ACE, EDN-1and PGI_2 were unchanged in $CaSR^{Ad-/-}$ PVAT compared to $CaSR^{fl/fl}$ controls (p>0.05; Fig. 6-22a; Tb 6-3). Vasoactive adipokines adiponectin, apelin, leptin, omentin, resistin and visfatin were also assessed in $CaSR^{Ad-/-}$ PVAT, but mRNA levels were unchanged (p>0.05; Fig. 6-22b; Tb. 6-3).

Figure 6-21

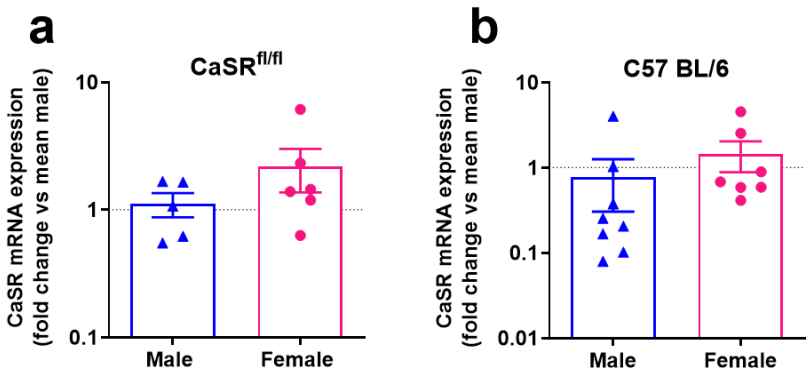

Figure 6-21: CaSR expression in male versus female PVAT in mice.

(a) CaSR mRNA expression in PVAT is comparable between male and female $CaSR^{fl/fl}$ mice. **(b)** CaSR mRNA expression in PVAT is comparable between male and female C57BL/6 mice. Mean±SEM. Unpaired t-test (a,b). PVAT=Perivascular adipose tissue.

Figure 6.22

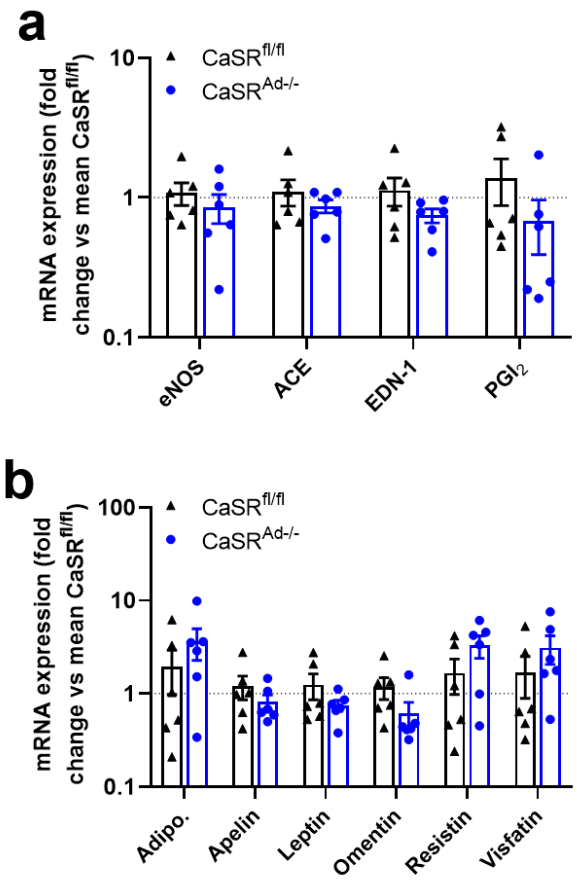

Figure 6-22: Gene expression of PVAT adipokines in female CaSR$^{Ad-/-}$ mice. **(a)** mRNA expression of eNOS, ACE, EDN-1 and PGI_2 is unaltered in CaSR$^{Ad-/-}$ PVAT compared to CaSR$^{fl/fl}$ controls. **(b)** mRNA expression of adipokines adiponectin (Adipo.), apelin, leptin, omentin, resistin and visfatin is unaltered in CaSR$^{Ad-/-}$ PVAT compared to CaSR$^{fl/fl}$ controls. Mean±SEM. Unpaired t-test (a,b). ACE=Angiotensin converting enzyme; EDN-1=Endothelin-1; eNOS=Endothelial nitric oxide synthase; PGI_2=Prostacyclin; PVAT=Perivascular adipose tissue.

Table 6-3

Gene target	$CaSR^{fl/fl}$	$CaSR^{Ad-/-}$	*p* -value
	(Mean fold change±SEM)		(*t* -test)
Non-adipokines			
eNOS	1.1±0.2	0.9±0.2	>0.05
ACE	1.1±0.2	0.9±0.1	>0.05
EDN-1	1.1±0.3	0.7±0.1	>0.05
PGI2	1.4±0.5	0.7±0.3	>0.05
Adipokines			
Adipo.	1.6±1.0	3.6±1.4	>0.05
Apelin	1.2±0.3	0.8±0.2	>0.05
Leptin	1.2±0.4	0.7±0.1	>0.05
Omentin	1.2±0.3	0.6±0.2	>0.05
Resistin	1.7±0.7	3.3±0.9	>0.05
Visfatin	1.7±0.8	3.1±1.1	>0.05

Table 6-3: Gene expression of PVAT adipokines in female $CaSR^{Ad-/-}$ mice.
Genes linked with PVAT endocrine signalling are unchanged in $CaSR^{Ad-/-}$ mice when compared to $CaSR^{fl/fl}$ controls. ACE=Angiotensin converting enzyme; EDN-1=Endothelin-1; eNOS=Endothelial nitric oxide synthase; PGI_2=Prostacyclin; PVAT=Perivascular adipose tissue.

6.3.13 gAT transfer studies

In female mice, PVAT increased maximal PE induced contraction in $CaSR^{fl/fl}$ aortas with intact endothelium, but this effect was not recapitulated in $CaSR^{Ad-/-}$ aortas. To dissect the mechanisms underpinning PVAT insensitivity in $CaSR^{Ad-/-}$ mice, adipose transfer studies were performed in aortas with intact endothelium using gAT.

As previously observed in section 6.3.11, PVAT acted to enhance PE-mediated contraction in control $CaSR^{fl/fl}$ aortas. Pilot studies in $CaSR^{fl/fl}$ aortas confirmed that gAT (from the same animal) had the same effect on vascular function, increasing contraction in response to PE. To characterise baseline vascular responses, an initial comparison of PE responses in $CaSR^{fl/fl}$ and $CaSR^{Ad-/-}$ aortas was performed in the absence of gAT. When compared to PE contraction in $CaSR^{fl/fl}$ aortas (pEC_{50}=6.6±0.2, E_{max}=55.5±4.1%), PE-mediated contraction in $CaSR^{Ad-/-}$ aortas was unaltered, as both pEC_{50} values and maximum PE contraction were similar (pEC_{50}=6.7±0.2, E_{max}=57.5±3.9%, p>0.05).

In the absence of gAT, PE induced contraction in $CaSR^{fl/fl}$ aortas (pEC_{50}=6.6±0.2, E_{max}=55.5±4.1%). When incubated with $CaSR^{fl/fl}$ gAT from the same animal, PE contraction in $CaSR^{fl/fl}$ aortas was enhanced, demonstrated by a significant increase in maximum PE induced contraction similar to that seen with PVAT (pEC_{50}= 6.8±0.1, E_{max}=78.2±4.6%, p<0.0001; Fig. 6-23a). To test whether adipocyte-specific CaSR deletion leads to altered gAT function, $CaSR^{fl/fl}$ aortas were incubated with gAT from $CaSR^{Ad-/-}$ mice. Unexpectedly, maximum PE contraction was also increased when $CaSR^{fl/fl}$ aortas were exposed to $CaSR^{Ad-/-}$ gAT (pEC_{50}= 6.9±0.2, E_{max}=90.1±6.3%, p<0.0001; Fig. 6-23a). Consistent with these data, the PE responses which were mediated by $CaSR^{fl/fl}$ gAT and $CaSR^{Ad-/-}$ gAT in $CaSR^{fl/fl}$ aortas were highly comparable (p>0.05; Fig 6-23a; Tb. 6-4).

As above, $CaSR^{fl/fl}$ gAT and $CaSR^{Ad-/-}$ gAT had a comparable effect on PE contraction in $CaSR^{fl/fl}$ aortas. Next, to test whether adipocyte-specific CaSR deletion impacted upon aortic function specifically, the effect of gAT was studied in $CaSR^{Ad-/-}$ aortas. In the absence of gAT, PE had a contractile effect in $CaSR^{Ad-/-}$ aortas (pEC_{50}=6.7±0.2, E_{max}=57.5±3.9%). In contrast to the response in $CaSR^{fl/fl}$ aortas, $CaSR^{fl/fl}$ gAT was unable to enhance PE contraction in $CaSR^{Ad-/-}$ aortas, as both maximum PE contraction and the pEC_{50} for PE were unaltered from baseline (pEC_{50}=6.8±0.1, E_{max}=59.7±3.5%, p>0.05; Fig. 6-23b). Again, in stark contrast to responses in $CaSR^{fl/fl}$ aortas, baseline PE responses in $CaSR^{Ad-/-}$ aortas were unchanged by $CaSR^{Ad-/-}$ gAT, which had no influence on maximum PE responses or the pEC_{50} for PE (pEC_{50}=6.7±0.2, E_{max}=54.0±5.7%, p>0.05; Fig. 6-23b). Collectively, neither $CaSR^{fl/fl}$ gAT or $CaSR^{Ad-/-}$ potentiated baseline PE contraction in $CaSR^{Ad-/-}$ aortas. Unsurprisingly, the PE contractile responses which were observed in $CaSR^{Ad-/-}$ aortas following $CaSR^{fl/fl}$ gAT or $CaSR^{Ad-/-}$ gAT were highly similar (p>0.05; Fig. 6-23b; Tb. 6-4).

$CaSR^{fl/fl}$ gAT and $CaSR^{Ad-/-}$ gAT increased PE contraction in $CaSR^{fl/fl}$ aortas. However, $CaSR^{Ad-/-}$ aortas were insensitive to both $CaSR^{fl/fl}$ gAT and $CaSR^{Ad-/-}$ gAT. As short-term AT treatments do not appear to alter vascular function, vascular reactivity could therefore be altered via changes in the aorta triggered by chronically dysregulated AT in $CaSR^{Ad-/-}$ mice. Therefore, mRNA expression of vasoactive mediators were interrogated in the aorta. As PVAT-mediated PE contraction in female $CaSR^{Ad-/-}$ mice was shown to differ depending on

endothelial integrity, the study focused on molecular mediators which are particularly relevant in endothelial function, namely those involved in NO signalling. Comparison of mRNA expression in $CaSR^{fl/fl}$ and $CaSR^{Ad-/-}$ aortas revealed no difference in eNOS, nor any differences in mediators which regulate the cellular response to NO, soluble guanylate cyclase (sGC)-1a, scGC1b and protein kinase G (PKG) ($p>0.05$; Fig. 6-24a; Tb. 6-4). To further interrogate the status of NO signalling in $CaSR^{Ad-/-}$ mice, molecular mediators of ROS signalling were also investigated Fig. 6-24b; Tb. 6-4). Prooxidant NADPH oxidases (NOX)-1 and NOX2 were unchanged in $CaSR^{Ad-/-}$ mice ($p>0.05$). The antioxidant catalase was also unaltered ($p>0.05$). $CaSR^{Ad-/-}$ aortas tended to show greater expression of antioxidant mediators superoxide dismutase (SOD; $p=0.0529$) and nuclear factor erythroid 2-related factor 2 (NRF2; $p=0.0709$), though this did not reach statistical significance. Further experiments are required to improve the statistical power of qPCR data examining SOD and NRF2 mRNA expression.

Figure 6-23

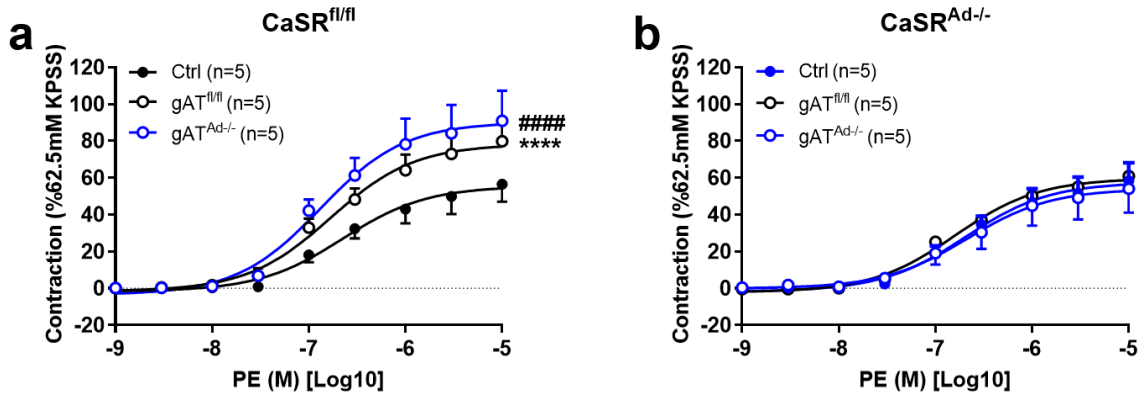

Figure 6-23: gAT-mediated vascular responses are altered in female $CaSR^{Ad-/-}$ mice.

(a) In vessels with intact endothelium (+E), maximum PE-mediated contraction in $CaSR^{fl/fl}$ control (ctrl) aortas is potentiated in the presence of $CaSR^{fl/fl}$ gAT and $CaSR^{Ad-/-}$ gAT. **(b)** In vessels with intact endothelium (+E), maximum PE-mediated contraction in $CaSR^{Ad-/-}$ control (ctrl) aortas is unaffected by incubation with $CaSR^{fl/fl}$ gAT or $CaSR^{Ad-/-}$ gAT. Mean ±SEM. F-test (a, b). ****p=<0.0001 $CaSR^{fl/fl}$ ctrl vs $CaSR^{fl/fl}$ gAT, ####p=<0.0001 $CaSR^{fl/fl}$ ctrl vs $CaSR^{Ad-/-}$ gAT. gAT=Gonadal adipose tissue; PE=Phenylephrine; PVAT=Perivascular adipose tissue.

Table 6-4

D-R Curve	PE (+E)		
	pEC_{50} ($-Log_{10}$)	E_{max} (%)	*p*
$CaSR^{fl/fl}$			
Ctrl	6.6±0.2	55.45±4.14	
$CaSR^{fl/fl}$ gAT	6.7±0.1	78.20±4.63	****
$CaSR^{Ad-/-}$ gAT	6.9±0.2	90.12±6.29	####
$CaSR^{Ad-/-}$			
Ctrl	6.7±0.2	57.51±3.89	
$CaSR^{fl/fl}$ gAT	6.8±0.1	59.67±3.46	
$CaSR^{Ad-/-}$ gAT	6.7±0.2	53.99±5.65	

Table 6-4: gAT-mediated vascular responses are altered in female $CaSR^{Ad-/-}$ mice.

Dose-response curves were conducted on aorta segments with intact endothelium (+E; >60% function preserved). Results are provided for PE dose-response curves in the absence (Ctrl) and presence of gAT. PE response is expressed as % contraction relative to the mean KPSS contraction. Mean ±SEM.). ****p=<0.0001 $CaSR^{fl/fl}$ ctrl vs $CaSR^{fl/fl}$ gAT, ####p=<0.0001 $CaSR^{fl/fl}$ vs $CaSR^{Ad-/-}$ gAT. gAT=Gonadal adipose tissue; PE=Phenylephrine.

Figure 6-24

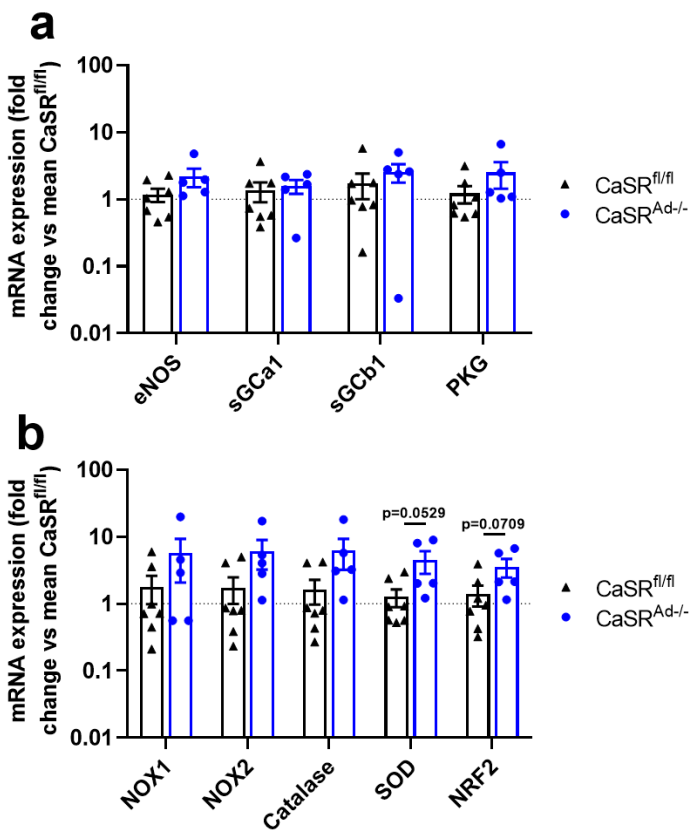

Figure 6-24: Gene expression of key signalling proteins in female CaSR$^{Ad-/-}$ aortas.

(a) mRNA expression of eNOS, sGCa1, sGCb1 and PKG is unaltered in CaSR$^{Ad-/-}$ aortas compared to CaSR$^{fl/fl}$ controls. **(b)** mRNA expression of mediators of ROS signalling mediators NOX1, NOX2, catalase, SOD and NRF2 is unaltered in CaSR$^{Ad-/-}$ aortas compared to CaSR$^{fl/fl}$ controls. Mean±SEM. Unpaired t-test (a,b). eNOS=Endothelial nitric oxide synthase; sGC=Soluble guanylate cyclase; NOX=NADPH oxidase; NRF2=Nuclear factor erythroid 2–related factor 2; PKG=Protein kinase G; ROS=Reactive oxygen species; SOD=Superoxide dismutase.

Table 6-5

Gene target	$CaSR^{fl/fl}$	$CaSR^{Ad-/-}$	*p* -value
	(Mean fold change±SEM)		(*t* -test)
NO signalling			
eNOS	1.2±0.3	2.2±0.7	>0.05
sGCa1	1.3±0.4	1.6±0.4	>0.05
sGCb1	1.7±0.7	2.6±0.8	>0.05
PKG	1.2±0.4	2.5±1.1	>0.05
ROS signalling			
NOX1	1.8±0.8	5.7±3.6	>0.05
NOX2	1.7±0.7	6.1±2.8	>0.05
Catalase	1.6±0.7	6.2±3.0	>0.05
SOD	1.3±0.4	4.5±1.7	0.0529
NRF2	1.4±0.5	3.6±1.1	0.0709

Table 6-5: Gene expression of key signalling proteins in female $CaSR^{Ad-/-}$ aortas.

Expression of several genes responsible for NO and ROS signalling are unaltered in $CaSR^{Ad-/-}$ mice when compared to $CaSR^{fl/fl}$ controls. Mean±SEM. eNOS=Endothelial nitric oxide synthase; sGC=Soluble guanylate cyclase; NOX=NADPH oxidase; NRF2=Nuclear factor erythroid 2–related factor 2; PKG=Protein kinase G; SOD=Superoxide dismutase.

6.3.14 Haemodynamic function

Female $CaSR^{Ad-/-}$ aortas are insensitive to PVAT- and gAT-mediated increases in PE induced contraction. To address whether attenuated vascular contraction affects haemodynamic function, blood pressure and heart rate were examined from 12-18 weeks of age in female $CaSR^{Ad-/-}$ mice using tail cuff plethysmography. At the beginning of the study, systolic blood pressure (SBP) was 117±3mmHg in $CaSR^{fl/fl}$ mice and 126±3mmHg in $CaSR^{Ad-/-}$. At 18-weeks, $CaSR^{fl/fl}$ and $CaSR^{Ad-/-}$ SBP was 119±3mmHg and 121±2mmHg. SBP was unaltered between groups throughout the study ($p>0.05$; Fig. 6-25a). In $CaSR^{fl/fl}$ mice, diastolic blood pressure (DBP) was determined as 64±4mmHg at the study outset and 76±5mmHg at the study end. Initial and final DBP measurements in $CaSR^{Ad-/-}$ were 68±4mmHg and 76±4mmHg respectively, comparable to $CaSR^{fl/fl}$ counterparts ($p>0.05$; Fig. 6-25b). Mean arterial blood pressure (MAP) at the beginning of the study was 82±4mmHg in $CaSR^{fl/fl}$ mice and 87±4mmHg in $CaSR^{Ad-/-}$. At the end of the study, $CaSR^{fl/fl}$ SBP was 90±3mmHg and $CaSR^{Ad-/-}$ SBP 91±3mmHg, with SBP across time comparable between groups ($p>0.05$; Fig. 6-25c). Heart rate (HR) at the study

outset was 539±23bpm in CaSR$^{fl/fl}$ mice and 588±17bpm in CaSR$^{Ad-/-}$. At 18-weeks, CaSR$^{fl/fl}$ and CaSR$^{Ad-/-}$ HR was determined as 587±13bpm and 576±12bpm respectively and was not different between groups ($p>0.05$) (Fig. 6-25d).

Figure 6-25

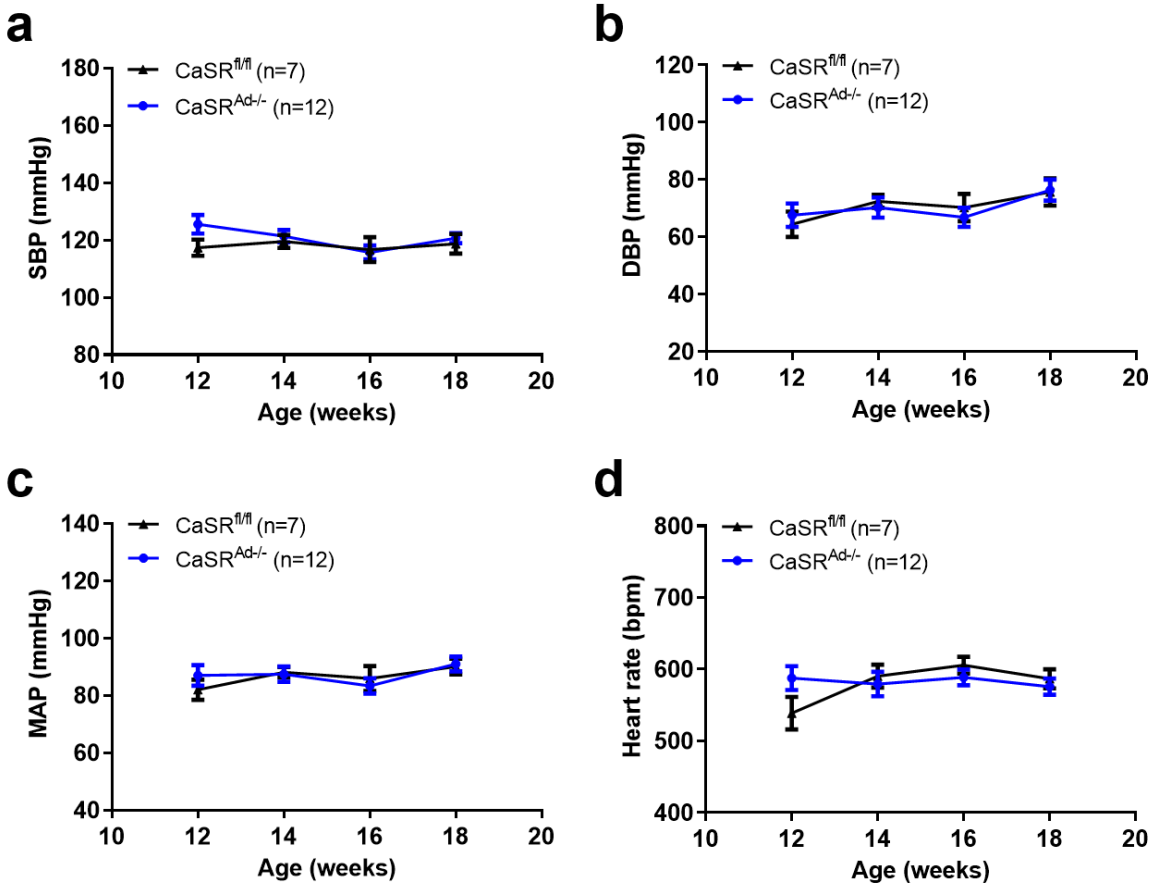

Figure 6-25: Haemodynamic function in female CaSR$^{Ad-/-}$ mice.

(a) Compared to CaSR$^{fl/fl}$ controls, CaSR$^{Ad-/-}$ mice show no difference in SBP **(b)** DBP **(c)** MAP **(d)** or HR. Mean±SEM. Two-way ANOVA (a-d). DBP=Diastolic blood pressure, HR=Heart rate, MAP=Mean arterial blood pressure, SBP=Systolic blood pressure.

6.4 Discussion

6.4.1 Adipocyte-specific CaSR deletion

To interrogate the effect of reduced adipocyte CaSR activity *in vivo*, this study examined mice with adipocyte-targeted, Cre recombinase-driven deletion of CaSR. This model was generated based on the CaSR exon 3, LoxP floxed mouse developed by Toka et al. (2012) utilising the Adipoq(adiponectin)-Cre developed by Eguchi et al. (2011). Excision of exon 3 and the neomycin cassette was demonstrated in gAT and scAT, but was in lacking in mice without Cre recombinase expression, confirming successful recombination. CaSR-postneo bands were broadly absent in lung homogenate, demonstrating that Cre-mediated exon 3 deletion was restricted to adipocytes. As adiponectin production has been described in mesenchymal stem cell lineages (Mukohira *et al.*, 2019), BMSCs were examined for ectopic Cre expression and inappropriate CaSR deletion. CaSR-postneo bands were again absent across all groups, suggesting that CaSR is preserved in non-targeted tissues.

To confirm that genetic disruption of CaSR exon 3 in targeted tissues leads to a decline in CaSR, mRNA and protein expression were assessed in gAT adipocytes. Surprisingly, CaSR protein levels tended to be decreased in $CaSR^{Ad-/-}$ mice, though the difference was not statistically significant. It is unclear why differences in protein levels were not evident in this study. The original investigation responsible for developing the murine CaSR exon 3 deletion model demonstrated robust, kidney-specific deletion of CaSR protein (Toka *et al.*, 2012). However, they used an antibody targeted toward a short sequence (amino acids 214-235) encoded by CaSR exon 4. In contrast, the antibody used here may demonstrate immunoreactivity towards a longer sequence (amino acids 200-300). Several examples of CaSR splice variants lacking exon 3 have been reported previously (Breitwieser, 2012). Possibly, exon 3 deletion gives rise to a mutant form of CaSR, which when translated produces a protein which remains partially detectable by immunoreactivity assays used here. However, this would need to be examined in further studies. Irrespective, successful genomic recombination of CaSR exon 2-exon 4 in addition to reduced mRNA expression of CaSR was considered sufficient evidence of CaSR deletion in $CaSR^{Ad-/-}$ adipocytes.

Intending to characterise $CaSR^{Ad-/-}$ mice, sex, genotype and mortality were assessed in offspring generated from $CaSR^{fl/fl}$ x $CaSR^{Ad-/-}$matings. These matings resulted in a greater proportion of female pups, suggesting that female embryo survival may be favoured *in utero*. Despite these findings, the genotypic distribution of female as well as male pups aligned with an expected distribution of 50%, suggesting that offspring genotype and thus adipocyte-specific CaSR deficiency does not contribute significantly towards an increased birth rate of female pups or general embryonic development. Maternal nutritional status and AT health also influences foetal development (Moreno-Mendez *et al.*, 2020). To establish whether maternal adipocyte CaSR deficiency could influence offspring viability, offspring mortality rate was investigated in litters derived from $CaSR^{Ad-/-}$ mothers and $CaSR^{Ad-/-}$ fathers. However, there was no evidence that offspring mortality was related to parental adipocyte-CaSR deficiency. Though more female mice were generated as a result of this study, the mechanism(s) responsible are unclear.

6.4.2 Fat accumulation and adipocyte biology

CaSR activation increases adipocyte proinflammatory cytokine expression, alters lipid handling and mediates adipogenesis; these observations underpin the proposition that CaSR signalling may act as mechanistic link between obesity, adipose dysfunction and cardiometabolic derangement (Bravo-Sagua *et al.*, 2016). Thus, reduced CaSR activity might regulate adipocyte biology and adipose accumulation *in vivo*. When measured across time, body weight was found to be reduced by ~5% in female $CaSR^{Ad-/-}$ mice. This would suggest that adipocyte CaSR signalling plays a role in body weight regulation. Interestingly, although absolute weight differed in $CaSR^{Ad-/-}$ mice, % growth across the study period was unchanged. As CaSR deficiency had no impact on body weight accumulated after 5-weeks of age, it is likely that reduced body weight in female $CaSR^{Ad-/-}$ mice is established before the study outset. This may be related to adipocyte maturation timelines in developing mice. For example, differentiation of scAT adipocytes is initiated during embryonic days 14-18 and continues until 8-weeks of age. On the other hand, gAT adipocyte commitment occurs postnatally, with many adipocytes reaching maturation by postnatal week 4 (Wang *et al.*, 2013). These data suggest that adipocyte CaSR deletion would be established by 4-8

weeks of age, since Adipoq-Cre-mediated CaSR deletion only occurs upon expression of adiponectin in mature adipocytes. The importance of CaSR signalling in body weight regulation may then vary depending on perinatal developmental stage, perhaps demonstrating greater significance during earlier points where adipocytes initially mature. In a recently generated murine model of adipocyte-specific CaSR deletion, weight was unaltered (Sundararaman *et al.*, 2021). However, this analysis was performed on cohorts of both sexes. Given that male and female weights were significantly different in the present study, the weight data provided by Sundararaman et al. is likely confounded. Further, the Sundararaman lab used a tamoxifen-inducible system to promote adipocyte CaSR deletion conditionally in mice aged 8-10-weeks of age. Based on the data presented in the present study, CaSR deficiency would not be predicted to significantly influence body weight at this late developmental stage. Accordingly, the present study is the first to report that adipocyte CaSR regulates body weight in female mice *in vivo*.

The primary hallmarks of adipogenesis are increased adipocyte number (hyperplasia) and increased adipocyte size (hypertrophy); while healthy adipose function can be preserved via hyperplasic responses, adipocyte hypertrophy is considered to be maladaptive (Oikonomou and Antoniades, 2019). To investigate the physiological significance of adipocyte CaSR, this study examined whether decreased weight in $CaSR^{Ad-/-}$ mice was correlated with altered adiposity and adipocyte morphology. Inconsistent with the finding that body weight is reduced in female $CaSR^{Ad-/-}$ mice, individual fat pad mass was unchanged. However, small differences in AT mass may not be distinguishable when assessed by simple weighing of AT depots. Compared to $CaSR^{fl/fl}$ mice here, previous studies demonstrate similar body weight in 21 week old female C57BL/6 mice. Notably, DEXA scanning determined that these mice possess 15.7% total body fat (Gargiulo *et al.*, 2014). In $CaSR^{fl/fl}$ mice, gAT (0.39g) and scAT (0.36g) contribute 3.1% to overall mass. Based on the work by Gargiulo et al., the AT depots examined here would comprise only ~20% of total fat mass. At the timepoint where this study examines fat mass, $CaSR^{Ad-/-}$ body weight is ~3% lower than $CaSR^{fl/fl}$ counterparts. Assuming that reduced body weight in $CaSR^{Ad-/-}$ mice is underpinned by decreased AT, then scAT and gAT mass may only be reduced by 0.6%. Thus, subtle reductions in adipose accumulation caused by CaSR deficiency might not

be detectable without a comprehensive assessment of total body fat in $CaSR^{Ad-/-}$ mice.

In chapter 4, this study demonstrated that the CaSR activator cinacalcet and the positive allosteric modulator NPS-R568 causes hypertrophy in 3T3-L1 adipocyte-like cells. As CaSR activity promotes adipocyte expansion, this study wanted to examine whether adipocyte size could be regulated *in vivo* by CaSR. Decreased weight in female $CaSR^{Ad-/-}$ mice occurred alongside reduced adipocyte size and increased cell number in gAT depots, suggesting that adipocyte phenotype is controlled by CaSR. This study therefore provides the first evidence that CaSR influences adipocyte morphology *in vivo*. Adipocyte size is an important determinant of adipocyte function. For instance, increased adipocyte size is correlated with enhanced lipid accumulation, inflammatory stress, insulin resistance and cell death in cardiometabolic disorders (Oikonomou and Antoniades, 2019). On the other hand, obesity resolution therapies which decrease adipocyte size coincide with improved metabolic function. Reduced adipocyte inflammation and lipid content may play a role in this effect (Stenkula and Erlanson-Albertsson, 2018). Though adipocyte size is important in the obese state, adipocyte size is also linked with physiological function. In gAT adipocytes derived from lean rats, expression of lipolytic enzymes and lipolytic capacity are decreased in small compared to large cells (Farnier *et al.*, 2003), implying that physiological variation in cell size can regulate adipocyte function under non-pathological conditions. As such, CaSR regulation of adipocyte size could have important implications for adipocyte function in health and disease.

Body weight and adipocyte size was decreased in female $CaSR^{Ad-/-}$ mice, but adipocyte-specific deletion was not similarly associated with decreased body weight or adipocyte size in male mice. These data suggest that adipocyte CaSR regulation of body composition and adipocyte biology could be less significant in males. Interestingly, though adipocyte CaSR mRNA expression was comparable between sexes, decreased body weight was linked with increased fat pad mass in female $CaSR^{fl/fl}$ mice. Differences in AT distribution, quantity, metabolism and hormonal/autonomic inputs contribute to sex-dependent differences in adipose function and wider metabolism (Fuente-Martín *et al.*, 2013). Therefore, sex-dependent differences in the effect of CaSR deficiency may be explained by the

greater abundance of AT and comparatively enlarged adipocytes at baseline in female mice compared to male counterparts, rather that differences in CaSR expression. The impact of CaSR deletion appears more significant in female mice, but it should be noted that these data are gathered in murine models under physiological conditions. Though the link between adipose accumulation and cardiovascular risk is well recognised, this paradigm has shifted markedly rapidly in recent years to accommodate a growing consensus that AT phenotype plays a crucial role in cardiovascular risk. For instance, visceral fat expansion tends to correlate with harmful cardiometabolic outcomes, but some fat depots, particularly those located in gluteal and femoral regions, may confer cardioprotection (Kwok, Lam and Xu, 2016). Though females typically accrue subcutaneous rather than visceral fat, the opposite is true of males. Consequentially, sex-specific differences in mammalian adipose distribution has important implications for adipose-associated cardiovascular risk (Fuente-Martín *et al.*, 2013). Though this study found that adipocyte size was reduced in female gAT, a visceral AT depot, subcutaneous AT adipocytes were not assessed. As visceral and subcutaneous AT have opposing influences on cardiovascular health, the role played by CaSR could also be substantially different between sexes in the context of adiposopathy and the development of cardiovascular disease. Supporting the idea that CaSR function could be sexually dimorphic in disease states, sex-dependent CaSR effects are traceable in clinical studies which examine the therapeutic lowering effect of cinacalcet on parathyroid hormone (PTH) in secondary hyperparathyroidism (Peter *et al.*, 2015). Though anecdotal, cinacalcet induced PTH reduction was greatest in groups predominated (>50%) by women, suggesting that the biological significance of parathyroid CaSR in disease could be greater in females versus males. Though CaSR has not been directly examined in the context of obesity, data presented here underscores the need to examine cohorts of both sexes in future investigations.

Cellular lipogenesis describes the process by which fatty acids are synthesised from carbohydrate substrates, then subsequently converted to triglyceride esters (Saponaro *et al.*, 2015). PPARγ and SREBP1 regulate lipogenesis via recruitment of genes involved in fatty acid biosynthesis and lipid handling (Rosen, Eguchi and Xu, 2009). Downstream, FASN and ACC1 mediate fatty acid synthesis (Saponaro *et al.*, 2015), while FABP4 (aP2) is involved in intracellular lipid

mobilisation (Furuhashi *et al.*, 2014). Previous studies suggest that CaSR regulates lipogenesis, as CaSR stimulation induces expression of PPARγ and FABP4 in SW82 adipocytes (He *et al.*, 2012). Consequentially, reduced CaSR activity *in vivo* may associate with decreased recruitment of PPARγ and its transcriptional activities in adipocytes. To investigate the effect of CaSR deficiency on adipocyte phenotype, this study examined gene expression in $CaSR^{Ad-/-}$ gAT adipocytes. However, mRNA expression of lipogenic mediators, including PPARγ, were broadly unchanged in $CaSR^{Ad-/-}$ adipocytes. These findings are not consistent with the effect of CaSR deficiency on adipocyte size, since decreased adipocyte size might be expected to coincide with reduced lipid accumulation and altered metabolism. As previously discussed, CaSR is implicated in body weight regulation, though its influence on weight seems negligible in mice beyond 5-weeks of age. In line with this observation, gAT adipocyte maturation is largely completed in mice 4-weeks of age (Wang *et al.*, 2013). If CaSR plays a more significant role in adipocyte biology at early developmental timepoints, then alterations in lipogenic and metabolic mediators might not be expected at the 18-22 week timepoint studied here. Another possible explanation could be that CaSR does not actively regulate these lipogenic mediators under physiological conditions. Studies demonstrating the effect of CaSR on lipogenic gene expression observe increased PPARγ expression following stimulation with orthosteric CaSR agonists such $GdCl_2$ (He *et al.*, 2012). Although this study associates CaSR activation and lipogenesis, it reveals little about CaSR signalling in adipocytes under resting, basal conditions. Interestingly, obesity elevates serum $[Ca^{2+}]_o$ in rat (Hakkak, Kaufmann and Stack, 2019), suggesting that adipocyte CaSR stimulation may be enhanced in the obese state. Possibly, increased lipogenic gene expression could be evident during the development of obesity in the context of raised circulating $[Ca^{2+}]_o$. Taken together, CaSR may impose greater effects on lipogenic gene expression under pathological compared to physiological conditions. Curiously, UCP-1 mRNA expression was highly variable in $CaSR^{Ad-/-}$ adipocytes, but frequently low in $CaSR^{fl/fl}$ adipocytes. UCP-1 is a key mediator of lipid catabolism in adipocyte mitochondria, particularly in metabolically active brown AT (Kwok, Lam and Xu, 2016). In mice, brown AT transplantation and increased white AT expression of UCP-1 (i.e. beiging) is linked with weight loss (Oikonomou and Antoniades, 2019). Though UCP-1 expression was not significantly altered in $CaSR^{Ad-/-}$ mice, there

could be a biological effect. This observation warrants further interrogation of UCP-1 and its transcriptional activities in future work. To further examine the effect of CaSR deletion on adipocyte biology, future studies should examine gene expression in $CaSR^{Ad-/-}$ adipocytes during early postnatal stages where gAT adipocytes begin to reach maturation.

Through $[Ca^{2+}]_i$ and cAMP second messenger pathways, CaSR regulates key intracellular signalling enzymes, such as CAM, PGE_2, $ERK_{1/2}$ and AKT, among others (Gerbino and Colella, 2018). To investigate the effect of adipocyte CaSR deficiency on adipocyte biology, this study examined total and phosphorylated $ERK_{1/2}$ and $CaSR^{Ad-/-}$ gAT adipocytes but found the enzyme to be unmodified. In chapter 4, this study showed that $ERK_{1/2}$ activation in 3T3-L1 adipocytes is strongly regulated by $[Ca^{2+}]_o$, but is unchanged following (short term) CaSR stimulation. However, adipocytes isolated from gAT show decreased total $ERK_{1/2}$ and reduced $ERK_{1/2}$ activation in small relative to large adipocytes (Farnier *et al.*, 2003), suggesting that cell size is associated with $ERK_{1/2}$ signalling *in vivo*. Accordingly, unchanged $ERK_{1/2}$ activation does not align with the previous finding here that cell size is decreased in $CaSR^{Ad-/-}$ adipocytes. In mice, genetic deletion of ERK_1 in fibroblasts and preadipocytes leads to decreased adipose, adipocyte size and differentiation (Bost *et al.*, 2005). Interestingly, $ERK_{1/2}$ signalling in LS14 preadipocytes plays a role in cinacalcet induced inflammatory signalling (D'Espessailles *et al.*, 2018) and proliferation (Rocha *et al.*, 2015). Though $ERK_{1/2}$ signalling seems relevant in preadipocytes, this pathway may be less significant in mature adipocytes. As such, the importance of CaSR induced $ERK_{1/2}$ signalling may be limited to adipocyte progenitors.

6.4.3 Lipid metabolism and adipokines

In vitro, CaSR lowers glycerol release and decreases expression of lipolytic enzymes in SW872 adipocytes (He, Zhang, *et al.*, 2011), suggesting that CaSR activity supports lipid retention in adipocytes. Subsequent work in SW872 adipocytes demonstrated that CaSR signalling raises PPARγ and CCAAT/enhancer-binding-protein (C/EBPα) expression, which is linked with lipogenesis (He *et al.*, 2012). Collectively, these data suggest that CaSR activation favours lipid accumulation. To assess whether adipocyte CaSR regulates lipid handling *in vivo*, this study examined the status of plasma lipids

in $CaSR^{Ad-/-}$ mice. Though circulating FFA levels remained constant, triglycerides were in contrast significantly lowered in female $CaSR^{Ad-/-}$ plasma, suggesting that adipocyte CaSR influences circulating lipid levels. Interestingly, human studies report that scAT adipocyte lipolysis determines 15% of individual plasma triglyceride variability, suggesting that adipocyte-specific lipid handling is an important mechanism contributing to systemic lipid levels (Rydén and Arner, 2017). Therefore, reduced plasma triglyceride levels in $CaSR^{Ad-/-}$ may arise through altered intracellular lipid handling at the level of the adipocyte. In previous studies, the role played by CaSR in regulating intracellular triglyceride levels in adipocytes has not been intensively investigated and is somewhat unclear. In preadipocytes, triglyceride accumulation is potentiated by $GdCl_3$ during differentiation, while siRNA targeting of CaSR reverses this effect (Cifuentes and Rojas, 2008). However, others report the opposite effect in mature adipocytes, which show reduced intracellular triglyceride levels in response to cinacalcet (Villarroel *et al.*, 2016). While decreased cell size in $CaSR^{Ad-/-}$ adipocytes would be consistent with lowered intracellular triglyceride content, this link remains speculative since the effect of adipocyte CaSR deletion on intracellular lipid levels was not examined here. Aside from directly influencing lipid handling in adipocytes, CaSR deficiency may also impact on systemic lipid levels by altering adipocyte secretion. Lipoprotein lipase (LPL) is the major enzyme responsible for degrading circulating triglycerides and is strongly expressed in AT (Klop, Elte and Cabezas, 2013) and is decreased by CaSR activity in LS14 adipocytes (Villarroel *et al.*, 2016). Therefore, adipocyte CaSR deficiency may decrease plasma triglycerides by elevating adipocyte LPL secretion and increasing systemic triglyceride degradation. Metabolic dysregulation is characterised by excess circulating triglycerides (hypertriglyceridemia) as well as raised FFAs (Kolovou, Anagnostopoulou and Cokkinos, 2005). However, plasma FFAs were not influenced by adipocyte CaSR deficiency here. Hypertriglyceridemia is proposed as the predominant driving mechanism in dyslipidaemia (Klop, Elte and Cabezas, 2013), so altered triglyceride levels may precede raised circulating FFAs and thus represent a more sensitive marker of metabolic status. Systemic triglyceride concentrations independently predict cardiovascular risk (Kolovou, Anagnostopoulou and Cokkinos, 2005). In $CaSR^{fl/fl}$ mice, plasma triglyceride levels (1.5nmol/uL /132.6mg/dL) are similar to those reported in healthy C57BL/6 mice (130mg/dL)

and that of dyslipidemic humans (154mg/dL) (Yin *et al.*, 2012). In the present study, adipocyte-specific CaSR deficiency reduced circulating triglycerides by 27%, which could prove significant in the context of human cardiometabolic disorders. However, future studies should assess intracellular triglyceride levels alongside LPL expression in mature adipocytes to probe the link between adipocyte $CaSR^{Ad-/-}$ deficiency and systemic triglyceride levels *in vivo*.

In obesity, adipocyte cell enlargement associated with a shift in secretory function, particularly that of key adipokines such as adiponectin and leptin (Oikonomou and Antoniades, 2019). In chapter 4, cinacalcet mediated stimulation of CaSR increased leptin secretion in 3T3-L1 cells. To test whether adipocyte CaSR deficiency regulates adipokine balance in *vivo*, adiponectin and leptin production were examined in $CaSR^{Ad-/-}$ mice. In this study, adiponectin and leptin mRNA and protein levels were unaltered in $CaSR^{Ad-/-}$ gAT adipocytes, while plasma levels were similarly unchanged. Adiponectin and leptin are involved in physiological adipocyte function, but their respective anti- and pro-inflammatory roles are especially important in CVD pathogenesis (Ha and Bauer, 2018). Although CaSR does not regulate adipocyte adipokine secretion under physiological conditions, these data do not preclude a role for CaSR in adipokine regulation during states of metabolic stress. Future studies in $CaSR^{Ad-/-}$ mice should therefore re-examine adiponectin and leptin following an obesity challenge to ascertain whether adipocyte CaSR deficiency modulates adipocyte adipokine secretion under pathological conditions.

6.4.4 Vascular function

To assess the importance of adipocyte CaSR in vascular function, this study examined aortic responses in $CaSR^{Ad-/-}$ mice. In both male and female $CaSR^{fl/fl}$ mice, PVAT increased PE induced vascular contraction and attenuated ACh endothelial-dependent and SNP endothelial-independent vascular relaxation. PVAT is a well-recognised mediator of vascular function. Though frequently associated with anticontractile vascular effects, PVAT can also be procontractile. PVAT-mediated contractile effects in the vasculature have been ascribed to its production of angiotensin-II, serotonin, noradrenaline, prostanoids, cytokines, ROS and adipokines (Ramirez, O'Malley and Ho, 2017; Chang, Garcia-Barrio and Chen, 2020). PVAT also expresses vasoactive contractile factors such as EDN-1

(Nava and Llorens, 2019). Accordingly, this study examined the effect of adipocyte-specific CaSR deficiency on PVAT-mediated contraction. Upon examination of PVAT vascular responses, the PVAT-mediated increase in PE contraction seen in intact $CaSR^{fl/fl}$ aortas was not conserved in $CaSR^{fl/fl}$ aortas with endothelial denudation, suggesting a critical role for the endothelium in PVAT-mediated enhancement of PE contraction. In contrast, PVAT did not influence contraction in intact $CaSR^{Ad-/-}$ aortas, suggesting that the mechanism(s) responsible for PVAT-mediated vascular contraction are blunted in $CaSR^{Ad-/-}$ mice. Interestingly, this effect was not reproduced in male $CaSR^{Ad-/-}$ aortas, indicating that adipocyte CaSR deletion impacts on vascular function, but specifically in females.

As aforementioned, PVAT-mediated contractile responses in $CaSR^{fl/fl}$ aortas were abolished following endothelial denudation, suggesting that the endothelium plays a key role in PVAT-mediated vascular contraction. Given the importance of EC function in PVAT-mediated vascular responses, PVAT-mediated responses in $CaSR^{fl/fl}$ and $CaSR^{Ad-/-}$ aortas were expected to be comparable in denuded aortas. Interestingly, instead of having no effect in $CaSR^{Ad-/-}$ aortas, PVAT-mediated PE contraction was decreased with denudation $CaSR^{Ad-/-}$ aortas. Importantly, the difference in PVAT-responses between $CaSR^{fl/fl}$ and $CaSR^{Ad-/-}$ aortas seen in intact vessels was conserved following endothelial denudation. Given that PVAT-mediated contractility is lost following endothelial removal, these data suggest that adipocyte-specific CaSR deficiency has an anticontractile effect on PVAT-mediated responses through additional, VSMC mediated mechanisms. Taken together, adipocyte CaSR deficiency augments PVAT-vascular signalling, indicating a role for adipocyte CaSR in vascular regulation *in vivo*. Though this effect may be primarily mediated by ECs, VSMC function is also impacted by adipocyte-specific CaSR deficiency.

As previously discussed, PVAT can mediate contractile vascular effects via a variety of bioactive substances including adipokines, prostanoids and ROS species, among others (Nava and Llorens, 2019). These mediators represent possible candidates through which PVAT regulates contractile effects in the present study. To test whether PVAT function was augmented by adipocyte CaSR deficiency in

female mice, mRNA levels of eNOS, EDN-1, ACE and PGI_2 were assessed in $CaSR^{Ad-/-}$ PVAT, but were not altered. A comprehensive panel of adipokines were also examined, but mRNA levels were similarly unchanged. Despite these findings, CaSR could regulate vasoactive mediators by controlling intracellular protein handling and secretion. For instance, catabolism of inactive big endothelin to active ET-1 is tightly regulated by endothelin converting enzyme. The expression, intracellular transport and cell surface trafficking of endothelin converting enzyme is dependent on its phosphorylation by protein kinase C (Kuruppu and Smith, 2012), a known target of CaSR (Conigrave and Ward, 2013). Plausibly, adipocyte CaSR could regulate paracrine PVAT activities *in vivo* by altering post-translational processing, such as trafficking to the cell surface, which in turn could modify adipocyte secretion.

Many procontractile factors produced by PVAT are also generated by peripheral AT (Nava and Llorens, 2019). To dissect the mechanisms underpinning PVAT insensitivity in $CaSR^{Ad-/-}$ mice, fat transfer studies were performed with gAT using aortas possessing intact endothelium. An initial comparison of $CaSR^{fl/fl}$ and $CaSR^{Ad-/-}$ aortic responses showed no difference in PE contraction, indicating that adipocyte-specific CaSR deficiency does not affect aortic contraction in the unstimulated state. Interestingly, while gAT isolated from $CaSR^{fl/fl}$ and $CaSR^{Ad-/-}$ mice increased PE contraction in $CaSR^{fl/fl}$ aortas, PE contraction was not enhanced by either $CaSR^{fl/fl}$ or $CaSR^{Ad-/-}$ gAT in $CaSR^{Ad-/-}$ aortas. As $CaSR^{fl/fl}$ responded similarly to both gAT preparations, acute AT function is preserved in $CaSR^{Ad-/-}$ gAT. On the other hand, $CaSR^{Ad-/-}$ aortas were completely insensitive to both $CaSR^{fl/fl}$ and $CaSR^{Ad-/-}$ gAT preparations, suggesting that the mechanism(s) controlling the aortic response to AT are chronically impaired in $CaSR^{Ad-/-}$ aortas. Accordingly, rather than directly influencing (acute) AT secretion, these data would instead suggest that adipocyte CaSR deletion modifies the aortic response to AT chronically, which in turn attenuates the contractile effect of AT.

To investigate the mechanism(s) underpinning chronically impaired AT responses in $CaSR^{Ad-/-}$ aortas, this study examined aortic mRNA expression. Due to the clear importance of endothelial function in $CaSR^{Ad-/-}$ responses, investigations were targeted towards key mediators and effectors of endothelial signalling, specifically those involved in NO signalling pathways. eNOS was unchanged in

this study, suggesting NO production is not modified in $CaSR^{Ad-/-}$ aortas. sGCa1 and -b1 and PKG which are recruited downstream of NO and were similarly unaffected. ROS species mediate vascular tone directly via stimulation of vascular cells and indirectly by sequestering NO (Touyz and Briones, 2010), so ROS mediators were also interrogated. Prooxidant enzymes NOX1 and NOX2 as well as the antioxidant catalase were unchanged in $CaSR^{Ad-/-}$ aortas. Though non-significant, both SOD (p=0.0529) and NRF2 (p=0.0709) tended to be raised in $CaSR^{Ad-/-}$ aortas. SOD is considered to be an important antioxidant system within the vascular wall due to its role in the conversion of reactive superoxide to hydrogen peroxide (Touyz and Briones, 2010). Meanwhile, NRF2 exerts significant antioxidant actions in the vasculature via its key role in regulating the transcription of ROS-related genes (Satta *et al.*, 2017). Therefore, increased SOD and NRF2 expression would be expected to mediate beneficial effects in the vasculature. Indeed, decreased oxidant stress and/or increased NO bioavailability would be consistent with anticontractile properties observed in $CaSR^{Ad-/-}$ aortas. Though this study was unable to demonstrate that these mediators were altered, the present findings warrant further examination of ROS status in $CaSR^{Ad-/-}$ aortas in future work.

PVAT-mediated PE contraction was attenuated in female $CaSR^{Ad-/-}$ aortas, but this effect was not similarly evident in males, suggesting that adipocyte CaSR signalling is comparably less significant in male vascular reactivity. Earlier in this chapter, body weight and adipocyte size were shown to be reduced in female $CaSR^{Ad-/-}$ mice. As discussed previously, smaller adipocytes are associated with improved adipocyte function, which could be linked to the vascular effects of adipocyte-specific CaSR deficiency in females. As with gAT adipocytes, sexually dimorphic CaSR expression was not evident in C57BL/6 or $CaSR^{fl/fl}$ PVAT. Accordingly, sex-dependent differences in vascular function during adipocyte CaSR deficiency likely arise due to baseline differences in AT between male and female mice, which in turn would augment CaSR signalling outputs. Due to its proximity to the vasculature, PVAT derived paracrine signalling is an influential determinant of vascular reactivity. However, vascular function is also amenable to circulating endocrine factors arising from peripheral AT depots (Oikonomou and Antoniades, 2019). This study has determined that aortic function is chronically impacted by adipocyte CaSR deficiency, but it is unclear whether

this effect occurs due to altered PVAT function, altered systemic AT function, or both.

Despite the identification of altered vascular function is $CaSR^{Ad-/-}$ mice, this does not appear to impact haemodynamic function, since BP and HR were comparable between $CaSR^{Ad-/}$ mice and $CaSR^{fl/fl}$ counterparts. However, this might be expected given that $CaSR^{fl/fl}$ and $CaSR^{Ad-/-}$ aortic responses are comparable in the absence of AT and that adipocyte $CaSR^{Ad-/-}$ deficiency impacts specifically on the vascular response to AT. As such, a difference in $CaSR^{Ad-/-}$ BP may only become apparent following a haemodynamic challenge, especially that in which AT is implicated in the vascular response. In myography studies, a key role for CaSR has been identified in VSMC contraction (Schepelmann *et al.*, 2016) and EC-mediated vasodilation (Greenberg, Shi, *et al.*, 2016). While other data contradict these studies (Thakore and Vanessa Ho, 2011; Loot *et al.*, 2013), they nonetheless demonstrate an important role for CaSR signalling in maintaining vascular tone. In the present study, adipocyte CaSR deficiency exerted an anticontractile effect AT mediated contraction, suggesting that adipocyte CaSR signalling may act to enhance procontractile AT signalling *in vivo*. Clearly, a greater understanding of VSMC-, EC- and adipocyte-specific CaSR effects is required to fully delineate the role of CaSR in vascular (patho)biology.

6.5 Conclusions

In summary, adipocyte-specific CaSR deletion results in decreased body weight and decreased adipocyte size in female mice. Inconsistent with its effect on cell size, CaSR did not influence PPARγ and its transcriptional targets in female $CaSR^{Ad-/-}$ adipocytes. However, CaSR regulation of lipogenic mediators may be more significant during earlier developmental timepoints, or in the context of pathology. Future investigations should examine lipogenic mediators earlier in perinatal development, perhaps focusing on the role UCP-1, which was highly variable in $CaSR^{Ad-/-}$ adipocytes. In female mice, reduced body weight and adipocyte size was associated with decreased plasma triglyceride levels, possibly arising due to altered adipocyte lipid handling or secretion of LPL. $CaSR^{Ad-/-}$ aortas demonstrated blunted responses to PVAT and gAT, indicating that CaSR may regulate the vascular response to AT. This effect was thought to arise due to chronic alteration of aortic vascular reactivity caused by long term depletion of CaSR in adipocytes, since $CaSR^{fl/fl}$ and $CaSR^{Ad-/-}$ gAT produced comparable responses in $CaSR^{fl/fl}$ aortas. Impaired vascular contractility in female $CaSR^{Ad-/-}$ mice may be linked to aortic ROS balance, though further work is required to explore the role of ROS signalling in $CaSR^{Ad-/-}$ vascular function. Body weight, adipocyte size and vascular function were unchanged in male mice. Collectively, these findings suggest that CaSR plays an important role in regulating adipocyte size, systemic lipid balance and vascular function in mice, but the biological significance of CaSR is greater in females versus males.

Chapter Seven

General Discussion

Chapter 7: General Discussion

7.1 Summary of results

Adipose is a highly complex tissue capable of regulating a variety of endocrine and metabolic functions. Derangement of adipocyte function leading to adipose tissue (AT) and metabolic dysfunction is a key etiological mechanism driving the elevation of cardiovascular disease (CVD) risk factors and CVD itself (Oikonomou and Antoniades, 2019). The calcium-sensing receptor (CaSR) has been identified in a variety of adipocyte model cell lines where it has been shown to play a role in adipocyte biology (Cifuentes, Albala and Rojas, 2005; Bravo-Sagua *et al.*, 2016). However, the biological relevance of adipocyte CaSR in the context of AT physiology and cardiovascular function had not been well explored.

Previous studies have shown that L-amino acids can act as allosteric modulators at CaSR (Conigrave, Quinn and Brown, 2000), but CaSR signalling pathways invoked by L-amino acids are not well characterised. The amino acid asymmetric dimethyl arginine (ADMA) is thought to invoke its biological effects via inhibition of endogenous nitric oxide (NO) production (Leone *et al.*, 1992). However, recent studies in our lab examining the effect of ADMA in 3T3-L1 adipocytes found that ADMA stimulated NO-independent cellular hypertrophy. Interestingly, the response could be recapitulated by the CaSR agonist cinacalcet and was abolished by calcilytic treatment, suggesting that ADMA might regulate adipocyte biology via a CaSR mechanism. Subsequent experiments interrogating the effect of ADMA in HEK293 cells overexpressing CaSR showed that CaSR-mediated cytosolic calcium ($[Ca^{2+}]_i$) signalling was potentiated in the presence of ADMA (Dowsett *et al.*, 2022). However, the downstream intracellular signalling mechanisms governing ADMA/CaSR signalling were unclear.

Using CaSR overexpressing HEK293 cells and 3T3-L1 adipocytes to model CaSR signalling pathways, the first aim of this thesis was to characterise CaSR signalling *in vitro*. This thesis then aimed to determine whether ADMA influences CaSR signalling and investigate the biological relevance of ADMA/CaSR signalling in cellular and vascular function, initially using the *in vitro* models above, and then moving to explore this pathway in vascular and perivascular adipose tissue

(PVAT) function using *ex vivo* vascular myography. Finally, this thesis aimed to determine the significance of adipocyte CaSR in adipose biology and cardiovascular health, firstly by examining CaSR function in 3T3-L1 adipocytes, then by interrogating a murine model of adipocyte-specific CaSR deficiency utilising *ex vivo and in vivo* approaches. In the following sections I will provide a brief summary of the significant findings of my studies and describe how these findings have advanced our understanding of the role of CaSR in adipocyte biology and vascular function. Finally, I will briefly outline potential future studies that might improve understanding of this field.

7.1.1 ADMA stimulates CaSR-dependent ERK signalling

In chapter 3, inducible expression of CaSR was demonstrated in HEK293 cells, which in turn showed CaSR-dependent phosphorylation of $ERK_{1/2}$ but not AKT. Cells exposed to low ADMA concentrations also demonstrated enhanced $ERK_{1/2}$ activation. ADMA-mediated $ERK_{1/2}$ activation seemed to be mediated by CaSR, since the effect relied on CaSR expression and was independent of NO. However, the impact of the synthetic CaSR modulator NPS R-568 in HEK293-CaSR cells were not fully recapitulated by ADMA, highlighting discrete downstream targets for CaSR agonists and ADMA acting in HEK293-CaSR cells.

7.1.2 CaSR and ADMA influence 3T3-L1 adipocyte biology

Differentiated 3T3-L1 cells were used as a model of adipocyte physiology to investigate the role of ADMA and CaSR in adipocytes. These cells showed robust expression of dimethylarginine dimethylaminohydrolase (DDAH) mRNA indicative of ADMA catabolism in 3T3-L1 adipocytes. Further, the identification of CaSR mRNA showed that CaSR was likely to be involved in adipocyte biology. Both ADMA and CaSR agonists stimulated NO-independent adipocyte hypertrophy. Confirming that CaSR regulates adipocyte biology, the CaSR agonist cinacalcet increased the expression of lipogenic mediators and leptin protein secretion. Interestingly, the major lipogenic gene PPARγ was significantly reduced in ADMA-treated cells following synthetic CaSR inhibition, suggesting a role for ADMA/CaSR crosstalk in adipocyte biology. Raised $[Ca^{2+}]_o$ caused acute $ERK_{1/2}$ activation but the effect was not sensitised by ADMA or CaSR allosteric

modulators. Therefore, the biological effects of ADMA and CaSR acting in 3T3-L1 adipocytes are not likely to depend on $ERK_{1/2}$ signalling.

7.1.3 $[Ca^{2+}]_o$ induced vascular contraction is CaSR-independent

To determine whether adipocyte CaSR could be relevant in vascular function, murine aortas were treated with CaSR modulators, CaSR-active L-Phenylalanine (L-Phe) and ADMA. Raised $[Ca^{2+}]_o$ increased endothelium-independent vascular contractility and also blocked PVAT-mediated inhibition of vascular contraction, but both effects were CaSR-independent. Broadly, there was no effect of the CaSR-active amino acid L-Phe or ADMA in augmenting vascular contraction or PVAT function. These data combined with that of prior studies lack consensus; the CaSR is expressed through all layers of the vascular wall where it mediates diverse and antagonist actions, so the pharmacological methods used may not be appropriate to define the role of vascular CaSR.

7.1.4 CaSR deletion alters adipocyte biology and cardiovascular function

This thesis establishes a model of conditional CaSR deletion in adipocytes ($CaSR^{Ad-/-}$) therein generating a new model for exploring how CaSR regulates adipocyte physiology. An important step in phenotyping this model was to investigate the effect of adipocyte-specific CaSR deletion on adipose tissue (AT). Female $CaSR^{Ad-/-}$ mice showed decreased body weight and visceral adipocyte size implicating CaSR in adipocyte morphology. Triglyceride levels were decreased in female $CaSR^{Ad-/-}$ plasma suggesting that CaSR in adipocytes impacts on systemic lipid handling, though the mechanism was not explored here. To determine whether altered adipose biology in $CaSR^{Ad-/-}$ mice influenced cardiovascular physiology, vascular myography was performed on aortic vessel segments. Contractile responses to PVAT and gonadal adipose tissue (gAT) were markedly reduced in female $CaSR^{Ad-/-}$ mice indicating that adipocyte CaSR mediates the vascular response to AT. Interestingly, this effect seemed to be due to chronic impairment of aortic contractility. Male mice showed no change in adipocyte size, triglyceride levels or vascular reactivity, indicating that that adipocyte CaSR is more significant in female relative to male mice.

7.2 Significance of findings

7.2.1 CaSR signalling *in vitro*

Transgenic modification of HEK293 cells leading to increased CaSR expression has historically been a key tool for investigating CaSR signalling pathways (Gerbino and Colella, 2018). In HEK293-CaSR cells here, $[Ca^{2+}]_o$- and agonist-induced CaSR signalling caused robust activation of its target p-$ERK_{1/2}$. Surprisingly however, CaSR had no effect on ERK in 3T3-L1 cells, and ERK was unaltered in $CaSR^{Ad-/-}$ adipocytes suggesting that the biological effects of CaSR in adipocytes are mediated via ERK-independent pathways. As result, this thesis reveals a key difference between two cell models used here to study CaSR signalling pathways (Fig. 7-1). Contributing to prior studies characterising cell-specific CaSR signalling behaviour, this work emphasises the diversity of CaSR signalling networks *in vitro*, underscoring the need for careful and tailored selection of cell model systems in studies investigating CaSR.

As further instances of cell-specific CaSR signalling are identified, the need to characterise the biological role of CaSR and its molecular pathways acting in discrete tissues is of clinical importance. Cinacalcet has been used therapeutically for nearly 20 years (U.S. Food and Drug Administration, 2004). Though cinacalcet is primarily used to regulate derangements in calcium homeostasis, large multinational clinical trials indicate that calcimimetics may have a beneficial effect on cardiovascular function (Chang *et al.*, 2016). As the applications of clinical calcimimetics are further explored, a detailed characterisation of CaSR function and signalling is essential to understand the potential for off-target effects. To improve understanding of adipocyte CaSR and its (patho)physiology, future studies modelling CaSR signalling must be validated in adipocyte cell-line and primary models.

Figure 7-1:

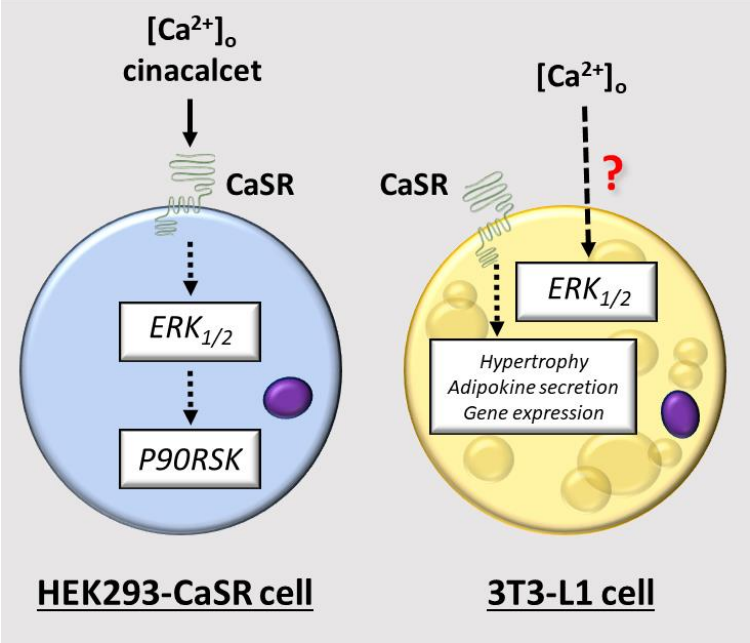

Figure 7-1: CaSR signalling *in vitro*.

Extracellular calcium ($[Ca^{2+}]_o$) and cinacalcet promote CaSR-dependent $ERK_{1/2}$ and P90RSK activation in transgenic HEK293-CaSR cells overexpressing CaSR. $[Ca^{2+}]_o$ stimulates $ERK_{1/2}$ activation in 3T3-L1 adipocytes through CaSR-independent mechanisms. $ERK_{1/2}$= Extracellular signal-regulated kinase; CaSR=Calcium-sensing receptor; P90RSK=p90 ribosomal S6 kinase.

7.2.2 The ADMA/CaSR pathway

Numerous studies have identified ADMA is an independent risk factor for CVD (Zoccali *et al.*, 2001; Meinitzer *et al.*, 2007; Cavusoglu *et al.*, 2010). It has long been known that (supraphysiological) doses of ADMA competes with L-Arg at cellular NOS decreasing NO synthesis (Leone *et al.*, 1992). As a result, the cardiovascular effects of ADMA have been largely ascribed to ADMA-mediated NOS inhibition and subsequent dysregulation of NO-dependent cardiovascular functions (Caplin and Leiper, 2012). Arguably however, ADMA concentrations influencing vascular reactivity and those measured in CVD are too low to mediate significant inhibition of NOS. In this thesis, ADMA stimulated $ERK_{1/2}$ signalling in HEK293-CaSR cells, and caused enlargement of 3T3-L1 adipocytes. In both model systems, ADMA-mediated effects appeared to be NO-independent. Crucially, ADMA effects in HEK293-CaSR cells relied on CaSR expression, suggesting that CaSR mediates cellular ADMA responses. Studies seeking to ameliorate the harmful effects of ADMA in CVD have used L-Arg supplementation with a view to

improve NO bioavailability. Frequently however, they could not identify a beneficial vascular effect of L-Arg (Walker *et al.*, 2001; Veresh *et al.*, 2012), indicating that ADMA might act through alternative targets. This study reveals a compelling additional mechanism through which ADMA might impact on cardiovascular health. As a highly amenable GPCR, the CaSR is an attractive therapeutic target in CVD, and may well represent a novel target for ameliorating harmful ADMA actions in the cardiovascular system.

7.2.3 Adipocyte CaSR, adipose and cardiovascular function

Adipocyte function and cardiovascular (patho)physiology are known to be intimately associated (Coelho, Oliveira and Fernandes, 2013; Oikonomou and Antoniades, 2019). In 3T3-L1 cells modelling mature adipocytes, synthetic CaSR agonism enhanced cellular hypertrophy, leptin secretion and lipogenic gene expression, underscoring a key role for CaSR in regulating adipocyte growth, adipokine secretion and lipogenesis, respectively. These findings show CaSR to be a mediator of adipocyte biology, consistent with previous work performed in adipocyte model systems (Cifuentes and Rojas, 2008; He, Zhang, *et al.*, 2011; He *et al.*, 2012; Villarroel *et al.*, 2016). In line with *in vitro* data, body weight and adipocyte size was decreased in adipocyte-specific CaSR deficient mice, demonstrating that CaSR regulation of adipocyte size is conserved *in vivo*. For some time, $[Ca^{2+}]_o$ metabolism and its signalling pathways have been implicated in body weight regulation. Despite emerging indications that obesity is positively associated with CaSR regulation, a direct causal role has not been explicitly demonstrated (Villarroel *et al.*, 2014). By showing a clear link between CaSR regulation, adipocyte size and body weight, this thesis implicates adipocyte CaSR as possible mechanism underpinning relationships between $[Ca^{2+}]_o$, body weight and metabolism in humans. CaSR activation *in vitro* is associated with an proinflammatory adipocyte phenotype (Bravo-Sagua *et al.*, 2016). Thus, CaSR may prove to be a highly interesting therapeutic target in disorders implicating AT dysfunction, such as obesity or diabetes.

The CaSR has a profound influence on vascular reactivity through its combined effects on VSMCs, ECs and nerve cells (Thakore and Vanessa Ho, 2011; Loot *et al.*, 2013; Greenberg, Shi, *et al.*, 2016). In this thesis, $CaSR^{Ad-/-}$ mice showed improved vascular function, revealing a previously unrealised link between

adipocyte CaSR and vascular reactivity. Both peripheral AT and PVAT secrete a panel of adipokines mediating vasoactive effects (Nava and Llorens, 2019). Importantly, AT-related pathologies such as obesity are readily characterised by a distinct shift in AT function. These changes have a detrimental impact on vascular health leading to increased CVD risk (Ha and Bauer, 2018). As such, pathological states leading to CaSR dysregulation in adipocytes could alter adipocyte biology, in turn causing AT derangement and vascular dysfunction. Supporting this hypothesis, CaSR polymorphisms have been identified as an independent risk factor for CAD and myocardial infarction (März *et al.*, 2007). Moreover, heritable and *de novo* CaSR mutations promoting calcitropic disorders have been associated with altered glucose, insulin and lipid handling (Vahe *et al.*, 2017). Collectively, these studies and the findings of this thesis support the view that CaSR function and/or expression is related to cardiovascular as well as metabolic health.

Interestingly, changes in adipose and vascular biology arising from adipocyte CaSR deficiency were limited strictly to female mice. There are distinct differences in the pattern of AT accumulation between males and females in humans; male adipose expansion primarily occurs in visceral depots, whereas females accrue greater subcutaneous AT (Fuente-Martín *et al.*, 2013). Plausibly, adipocyte CaSR signalling comprises a potential mechanism contributing to the differential accumulation of visceral adipose in men and women. There is a strong positive correlation between 'male-type' fat distribution and cardiometabolic risk (Fuente-Martín *et al.*, 2013). Therefore, establishing whether CaSR contributes to sex-specific adipose tissue deposition, and investigating the possible role of CaSR in sex-dependent CVD risk stratification, are important pending issues. Arguably, sex-dependent differences in CaSR biology might also impact on the clinical response to therapeutic calcimimetics, so there is a clear need to explore this phenomenon further, in adipocytes but also in other tissues known to influence cardiovascular physiology.

Due to its critical influence on cardiometabolic health, this thesis studied CaSR function primarily in visceral AT. GPCR expression, sensitivity and signal transduction is known to differ between AT depots (Ibrahim, 2010). At this stage it is not possible to say whether CaSR also reduces adipocyte size similarly in

female subcutaneous or brown AT, or if CaSR mediates cell size in male adipose depots besides visceral AT. Considering the opposing influence of visceral and subcutaneous AT on cardiovascular health, the importance of CaSR in each could differ greatly depending on its specific activity and function in each depot. The data presented here links CaSR, AT and cardiovascular function, highlighting CaSR as a potentially promising target in disorders typified by AT dysfunction, and in CVD. However, a comprehensive appraisal of CaSR function in subcutaneous and brown AT of both sexes is required to gain a thorough understanding of how CaSR regulates AT and cardiovascular (patho)physiology.

7.3 Future work

At its outset, this thesis originally planned to develop and phenotype $CaSR^{Ad-/-}$ mice, later using this model to perform diet-induced obesity studies. However, this work was prevented as a result of the covid pandemic. As this study and others continue to highlight new, potentially pathogenic roles for adipocyte CaSR, there is an increasing need to address the role of adipocyte CaSR in the obese state. For a better understanding of how CaSR might function as an etiological factor in the development of obesity and AT dysfunction, future studies should examine how CaSR modulation affects AT accumulation, adipokine signalling and lipid metabolism using genetic and diet-induced obesity models.

Genetic strategies may be employed in future work to interrogate causal links between adipocyte CaSR, AT and cardiovascular function. Previously, Babinsky *et al.* demonstrated that glucose homeostasis was impaired in murine models of global CaSR activation. The study confirmed a causal role for CaSR in metabolic dysfunction since the effect was normalised by the CaSR antagonist roncalaret (Babinsky *et al.*, 2017). Though this work associates CaSR and metabolic dysfunction, the relative contribution of CaSR overexpression occurring specially in adipocytes has not been determined. At present, murine models of adipocyte CaSR overexpression have yet to be developed, but would provide valuable insight into understanding CaSR (patho)physiology in adipocytes. For instance, one could speculate that mice overexpressing adipocyte CaSR would produce a phenotype opposing that observed in $CaSR^{Ad-/-}$ mice, demonstrating adipocyte

enlargement and enhanced vascular contraction. In the present study, adipocyte functions shown to be regulated by CaSR in cell line models was not fully consistent with those seen following targeted deletion of CaSR *in vivo*, possibly due to low baseline CaSR activation levels in settings of physiological health. As such, adipocyte-specific CaSR overexpressing systems could be key for exploring how CaSR mediates adipocyte function such as lipogenesis and leptin signalling, which could not be concluded here with the current model.

Clinically, cinacalcet is used to manage a variety of conditions; the most well-known of its therapeutic applications is its use in the treatment hyperparathyroidism arising secondary to chronic kidney disease (Block *et al.*, 2004). In this thesis, adipocyte hypertrophy was triggered by cinacalcet, and there was negative regulation of body weight, adipocyte size and lipid profiles in female mice lacking adipocyte CaSR. The effect of therapeutic CaSR allosteric agonists such as cinacalcet on AT and body weight regulation in humans is therefore of considerable intrigue. Cinacalcet has been in clinical use for over two decades, so it is likely that our understanding of adipocyte CaSR could be significantly advanced using patient data already available. For instance, biobank data could be used to interrogate relationships between cinacalcet dose and human metabolism by examining weight, body mass index, or lipid profiles. These datasets could also be examined to probe sexually dimorphic CaSR effects in humans, since data from cinacalcet-treated cohorts could be compared to assess therapeutic responses as well as off-target effects in men versus women, within a range of tissues.

7.4 Summary

This thesis aimed to characterise CaSR signalling *in vitro*, then subsequently sought to determine whether the CaSR could be amenable to stimulation by the amino acid ADMA in adipocytes. The CaSR is linked with CVD but the relevance of adipocyte CaSR is unknown, thus this thesis also aimed to examine the function of CaSR in adipocytes, later determining its wider significance in AT and cardiovascular biology. Initial studies performed in HEK293 models of CaSR overexpression showed that CaSR signalling pathways can be modulated by ADMA. An examination of 3T3-L1 cells modelling mature adipocytes showed that CaSR

and ADMA signalling caused adipocyte enlargement and may interact to regulate lipogenesis, but CaSR effects were not fully replicated by ADMA suggesting that ADMA/CaSR interactions are complex requiring further exploration. Characterisation of an adipocyte-specific CaSR deficient mouse model provided a novel insight into the biological role of adipocyte CaSR *in vivo*; the most interesting aspects of this work showed that adipocyte CaSR regulates adipocyte size and vasoreactivity, and that these effects occurred specifically in female mice indicating sexually dimorphic function. This thesis establishes ADMA as a potentially novel ligand of CaSR, and reveals adipocyte CaSR as an important mediator of adipose and cardiovascular function *in vivo*.

References

Abate, N. *et al.* (1995) 'Relationships of generalized and regional adiposity to insulin sensitivity in men', *Journal of Clinical Investigation*. American Society for Clinical Investigation, 96(1), pp. 88–98. doi: 10.1172/JCI118083.

Abbasi, F. *et al.* (2001) 'Plasma concentrations of asymmetric dimethylarginine are increased in patients with type 2 diabetes mellitus', *The American Journal of Cardiology*. Excerpta Medica, 88(10), pp. 1201–1203. doi: 10.1016/S0002-9149(01)02063-X.

Abhary, S. *et al.* (2010) 'Sequence variation in DDAH1 and DDAH2 genes is strongly and additively associated with serum ADMA concentrations in individuals with type 2 diabetes', *PLoS ONE*, 5(3), pp. 9462–9470. doi: 10.1371/journal.pone.0009462.

Acar, I. *et al.* (2020) 'The role of calcium sensing receptors in GLP-1 and PYY secretion after acute intraduodenal administration of L-Tryptophan in rats', *Nutritional Neuroscience*. Taylor & Francis, 23(6), pp. 481–489. doi: 10.1080/1028415X.2018.1521906.

Achan, V. *et al.* (2003) 'Asymmetric dimethylarginine causes hypertension and cardiac dysfunction in humans and is actively metabolized by dimethylarginine dimethylaminohydrolase.', *Arteriosclerosis, Thrombosis, and Vascular Biology*. American Heart Association, Inc., 23(8), pp. 1455–1459. doi: 10.1161/01.ATV.0000081742.92006.59.

Achari, A. E. and Jain, S. K. (2017) 'Adiponectin, a therapeutic target for obesity, diabetes, and endothelial dysfunction', *International Journal of Molecular Sciences*. MDPI, 18(6), pp. 1321–1338. doi: 10.3390/ijms18061321.

Akoumianakis, I. and Antoniades, C. (2017) 'The interplay between adipose tissue and the cardiovascular system: is fat always bad?', *Cardiovascular Research*. European Society of Cardiology, 113(9), pp. 999–1008. doi: 10.1093/cvr/cvx111.

Al-Zobaidy, M. J., Craig, J. and Martin, W. (2010) 'Differential sensitivity of basal and acetylcholine-induced activity of nitric oxide to blockade by asymmetric dimethylarginine in the rat aorta', *British Journal of Pharmacology*. John Wiley and Sons Inc., 160(6), pp. 1476–1483. doi: 10.1111/j.1476-5381.2010.00802.x.

Alamshah, A. *et al.* (2017) 'l-phenylalanine modulates gut hormone release and glucose tolerance, and suppresses food intake through the calcium-sensing receptor in rodents', *International journal*

of obesity. Nature, 41(11), pp. 1693–1701. doi: 10.1038/IJO.2017.164.

Altinova, A. E. *et al.* (2007) 'Uncomplicated Type 1 Diabetes Is Associated with Increased Asymmetric Dimethylarginine Concentrations', *The Journal of Clinical Endocrinology & Metabolism*. The Endocrine Society, 92(5), pp. 1881–1885. doi: 10.1210/jc.2006-2643.

Amir, M. *et al.* (2018) 'AGXT2 and DDAH-1 genetic variants are highly correlated with serum ADMA and SDMA levels and with incidence of coronary artery disease in Egyptians', *Molecular Biology Reports*. Springer Netherlands, 45(6), pp. 2411–2419. doi: 10.1007/s11033-018-4407-1.

Arita, Y. *et al.* (2002) 'Adipocyte-Derived Plasma Protein Adiponectin Acts as a Platelet-Derived Growth Factor-BB–Binding Protein and Regulates Growth Factor–Induced Common Postreceptor Signal in Vascular Smooth Muscle Cell', *Circulation*. Lippincott Williams & Wilkins, 105(24), pp. 2893–2898. doi: 10.1161/01.CIR.0000018622.84402.FF.

Arlouskaya, Y. *et al.* (2019) 'Asymmetric dimethylarginine (ADMA) and symmetric dimethylarginine (SDMA) concentrations in patients with obesity and the risk of obstructive sleep apnea (OSA)', *Journal of Clinical Medicine*. MDPI AG, 8(6), pp. 897–912. doi: 10.3390/jcm8060897.

El Assar, M. *et al.* (2016) 'Asymmetric dimethylarginine (ADMA) elevation and arginase up-regulation contribute to endothelial dysfunction related to insulin resistance in rats and morbidly obese humans', *Journal of Physiology*. The Physiological Society, 594(11), pp. 3045–3060. doi: 10.1113/JP271836.

Avlani, V. A. *et al.* (2013) 'Calcium-sensing receptor-dependent activation of CREB phosphorylation in HEK293 cells and human parathyroid cells', *American Journal of Physiology - Endocrinology and Metabolism*. American Physiological Society, 304(10), pp. E1097–E1104. doi: 10.1152/ajpendo.00054.2013.

Ayachi, S. (1979) 'Increased dietary calcium lowers blood pressure in the spontaneously hypertensive rat', *Metabolism: clinical and experimental*. Elsevier, 28(12), pp. 1234–1238. doi: 10.1016/0026-0495(79)90136-7.

Babinsky, V. N. *et al.* (2017) 'Mutant Mice With Calcium-Sensing Receptor Activation Have Hyperglycemia That Is Rectified by Calcilytic Therapy', *Endocrinology*. Oxford University Press, 158(8), pp. 2486–2502. doi: 10.1210/en.2017-00111.

Bai, M., Trivedi, S. and Brown, E. M. (1998) 'Dimerization of the extracellular calcium-sensing

receptor (CaR) on the cell surface of CaR-transfected HEK293 cells.', *The Journal of biological chemistry*. American Society for Biochemistry and Molecular Biology, 273(36), pp. 23605–10. doi: 10.1074/JBC.273.36.23605.

Bedford, M. T. and Clarke, S. G. (2009) 'Protein arginine methylation in mammals: who, what, and why.', *Molecular cell*. NIH Public Access, 33(1), pp. 1–13. doi: 10.1016/j.molcel.2008.12.013.

Bedford, M. T. and Richard, S. (2005) 'Arginine Methylation: An Emerging Regulatorof Protein Function', *Molecular Cell*. Cell Press, 18(3), pp. 263–272. doi: 10.1016/J.MOLCEL.2005.04.003.

Block, G. A. *et al.* (2004) 'Cinacalcet for Secondary Hyperparathyroidism in Patients Receiving Hemodialysis', *N Engl J Med*. Massachusetts Medical Society, 350(15), pp. 1516–1525. doi: 10.1056/NEJMOA031633.

Bode-Böger, S. M., Scalera, F. and Ignarro, L. J. (2007) 'The l-arginine paradox: Importance of the l-arginine/asymmetrical dimethylarginine ratio', *Pharmacology and Therapeutics*. Pergamon, 114(3), pp. 295–306. doi: 10.1016/j.pharmthera.2007.03.002.

Böger, R. H. *et al.* (1998) 'Asymmetric dimethylarginine (ADMA): a novel risk factor for endothelial dysfunction: its role in hypercholesterolemia.', *Circulation*. American Heart Association Inc., 98(18), pp. 1842–1847. doi: 10.1161/01.CIR.98.18.1842.

Böger, R. H. *et al.* (2000) 'An endogenous inhibitor of nitric oxide synthase regulates endothelial adhesiveness for monocytes', *Journal of the American College of Cardiology*. Elsevier, 36(7), pp. 2287–2295. doi: 10.1016/S0735-1097(00)01013-5.

Bohr, D. F. (1963) 'Vascular smooth muscle: Dual effect of calcium', *Science*. American Association for the Advancement of Science, 139(3555), pp. 597–599. doi: 10.1126/SCIENCE.139.3555.597.

Bost, F. *et al.* (2005) 'The Extracellular Signal–Regulated Kinase Isoform ERK1 Is Specifically Required for In Vitro and In Vivo Adipogenesis', *Diabetes*. American Diabetes Association, 54(2), pp. 402–411. doi: 10.2337/DIABETES.54.2.402.

Bravo-Sagua, R. *et al.* (2016) 'Calcium Sensing Receptor as a Novel Mediator of Adipose Tissue Dysfunction: Mechanisms and Potential Clinical Implications.', *Frontiers in physiology*. Frontiers Media SA, 7, pp. 395–402. doi: 10.3389/fphys.2016.00395.

Breitwieser, G. E. (2012) ‘Minireview: The intimate link between calcium sensing receptor trafficking and signaling: Implications for disorders of calcium homeostasis’, *Molecular Endocrinology*. The Endocrine Society, 26(9), pp. 1482–1495. doi: 10.1210/me.2011-1370.

Breitwieser, G. E. (2013) ‘The calcium sensing receptor life cycle: Trafficking, cell surface expression, and degradation’, *Best Practice & Research Clinical Endocrinology & Metabolism*. Elsevier, 27(3), pp. 303–313. doi: 10.1016/J.BEEM.2013.03.003.

Broadhead, G. K. *et al.* (2011) ‘Allosteric modulation of the calcium-sensing receptor by γ-glutamyl peptides: Inhibition of pth secretion, suppression of intracellular cAMP levels, and a common mechanism of action with L-amino acids’, *Journal of Biological Chemistry*. Elsevier, 286(11), pp. 8786–8797. doi: doi: 10.1074/jbc.M110.149724.

Brown, E. M. *et al.* (1993) ‘Cloning and characterization of an extracellular Ca2+-sensing receptor from bovine parathyroid’, *Nature*. Nature Publishing Group, 366(6455), pp. 575–580. doi: 10.1038/366575a0.

Brozovich, F. V. *et al.* (2016) ‘Mechanisms of vascular smooth muscle contraction and the basis for pharmacologic treatment of smooth muscle disorders’, *Pharmacological Reviews*. American Society for Pharmacology and Experimental Therapeutics, 68(2), pp. 476–532. doi: 10.1124/pr.115.010652.

Bruce, J. I. E. *et al.* (1999) ‘Molecular and Functional Identification of a Ca2+ (Polyvalent Cation)-sensing Receptor in Rat Pancreas’, *Journal of Biological Chemistry*. Elsevier, 274(29), pp. 20561–20568. doi: 10.1074/JBC.274.29.20561.

Bruun, J. M. *et al.* (2004) ‘Higher production of IL-8 in visceral vs. subcutaneous adipose tissue. Implication of nonadipose cells in adipose tissue’, *American Journal of Physiology - Endocrinology and Metabolism*. American Physiological Society, 286(1), pp. e8–e13. doi: 10.1152/ajpendo.00269.2003.

Bruun, J. M. *et al.* (2005) ‘Monocyte chemoattractant protein-1 release is higher in visceral than subcutaneous human adipose tissue (AT): Implication of macrophages resident in the AT’, *Journal of Clinical Endocrinology and Metabolism*. The Endocrine Society, 90(4), pp. 2282–2289. doi: 10.1210/jc.2004-1696.

Canaff, L. and Hendy, G. N. (2002) ‘Human calcium-sensing receptor gene. Vitamin D response elements in promoters P1 and P2 confer transcriptional responsiveness to 1,25-dihydroxyvitamin D.’, *The Journal of biological chemistry*. Elsevier, 277(33), pp. 30337–30350. doi:

10.1074/jbc.M201804200.

Canaff, L. and Hendy, G. N. (2005) 'Calcium-sensing Receptor Gene Transcription Is Up-regulated by the Proinflammatory Cytokine, Interleukin-1β: Role of the NF-κB Pathway and κB Elements', *Journal of Biological Chemistry*. Elsevier, 280(14), pp. 14177–14188. doi: 10.1074/JBC.M408587200.

Canaff, L., Zhou, X. and Hendy, G. N. (2008) 'The Proinflammatory Cytokine, Interleukin-6, Up-regulates Calcium-sensing Receptor Gene Transcription via Stat1/3 and Sp1/3', *Journal of Biological Chemistry*. Elsevier, 283(20), pp. 13586–13600. doi: 10.1074/JBC.M708087200.

Caplin, B. and Leiper, J. (2012) 'Endogenous nitric oxide synthase inhibitors in the biology of disease: markers, mediators, and regulators?', *Arteriosclerosis, thrombosis, and vascular biology*. Europe PMC Funders, 32(6), pp. 1343–53. doi: 10.1161/ATVBAHA.112.247726.

Carafoli, E. (2003) 'The calcium-signalling saga: tap water and protein crystals', *Nature Reviews Molecular Cell Biology*. Nature Publishing Group, 4(4), pp. 326–332. doi: 10.1038/nrm1073.

Cardounel, A. J. *et al.* (2007) 'Evidence for the Pathophysiological Role of Endogenous Methylarginines in Regulation of Endothelial NO Production and Vascular Function', *Journal of Biological Chemistry*. The American Society for Biochemistry and Molecular Biology, 282(2), pp. 879–887. doi: 10.1074/jbc.M603606200.

Care, A. D. *et al.* (1966) 'Evaluation by Radioimmunoassay of Factors Controlling the Secretion of Parathyroid Hormone: Perfusion of the Isolated Parathyroid Gland of the Goat and Sheep', *Nature*. Nature Publishing Group, 209(5018), pp. 55–57. doi: 10.1038/209055a0.

La Cava, A. and Matarese, G. (2004) 'The weight of leptin in immunity', *Nature Reviews Immunology 2004 4:5*. Nature Publishing Group, 4(5), pp. 371–379. doi: 10.1038/nri1350.

Cavusoglu, E. *et al.* (2010) 'Relation of baseline plasma ADMA levels to cardiovascular morbidity and mortality at two years in men with diabetes mellitus referred for coronary angiography', *Atherosclerosis*. Elsevier, 210(1), pp. 226–231. doi: 10.1016/J.ATHEROSCLEROSIS.2009.10.034.

Chang, L., Garcia-Barrio, M. T. and Chen, Y. E. (2020) 'Perivascular Adipose Tissue Regulates Vascular Function by Targeting Vascular Smooth Muscle Cells', *Arteriosclerosis, thrombosis, and vascular biology*. American Heart Association Inc., 40(5), pp. 1094–1109. doi: 10.1161/ATVBAHA.120.312464.

Chang, T. I. *et al.* (2016) 'The effects of cinacalcet on blood pressure, mortality and cardiovascular endpoints in the EVOLVE trial', *Journal of Human Hypertension*. Nature Publishing Group, 30(3), pp. 204–209. doi: 10.1038/jhh.2015.56.

Chang, W. *et al.* (2008) 'The extracellular calcium-sensing receptor (CaSR) is a critical modulator of skeletal development', *Science signaling*. Science, 2;1(35), pp. 1–13. doi: 10.1126/SCISIGNAL.1159945.

Chatterjee, T. K. *et al.* (2009) 'Pro-inflammatory phenotype of perivascular adipocytes: influence of high fat feeding', *Circulation research*. NIH Public Access, 104(4), pp. 541–549. doi: 10.1161/CIRCRESAHA.108.182998.

Chen, H. *et al.* (1996) 'Evidence that the diabetes gene encodes the leptin receptor: Identification of a mutation in the leptin receptor gene in db/db mice', *Cell*. Cell Press, 84(3), pp. 491–495. doi: 10.1016/S0092-8674(00)81294-5.

Cheng, C. K. *et al.* (2018) 'Perivascular Adipose Tissue: the Sixth Man of the Cardiovascular System', *Cardiovascular drugs and therapy*. Springer, 32(5), pp. 481–502. doi: 10.1007/S10557-018-6820-Z.

Chikatsu, N. *et al.* (2000) 'Cloning and Characterization of Two Promoters for the Human Calcium-sensing Receptor (CaSR) and Changes of CaSR Expression in Parathyroid Adenomas', *Journal of Biological Chemistry*. Elsevier, 275(11), pp. 7553–7557. doi: 10.1074/JBC.275.11.7553.

Chow, J. Y. C. *et al.* (2011) 'Calcium-sensing receptor modulates extracellular ca 2+ entry via TRPC-encoded receptor-operated channels in human aortic smooth muscle cells', *American Journal of Physiology - Cell Physiology*. American Physiological Society, 301(2), pp. 461–468. doi: 10.1152/ajpcell.00389.2010.

Chusyd, D. E. *et al.* (2016) 'Relationships between Rodent White Adipose Fat Pads and Human White Adipose Fat Depots', *Frontiers in Nutrition*. Frontiers Media SA, 19;3(10), pp. 1–12. doi: 10.3389/fnut.2016.00010.

Cifuentes, M. *et al.* (2010) 'Obesity-associated proinflammatory cytokines increase calcium sensing receptor (CaSR) protein expression in primary human adipocytes and LS14 human adipose cell line', *Archives of Biochemistry and Biophysics*. Elsevier, 500(2), pp. 151–156. doi: 10.1016/j.abb.2010.05.033.

Cifuentes, M. *et al.* (2012) 'Calcium sensing receptor activation elevates proinflammatory factor expression in human adipose cells and adipose tissue.', *Molecular and cellular endocrinology*. NIH Public Access, 361(1–2), pp. 24–30. doi: 10.1016/j.mce.2012.03.006.

Cifuentes, M., Albala, C. and Rojas, C. (2005) 'Calcium-sensing receptor expression in human adipocytes', *Endocrinology*. The Endocrine Society, 146(5), pp. 2176–2179. doi: 10.1210/EN.2004-1281.

Cifuentes, M. and Rojas, C. V. (2008) 'Antilipolytic effect of calcium-sensing receptor in human adipocytes', *Molecular and Cellular Biochemistry*. Springer, 319(1–2), pp. 17–21. doi: 10.1007/S11010-008-9872-8/TABLES/2.

Coelho, M., Oliveira, T. and Fernandes, R. (2013) 'Biochemistry of adipose tissue: an endocrine organ', *Archives of Medical Science : AMS*. Termedia Publishing, 9(2), pp. 191–200. doi: 10.5114/AOMS.2013.33181.

Colella, M. *et al.* (2016) 'Recent advances in understanding the extracellular calcium-sensing receptor.', *F1000Research*. Faculty of 1000 Ltd, 5, pp. 2535–2547. doi: 10.12688/f1000research.8963.1.

Conigrave, A. D. *et al.* (2004) 'L-Amino acids regulate parathyroid hormone secretion', *Journal of Biological Chemistry*. The American Society for Biochemistry and Molecular Biology, Inc., 279(37), pp. 38151–38159. doi: 10.1074/jbc.M406373200.

Conigrave, A. D., Mun, H. C. and Lok, H. C. (2007) 'Aromatic L-amino acids activate the calcium-sensing receptor', *The Journal of nutrition*. American Society for Nutrition, 137(6), pp. 1524S-1527S. doi: 10.1093/JN/137.6.1524S.

Conigrave, A. D., Quinn, S. J. and Brown, E. M. (2000) 'L-amino acid sensing by the extracellular Ca2+-sensing receptor', *Proceedings of the National Academy of Sciences of the United States of America*. National Academy of Sciences, 97(9), pp. 4814–4819. doi: 10.1073/pnas.97.9.4814.

Conigrave, A. D. and Ward, D. T. (2013) 'Calcium-sensing receptor (CaSR): Pharmacological properties and signaling pathways', *Best Practice & Research Clinical Endocrinology & Metabolism*. Baillière Tindall, 27(3), pp. 315–331. doi: 10.1016/J.BEEM.2013.05.010.

Cook, K. S. *et al.* (1987) 'Adipsin: A circulating serine protease homolog secreted by adipose tissue and sciatic nerve', *Science*. Science, 237(4813), pp. 402–405. doi: 10.1126/science.3299705.

D'Espessailles, A. *et al.* (2018) 'Calcium-sensing receptor activates the NLRP3 inflammasome in LS14 preadipocytes mediated by ERK1/2 signaling', *Journal of Cellular Physiology*. Elsevier, 233(8), pp. 6232–6240. doi: 10.1002/jcp.26490.

Davey, A. E. *et al.* (2012) 'Positive and negative allosteric modulators promote biased signaling at the calcium-sensing receptor', *Endocrinology*. Oxford University Press, USA, 153(3), pp. 1232–1241. doi: 10.1210/EN.2011-1426.

Dayoub, H. *et al.* (2003) 'Dimethylarginine Dimethylaminohydrolase Regulates Nitric Oxide Synthesis: Genetic and Physiological Evidence', *Circulation*. Lippincott Williams & Wilkins, 108(24), pp. 3042–3047. doi: 10.1161/01.CIR.0000101924.04515.2E.

Ding, H. *et al.* (2010) *A novel loss-of-function DDAH1 promoter polymorphism is associated with increased susceptibility to thrombosis stroke and coronary heart disease*, *Circulation Research*. Lippincott Williams & Wilkins. doi: 10.1161/CIRCRESAHA.109.215616.

Dowsett, L. *et al.* (2015) 'Endothelial dimethylarginine dimethylaminohydrolase 1 is an important regulator of angiogenesis but does not regulate vascular reactivity or hemodynamic homeostasis', *Circulation*. Lippincott Williams and Wilkins, 131(25), pp. 2217–2225. doi: 10.1161/CIRCULATIONAHA.114.015064.

Dowsett, L. *et al.* (2020) 'ADMA: A Key Player in the Relationship between Vascular Dysfunction and Inflammation in Atherosclerosis', *Journal of clinical medicine*. J Clin Med, 9(9), pp. 1–17. doi: 10.3390/JCM9093026.

Dowsett, L. *et al.* (2022) *Asymmetric dimethylarginine positively modulates Calcium-Sensing Receptor signalling to promote lipid accumulation and adiposity*, *bioRxiv [Preprint]*. Cold Spring Harbor Laboratory. doi: 10.1101/2022.07.26.501411.

Dowsett, L. B. (2014) *The Role of the NOS-ADMA-DDAH1 Pathway in Adipocytes and Obesity*, *PhD Thesis*. Imperial College London.

Drenjancevic, I. *et al.* (2018) 'The Markers of Endothelial Activation', in *Endothelial Dysfunction - Old Concepts and New Challenges*. InTechOpen, pp. 391–417. doi: 10.5772/intechopen.74671.

Dubrovska, G. *et al.* (2004) 'Mechanisms of ADRF release from rat aortic adventitial adipose tissue', *American Journal of Physiology - Heart and Circulatory Physiology*. American Physiological Society, 286(3 55-3), pp. 1107–1113. doi: 10.1152/ajpheart.00656.2003.

Eguchi, J. *et al.* (2011) 'Transcriptional control of adipose lipid handling by IRF4', *Cell Metabolism*. Cell Press, 13(3), pp. 249–259. doi: 10.1016/J.CMET.2011.02.005.

Eid, H. M. A. *et al.* (2004) 'Relationship between obesity, smoking, and the endogenous nitric oxide synthase inhibitor, asymmetric dimethylarginine', *Metabolism*. W.B. Saunders, 53(12), pp. 1574–1579. doi: 10.1016/J.METABOL.2004.06.026.

Farnier, C. *et al.* (2003) 'Adipocyte functions are modulated by cell size change: potential involvement of an integrin/ERK signalling pathway', *International Journal of Obesity*. Nature Publishing Group, 27(10), pp. 1178–1186.

Farooqi, I. S. *et al.* (2002) 'Beneficial effects of leptin on obesity, T cell hyporesponsiveness, and neuroendocrine/metabolic dysfunction of human congenital leptin deficiency', *The Journal of Clinical Investigation*. American Society for Clinical Investigation, 110(8), pp. 1093–1103. doi: 10.1172/JCI15693.

Fitzgibbons, T. P. *et al.* (2011) 'Similarity of mouse perivascular and brown adipose tissues and their resistance to diet-induced inflammation', *American Journal of Physiology - Heart and Circulatory Physiology*. American Physiological Society, 301(4), pp. H1425–H1437. doi: 10.1152/AJPHEART.00376.2011.

Frayn, K. N. (2000) 'Visceral fat and insulin resistance ' causative or correlative?', *British Journal of Nutrition*. Cambridge University Press, 83(S1), pp. S71–S77. doi: 10.1017/S0007114500000982.

Freedland, E. S. (2004) 'Role of a critical visceral adipose tissue threshold (CVATT) in metabolic syndrome: Implications for controlling dietary carbohydrates: A review', *Nutrition and Metabolism*. BioMed Central, 1(12), pp. 1–24. doi: 10.1186/1743-7075-1-12.

Frees, S. *et al.* (2018) 'Calcium-sensing receptor (CaSR) promotes development of bone metastasis in renal cell carcinoma', *Oncotarget*. Impact Journals, LLC, 9(21), pp. 15766–15779. doi: 10.18632/ONCOTARGET.24607.

Fried, S. K., Bunkin, D. A. and Greenberg, A. S. (1998) 'Omental and Subcutaneous Adipose Tissues of Obese Subjects Release Interleukin-6: Depot Difference and Regulation by Glucocorticoid 1', *The Journal of Clinical Endocrinology & Metabolism*. The Endocrine Society, 83(3), pp. 847–850. doi: 10.1210/jcem.83.3.4660.

Fuente-Martín, E. *et al.* (2013) 'Sex differences in adipose tissue: It is not only a question of quantity

and distribution', *Adipocyte*. Taylor & Francis, 2(3), pp. 128–134. doi: 10.4161/ADIP.24075.

Furuhashi, M. *et al.* (2014) 'Fatty acid-binding protein 4 (FABP4): Pathophysiological insights and potent clinical biomarker of metabolic and cardiovascular diseases', *Clinical Medicine Insights: Cardiology*. SAGE Publications, pp. 23–33. doi: 10.4137/CMC.S17067.

Gao, Y. J. *et al.* (2006) 'Perivascular adipose tissue promotes vasoconstriction: the role of superoxide anion', *Cardiovascular Research*. Oxford Academic, 71(2), pp. 363–373. doi: 10.1016/j.cardiores.2006.03.013.

Gao, Y. J. *et al.* (2007) 'Modulation of vascular function by perivascular adipose tissue: the role of endothelium and hydrogen peroxide', *British journal of pharmacology*. Nature Publishing Group, 151(3), pp. 323–331. doi: 10.1038/SJ.BJP.0707228.

Gargiulo, S. *et al.* (2014) 'Evaluation of Growth Patterns and Body Composition in C57Bl/6J Mice Using Dual Energy X-Ray Absorptiometry', *BioMed Research International*. Hindawi Limited, 4(11), pp. 1–11. doi: 10.1155/2014/253067.

Garrett, J. E. *et al.* (1995) 'Molecular Cloning and Functional Expression of Human Parathyroid Calcium Receptor cDNAs', *Journal of Biological Chemistry*. Elsevier, 270(21), pp. 12919–12925. doi: 10.1074/JBC.270.21.12919.

De Gennaro Colonna, V. *et al.* (2007) 'Asymmetric dimethylarginine (ADMA) induces vascular endothelium impairment and aggravates post-ischemic ventricular dysfunction in rats', *European Journal of Pharmacology*. Elsevier, 557(2–3), pp. 178–185. doi: 10.1016/j.ejphar.2006.11.034.

Gerbino, A. and Colella, M. (2018) 'The different facets of extracellular calcium sensors: Old and new concepts in calcium-sensing receptor signalling and pharmacology', *International Journal of Molecular Sciences*. MDPI AG, pp. 999–1037. doi: 10.3390/ijms19040999.

Ghantous, C. M. *et al.* (2015) 'Differential Role of Leptin and Adiponectin in Cardiovascular System', *International Journal of Endocrinology*. Hindawi Limited, 2015(6), pp. 1–13. doi: 10.1155/2015/534320.

Goldstein, B. J., Scalia, R. G. and Ma, X. L. (2009) 'Protective vascular and myocardial effects of adiponectin', *Nature Clinical Practice Cardiovascular Medicine*. Nature, 6(1), pp. 27–35. doi: 10.1038/ncpcardio1398.

Greenberg, H. Z. E., Shi, J., *et al.* (2016) 'Stimulation of calcium-sensing receptors induces endothelium-dependent vasorelaxations via nitric oxide production and activation of IKCa channels', *Vascular pharmacology*. Elsevier Inc., 80(2016), pp. 75–84. doi: 10.1016/j.vph.2016.01.001.

Greenberg, H. Z. E., Jahan, K. S., *et al.* (2016) 'The calcilytics Calhex-231 and NPS 2143 and the calcimimetic Calindol reduce vascular reactivity via inhibition of voltage-gated Ca2+channels', *European Journal of Pharmacology*. Elsevier B.V., 791, pp. 659–668. doi: 10.1016/j.ejphar.2016.10.008.

Grundy, S. M. (2015) 'Adipose tissue and metabolic syndrome: Too much, too little or neither', *European Journal of Clinical Investigation*. Wiley-Blackwell, 45(11), pp. 1209–1217. doi: 10.1111/eci.12519.

Grundy, S. M., Adams-Huet, B. and Vega, G. L. (2008) 'Variable contributions of fat content and distribution to metabolic syndrome risk factors', *Metabolic Syndrome and Related Disorders*. Mary Ann Liebert, Inc., 6(4), pp. 281–288. doi: 10.1089/met.2008.0026.

Guo, Y. *et al.* (2020) 'ERK/MAPK signalling pathway and tumorigenesis (Review)', *Experimental and Therapeutic Medicine*. Spandidos Publications, 19(3), pp. 1997–2007. doi: 10.3892/ETM.2020.8454.

Ha, E. E. and Bauer, R. C. (2018) 'Emerging Roles for Adipose Tissue in Cardiovascular Disease', *Arteriosclerosis, thrombosis, and vascular biology*. NLM (Medline), 38(8), pp. e137–e144. doi: 10.1161/ATVBAHA.118.311421.

Hakkak, R., Kaufmann, Y. and Stack, B. (2019) 'Effects of Obesity on Serum Calcium and Parathyroid Hormone in Zucker Rat Model (P08-032-19) [abstract]', *Current Developments in Nutrition*. Oxford Academic, 3(Supplement_1), p. 2093. doi: 10.1093/cdn/nzz044.p08-032-19.

Harris, R. B. S. *et al.* (1998) 'A Leptin Dose-Response Study in Obese (ob/ob) and Lean (+/?) Mice', *Endocrinology*. Oxford Academic, 139(1), pp. 8–19. doi: 10.1210/ENDO.139.1.5675.

Hasegawa, K. *et al.* (2007) 'Role of Asymmetric Dimethylarginine in Vascular Injury in Transgenic Mice Overexpressing Dimethylarginie Dimethylaminohydrolase 2', *Circulation Research*. Lippincott Williams & Wilkins, 101(2), pp. e2-10. doi: 10.1161/CIRCRESAHA.107.156901.

Hauner, H., Wabitsch, M. and Pfeiffer, E. F. (1988) 'Differentiation of adipocyte precursor cells from

obese and nonobese adult women and from different adipose tissue sites', *Hormone and Metabolic Research*. Thieme, 19(Suppl.), pp. 35–39.

He, Y.-H., Zhang, H., *et al.* (2011) 'Involvement of calcium-sensing receptor in inhibition of lipolysis through intracellular cAMP and calcium pathways in human adipocytes', *Biochemical and Biophysical Research Communications*. Academic Press, 404(1), pp. 393–399. doi: 10.1016/J.BBRC.2010.11.129.

He, Y.-H., Song, Y., *et al.* (2011) 'The Calcium-Sensing Receptor Affects Fat Accumulation via Effects on Antilipolytic Pathways in Adipose Tissue of Rats Fed Low-Calcium Diets', *The Journal of Nutrition*. Oxford University Press, 141(11), pp. 1938–1946. doi: 10.3945/jn.111.141762.

He, Y. Y.-H. H. Y. *et al.* (2012) 'The calcium-sensing receptor promotes adipocyte differentiation and adipogenesis through PPARγ pathway.', *Molecular and cellular biochemistry*. Springer US, 361(1–2), pp. 321–328. doi: 10.1007/s11010-011-1118-5.

Heikal, L. *et al.* (2018) 'L-Phenylalanine Restores Vascular Function in Spontaneously Hypertensive Rats Through Activation of the GCH1-GFRP Complex', *JACC: Basic to Translational Science*. Elsevier, 3(3), pp. 366–377. doi: 10.1016/j.jacbts.2018.01.015.

Hénaut, L. *et al.* (2014) 'Calcimimetics increase CaSR expression and reduce mineralization in vascular smooth muscle cells: Mechanisms of action', *Cardiovascular Research*. Oxford Academic, 101(2), pp. 256–265. doi: 10.1093/cvr/cvt249.

Hendy, G. N. and Canaff, L. (2016) 'Calcium-sensing receptor gene: Regulation of expression', *Frontiers in Physiology*. Frontiers Media S.A., 7(394), pp. 1–12. doi: 10.3389/FPHYS.2016.00394/BIBTEX.

Hildebrand, S., Stümer, J. and Pfeifer, A. (2018) 'PVAT and its relation to brown, beige, and white adipose tissue in development and function', *Frontiers in Physiology*. Frontiers Media S.A., 9(70), pp. 1–10. doi: 10.3389/fphys.2018.00070.

Ho, C. *et al.* (1995) 'A mouse model of human familial hypocalciuric hypercalcemia and neonatal severe hyperparathyroidism', *Nature Genetics 1995 11:4*. Nature Publishing Group, 11(4), pp. 389–394. doi: 10.1038/ng1295-389.

Hocking, S. L. *et al.* (2010) 'Intrinsic depot-specific differences in the secretome of adipose tissue, preadipocytes, and adipose tissue-derived microvascular endothelial cells', *Diabetes*. American

Diabetes Association, 59(12), pp. 3008–3016. doi: 10.2337/db10-0483.

Holstein, D. M. *et al.* (2004) 'Calcium-sensing Receptor-mediated ERK1/2 Activation Requires Gα i2 Coupling and Dynamin-independent Receptor Internalization', *Journal of Biological Chemistry*. The American Society for Biochemistry and Molecular Biology, Inc. Vol., 279(11), pp. 10060–10069. doi: 10.1074/jbc.M312039200.

Horinouchi, T. *et al.* (2020) 'Extracellular Ca2+ promotes nitric oxide production via Ca2+-sensing receptor-Gq/11 protein-endothelial nitric oxide synthase signaling in human vascular endothelial cells', *Journal of Pharmacological Sciences*. Japanese Pharmacological Society, 143(4), pp. 315–319. doi: 10.1016/j.jphs.2019.06.009.

Horowitz, J. D. and Heresztyn, T. (2007) 'An overview of plasma concentrations of asymmetric dimethylarginine (ADMA) in health and disease and in clinical studies: Methodological considerations', *Journal of Chromatography B: Analytical Technologies in the Biomedical and Life Sciences*. Elsevier, 851(1–2), pp. 42–50. doi: 10.1016/j.jchromb.2006.09.023.

Hu, J. and Spiegel, A. M. (2007) 'Structure and function of the human calcium-sensing receptor: insights from natural and engineered mutations and allosteric modulators.', *Journal of cellular and molecular medicine*. Wiley-Blackwell, 11(5), pp. 908–22. doi: 10.1111/j.1582-4934.2007.00096.x.

Hu, X. *et al.* (2009) 'Vascular endothelial-specific dimethylarginine dimethylaminohydrolase-1-deficient mice reveal that vascular endothelium plays an important role in removing asymmetric dimethylarginine', *Circulation*. American Heart Association, Inc., 120(22), pp. 2222–2229. doi: 10.1161/CIRCULATIONAHA.108.819912.

Huang, Y. and Breitwieser, G. E. (2007) 'Rescue of calcium-sensing receptor mutants by allosteric modulators reveals a conformational checkpoint in receptor biogenesis', *Journal of Biological Chemistry*. The American Society for Biochemistry and Molecular Biology, Inc. Printed, 282(13), pp. 9517–9525. doi: 10.1074/jbc.M609045200.

Ibrahim, M. M. (2010) 'Subcutaneous and visceral adipose tissue: structural and functional differences', *Obesity reviews : an official journal of the International Association for the Study of Obesity*. Wiley-Blackwell, 11(1), pp. 11–18. doi: 10.1111/J.1467-789X.2009.00623.X.

Jacobi, J. *et al.* (2010) 'Dimethylarginine dimethylaminohydrolase overexpression ameliorates atherosclerosis in apolipoprotein E-deficient mice by lowering asymmetric dimethylarginine', *American Journal of Pathology*. Elsevier Inc., 176(5), pp. 2559–2570. doi: 10.2353/ajpath.2010.090614.

Jang, B. C. (2016) ‘Artesunate inhibits adipogeneis in 3T3-L1 preadipocytes by reducing the expression and/or phosphorylation levels of C/EBP-α, PPAR-γ, FAS, perilipin A, and STAT-3’, *Biochemical and Biophysical Research Communications*. Academic Press, 474(1), pp. 220–225. doi: 10.1016/J.BBRC.2016.04.109.

Janicic, N. *et al.* (1995) ‘Mapping of the calcium-sensing receptor gene (CASR) to human Chromosome 3q13.3-21 by fluorescence in situ hybridization, and localization to rat Chromosome 11 and mouse Chromosome 16’, *Mammalian Genome*. Springer, 6(11), pp. 798–801. doi: 10.1007/BF00539007.

Jayachandran, I. *et al.* (2020) ‘Asymmetric dimethylarginine (ADMA) accelerates renal cell fibrosis under high glucose condition through NOX4/ROS/ERK signaling pathway’, *Scientific Reports*. Nature Research, 10(1), pp. 1–17. doi: 10.1038/s41598-020-72943-2.

Jensen, B. *et al.* (2004) ‘High extracellular calcium attenuates adipogenesis in 3T3-L1 preadipocytes’, *Experimental Cell Research*. Elsevier, 301(2), pp. 280–292. doi: 10.1016/j.yexcr.2004.08.030.

Jiang, J.-L. L. *et al.* (2007) ‘The inhibitory effect of simvastatin on the ADMA-induced inflammatory reaction is mediated by MAPK pathways in endothelial cells’, *Biochemistry and Cell Biology*. Canadian Science Publishing, 85(1), pp. 66–77. doi: 10.1139/O06-146.

Kielstein, J. T. *et al.* (2004) ‘Cardiovascular Effects of Systemic Nitric Oxide Synthase Inhibition With Asymmetrical Dimethylarginine in Humans’, *Circulation*. Lippincott Williams & Wilkins, 109(2), pp. 172–177. doi: 10.1161/01.CIR.0000105764.22626.B1.

Kielstein, J. T. *et al.* (2006) ‘ADMA Increases Arterial Stiffness and Decreases Cerebral Blood Flow in Humans’, *Stroke*. American Heart Association Inc., 37(8), pp. 2024–2029. doi: 10.1161/01.STR.0000231640.32543.11.

Klop, B., Elte, J. W. F. and Cabezas, M. C. (2013) ‘Dyslipidemia in Obesity: Mechanisms and Potential Targets’, *Nutrients*. Multidisciplinary Digital Publishing Institute (MDPI), 5(4), pp. 1218–1240. doi: 10.3390/NU5041218.

Klöting, N. *et al.* (2010) ‘Insulin-sensitive obesity’, *Am J Physiol Endocrinol Metab*. American Physiological Society, 299, pp. 506–515. doi: 10.1152/ajpendo.00586.2009.-The.

Klöting, N. and Blüher, M. (2014) ‘Adipocyte dysfunction, inflammation and metabolic syndrome’,

Reviews in Endocrine and Metabolic Disorders. Kluwer Academic Publishers, 15(4), pp. 277–287. doi: 10.1007/S11154-014-9301-0/FIGURES/3.

Kniazeff, J. *et al.* (2011) 'Dimers and beyond: The functional puzzles of class C GPCRs', *Pharmacology and Therapeutics*. Elsevier, 130(1), pp. 9–25. doi: 10.1016/j.pharmthera.2011.01.006.

Kolovou, G. D., Anagnostopoulou, K. K. and Cokkinos, D. V. (2005) 'Pathophysiology of dyslipidaemia in the metabolic syndrome', *Postgraduate Medical Journal*. BMJ Publishing Group, 81(956), pp. 358–366. doi: 10.1136/PGMJ.2004.025601.

Krahmer, N. *et al.* (2013) 'Balancing the fat: lipid droplets and human disease.', *EMBO molecular medicine*. Wiley-Blackwell, 5(7), pp. 973–83. doi: 10.1002/emmm.201100671.

Kuczera, P., Adamczak, M. and Wiecek, A. (2015) 'Treatment with cinacalcet decreases systolic blood pressure in haemodialysed patients with chronic kidney disease and secondary hyperparathyroidism', *Arterial Hypertension*. Via Medica, 19(3), pp. 129–134. doi: 10.5603/AH.2015.0016.

Kuruppu, S. and Smith, A. I. (2012) 'Endothelin converting enzyme-1 phosphorylation and trafficking', *FEBS Letters*. Elsevier, 586(16), pp. 2212–2217. doi: 10.1016/J.FEBSLET.2012.06.020.

Kwok, K. H. M., Lam, K. S. L. and Xu, A. (2016) 'Heterogeneity of white adipose tissue: molecular basis and clinical implications', *Experimental & molecular medicine*. Korean Society for Biochemistry and Molecular Biology, 48(3), p. e215. doi: 10.1038/emm.2016.5.

Kypreos, K. E. *et al.* (2018) 'Apolipoprotein E in diet-induced obesity: a paradigm shift from conventional perception', *Journal of Biomedical Research*. Education Department of Jiangsu Province, 32(3), p. 183. doi: 10.7555/JBR.32.20180007.

Lambden, S. *et al.* (2015) 'Dimethylarginine Dimethylaminohydrolase 2 Regulates Nitric Oxide Synthesis and Hemodynamics and Determines Outcome in Polymicrobial Sepsis', *Arteriosclerosis, Thrombosis, and Vascular Biology*. Lippincott Williams and Wilkins, 35(6), pp. 1382–1391. doi: 10.1161/ATVBAHA.115.305278.

Laurencikiene, J. *et al.* (2011) 'Regulation of lipolysis in small and large fat cells of the same subject', *Journal of Clinical Endocrinology and Metabolism*. The Endocrine Society, 96(12), pp.

E2045–E2049. doi: 10.1210/jc.2011-1702.

Lee, H. J. *et al.* (2007) 'Allosteric activation of the extracellular Ca2+-sensing receptor by L-amino acids enhances ERK1/2 phosphorylation', *Biochemical Journal*. Biochemical Society, 404(1), pp. 141–149. doi: 10.1042/BJ20061826.

Lee, R. M. K. W. *et al.* (2009) 'Endothelium-dependent relaxation factor released by perivascular adipose tissue', *Journal of Hypertension*. Wolters Kluwer -- Medknow Publications, 27(4), pp. 782–790. doi: 10.1097/HJH.0b013e328324ed86.

Leiper, J. *et al.* (2007) 'Disruption of methylarginine metabolism impairs vascular homeostasis', *Nature Medicine*. Nature Publishing Group, 13(2), pp. 198–203. doi: 10.1038/nm1543.

Leiper, J. M. and Vallance, P. (2006) 'The synthesis and metabolism of asymmetric dimethylarginine (ADMA)', *European Journal of Clinical Pharmacology*. Springer Verlag, 62(1), pp. 33–38. doi: 10.1007/s00228-005-0013-y.

Leiper, J. and Nandi, M. (2011) 'The therapeutic potential of targeting endogenous inhibitors of nitric oxide synthesis', *Nature Reviews Drug Discovery*. Nature Publishing Group, 10(4), pp. 277–291. doi: 10.1038/nrd3358.

Leiper, J. and Vallance, P. (2006) 'New tricks from an old dog: nitric oxide-independent effects of dimethylarginine dimethylaminohydrolase', *Arteriosclerosis, thrombosis, and vascular biology*. American Heart Association Inc., 26(7), p. 1419—1420. doi: 10.1161/01.atv.0000229598.55602.17.

Leone, A. *et al.* (1992) 'Accumulation of an endogenous inhibitor of nitric oxide synthesis in chronic renal failure', *The Lancet*. Elsevier, 339(8793), pp. 572–575. doi: 10.1016/0140-6736(92)90865-Z.

Lerman, A. *et al.* (1998) 'Long-term L-arginine supplementation improves small-vessel coronary endothelial function in humans', *Circulation*. Lippincott Williams and Wilkins, 97(21), pp. 2123–2128. doi: 10.1161/01.CIR.97.21.2123.

Li, C. *et al.* (2015) 'Perivascular adipose tissue-derived adiponectin inhibits collar-induced carotid atherosclerosis by promoting macrophage autophagy', *PLoS ONE*. PLoS One, 10(5), pp. 1–12. doi: 10.1371/journal.pone.0124031.

Li, G. W. *et al.* (2011) 'The functional expression of extracellular calcium-sensing receptor in rat

pulmonary artery smooth muscle cells', *Journal of Biomedical Science*. BioMed Central, 18(1), pp. 1–8. doi: 10.1186/1423-0127-18-16/FIGURES/5.

Li, H. *et al.* (2014) 'Perivascular adipose tissue-derived leptin promotes vascular smooth muscle cell phenotypic switching via p38 mitogen-activated protein kinase in metabolic syndrome rats':, *Experimental Biology and Medicine*. SAGE Publications, 239(8), pp. 954–965. doi: 10.1177/1535370214527903.

Li, T. *et al.* (2017) 'Dimethylarginine Dimethylaminohydrolase 1 Protects Against High-Fat Diet-Induced Hepatic Steatosis and Insulin Resistance in Mice', *Antioxidants & Redox Signaling*. Mary Ann Liebert, Inc., 26(11), pp. 598–609. doi: 10.1089/ars.2016.6742.

Liu, H. *et al.* (2020) 'Illuminating the allosteric modulation of the calcium-sensing receptor', *Proceedings of the National Academy of Sciences of the United States of America*. National Academy of Sciences, 117(35), pp. 21711–21722. doi: 10.1073/PNAS.1922231117/-/DCSUPPLEMENTAL.

Löhn, M. *et al.* (2002) 'Periadventitial fat releases a vascular relaxing factor', *The FASEB Journal*. Wiley-Blackwell, 16(9), pp. 1057–1063. doi: 10.1096/fj.02-0024com.

Longo, M. *et al.* (2019) 'Adipose Tissue Dysfunction as Determinant of Obesity-Associated Metabolic Complications', *International journal of molecular sciences*. MDPI AG, 20(9), pp. 2358–2365. doi: 10.3390/IJMS20092358.

Loot, A. E. *et al.* (2013) 'Ca2+-sensing receptor cleavage by calpain partially accounts for altered vascular reactivity in mice fed a high-fat diet', *Journal of Cardiovascular Pharmacology*. Wolters Kluwer -- Medknow Publications, 61(6), pp. 528–535. doi: 10.1097/FJC.0b013e31828d0fa3.

Lundman, P. *et al.* (2001) 'Mild-to-moderate hypertriglyceridemia in young men is associated with endothelial dysfunction and increased plasma concentrations of asymmetric dimethylarginine', *Journal of the American College of Cardiology*. American College of Cardiology Foundation, 38(1), pp. 111–116. doi: 10.1016/S0735-1097(01)01318-3.

Lynch, F. M. *et al.* (2013) 'Perivascular adipose tissue-derived adiponectin activates BKCa channels to induce anticontractile responses', *American Journal of Physiology - Heart and Circulatory Physiology*. American Physiological Society Bethesda, MD, 304(6), pp. 786–795. doi: 10.1152/AJPHEART.00697.2012/ASSET/IMAGES/LARGE/ZH40051306710005.JPEG.

Mace, O. J., Schindler, M. and Patel, S. (2012) 'The regulation of K- and L-cell activity by GLUT2 and the calcium-sensing receptor CasR in rat small intestine', *Journal of Physiology*. The Physiological Society, 590(12), pp. 2917–2936. doi: 10.1113/jphysiol.2011.223800.

Magno, A. L., Ward, B. K. and Ratajczak, T. (2011) 'The calcium-sensing receptor: A molecular perspective', *Endocrine Reviews*. Oxford Academic, 32(1), pp. 3–30. doi: 10.1210/er.2009-0043.

Makita, N. *et al.* (2007) 'An acquired hypocalciuric hypercalcemia autoantibody induces allosteric transition among active human Ca-sensing receptor conformations', *Proceedings of the National Academy of Sciences of the United States of America*. National Academy of Sciences, 104(13), pp. 5443–5448. doi: 10.1073/PNAS.0701290104.

Mamillapalli, R. *et al.* (2008) 'Switching of G-protein usage by the calcium-sensing receptor reverses its effect on parathyroid hormone-related protein secretion in normal versus malignant breast cells', *Journal of Biological Chemistry*. The American Society for Biochemistry and Molecular Biology, Inc, 283(36), pp. 24435–24447. doi: 10.1074/jbc.M801738200.

Mårin, P. *et al.* (1992) 'The morphology and metabolism of intraabdominal adipose tissue in men', *Metabolism*. Elsevier, 41(11), pp. 1242–1248. doi: 10.1016/0026-0495(92)90016-4.

März, W. *et al.* (2007) 'Alanine to serine polymorphism at position 986 of the calcium-sensing receptor associated with coronary heart disease, myocardial infarction, all-cause, and cardiovascular mortality', *Journal of Clinical Endocrinology and Metabolism*. The Endocrine Society, 92(6), pp. 2363–2369. doi: 10.1210/jc.2006-0071.

Maslowska, M. H. *et al.* (1993) 'Regional differences in triacylglycerol synthesis in adipose tissue and in cultured preadipocytes.', *Journal of Lipid Research*. Elsevier, 34(2), pp. 219–228. doi: 10.1016/S0022-2275(20)40749-7.

Matsuguma, K. *et al.* (2006) 'Molecular mechanism for elevation of asymmetric dimethylarginine and its role for hypertension in chronic kidney disease', *Journal of the American Society of Nephrology*. American Society of Nephrology, 17(8), pp. 2176–2183. doi: 10.1681/ASN.2005121379.

Mattar, P. *et al.* (2020) 'Calcium-sensing receptor in adipose tissue: Possible association with obesity-related elevated autophagy', *International Journal of Molecular Sciences*. MDPI AG, 21(20), pp. 1–14. doi: 10.3390/ijms21207617.

McDermott, J. R. (1976) ‘Studies on the Catabolism of NG-Methylargire, NG,NlG-Dimty1arginie and; NG,NG Dimethy1arginine in the Rabbit’, *The Biochemical journal*. Portland Press Ltd, 154(1), pp. 179–184.

Meinitzer, A. *et al.* (2007) ‘Asymmetrical dimethylarginine independently predicts total and cardiovascular mortality in individuals with angiographic coronary artery disease (The Ludwigshafen Risk and Cardiovascular Health Study)’, *Clinical Chemistry*. Oxford Academic, 53(2), pp. 273–283. doi: 10.1373/clinchem.2006.076711.

Minakuchi, H. *et al.* (2016) ‘The role of adipose tissue asymmetric dimethylarginine/dimethylarginine dimethylaminohydrolase pathway in adipose tissue phenotype and metabolic abnormalities in subtotally nephrectomized rats’, *Nephrology Dialysis Transplantation*. Oxford Academic, 31(3), pp. 413–423. doi: 10.1093/ndt/gfv367.

Miyazaki, H. *et al.* (1999) ‘Endogenous nitric oxide synthase inhibitor: a novel marker of atherosclerosis’, *Circulation*. Lippincott Williams & Wilkins, 99(9), pp. 1141–1146. doi: 10.1161/01.CIR.99.9.1141.

Molostvov, G. *et al.* (2007) ‘Extracellular calcium-sensing receptor is functionally expressed in human artery’, *American Journal of Physiology - Renal Physiology*. American Physiological Society, 293(3), pp. F5946–F955. doi: 10.1152/ajprenal.00474.2006.

Morales, Y. *et al.* (2016) ‘Biochemistry and regulation of the protein arginine methyltransferases (PRMTs)’, *Archives of Biochemistry and Biophysics*. Academic Press, 590(2016), pp. 138–152. doi: 10.1016/J.ABB.2015.11.030.

Moreno-Mendez, E. *et al.* (2020) ‘Early-life programming of adipose tissue’, *Nutrition Research Reviews*. Cambridge University Press, 33(2), pp. 244–259. doi: 10.1017/S0954422420000037.

Mukohira, H. *et al.* (2019) ‘Mesenchymal stromal cells in bone marrow express adiponectin and are efficiently targeted by an adiponectin promoter-driven Cre transgene’, *International Immunology*. Oxford Academic, 31(11), pp. 729–741. doi: 10.1093/intimm/dxz042.

Mundy, G. R. and Guise, T. A. (1999) ‘Hormonal Control of Calcium Homeostasis’, *Clinical Chemistry*. Oxford Academic, 45(8), pp. 1347–1352. doi: 10.1093/CLINCHEM/45.8.1347.

Muresan, A. A. *et al.* (2021) ‘Circulating amino acids as fingerprints of visceral adipose tissue independent of insulin resistance: a targeted metabolomic research in women’, *Revista Romana*

de Medicina de Laborator. Walter de Gruyter GmbH, 29(4), pp. 439–451. doi: 10.2478/rrlm-2021-0033.

Murphey, E. D. *et al.* (2000) 'Up-regulation of the parathyroid calcium-sensing receptor after burn injury in sheep: a potential contributory factor to postburn hypocalcemia.', *Critical Care Medicine*. Lippincott Williams and Wilkins, 28(12), pp. 3885–3890. doi: 10.1097/00003246-200012000-00024.

Nava, E. and Llorens, S. (2019) 'The local regulation of vascular function: From an inside-outside to an outside-inside model', *Frontiers in Physiology*. Frontiers Media S.A., 10(729), pp. 1–15. doi: 10.3389/fphys.2019.00729.

Nemeth, E. F. *et al.* (1998) 'Calcimimetics with potent and selective activity on the parathyroid calcium receptor', *Proceedings of the National Academy of Sciences of the United States of America*. National Academy of Sciences, 95(7), pp. 4040–4045. doi: 10.1073/pnas.95.7.4040.

Nemeth, E. F. *et al.* (2004) 'Pharmacodynamics of the Type II Calcimimetic Compound Cinacalcet HCl', *Journal of Pharmacology and Experimental Therapeutics*. American Society for Pharmacology and Experimental Therapeutics, 308(2), pp. 627–635. doi: 10.1124/jpet.103.057273.

Nemeth, E. F. and Carafoli, E. (1990) 'The role of extracellular calcium in the regulation of intracellular calcium and cell function', *Cell Calcium*. Longman Group, 11(5), pp. 319–321. doi: 10.1016/0143-4160(90)90032-P.

Nemeth, E. F. and Scarpa, A. (1987) 'Rapid Mobilization of Cellular Ca2+ in Bovine Parathyroid Cells Evoked by Extracellular Divalent Cations', *Journal of Biological Chemistry*. American Society of Biological Chemists, Inc., 262(11), pp. 5188–5196. doi: 10.1016/S0021-9258(18)61172-X.

Oda, Y. *et al.* (2000) 'The calcium sensing receptor and its alternatively spliced form in murine epidermal differentiation', *Journal of Biological Chemistry*. Elsevier, 275(2), pp. 1183–1190. doi: 10.1074/jbc.275.2.1183.

Ogawa, T. *et al.* (1987) 'Metabolism of NG,NG- and NG,NG-dimethylarginine in rats', *Archives of Biochemistry and Biophysics*. Elsevier, 252(2), pp. 526–537. doi: 10.1016/0003-9861(87)90060-9.

Oh, J. *et al.* (2011) 'Stimulation of the calcium-sensing receptor stabilizes the podocyte cytoskeleton, improves cell survival, and reduces toxin-induced glomerulosclerosis', *Kidney*

International. International Society of Nephrology, 80(5), pp. 483–492. doi: 10.1038/ki.2011.105.

Ohanian, J. *et al.* (2005) 'Evidence for a functional calcium-sensing receptor that modulates myogenic tone in rat subcutaneous small arteries', *American Journal of Physiology - Heart and Circulatory Physiology*. American Physiological Society, 288(4), pp. H1756–H1762. doi: 10.1152/ajpheart.00739.2004.

Oikonomou, E. K. and Antoniades, C. (2019) 'The role of adipose tissue in cardiovascular health and disease', *Nature Reviews Cardiology*. Nature Publishing Group, 16(2), pp. 83–99. doi: 10.1038/s41569-018-0097-6.

Östman, J. *et al.* (1979) 'Regional differences in the control of lipolysis in human adipose tissue', *Metabolism*. Elsevier, 28(12), pp. 1198–1205. doi: 10.1016/0026-0495(79)90131-8.

Ouchi, N. *et al.* (2003) 'Association of hypoadiponectinemia with impaired vasoreactivity', *Hypertension*. American Heart Association Inc., 42(3), pp. 231–234. doi: 10.1161/01.HYP.0000083488.67550.B8.

Ozaki, K. *et al.* (2016) 'Targeting the ERK signaling pathway as a potential treatment for insulin resistance and type 2 diabetes', *American Journal of Physiology-Endocrinology and Metabolism*. American Physiological Society, 310(8), pp. E643–E651. doi: 10.1152/ajpendo.00445.2015.

Payne, G. A. *et al.* (2009) 'Periadventitial adipose tissue impairs coronary endothelial function via PKC-β-dependent phosphorylation of nitric oxide synthase', *American Journal of Physiology - Heart and Circulatory Physiology*. American Physiological Society, 297(1), pp. H460–H465. doi: 10.1152/ajpheart.00116.2009.

Pearce, S. H. S. *et al.* (1996) 'Functional characterization of calcium-sensing receptor mutations expressed in human embryonic kidney cells', *Journal of Clinical Investigation*. American Society for Clinical Investigation, 98(8), pp. 1860–1866. doi: 10.1172/JCI118987.

Peng, X. *et al.* (2014) 'Involvement of calcium-sensing receptors in hypoxia-induced vascular remodeling and pulmonary hypertension by promoting phenotypic modulation of small pulmonary arteries', *Molecular and Cellular Biochemistry*. Springer, 396(1–2), pp. 87–98. doi: 10.1007/s11010-014-2145-9.

Pereira, S. S. and Alvarez-Leite, J. I. (2014) 'Adipokines: Biological functions and metabolically healthy obese profile', *Journal of Receptor, Ligand and Channel Research*. Dove Medical Press

Ltd, 2014(7), pp. 15–25. doi: 10.2147/JRLCR.S36060.

Peter, W. L. S. *et al.* (2015) 'Parathyroid hormone change after cinacalcet initiation and one-year clinical outcome risk: A retrospective cohort study', *BMC Nephrology*. BioMed Central, 16(1), pp. 1–8. doi: 10.1186/s12882-015-0030-8.

Pollak, M. R. *et al.* (1993) 'Mutations in the human Ca2+-sensing receptor gene cause familial hypocalciuric hypercalcemia and neonatal severe hyperparathyroidism', *Cell*. Cell Press, 75(7), pp. 1297–1303. doi: 10.1016/0092-8674(93)90617-Y.

Pramme-Steinwachs, I., Jastroch, M. and Ussar, S. (2017) 'Extracellular calcium modulates brown adipocyte differentiation and identity', *Scientific Reports 2017 7:1*. Nature Publishing Group, 7(1), pp. 1–10. doi: 10.1038/s41598-017-09025-3.

Qi, X. Y. *et al.* (2018) 'Perivascular adipose tissue (PVAT) in atherosclerosis: A double-edged sword', *Cardiovascular Diabetology*. BioMed Central, 17(1), pp. 134–154. doi: 10.1186/s12933-018-0777-x.

Ramirez, J. G., O'Malley, E. J. and Ho, W. S. V. (2017) 'Pro-contractile effects of perivascular fat in health and disease', *British Journal of Pharmacology*. The British Pharmacological Society, 174(20), pp. 3482–3495. doi: 10.1111/bph.13767.

Rey, O. *et al.* (2005) 'Amino acid-stimulated Ca2+ oscillations produced by the Ca 2+-sensing receptor are mediated by a phospholipase C/inositol 1,4,5-trisphosphate-independent pathway that requires G12, Rho, filamin-A, and the actin cytoskeleton', *Journal of Biological Chemistry*. The American Society for Biochemistry and Molecular Biology, Inc. Vol., 280(24), pp. 22875–22882. doi: 10.1074/jbc.M503455200.

Riccardi, D. (2012) 'Parathyroid hormone-independent role for the calcium-sensing receptor in the control of urinary calcium excretion', *Journal of the American Society of Nephrology*. American Physiological Society, 23(11), pp. 1766–1768. doi: 10.1681/ASN.2012090955.

Richard, A. J. *et al.* (2000) *Adipose Tissue: Physiology to Metabolic Dysfunction*, *Endotext*. MDText.com, Inc.

Ringer, S. (1883) 'A further Contribution regarding the influence of the different Constituents of the Blood on the Contraction of the Heart', *The Journal of Physiology*. Wiley-Blackwell, 4(1), pp. 29–42. doi: 10.1113/jphysiol.1883.sp000120.

Rizzatti, V. *et al.* (2013) 'Lipid droplets characterization in adipocyte differentiated 3T3-L1 cells: Size and optical density distribution', *European Journal of Histochemistry*. PAGEPress, 57(3), pp. 159–162. doi: 10.4081/ejh.2013.e24.

Rocha, G. *et al.* (2015) 'Preadipocyte proliferation is elevated by calcium sensing receptor activation', *Molecular and Cellular Endocrinology*. Elsevier, 412(2015), pp. 251–256. doi: 10.1016/j.mce.2015.05.011.

Rochlani, Y. *et al.* (2017) 'Metabolic syndrome: Pathophysiology, management, and modulation by natural compounds', *Therapeutic Advances in Cardiovascular Disease*. SAGE Publications, pp. 215–225. doi: 10.1177/1753944717711379.

Rodriguez, L. *et al.* (2005) 'Expression and Functional Assessment of an Alternatively Spliced Extracellular Ca2+-Sensing Receptor in Growth Plate Chondrocytes', *Endocrinology*. Oxford Academic, 146(12), pp. 5294–5303. doi: 10.1210/EN.2005-0256.

Rosen, E. D. and Spiegelman, B. M. (2003) 'Molecular Regulation of Adipogenesis', *Annual Review of Cell and Developmental Biology*. Annual Reviews, 16(2000), pp. 145–171. doi: 10.1146/ANNUREV.CELLBIO.16.1.145.

Rosen, E., Eguchi, J. and Xu, Z. (2009) 'Transcriptional targets in adipocyte biology', *Expert Opinion on Therapeutic Targets*. Taylor & Francis, pp. 975–986. doi: 10.1517/14728220903039706.

Ruiz-Ortega, M. *et al.* (2007) 'TGF-beta signaling in vascular fibrosis', *Cardiovascular research*. Elsevier, 74(2), pp. 196–206. doi: 10.1016/J.CARDIORES.2007.02.008.

Rydén, M. and Arner, P. (2017) 'Subcutaneous Adipocyte Lipolysis Contributes to Circulating Lipid Levels', *Arteriosclerosis, Thrombosis, and Vascular Biology*. American Heart Association, Inc., 37(9), pp. 1782–1787. doi: 10.1161/ATVBAHA.117.309759.

Salans, L. B., Knittle, J. L. and Hirsch, J. (1968) 'The role of adipose cell size and adipose tissue insulin sensitivity in the carbohydrate intolerance of human obesity', *Journal of Clinical Investigation*. American Society for Clinical Investigation, 47(1), pp. 153–165. doi: 10.1172/jci105705.

Saponaro, C. *et al.* (2015) 'The Subtle Balance between Lipolysis and Lipogenesis: A Critical Point in Metabolic Homeostasis.', *Nutrients*. Multidisciplinary Digital Publishing Institute (MDPI), 7(11),

pp. 9453–74. doi: 10.3390/nu7115475.

Satta, S. *et al.* (2017) 'The Role of Nrf2 in Cardiovascular Function and Disease', *Exercise and Sport Sciences Reviews*. American College of Sports Medicine, 41(3), pp. 162–168. doi: 10.1155/2017/9237263.

Sauer, B. and Henderson, N. (1988) 'Site-specific DNA recombination in mammalian cells by the Cre recombinase of bacteriophage P1.', *Proceedings of the National Academy of Sciences of the United States of America*. PNAS, 85(14), pp. 5166–5170. doi: 10.1073/pnas.85.14.5166.

Schepelmann, M. *et al.* (2016) 'The vascular Ca2+-sensing receptor regulates blood vessel tone and blood pressure', *Am J Physiol Cell Physiol.* American Physiological Society, 310(3), pp. C193–C204. doi: 10.1152/ajpcell.00248.2015.

Scherer, P. E. *et al.* (1995) 'A novel serum protein similar to C1q, produced exclusively in adipocytes', *Journal of Biological Chemistry*. The American Society for Biochemistry and Molecular Biology, Inc., 270(45), pp. 26746–26749. doi: 10.1074/jbc.270.45.26746.

Schreckenberg, R. and Schlüter, K.-D. D. (2018) 'Calcium sensing receptor expression and signalling in cardiovascular physiology and disease', *Vascular Pharmacology*. Elsevier, 107(2018), pp. 35–42. doi: 10.1016/J.VPH.2018.02.007.

Segarra, G. *et al.* (2000) 'Contractile effects of arginine analogues on human internal thoracic and radial arteries', *Journal of Thoracic and Cardiovascular Surgery*. Mosby Inc., 120(4), pp. 729–736. doi: 10.1067/mtc.2000.109537.

Shin, S., Thapa, S. K. and Fung, H. L. (2017) 'Cellular interactions between L-arginine and asymmetric dimethylarginine: Transport and metabolism', *PLoS ONE*. PLoS One, 12(5), p. e0178710. doi: 10.1371/journal.pone.0178710.

Shoback, D. *et al.* (1983) 'Effects of extracellular ca++ and mg++ on cytosolic ca++ and pth release in dispersed bovine parathyroid cells', *Endocrinology*. Wiley-Blackwell, 113(1), pp. 424–426. doi: 10.1210/endo-113-1-424.

Skurk, T. *et al.* (2007) 'Relationship between adipocyte size and adipokine expression and secretion', *Journal of Clinical Endocrinology and Metabolism*. Endocrine Society, 92(3), pp. 1023–1033. doi: 10.1210/jc.2006-1055.

Smajilovic, S. *et al.* (2006) ‘Extracellular calcium sensing in rat aortic vascular smooth muscle cells’, *Biochemical and Biophysical Research Communications*. Elsevier, 348(4), pp. 1215–1223. doi: 10.1016/j.bbrc.2006.07.192.

Smith, C. L. *et al.* (2005) ‘Effects of ADMA upon Gene Expression: An Insight into the Pathophysiological Significance of Raised Plasma ADMA’, *PLoS Medicine*. Edited by I. Benjamin. Public Library of Science, 2(10), p. e264. doi: 10.1371/journal.pmed.0020264.

Soltis, E. E. and Cassis, L. A. (1991) ‘Influence of perivascular adipose tissue on rat aortic smooth muscle responsiveness’, *Clinical and Experimental Hypertension*. Taylor & Francis, 13(2), pp. 277–296. doi: 10.3109/10641969109042063.

Song, Z., Xiaoli, A. M. and Yang, F. (2018) ‘Regulation and metabolic significance of De Novo lipogenesis in adipose tissues’, *Nutrients*. MDPI, 10(10), pp. 1383–1404. doi: 10.3390/nu10101383.

Spiegelman, B. M. *et al.* (1993) ‘Regulation of adipocyte gene expression in differentiation and syndromes of obesity/diabetes’, *Journal of Biological Chemistry*. Elsevier, 268(10), pp. 6823–6826. doi: 10.1016/s0021-9258(18)53107-0.

Spoto, B. *et al.* (2007) ‘The enzymatic machinery for ADMA synthesis and degradation is fully expressed in human adipocytes.’, *Journal of nephrology*. Springer, 20(5), pp. 554–9.

Stenkula, K. G. and Erlanson-Albertsson, C. (2018) ‘Adipose cell size: Importance in health and disease’, *American Journal of Physiology - Regulatory Integrative and Comparative Physiology*. American Physiological Society, 315(2), pp. R284–R295. doi: 10.1152/AJPREGU.00257.2017/ASSET/IMAGES/LARGE/ZH60061894830002.JPEG.

Stern, J. S. *et al.* (1972) ‘Adipose-cell size and immunoreactive insulin levels in obese and normal-weight adults’, *The Lancet*. Elsevier, 300(7784), pp. 948–951. doi: 10.1016/S0140-6736(72)92474-9.

Stühlinger, M. C. *et al.* (2002) ‘Relationship between insulin resistance and an endogenous nitric oxide synthase inhibitor’, *JAMA*. American Medical Association, 287(11), pp. 1420–1426. doi: 10.1001/jama.287.11.1420.

Suda, O. *et al.* (2004) ‘Asymmetric dimethylarginine produces vascular lesions in endothelial nitric oxide synthase-deficient mice: involvement of renin-angiotensin system and oxidative stress.’, *Arteriosclerosis, thrombosis, and vascular biology*. American Heart Association, Inc., 24(9), pp.

1682–8. doi: 10.1161/01.ATV.0000136656.26019.6e.

Sundararaman, S. S. *et al.* (2021) ‘Adipocyte calcium sensing receptor is not involved in visceral adipose tissue inflammation or atherosclerosis development in hyperlipidemic Apoe−/− mice’, *Scientific Reports 2021 11:1*. Nature Publishing Group, 11(1), pp. 1–9. doi: 10.1038/s41598-021-89893-y.

Sundararaman, S. S. and van der Vorst, E. P. C. (2021) ‘Calcium-Sensing Receptor (CaSR), Its Impact on Inflammation and the Consequences on Cardiovascular Health’, *International Journal of Molecular Sciences*. Multidisciplinary Digital Publishing Institute (MDPI), 22(5), pp. 1–16. doi: 10.3390/IJMS22052478.

Surdacki, A. *et al.* (1999) ‘Reduced urinary excretion of nitric oxide metabolites and increased plasma levels of asymmetric dimethylarginine in men with essential hypertension.’, *Journal of cardiovascular pharmacology*. SAGE Publications, 33(4), pp. 652–658. doi: 10.1097/00005344-199904000-00020.

Szasz, T., Bomfim, G. F. and Webb, R. C. (2013) ‘The influence of perivascular adipose tissue on vascular homeostasis.’, *Vascular health and risk management*. Dove Press, 2013(9), pp. 105–116. doi: 10.2147/vhrm.s33760.

Tain, Y.-L. and Hsu, C.-N. (2017) ‘Toxic Dimethylarginines: Asymmetric Dimethylarginine (ADMA) and Symmetric Dimethylarginine (SDMA).’, *Toxins*. MDPI, 9(3), pp. 92–102. doi: 10.3390/toxins9030092.

Tan, R. *et al.* (2020) ‘Phenylalanine induces pulmonary hypertension through calcium-sensing receptor activation’, *American Journal of Physiology - Lung Cellular and Molecular Physiology*. American Physiological Society, 319(6), pp. L1010–L1020. doi: 10.1152/AJPLUNG.00215.2020.

Tang, Q. Q. and Lane, M. D. (2012) ‘Adipogenesis: From stem cell to adipocyte’, *Annual Review of Biochemistry*. Annual Reviews, 2012(81), pp. 715–736. doi: 10.1146/annurev-biochem-052110-115718.

Tarnow, L. *et al.* (2004) ‘Elevated plasma asymmetric dimethylarginine as a marker of cardiovascular morbidity in early diabetic nephropathy in type 1 diabetes.’, *Diabetes care*. American Diabetes Association, 27(3), pp. 765–9. doi: 10.2337/DIACARE.27.3.765.

Teerlink, T. *et al.* (2009) ‘Cellular ADMA: regulation and action.’, *Pharmacological research*. NIH

Public Access, 60(6), pp. 448–60. doi: 10.1016/j.phrs.2009.08.002.

Thakore, P. and Vanessa Ho, W. S. (2011) 'Vascular actions of calcimimetics: Role of Ca 2+-sensing receptors versus Ca 2+ influx through L-type Ca 2+ channels', *British Journal of Pharmacology*. Wiley-Blackwell, 162(3), pp. 749–762. doi: 10.1111/j.1476-5381.2010.01079.x.

Thiel, G., Lesch, A. and Keim, A. (2012) 'Transcriptional response to calcium-sensing receptor stimulation', *Endocrinology*. The Endocrine Society, 153(10), pp. 4716–4728. doi: 10.1210/en.2012-1343.

Toka, H. R. *et al.* (2012) 'Deficiency of the calcium-sensing receptor in the kidney causes parathyroid hormone-independent hypocalciuria', *Journal of The American Society of Nephrology*. American Society of Nephrology, 23(11), pp. 1879–1890.

Torondel, B. *et al.* (2010) 'Adenoviral-mediated overexpression of DDAH improves vascular tone regulation', *Vascular Medicine*. SAGE Publications, 15(3), pp. 205–213. doi: 10.1177/1358863X09360264.

Touyz, R. M. and Briones, A. M. (2010) 'Reactive oxygen species and vascular biology: implications in human hypertension', *Hypertension Research 2011 34:1*. Nature Publishing Group, 34(1), pp. 5–14. doi: 10.1038/hr.2010.201.

Trayhurn, P. and Wood, I. S. (2004) 'Adipokines: inflammation and the pleiotropic role of white adipose tissue', *British Journal of Nutrition*. Cambridge University Press, 92(3), pp. 347–355. doi: 10.1079/BJN20041213.

Tsubai, T. *et al.* (2016) 'Insulin elevates leptin secretion and mRNA levels via cyclic AMP in 3T3-L1 adipocytes deprived of glucose', *Heliyon*. Elsevier, 2(11), pp. 1–16. doi: 10.1016/J.HELIYON.2016.E00194.

U.S. Food and Drug Administration (2004) *Drug Approval Package: Sensipar (Cinacalcet HCl) NDA #021688*.

Vahe, C. *et al.* (2017) 'Diseases associated with calcium-sensing receptor', *Orphanet Journal of Rare Diseases*. BioMed Central, p. 19. doi: 10.1186/s13023-017-0570-z.

Veresh, Z. *et al.* (2008) 'ADMA impairs nitric oxide-mediated arteriolar function due to increased superoxide production by angiotensin II-NAD(P)H oxidase pathway', *Hypertension*. Lippincott

Williams & Wilkins, 52(5), pp. 960–966. doi: 10.1161/HYPERTENSIONAHA.108.116731.

Veresh, Z. *et al.* (2012) 'Asymmetric dimethylarginine reduces nitric oxide donor-mediated dilation of arterioles by activating the vascular renin-angiotensin system and reactive oxygen species', *Journal of Vascular Research*. Karger Publishers, 49(4), pp. 363–372. doi: 10.1159/000337485.

Victorio, J. A. *et al.* (2016) 'Different anti-contractile function and nitric oxide production of thoracic and abdominal perivascular adipose tissues', *Frontiers in Physiology*. Frontiers Research Foundation, 7(295), pp. 1–10. doi: 10.3389/fphys.2016.00295.

Villarroel, P. *et al.* (2013) 'Adipogenic effect of calcium sensing receptor activation', *Molecular and Cellular Biochemistry*. Springer US, 384(1–2), pp. 139–145. doi: 10.1007/s11010-013-1791-7.

Villarroel, P. *et al.* (2014) 'Calcium, obesity, and the role of the calcium-sensing receptor', *Nutrition Reviews*. Oxford University Press, 72(10), pp. 627–637. doi: 10.1111/nure.12135.

Villarroel, P. *et al.* (2016) 'Calcium sensing receptor effects in adipocytes and liver cells: Implications for an adipose-hepatic crosstalk', *Archives of Biochemistry and Biophysics*. Academic Press, 607(2016), pp. 47–54. doi: 10.1016/j.abb.2016.08.017.

Vladimirova-Kitova, L. *et al.* (2008) 'Relationship of asymmetric dimethylarginine with flow-mediated dilatation in subjects with newly detected severe hypercholesterolemia', *Clinical Physiology and Functional Imaging*. John Wiley & Sons, Ltd, 28(6), pp. 417–425. doi: 10.1111/j.1475-097X.2008.00825.x.

Wajchenberg, B. L. (2000) 'Subcutaneous and visceral adipose tissue: Their relation to the metabolic syndrome', *Endocrine Reviews*. The Endocrine Society, 21(6), pp. 697–738. doi: 10.1210/edrv.21.6.0415.

Walker, H. A. *et al.* (2001) 'Endothelium-dependent vasodilation is independent of the plasma L-arginine/ADMA ratio in men with stable angina: Lack of effect of oral l-arginine on endothelial function, oxidative stress and exercise performance', *Journal of the American College of Cardiology*. Elsevier, 38(2), pp. 499–505. doi: 10.1016/S0735-1097(01)01380-8.

Wang, Q. A. *et al.* (2013) 'Tracking adipogenesis during white adipose tissue development, expansion and regeneration', *Nature Medicine 2013 19:10*. Nature Publishing Group, 19(10), pp. 1338–1344. doi: 10.1038/nm.3324.

Wang, R. *et al.* (2003) 'Calcium and polyamine regulated calcium-sensing receptors in cardiac tissues', *European Journal of Biochemistry*. Wiley-Blackwell, 270(12), pp. 2680–2688. doi: 10.1046/j.1432-1033.2003.03645.x.

Wang, Y. and Bukoski, R. D. (1998) 'Distribution of the perivascular nerve Ca2+ receptor in rat arteries', *British Journal of Pharmacology*. Nature Publishing Group, 125(7), pp. 1397–1404. doi: 10.1038/SJ.BJP.0702195.

Ward, D. T., Brown, E. M. and Harris, H. W. (1998) 'Disulfide Bonds in the Extracellular Calcium-Polyvalent Cation-sensing Receptor Correlate with Dimer Formation and Its Response to Divalent Cations in Vitro', *Journal of Biological Chemistry*. Elsevier, 273(23), pp. 14476–14483. doi: 10.1074/JBC.273.23.14476.

Ward, D. T. and Riccardi, D. (2012) 'New concepts in calcium-sensing receptor pharmacology and signalling', *British Journal of Pharmacology*. Wiley-Blackwell, 165(1), pp. 35–48. doi: 10.1111/j.1476-5381.2011.01511.x.

Ward, R. J., Alvarez-Curto, E. and Milligan, G. (2011) 'Using the Flp-In™ T-Rex™ system to regulate GPCR expression', *Methods in Molecular Biology*. Springer, 746, pp. 21–37. doi: 10.1007/978-1-61779-126-0_2.

Weisberg, S. P. *et al.* (2003) 'Obesity is associated with macrophage accumulation in adipose tissue', *Journal of Clinical Investigation*. The American Society for Clinical Investigation, 112(12), pp. 1796–1808. doi: 10.1172/jci19246.

Wellendorph, P. and Bräuner-Osborne, H. (2009) 'Molecular basis for amino acid sensing by family C G-protein-coupled receptors', *British Journal of Pharmacology*. The British Pharmacological Society, 156(6), pp. 869–884. doi: 10.1111/j.1476-5381.2008.00078.x.

Weston, A. H. *et al.* (2005) 'Evidence in favor of a calcium-sensing receptor in arterial endothelial cells: studies with calindol and Calhex 231', *Circulation research*. American Heart Association, Inc., 97(4), pp. 391–398. doi: 10.1161/01.RES.0000178787.59594.A0.

Wiklund, P. *et al.* (2016) 'Insulin resistance is associated with altered amino acid metabolism and adipose tissue dysfunction in normoglycemic women', *Scientific Reports*. Nature Publishing Group, 6(24540), pp. 1–11. doi: 10.1038/SREP24540.

Wonneberger, K., Scofield, M. A. and Wangemann, P. (2000) 'Evidence for a Calcium-Sensing

Receptor in the Vascular Smooth Muscle Cells of the Spiral Modiolar Artery', *The Journal of Membrane Biology*. Springer Verlag, 175(3), pp. 203–212. doi: 10.1007/s00232001068.

Xing, L. *et al.* (2019) 'γ-Glutamylvaline prevents low-grade chronic inflammation via activation of a calcium-sensing receptor pathway in 3T3-L1 Mouse adipocytes', *Journal of Agricultural and Food Chemistry*. ACS Publications, 67(30), pp. 8361–8369. doi: 10.1021/acs.jafc.9b02334.

Xuan, C. *et al.* (2016) 'Dimethylarginine dimethylaminohydrolase 2 (DDAH 2) gene polymorphism, asymmetric dimethylarginine (ADMA) concentrations, and risk of coronary artery disease: A case-control study', *Scientific Reports*. Nature Publishing Group, 6(1), pp. 1–6. doi: 10.1038/srep33934.

Yamamura, A. *et al.* (2012) 'Enhanced Ca 2+-sensing receptor function in idiopathic pulmonary arterial hypertension', *Circulation Research*. American Heart Association, Inc., 111(4), pp. 469–481. doi: 10.1161/CIRCRESAHA.112.266361.

Yeh, W. C. *et al.* (1995) 'Cascade regulation of terminal adipocyte differentiation by three members of the C/EBP family of leucine zipper proteins', *Genes and Development*. Cold Spring Harbor Laboratory Press, 9(2), pp. 168–181. doi: 10.1101/gad.9.2.168.

Yin, W. *et al.* (2012) 'Plasma lipid profiling across species for the identification of optimal animal models of human dyslipidemia', *Journal of Lipid Research*. The American Society for Biochemistry and Molecular Biology, Inc, 53(1), pp. 51–65. doi: 10.1194/jlr.M019927.

Yoo, J. H. and Lee, S. C. (2001) 'Elevated levels of plasma homocyst(e)ine and asymmetric dimethylarginine in elderly patients with stroke.', *Atherosclerosis*. Elsevier, 158(2), pp. 425–30. doi: 10.1016/s0021-9150(01)00444-0.

Zhang, C. *et al.* (2016) 'Molecular basis of the extracellular ligands mediated signaling by the calcium sensing receptor', *Frontiers in Physiology*. Springer, 7(441), pp. 1–17. doi: 10.3389/fphys.2016.00441.

Zhang, W. *et al.* (2019) 'CaSR participates in the regulation of vascular tension in the mesentery of hypertensive rats via the PLC-IP3/AC-V/cAMP/RAS pathway', *Molecular Medicine Reports*. Spandidos Publications, 20(5), pp. 4433–4448. doi: 10.3892/mmr.2019.10620.

Zhang, Y. *et al.* (1994) 'Positional cloning of the mouse obese gene and its human homologue', *Nature*. Nature Publishing Group, 372(6505), pp. 425–432.

Zhou, Y. M. *et al.* (2014) ‘Rho/ROCK signal cascade mediates asymmetric dimethylarginine-induced vascular smooth muscle cells migration and phenotype change.’, *BioMed research international*. Hindawi Limited, 2014, pp. 1–9. doi: 10.1155/2014/683707.

Ziegelstein, R. C. *et al.* (2006) ‘Expression of a functional extracellular calcium-sensing receptor in human aortic endothelial cells’, *Biochemical and biophysical research communications*. Elsevier, 342(1), pp. 153–163. doi: 10.1016/J.BBRC.2006.01.135.

Zoccali, C. *et al.* (2001) ‘Plasma concentration of asymmetrical dimethylarginine and mortality in patients with end-stage renal disease: A prospective study’, *Lancet*. Elsevier, 358(9299), pp. 2113–2117. doi: 10.1016/S0140-6736(01)07217-8.